

**CONTROLS ON THE ARCHITECTURE OF LOWER ISMAY ZONE OF THE  
HONAKER TRAIL FORMATION (PENNSYLVANIAN), SAN JUAN RIVER, UTAH,  
USA**

By

Karen S. Lechtenberg

Submitted to the graduate degree program in geology  
and the Graduate Faculty of the University of Kansas in partial fulfillment of the  
requirements for the degree of Master of Science.

2015

---

Co-chairperson Robert H. Goldstein

---

Co-chairperson Evan K. Franseen

---

Bruce Lieberman

Date Defended: 12/4/2015

The Thesis Committee for Karen S. Lechtenberg

certifies that this is the approved version of the following thesis:

**CONTROLS ON THE ARCHITECTURE OF LOWER ISMAY ZONE OF THE  
HONAKER TRAIL FORMATION (PENNSYLVANIAN), SAN JUAN RIVER, UTAH,  
USA**

---

Co-chairperson Robert H. Goldstein

---

Co-chairperson Evan K. Franseen

---

Bruce Lieberman

Date approved: 12/4/2015

## ABSTRACT

Karen S. Lechtenberg  
Department of Geology, August 2015  
The University of Kansas

This study of the Pennsylvanian Lower Ismay zone of the Paradox Formation, Paradox Basin, Utah, USA intends to improve understanding of build-and-fill processes and carbonate sequence stratigraphy. Closely spaced, centimeter-scale stratigraphic sections reveal lateral and vertical heterogeneities in phylloid algal bafflestone and packstone of a mound-building phase and in fossil-rich wacke-packstone of a topography-filling phase.

Ten lithofacies and one sublithofacies were documented through field study and petrographic analyses. Facies are organized into 10 units within 2 sequences distinguished by lateral geometries and surfaces representing changes in depositional environment. Sequence 1 comprises Units 1-5 and provides evidence of an overall relative shallowing from 50-100m depositional depth to subaerial exposure. A relative sea-level rise was recorded between Units 4 and 5. Sequence 1 consists of lithofacies 1 through 5: 1) Black Laminated Mudstone (BLM); 2) Spicule Mudstone (SM); 3) Crinoid Packstone (CP); 4) Algal Bafflestone (AB); and 5) Algal Packstone (AP). The algal facies (Lithofacies 4 and 5) created relief-building geometries. The sequence was exposed and 5-7m of the topographically highest beds were erosionally truncated to create the famous undulose geometries of the algal facies, commonly known as the “mounds.” Sequence 2 comprises Units 6-10, and shows evidence of an overall relative rise and fall in sea level. Facies of Sequence 2 fill in and drape underlying topography created by Sequence 1. It consists of the following lithofacies: Fusulinid Packstone (FP; 6); Skeletal Wacke-Packstone (SWP, 7); Skeletal Wacke-Packstone-*Chaetetes* (SWP-C, 7a); Peloidal Mudstone (PM, 8); Quartz Sandstone (QS,9); and Quartz Siltstone (QSt, 10).

The build-and-fill model is an enhancement of sequence stratigraphic models. It applies where carbonate strata exhibit subtle paleotopography, were subject to non-optimal carbonate productivity and high-amplitude sea-level changes. The stratigraphic succession in the Lower Ismay algal mounds shows evidence of relative shallowing and deepening during a relief-building phase. A subaerial exposure surface on the top of the algal facies indicates relative deepening was followed by shallowing during a relief-filling phase. The Lower Ismay zone provides an example of build-and-fill geometries that underwent different conditions than typical build-and-fill sequences, ultimately adding to our understanding of the processes that yield build-and-fill geometries.

## ACKNOWLEDGEMENTS

I would like to thank my advisers, Dr. Robert Goldstein and Dr. Evan Franseen, for their continued support throughout this project. On the river in Utah, Chris Klotz, Will Lytle, and Sera Mirchandani were my safety lifelines during 200+ ft rappels, week-long thunderstorms, and hidden rocks in the rapids, for which I am forever grateful. A special thanks to Travis Lechtenberg, my field assistant during the second trip to the field in below freezing temperatures. My gratitude to Wild River Expeditions for the many short-notice trips down the river. Thank you to both the Navajo Nation and the Bureau of Land Management for allowing me to respectfully study my area. Also, thank you to the residents of Blanding and Mexican Hat, Utah for welcoming us into their communities and offering lodging and storage space.

I would like to thank all of my University of Kansas professors, staff, and friends for their endless support. I would especially like to thank Luis Gonzalez for his petrography advice and the use of his old office. Also, a thank you to Wayne Dickerson and his lab's tireless work on preparing thin sections. Many thanks to my climbing teachers, Andrew McCallister and Rafferty Sweeney, for the valuable rappelling and climbing lessons from tall trees, porch balconies, and building rafters while in Kansas. And thank you to my family for their endless encouragement.

Finally, thank you to the Kansas Interdisciplinary Carbonates Consortium, the Society for Sedimentary Geology, the American Association of Petroleum Geologists, the Association for Women Geoscientists, and the University of Kansas for funding to make this project possible.

## TABLE OF CONTENTS

ACCEPTANCE PAGE.....	ii
ABSTRACT.....	iii
ACKNOWLEDGEMENTS.....	v
TABLE OF CONTENTS.....	vi
LIST OF FIGURES AND TABLES.....	viii
INTRODUCTION .....	1
AREA OF STUDY .....	7
GEOLOGICAL BACKGROUND.....	9
METHODOLOGY .....	18
LITHOFACIES AND DEPOSITIONAL ENVIRONMENTS.....	18
Lithofacies 1: Black Laminated Mudstone (BLM).....	19
Lithofacies 2: Spicule Mudstone (SM).....	28
Lithofacies 3: Crinoid Packstone (CP) .....	31
Lithofacies 4: Algal Bafflestone (AB).....	33
Lithofacies 5: Algal Packstone (AP).....	38
Lithofacies 6: Fusulinid Packstone (FP).....	41
Lithofacies 7: Skeletal Wacke-Packstone (SWP).....	43
Sublithofacies 7a: Skeletal Wacke-Packstone - <i>Chaetetes</i> (SWP-C) .....	45
Lithofacies 8: Peloidal Mudstone (PM).....	48
Lithofacies 9: Quartz Sandstone (QS) .....	50
Lithofacies 10: Quartz Siltstone (QSt).....	53
STRATIGRAPHY .....	56
Paleotopographic Reconstruction .....	58
Lower Ismay Zone Sequence Stratigraphy.....	65
Sequence 1 .....	65
Sequence 2 .....	80
Summary.....	88
DISCUSSION.....	90
Algal Facies Development.....	90

Build-and-Fill Model of the Lower Ismay Zone.....	97
Application.....	99
CONCLUSIONS.....	100
REFERENCES .....	103
APPENDICES .....	109
Appendix I: Stratigraphic Sections .....	109
Appendix II: Photomosaics.....	189
Appendix III: Thin Sections.....	195
Appendix IV: Algal Facies Measurements .....	239

## LIST OF FIGURES AND TABLES

Figure 1: Build-and-fill zone locations.....	2
Figure 2: Build-and-fill model summary.....	3-5
Figure 3: Map of study area.....	8
Figure 4: Photos of outcrop challenges.....	10
Figure 5: Map of present-day Paradox Basin.....	11
Figure 6: Pennsylvanian chronostratigraphy of the Paradox Basin.....	13
Figure 7: Generalized dip-oriented cross section of Paradox Basin.....	15
Figure 8: Isopach of Pennsylvanian strata, Paradox Basin.....	15
Figure 9: Generalized stratigraphic diagram of the Lower Ismay.....	16
Figure 10: Explanation of colors and symbols.....	17
Figure 11: Photos of Black Laminated Mudstone Facies (Lithofacies 1).....	25
Figure 12: Photos of Spicule Mudstone (Lithofacies 2).....	29
Figure 13: Photos of Crinoid Packstone (Lithofacies 3).....	32
Figure 14: Photos of Algal Bafflestone (Lithofacies 4).....	35-36
Figure 15: Photos of Algal Packstone (Lithofacies 5).....	39
Figure 16: Photos of Fusulinid Packstone (Lithofacies 6).....	42
Figure 17: Photos of Skeletal Wacke-Packstone (Lithofacies 7).....	44
Figure 18: Photos of Skeletal Wacke-Packstone (Subfacies 7a).....	47
Figure 19: Photos of Peloidal Mudstone (Lithofacies 8).....	49
Figure 20: Photos of Quartz Sandstone (Lithofacies 9).....	52
Figure 21: Photos of Quartz Siltstone (Lithofacies 10).....	54
Figure 22: Map of stratigraphic sections and cross-section locations.....	59
Figure 23: Cross-section A-A'.....	60
Figure 24: Cross-section B-B'.....	61

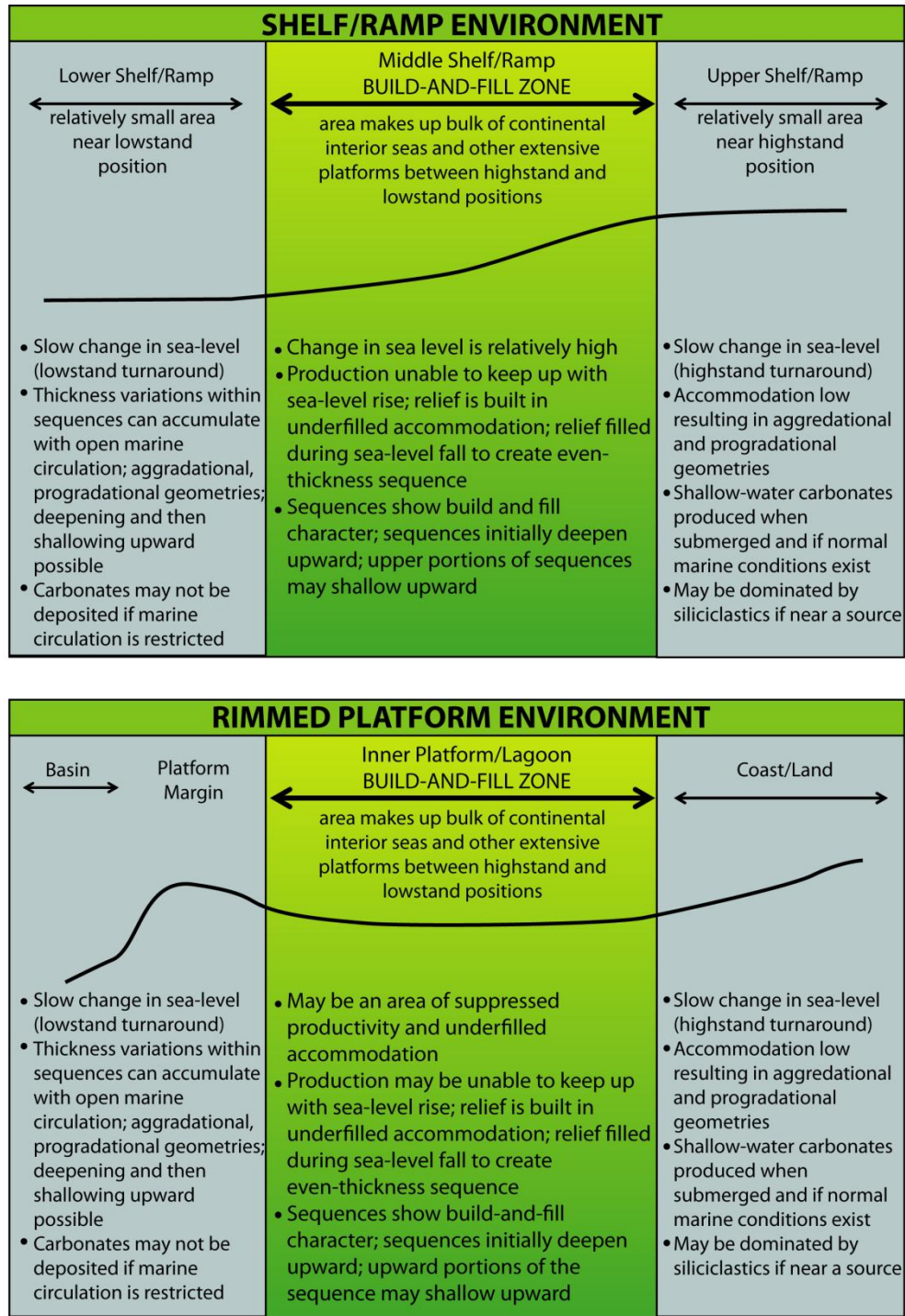


Figure 25:Cross-section C-C' .....	62
Figure 26: Cross-section D-D' .....	63
Figure 27: Fence diagram.....	64
Figure 28: 8FDN water depth curve.....	67
Figure 29: Map of Laura Leta-5 Location.....	69
Figure 30: Photo of algal facies at HTF.....	71
Figure 31:Photo of thinning and thickening of algal facies.....	73
Figure 32: Photo of Unit 4 pinch out.....	75
Figure 33: Photo of Unit 4 truncation.....	75
Figure 34: Photo of SB1.....	79
Figure 35: Illustration of algal facies geometries.....	81
Figure 36: Photo of Units 6 and 7 filling and smoothing.....	83
Figure 37: Photo of Unit 8 pinch out.....	85
Figure 38: Illustration of ring depositional model.....	91
Figure 39: Illustration of dune depositional model.....	94
Figure 40: Map of subsurface algal facies distribution.....	96
Figure 41: Isochron of Upper Ismay zone.....	96
Table 1: Lithofacies table.....	20-23

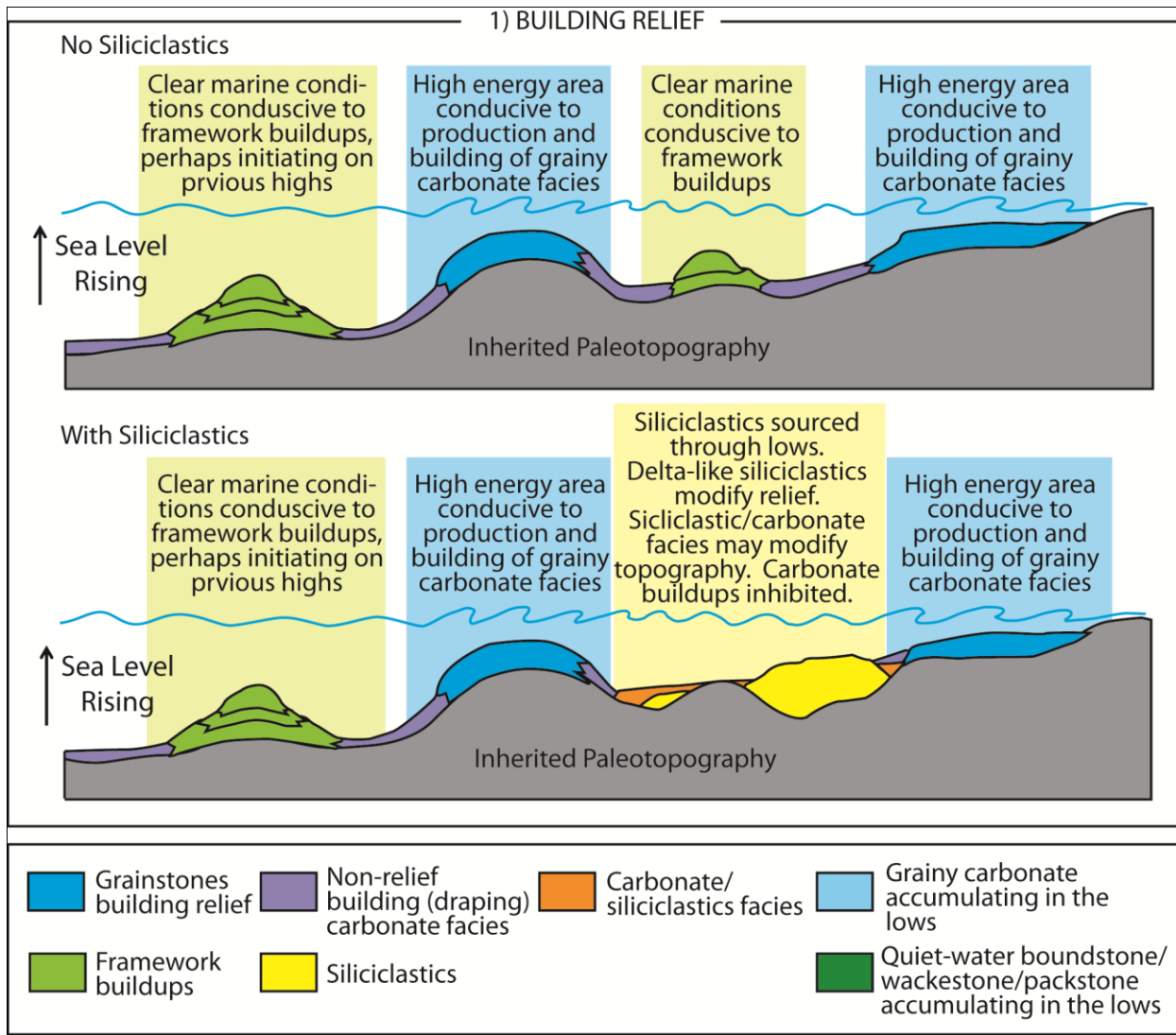
## INTRODUCTION

Standard carbonate sequence-stratigraphy models commonly illustrate sequences with volumetrically dominant highstand systems tracts and lowstand systems tracts (Sarg, 1988; Schlager, 2005). These models are likely less reliable where depositional settings of carbonates are intermediate between the highstand and lowstand positions, exhibit subtle paleotopography, and are subject to non-optimal carbonate productivity or high-amplitude sea-level changes (Franseen et al., 2007b; McKirahan et al., 2003). Typically carbonate and carbonate-siliciclastic sequences, deposited over gentle slopes, are thin in comparison to the amplitude of sea-level change and maintain a consistent thickness for 10s to 100s of kilometers laterally. Many of these sequences form in intermediate locations between the highstands and lowstands of sea level (Franseen et al., 2007b). Icehouse conditions, which are periods of high-frequency, high-amplitude sea-level fluctuations, are ideal for forming such thin laterally continuous sequences (Lehrmann and Goldhammer, 1999). During a sea-level cycle, sedimentation commonly has a topographic relief-building phase and a topographic relief-filling phase, considered a build-and-fill sequence (Franseen and Goldstein, 2004). Build-and-fill sequences typically appear in the middle of a ramp system or the inner platform/lagoon of a rimmed platform known as the build-and-fill zone (Figure 1, Franseen et al., 2007a).

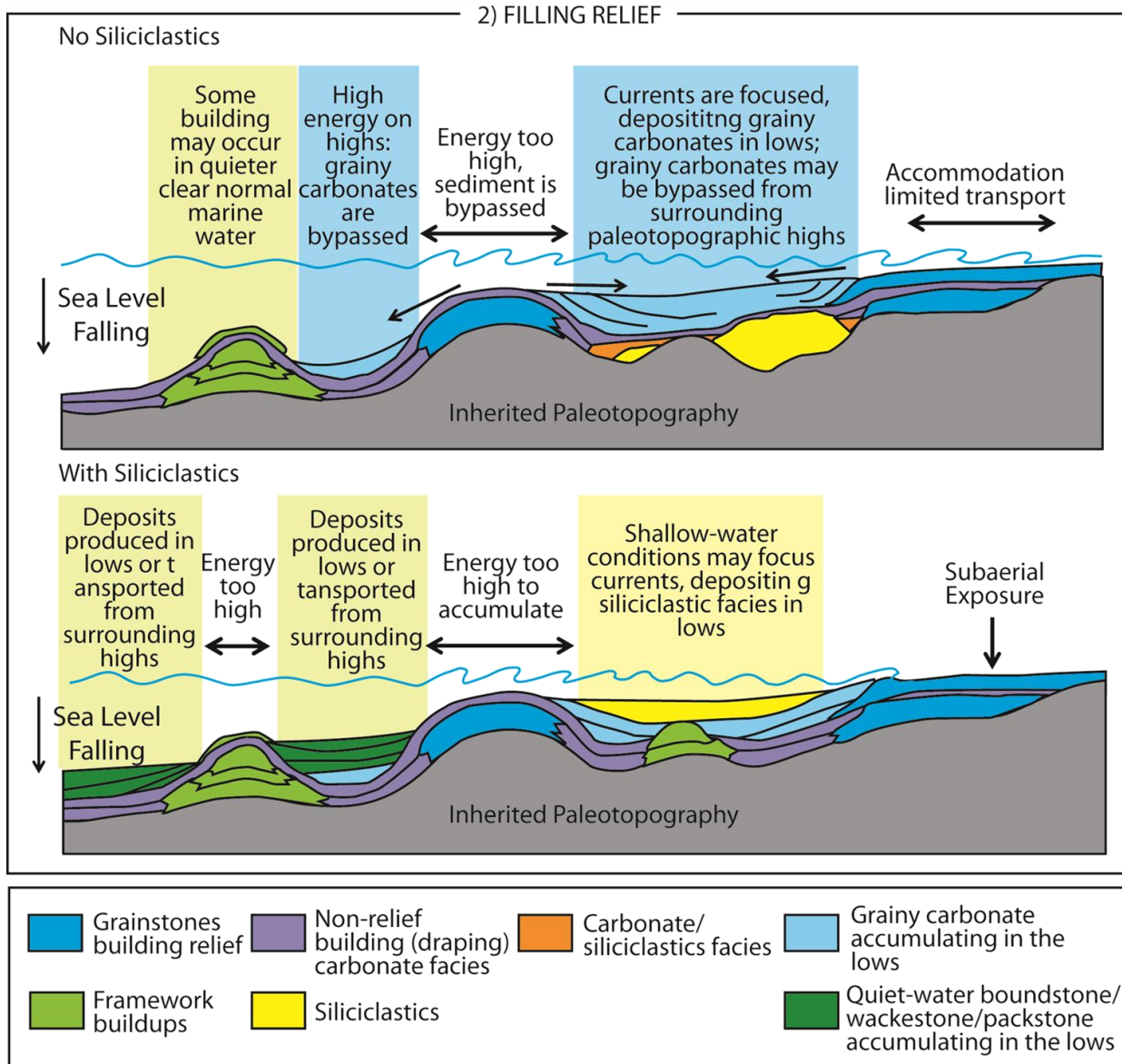
The build-and-fill model evolved from field-study results of numerous icehouse systems of the Upper Miocene of Spain and the Pennsylvanian Midcontinent USA (Figures 2a, 2b, and 2c; Emery et al., 2006; Fairchild et al., 2008; Franseen and Goldstein, 2004; Franseen et al., 2007b; Lipinski et al., 2008; McKirahan et al., 2003; Washburn and Franseen, 2003). Ongoing studies include additional field studies, like this one, and extensive literature research to better



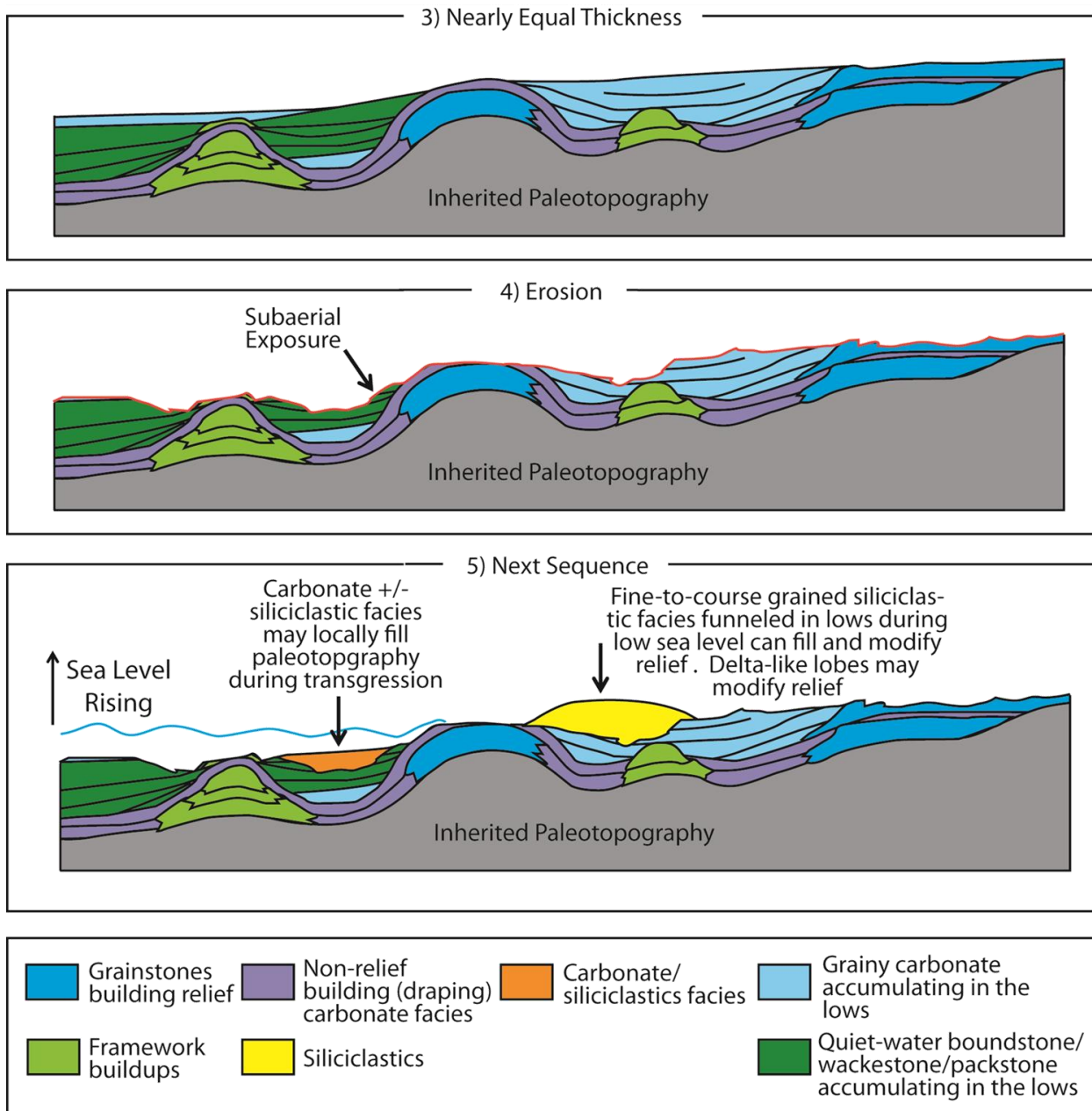
**Figure 1.** Schematic illustrating build-and-fill zone locations for shelf/ramp and rimmed platform environments. Modified from Franseen and Goldstein (2012) and Franseen et al. (2007b).



**Figure 2a.** Build-and-fill model summary: 1) Topography building and drape during sea-level rise (modified from Franseen, et al. (2007b)).



**Figure 2b.** Build-and-fill model summary: 2) Topography filling during sea-level fall (modified from Franseen, et al. (2007b)).



**Figure 2c.** Build-and-fill model summary: 3) Topography filled resulting in nearly equal-thickness sequences; 4) Erosion during lowstand re-initiates variable paleotopography prior to deposition of next sequence; and 5) Initiation of next build-and-fill sequence (modified from Franseen, et al. (2007b)).

understand the fundamental factors that lead to build-and-fill and those that do not lead to build-and-fill.

Build-and-fill sequences are observed throughout the rock record (Franseen and Goldstein, 2012). Examples were typically deposited as 4<sup>th</sup> or higher order sequences during icehouse and greenhouse conditions (Franseen and Goldstein, 2012). The building phases dominantly form during relative sea-level rise and are created by corals, stromatoporoids, thrombolites/stromatolites, sponges, red algae, green algae, and grainstone shoals (Franseen and Goldstein, 2004; Franseen and Goldstein, 2012). The filling phases dominantly form during relative sea-level fall and typically are composed of packstones and grainstones (Franseen and Goldstein, 2004; Franseen and Goldstein, 2012). As the overall thickness of build-and-fill sequences is far less than the amplitude of sea-level rise, it is clear that the carbonate factory was unable to keep up with the rate of relative sea-level rise. This leads to deeper water and unfilled accommodation (Lehrmann and Goldhammer, 1999). Other examples in the rock record demonstrate that the building phase can occur during a sea-level fall in more distal environments of platforms (Franseen and Goldstein, 2012). Further investigation is needed to increase understanding of the controls behind non-optimal carbonate productivity that might lead to build-and-fill conditions.

The Lower Ismay zone (Desmoinesian) of the Paradox Basin contains thin, laterally extensive sequences with complex internal geometries deposited during icehouse conditions (Goldhammer et al., 1991), on a gentle paleotopographic slope (Goldhammer et al., 1991; Peterson, 1966b). Strata exposed by the modern-day San Juan River through the Raplee anticline and Monument upwarp are interpreted to result from 4<sup>th</sup> and 5<sup>th</sup> order sea-level changes (Goldhammer et al., 1991; Grammer et al., 2000). Sequences contain relief-building algal facies

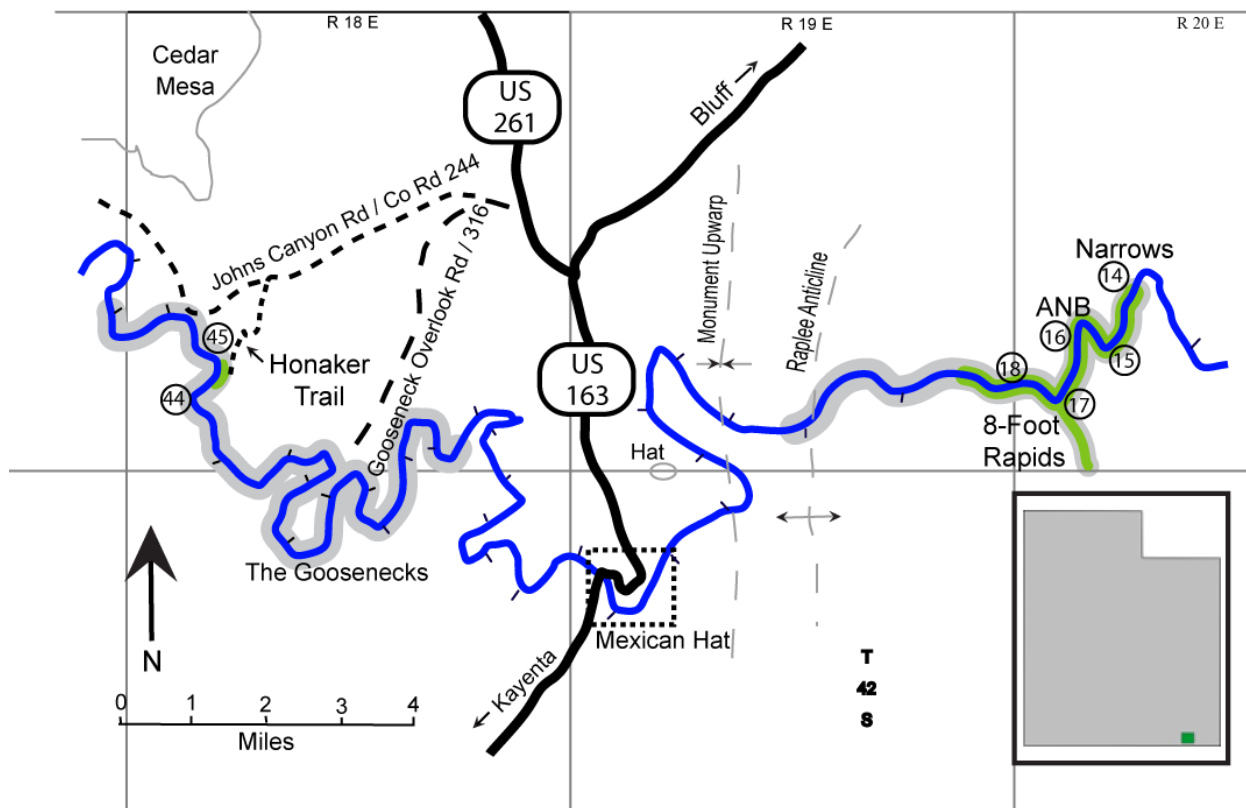
and relief-filling packstones and wackestones (Pray and Wray, 1963). This study investigates the controls on geometries and facies in the Lower Ismay zone. Outcrops of the Lower Ismay zone near Mexican Hat, Utah along the San Juan River, where accessible, can be analyzed for indicators of sea-level change to evaluate the origin of geometries that build relief and those that fill relief (Figure 3). Given the build-and-fill model, if the Lower Ismay is a typical build-and-fill sequence, then it would show indicators of sea-level deepening within the building geometries and indicators of sea-level shallowing within the filling geometries. If the Lower Ismay does not exhibit such characteristics, then different conditions are responsible for the observed build-and-fill geometries.

Outcrops of build-and-fill sequences are useful analogs to hydrocarbon reservoirs (Franseen and Goldstein, 2012). The Lower Ismay outcrops are direct analogs to heterogeneous reservoirs in the nearby Great Aneth Field and surrounding smaller fields (Amateis and Hall, 2005; Chidsey et al., 1996a; Chidsey et al., 1996b; Herrod et al., 1985; Montgomery et al., 1999; Peterson, 1966b). In the subsurface, the algal facies of the Lower Ismay and Desert Creek is known as a complex heterogeneous hydrocarbon reservoir (Grammer et al., 2000; Goldhammer et al., 1991; Chidsey et al., 1996a; Chidsey et al., 1996b; Choquette and Traut, 1963; Grammer and Ritter, 2008; Herrod et al., 1985; Montgomery et al., 1999; Peterson, 1966a; Peterson, 1966b; Peterson and Hite, 1969). The complexity of the system provides challenges for hydrocarbon exploitation. Results from this study can lead to better predictive reservoir models of such systems.

## **AREA OF STUDY**

This study analyzes well-known outcrops of the Honaker Trail area, 8-foot Rapids, and various outcrops along the San Juan River (Figure 3; Chidsey et al., 1996a; Chidsey





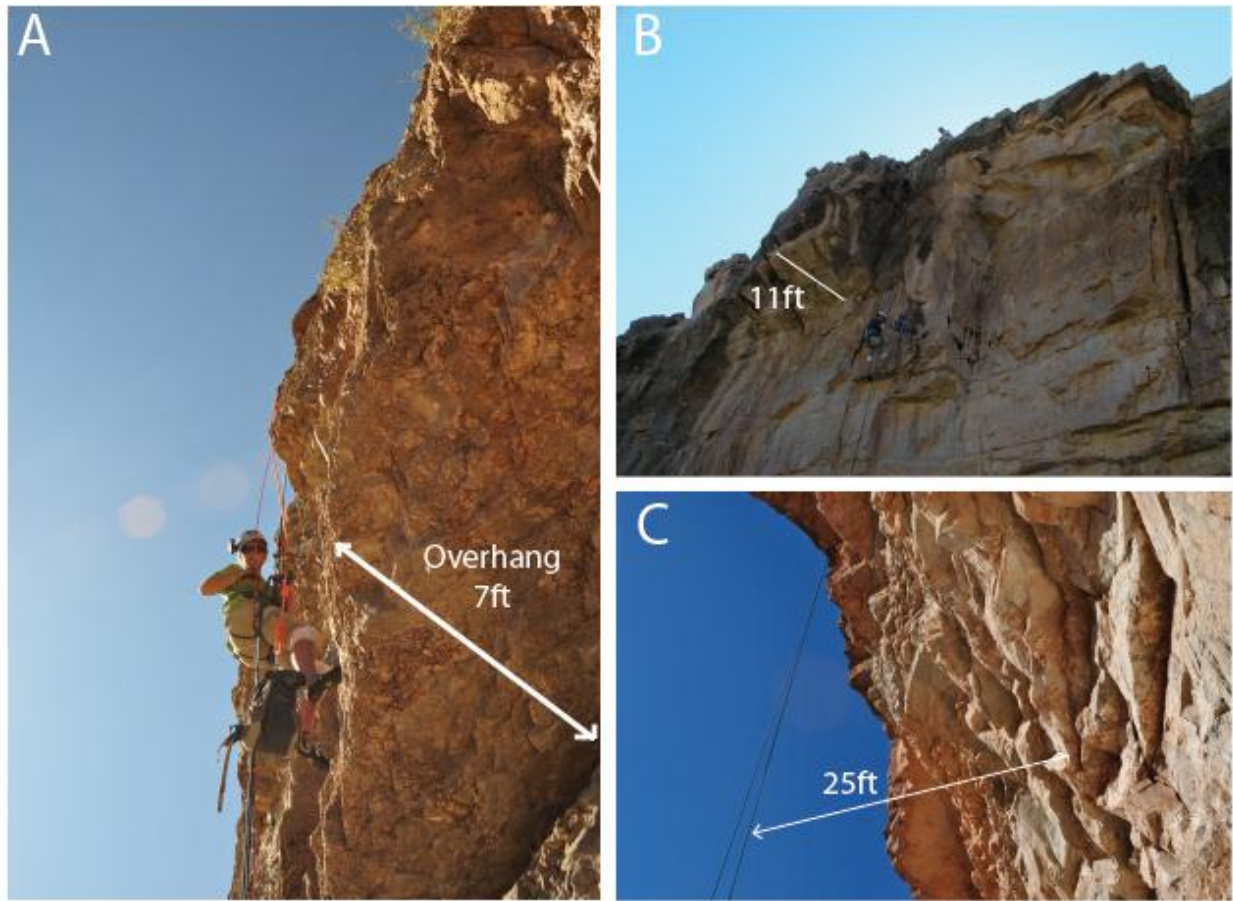
**Figure 3.** Study area map. The study area is located in southeast Utah along the San Juan River. The San Juan River is marked in blue with the river miles marked by circled numbers near study areas or tick marks elsewhere. Highways are solid black lines, paved roads are dashed lines, and dirt roads are smaller dashed lines. Lower Ismay outcrop is highlighted in gray along the river. Accessible locations of measured stratigraphic sections are highlighted in green and labeled with site names. Landmarks and towns are labeled. Map modified from Pray and Wray (1963).

et al., 1996b; Goldhammer et al., 1991; Grammer et al., 2000; Grammer and Ritter, 2008; Lerat et al., 2000; Montgomery et al., 1999; Ritter et al., 2002; Roylance, 1990). Outcrops of the Lower Ismay zone in this area are located on the sides of cliffs as a result of downcutting by the modern-day San Juan River through the Raplee anticline and Monument upwarp (Figure 3). A raft was taken down the San Juan River to reach the study area. Climbing ropes aided in the collection of data in hard-to-access areas. Rappelling proved difficult due to poor anchor rock types and overhangs created by overlying, more resistive formations (Figure 4). Cliff walls within the Raplee anticline between river-miles 13 and 19 expose the Lower Ismay zone of the Paradox Formation. The Honaker Trail at river-mile 45 is an abandoned gold-panning path that provides access to the San Juan River, 1,000 feet below the canyon rim. The manmade trail provides limited access to a Lower Ismay zone outcrop.

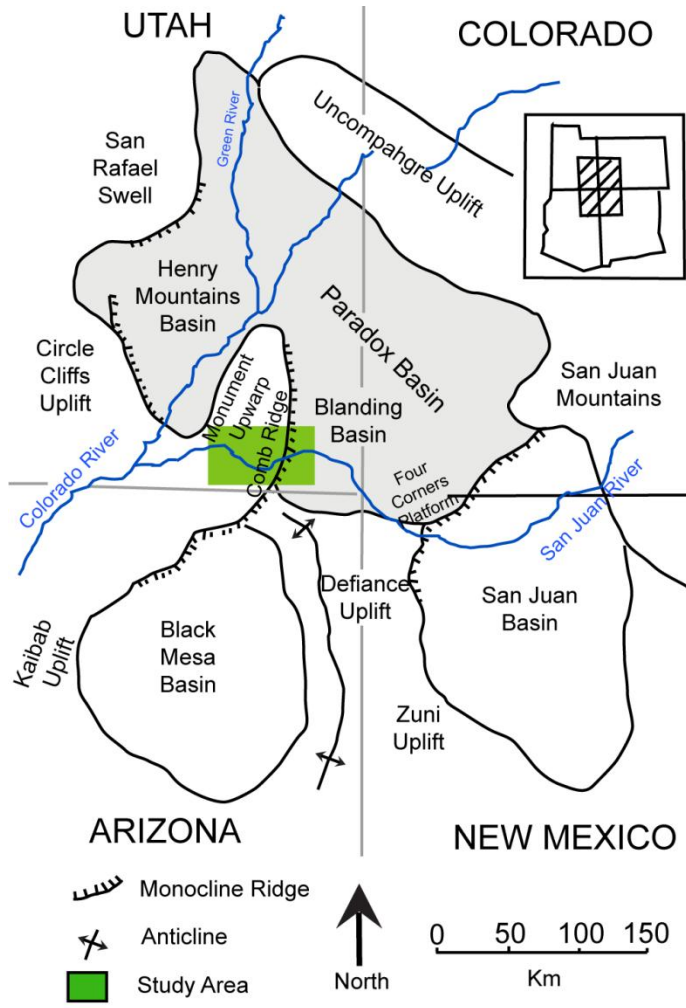
## **GEOLOGICAL BACKGROUND**

The Paradox basin is a northwest-southeast oriented, Pennsylvanian “trough-shaped” basin located in the Four Corners region, USA at the juncture of Utah, Colorado, New Mexico and Arizona (Figure 5) (Baars and Stevenson, 1981; Baars and Stevenson, 1982; Goldhammer et al., 1991; Stevenson, 1984). Today, the Paradox basin is bounded on the northeast by the Uncompahgre uplift, on the west by the San Rafael swell and the Circle Cliffs, and on the south by the Four Corners platform, the Defiance-Zuni uplift, and the Monument upwarp (Goldhammer et al., 1991; Peterson, 1966b).

During the early Mississippian, the Paradox basin was an extensive marine shelf across the Colorado plateau (Ohlen and McIntyre, 1965). In the late Mississippian, the area was uplifted, subaerially exposing the marine sediments and creating widespread red paleosol (Goldhammer et al., 1991; Peterson, 1966b).



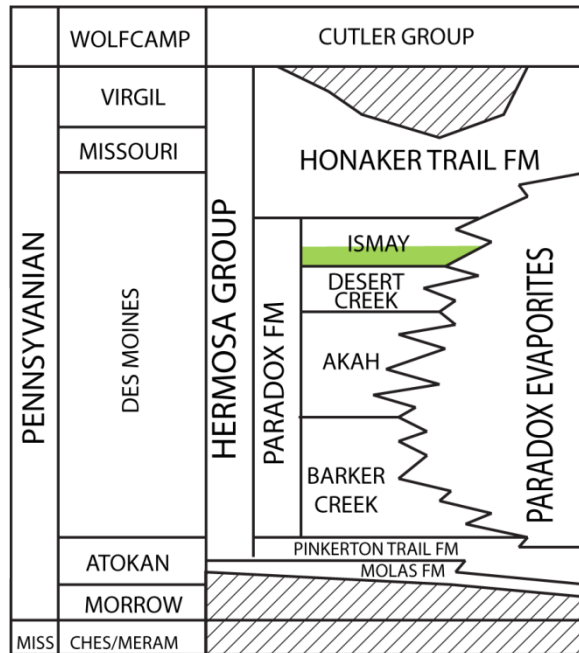
**Figure 4.** Photos illustrating overhangs created by Units 6-10. Overhangs made accessing lower units (1-5) difficult. A) 7ft overhang created by Lithofacies 7 facies at ANB locality. B) 11ft overhang created by Lithofacies 7. This example shows a rappelling route at the 8FR locality that allowed measurement of stratigraphic section without overhang, however, closely-spaced stratigraphic section along the entire outcrop was not possible. Person for scale. C) Overhang created by Lithofacies 7 created an overhang that created a 25ft gap between the rope and the outcrop.



**Figure 5.** The present-day Paradox Basin (light gray) is bounded by the Uncompahgre uplift (northeast), the San Rafael swell and Circle Cliffs (west), Four Corners Platform, the Defiance-Zuni uplift, and Monument upwarp (south). The green box indicates the area of this study. Modified from Ohlen and McIntyre (1965).

During the Pennsylvanian, uplifts associated with deformation in the Ancestral Rockies defined the geometries of the Paradox basin (Soreghan et al., 2012). Uplifts around the rim of the basin included the Uncompahgre uplift to the northeast, the Defiance-Zuni uplift to the south, and the Emery Uplift to the west (Peterson and Hite, 1969). The basin strike is interpreted to be northwest to southeast, and deepening to the northeast (Goldhammer et al., 1991). These uplifts restricted the basin from the open sea, with the exception of two connecting passageways, the Cabezón seaway to the southeast and another unnamed seaway to the southwest (Hite, 1970; Peterson and Hite, 1969).

The marine transgression of the Hermosa sea during the beginning of the Desmoinesian (Pennsylvanian) reworked the red paleosol, creating the Atokan Molas formation, and deposited the mixed siliciclastics and carbonates of the Pinkerton Trail formation (Goldhammer et al., 1991; Grammer et al., 2000). The rest of the Desmoinesian was dominated by thin, cyclic mixed-siliciclastics and carbonate deposits (Goldhammer et al., 1991). Open-marine carbonates were deposited on a low-angle, shallow-shelf environment located in the southeast portion of the basin and dipped northeast (Eberli, 2000; Goldhammer et al., 1991; Grammer et al., 2000; Montgomery et al., 1999; Picard and Brown, 1961). Siliciclastics, typically sourced from the surrounding uplifts, were also deposited on the shelf and near basin margins (Goldhammer et al., 1991). Basinward, thick, coeval evaporites were deposited and interfinger with thin siliciclastic-carbonate cycles (Baars and Stevenson, 1981; Peterson, 1966a; Peterson and Hite, 1969). The Desmoinesian shelfal carbonates and siliciclastics are grouped into four intervals of the Paradox Formation: Barker Creek, Akah, Desert Creek, and Ismay (Figure 6) (Grammer et al., 2000). Laterally extensive black shale beds are used to correlate the shelfal cycles to the basin

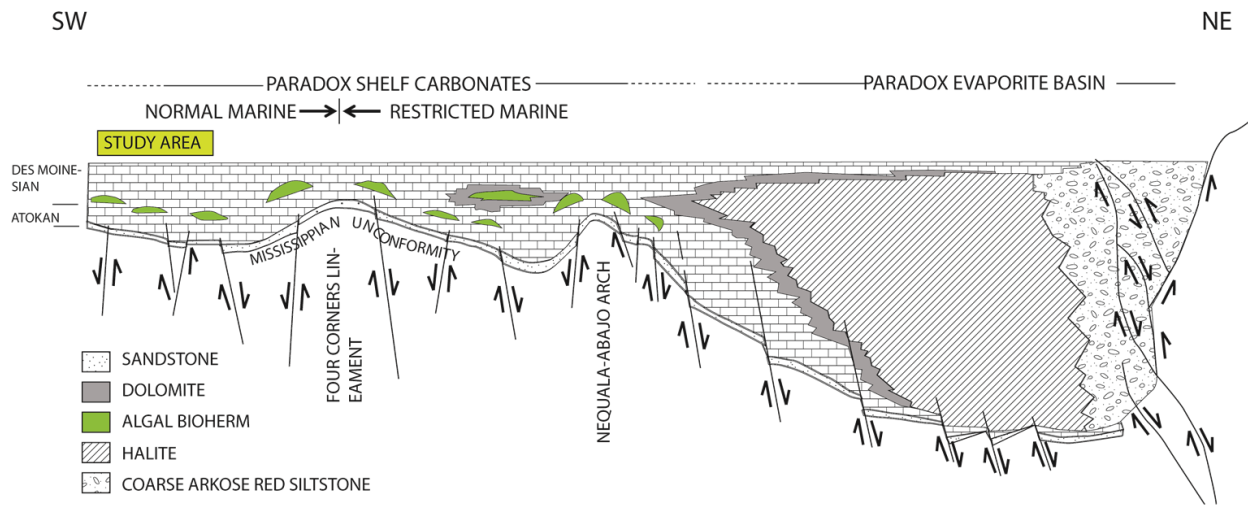


**Figure 6.** Pennsylvanian chronostratigraphy of the Paradox basin. The zone of interest, the Lower Ismay, is marked with green. Modified after Goldhammer et al. (1991) and Baars and Stevenson (1982).

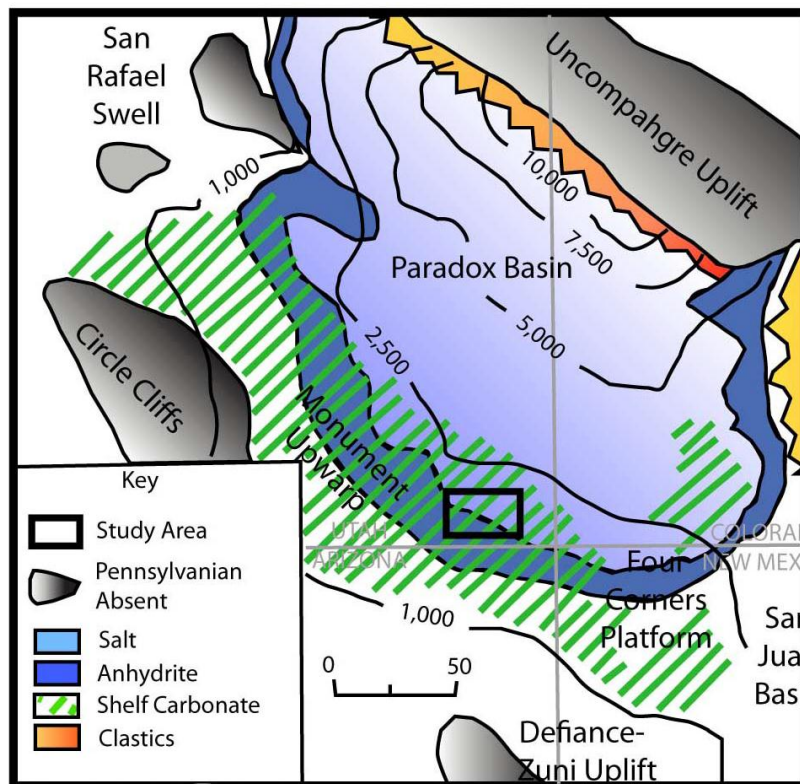
evaporites and mark the beginning of each cycle (Choquette and Traut, 1963; Goldhammer et al., 1991; Peterson, 1966b). Rapid subsidence occurred throughout Pennsylvanian deposition (Baars and Stevenson, 1981). Subsidence rates were nonuniform, and were higher towards the Uncompahgre Uplift and created the deepest part of the basin (Figure 7, Baars and Stevenson, 1981; Goldhammer et al., 1991).

The Honaker Trail formation, Desmoinesian-to-Virgilian age, overlies the four intervals of the Paradox Formation (Grammer et al., 1962). It grades from mixed siliciclastics and carbonates to massive sandstones towards the northwest (Grammer et al., 2000). With the end of the Pennsylvanian (Virgilian), the Hermosa sea retreated with a sudden final rise of the Uncompahgre uplift forming a widespread unconformity between the Carboniferous and the Permian (Figure 6, Elston et al., 1962; Grammer et al., 2000).

The zone of interest, the Lower Ismay of the Paradox Formation (Desmoinesian), was deposited on evolving topography during syndepositional deformation. An overall dip 0.4 degree was calculated from published isopach maps of the Desmoinesian strata (Figure 8, Goldhammer et al., 1991). Facies distributions discussed in the Sequence Stratigraphy section suggest a dip of approximately 0.1 degree throughout the study area. The deposition of the Lower Ismay occurred during active subsidence of basinward deposits and the depositional dip was changing throughout deposition (Grammer et al., 2000; Goldhammer et al., 1991). As a result, the shelfal deposits thicken basinward as they interfinger with basinal evaporites (Figure 6; Goldhammer et al., 1991). Figure 9 diagrams the general stratigraphy and distribution of the Lower Ismay facies in the study area from Honaker Trail (HTF) to 8-Foot localities. See Figure 10 for explanations of symbols and colors used in figures and appendices.

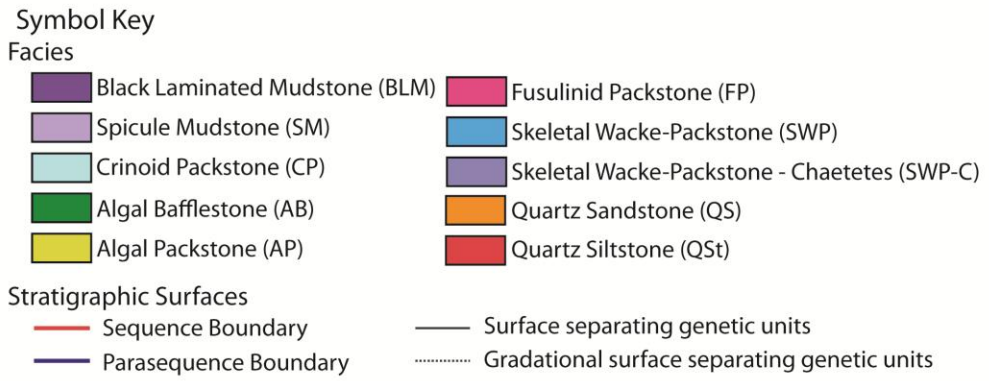
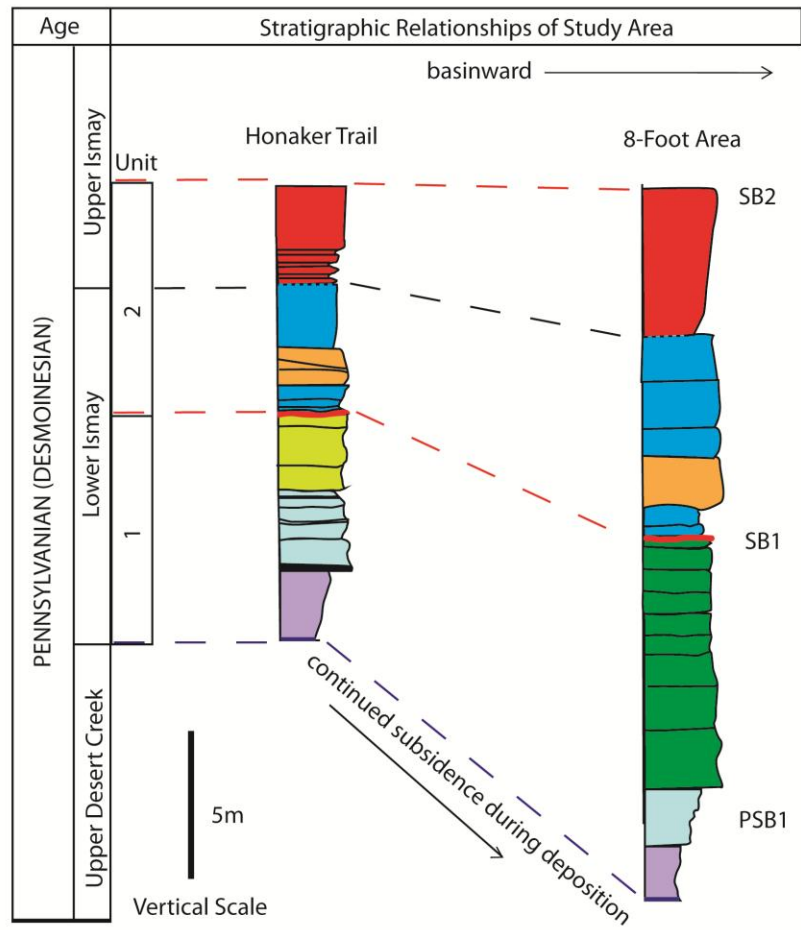


**Figure 7.** Generalized southwest-northeast dip-oriented cross-section across the Paradox basin illustrating relationships between Pennsylvanian shelf carbonates, basinal evaporites, and clastics proximal to the Uncompahgre uplift. The algal bioherm buildups are highlighted in green. The approximate study location within the cross-section is marked. Modified from Goldhammer et al. (1991).


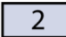
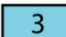


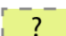


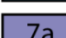








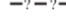


















**Figure 8.** Isopach map of Pennsylvanian strata (ft). The study area is marked with a black box. Modified from Goldhammer et al. (1991).





**Figure 9.** Illustration of stratigraphic relationships and facies distribution of the Lower Ismay study interval between HTF and 8-Foot locations. The Peloidal Mudstone (PM) facies, sedimentary structures, and grains are not shown at this scale. See Distribution of Stratigraphic Units for sequence stratigraphy definitions.

Symbol Explanation	
<b>Lithofacies</b>	
	Black Laminated Mudstone (BLM)
	Spicule Mudstone (SM)
	Crinoid Packstone (CP)
	Algal Bafflestone (AB)
	Algal Packstone (AP)
	Interpreted Algal Packstone (AP)
	Fusulinid Packstone (FP)
	Skeletal Wacke-Packstone (SWP)
	Skeletal Wacke-Packstone - Chaetetes SWP-C)
	Peloidal Mudstone (PM)
	Quartz Sandstone (QS)
	Quartz Siltstone (QSt)
<b>Stratigraphic Surfaces</b>	
	Sequence Boundary
	Parasequence Boundary
	Surface separating genetic units
	Gradational surface separating genetic units
	Bedding plane traced using photomosaics
	Bedding plane where exposure is poor, covered, or not preserved
<b>Sedimentary Structures</b>	
	Trough Crossbedding
	Styolite
	Flaser Bedding
<b>Grain Types</b>	
	Phylloid algae
	Individual crinoid fragments
	Crinoid column
	Thick brachiopod shells
	Thin brachiopod shells
	Rugose coral
	Chaetetes sponge
	Bryozoan
	Gastropod
	Fusulinids
	Mud clasts
	Brecciated mud clast
	Chert

**Figure 10.** Explanation of colors and symbols used in figures 23-36 and Appendices I-III.

## **METHODOLOGY**

Sedimentary units and contacts were measured and characterized with the creation of 27 stratigraphic sections between river miles 13 and 19, and at river-mile 45. The stratigraphic section localities include the Narrows (N), Rock Cairn Bend (RCB), Alligator Nose Bend (ANB), 8-Foot Rappel (8FR), 8-Foot Drainage Navajo (8FDN), 8-Foot Narrows (8FN), and Honaker Trail Fin (HTF). GPS locations for each stratigraphic section locality are listed in Appendix I. Stratigraphic sections were measured on a centimeter scale with emphasis on lithofacies, sedimentary structures, and surfaces (e.g. subaerial exposure surfaces) to determine depositional environments.

Lithofacies and surfaces were traced laterally on photomosaics or physically walked out, depending on accessibility. 128 samples were collected for petrographic analysis. A total of forty-three thin sections and fifty-one polished slabs were analyzed to further document facies and features diagnostic of depositional environment. A sequence-stratigraphic interpretation was constructed based on field and lab data.

### **LITHOFACIES AND DEPOSITIONAL ENVIRONMENTS**

A total of 10 lithofacies and 1 sublithofacies were defined from field observation, polished slabs, and petrographic analysis of thin sections. The general distribution of the facies is represented in Figure 9. Lithofacies were identified using texture, degree of sorting, grain components (type, volume percentage, and size), degree of abrasion, bedding, sedimentary structures, and any other diagnostic characteristics outlined in Table 1. Texture was determined using Dunham's classification (1962). Sorting was established using the qualitative observation of the deviation of grain sizes, excluding matrix and cement, and using Longiaru's (1987) visual comparison sorting charts as a reference. Volume percentages were visual estimates of polished

slabs and thin sections with reference to Baccelle and Bosellini (1965) and Scholle and Ulmer-Scholle (2003) carbonate visualization estimation diagrams. Volume percentages from thin sections and slabs were recorded for each grain type, mud, cement, and void space. Mud content was defined as depositional mud and internal sediment. The mud seen in thin section appears to be comprised of compressed peloids. Peloids that show evidence of early compaction are soft peloids, and are classified as mud. Peloids that have maintained shape and can confidently be identified are classified as hard peloids. Grain size was measured along the long dimension of each grain as seen in thin section. The degree of abrasion was determined using a visual abrasion estimation chart as a reference (Flügel, 2010). Bedding and sedimentary structures were defined from outcrop observations. Other diagnostic characteristics were noted including distinct coloration of beds, abundance of chert, or any other significant features that distinguish facies. See Appendix III for individual thin section data.

### **Lithofacies 1: Black Laminated Mudstone (BLM)**

**Description** - The Black Laminated Mudstone (BLM) Facies in the Lower Ismay Zone is commonly known to petroleum companies as the “Gothic Shale.” The BLM is 10-40 cm thick and is black to dark gray in color (Figure 11A). It consists of 60% mud, 20% subangular-subrounded quartz sand, 10% clay, 5% calcite, 5% pyrite, and sparse biotite grains, non-skeletal phosphate, sponge spicules and conodonts (*Idiognathodus n. sp. B*, *Idiognathodus n. sp. C*, *Gondolella bella*, *Neognathodus*, *I. Meekerensis*, and *I. Obliquus*; Ritter et al., 2002), and no visible porosity (Figure 11B). No skeletal phosphate is observed. It is organic-rich and smells of hydrocarbons when broken with a hammer. Millimeter-scale laminations are present every 0.2 cm, parallel underlying beds, and cause fissility. Some blockiness between laminations suggests possible bioturbation (Figure 11C).

**Table 1.** Lithofacies summary table.

Facies	Diagnostic Characteristics	Components	Bedding and Sedimentary Structures	Interpreted Depositional Environment
<p><b>1.</b> <b>Black Laminated Mudstone</b></p>	<p>dark gray to black; organic-rich; smells like hydrocarbons</p>	<p>peloidal mud (60%), quartz sand (20%), clay (10%), calcite (5%), pyrite (5%), biotite (sparse), sponge spicules (sparse), non-skeletal phosphate (sparse), and conodonts (<i>Idiognathodus n. sp. B</i>, <i>Idiognathodus n. sp. C</i>, <i>Gondolella bella</i>, <i>Neognathodus</i>, <i>I. Meekerensis</i>, and <i>I. Obliquus</i>) (sparse); No visible porosity</p>	<p>thin, laterally continuous bed (10-40cm thick); laminations every 0.2 cm; laminations parallel underlying bed</p>	<p>low energy, anoxic environment through settling of mud, fossils, and detrital very fine-grained quartz; 50-100m water depth</p>
<p><b>2.</b> <b>Spicule Mudstone</b></p>	<p>brownish gray (weathers yellow); forms recessive unit below resistive algal facies</p>	<p>peloidal mud (~35%), silt to very fine-grained quartz sand (~30%), sponge spicules (~20%), clay (~5%), calcite (~5%), marine fossils (brachiopods, crinoids, and bryozoa) (1-10%, increasing in abundance stratigraphically up); No visible porosity</p>	<p>thick, laterally continuous bed (~4m thick); undulose-to-nodular bedding; ~2 cm-scale vague laminations; possible burrowing; laterally traceable 10-20cm thick chert deposits</p>	<p>low energy, dysaerobic environment; between 50-100m and 15-20m water depth</p>
<p><b>3.</b> <b>Crinoid Packstone</b></p>	<p>yellow-brown; stylolitized bed below mounds</p>	<p>crinoids (20-30%), normal marine fossils (bryozoa, brachiopods, brachiopod spines, ostracods, and sponge spicules) (30%), peloidal mud (15%), calcite cements (5-10%), pellets (sparse); 0-1% visible porosity</p>	<p>thick laterally continuous bed (~3m thick); bioturbation throughout facies; stylolitized near base</p>	<p>low energy, aerobic environment; 15-20m water depth</p>

<p><b>4.</b> <b>Algal</b> <b>Bafflestone</b></p>	<p>brownish gray; vuggy porosity; cup-shaped phyllloid algae plates with sediment fills; appears massive due to weathering</p>	<p>whole phylloid algae (Ivanovia, 10-30%), and sparse-to-low abundance foraminifera (fusulinids, encrusting forams and biserial forams), calcite spar (25-40%), bryozoa, brachiopods, brachiopod spines, crinoids, gastropods, and ostracods, peloidal mud (15- 30%), hard peloids (1-5%), chalcedony (0-5%); 5-10% visual porosity</p>	<p>bed thickness ranges 10cm-3m; interfinger with AP; builds relief; possible bioturbation</p>	<p>moderate energy, aerobic environment; algae baffles current and traps sediment; 10- 15m water depth</p>
<p><b>5.</b> <b>Algal</b> <b>Packstone</b></p>	<p>brownish gray; vuggy porosity; appears massive due to weathering; well-sorted broken algal plates</p>	<p>fragmented phylloid algae (Ivanovia, 25-40%), and sparse-to-low abundance pellets, bryozoa, brachiopods, brachiopod spines, crinoids, gastropods, ostracods, and foraminifera (fusulinids, encrusting forams and biserial forams), peloidal mud (5-40%), calcite spar (20- 50%); 5-40% visual porosity</p>	<p>patches that interfinger with AB</p>	<p>moderate-high energy, aerobic environment; 5- 10m water depth</p>
<p><b>6.</b> <b>Fusulinid</b> <b>Packstone</b></p>	<p>gray; fills and drapes underlying topography</p>	<p>fusulinids (45-60%), normal marine fossils (bryozoa, brachiopod, ostracods, gastropod, and crinoids) (10-20%), peloidal mud (10- 20%), pore-filling and replacement calcite spar (5%); No visible porosity</p>	<p>beds thin or onlap onto underlying topography</p>	<p>low energy, aerobic environment; 20- 25m water depth</p>

<p><b>7.</b> <b>Skeletal Wacke-Packstone</b></p>	<p>dark gray; drapes and fills underlying topography</p>	<p>normal marine fossils (crinoids, bryozoa, brachiopods, brachiopod spines, foraminifera (<i>fusulinids</i>, <i>Endothyrids</i>, uniserial forams, and biserial forams, possibly <i>Deekereella</i>), pellets, ostracods, gastropods, rugose coral, <i>Chaetetes</i> sponges, and local phylloid algae (<i>Ivanovia</i>) (20-70%), peloidal mud (15-55%), pore-filling and replacement calcite spar (5-25%), chalcedony (1-6%), replacement quartz (1-5%); 0-5% visible porosity</p>	<p>thin-to-medium bedding ranging from 10cm-2m thick; fills or drapes relief; bioturbation; stylolites; chert lenses throughout facies</p>	<p>moderate-high energy, normal marine, aerobic environment; 5-10m water depth</p>
<p><b>7a.</b> <b>Skeletal Wacke-Packstone - Chatetes</b></p>	<p>dark gray; drapes and fills underlying topography; whole <i>Chaetetes</i> sponges and rugose corals; large, nearly intact crinoid stems</p>	<p>normal marine fossils (crinoids, bryozoa, brachiopods, brachiopod spines, foraminifera (<i>fusulinids</i>, <i>endothyrids</i>, uniserial forams, encrusting forams, and biserial forams, possibly <i>Deekereella</i>), ostracods, gastropods, rugose coral, <i>Chaetetes</i> sponges, and local phylloid algae (<i>Ivanovia</i>) (50-80%), peloidal mud (15-30%), pore-filling and replacement calcite spar (5-40%), chalcedony (1-5%), replacement quartz (1-5%). pellets (sparse); 0-5% visible porosity</p>	<p>undulose medium bedding ranging from 20cm-1m thick; onlaps, fills or drapes relief; bioturbation; stylolites; chert lenses throughout facies</p>	<p>low-moderate energy, normal marine, aerobic environment; approximately 10-15m water depth</p>
<p><b>8.</b> <b>Peloid Mudstone</b></p>	<p>dark gray-brown; discontinuous</p>	<p>peloidal mud (80-90%), pore-filling calcite cement (&lt;5%), normal marine fauna (brachiopods, crinoids, foraminifera, gastropods) (sparse); &lt;5% visible porosity</p>	<p>discontinuous, thin bedding 1-50cm thick; fills and onlaps relief</p>	<p>high energy, storm deposits later bioturbated and eroded or protected areas within SWP environment; approximately 4-10m water depth</p>

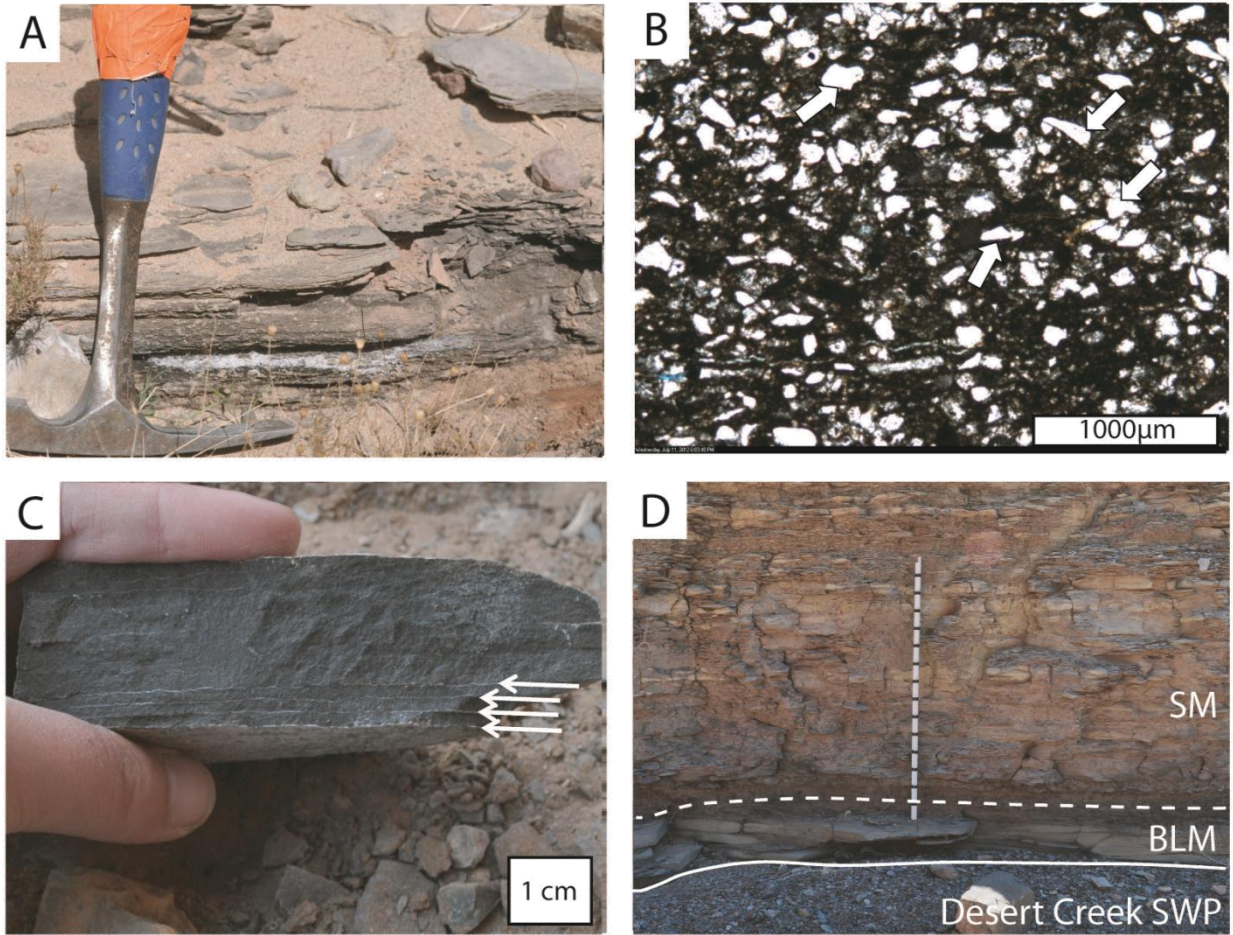
<p><b>9. Quartz Sandstone</b></p>	<p>yellow-brown; distinct crossbeds; wedge-shaped</p>	<p>very fine to silt sized quartz (~70%), feldspars (1%), pyrite (sparse), and diverse fauna (brachiopods, brachiopod spines, foraminifera, crinoids, ostracods) concentrated in peloidal mud along crossbed planes (&lt;5%);  ~5% visible porosity</p>	<p>discontinuous, wedge-shaped medium bed up to 3.5m thick; low- angle trough- crossbedding</p>	<p>high energy, within fair-weather wave base; 5-10m water depth</p>
<p><b>10. Quartz Siltstone</b></p>	<p>distinct yellow color; known to locals as "Old Yeller"</p>	<p>quartz silt (60-80%), peloidal mud (20-30%), marine fossils (brachiopods, brachiopod spines, foraminifera, bryozoa, ostracods) along planes (5-30%), calcite cements (&lt;10%);  &lt;5% visible porosity</p>	<p>thick bedding ~7m thick; laterally continuous; flaser bedded; abundant chert throughout facies</p>	<p>subtidal environment; less than 5m water depth</p>



The BLM is the basal facies of the Lower Ismay Zone of the Paradox Formation. It overlies, in sharp contact, Skeletal Wacke-Packstone of the Upper Desert Creek zone (see description below). The BLM grades upward into the Spicule Mudstone (see below) (Figure 11D).

**Interpretation** – The water depth of deposition of BLM has been debated in the literature. Byers' (1977) general model of euxinic basins places deposition of similar lithologies at 150+m, below the pycnocline. Grammer et al. (2000), however, placed depositional depth at 1-20m during a rapid transgression that caused poor circulation and hypersaline conditions. Macquaker (2011) and Schieber (1999) demonstrated that mudstones, especially source rocks, can have more dynamic depositional conditions than typically interpreted based on micro-sedimentary structures. Such micro-sedimentary structures were not observed in thin section. The lack of sedimentary structures that would indicate wave-sediment interaction suggests that deposition was below storm wave-base and in calm waters, typically greater than 25 meters depth (Immenhauser, 2009). General agreements on the BLM include that it is a laterally persistent, thin, dark, fissile deposit that lacks diverse marine benthic fossil assemblages and was deposited in anoxic conditions through sedimentation in a low-energy environment.

The Pennsylvanian deposits of the Paradox Basin are comparable to typical Pennsylvanian Kansas Cyclothems, which were also deposited during rapid transgressions and regressions during icehouse conditions (Heckel, 1986). The BLM is analogous to the core shale of Kansas-Iowa cyclothems, sharing many characteristics, including three of the same conodont faunas (Heckel, 1977; Ritter et al., 2002). The BLM harbors a diverse conodont fauna including *Idiognathodus n. sp. B*, *Idiognathodus n. sp. C*, *Gondolella bella*, *Neognathodus*, *I. Meekerensis*,



**Figure 11.** Photos and photomicrograph of Black Laminated Shale Facies (Lithofacies 1). A) Field photo of BLM showing laminations. B) Thin section of BLM showing quartz sand (white arrows) and muddy matrix. C) Hand sample showing laminations and dark color after being broken with a hammer. D) Field photo of underlying Skeletal Wacke-Packstone (SWP) in sharp contact with BLM. BLM grades into overlying Spicule Mudstone (SM). 1.5m jacob staff with 10cm black markings for scale.

and *I. Obliquus* (Ritter et al., 2002). This diverse conodont assemblage may indicate a deep-water depositional environment (Heckel and Baesemann, 1975). The high diversity of conodonts indicates a stable environment that includes offshore deep-water deposition secluded from salinity, temperature, and energy changes of nearshore, shallow waters (Buzas and Gibson, 1969; Heckel, 1977; Heckel and Baesemann, 1975; Hessler and Sanders, 1967). Core shales and the BLM share *Gondolella* and *Idiognathodus* conodonts (Heckel and Baesemann, 1975; Ritter et al., 2002). *Gondolella* and *Idiognathodus* are interpreted as deep-water, offshore organisms, with *Gondolella* representing the deepest conditions (Heckel and Baesemann, 1975; von Bitter, 1972; Boardman et al., 1995). The Black Laminated Mudstone Facies was deposited through settling of mud in suspension and detrital very fine-grained quartz in an anoxic, offshore environment that was deep enough to establish a thermocline or oxygen-minimum zone caused by decay of organics.

Similar to the core shales, the BLM exhibits non-skeletal phosphate (Heckel, 1977; Choquette, 1983; Goldhammer et al., 1991). The sparse phosphate was not concentrated around fossils. Non-skeletal phosphate occurs in waters deeper than 50m below the habitat of phosphate-digesting phytoplankton (Kazakov, 1937; Tucker, 2009). Bushinski (1964) placed non-skeletal phosphate deposition between 30m and 200m in modern analogues. Heckel (1977) determined the depositional depth of Kansas core shales to be “no deeper than 100m.” The non-phosphate concentrations in the BLM suggest its depositional depth to be 50-100m.

Another interpretation popularized by (Goldhammer et al., 1991) was that the Paradox Basin was a barred evaporite basin which was restricted from open-ocean circulation by topographic barriers (Hite, 1970), much like the Baltic Sea. Fischer (1961) argued that restriction cannot be the only mechanism for cutting off open-ocean circulation and depositing

anoxic facies. “If a sill...were effective enough to cut off bottom circulation with [the] more open sea during maximum transgression, then later shallowing should cause the sill to become increasingly effective and eventually to isolate the sea completely” (Fischer, 1961). Instead, the Lower Ismay Zone exhibits an increase in marine fauna diversity upsection. Hite (1970) suggested that brine reflux was the control for anoxic conditions on the shelf. During the highest sea level and beginning of sea-level fall, high reflux caused an anoxic brine to cover the entire basin; therefore, depositing the widespread, fossil-poor black mudstone (Hite, 1970). With continued falling sea level, reflux decreased allowing more oxygen circulation within the basin and the deposition of successive diverse marine facies (Hite, 1970). Peterson and Hite’s (1969) subsurface stratigraphic reconstructions of the Paradox Basin and Hite’s (1970) barred evaporite basin model places the BLM’s depositional depth at 30+m. The possibility that the BLM was deposited in association with brine reflux can be ruled out due to the presence of diverse conodont fauna.

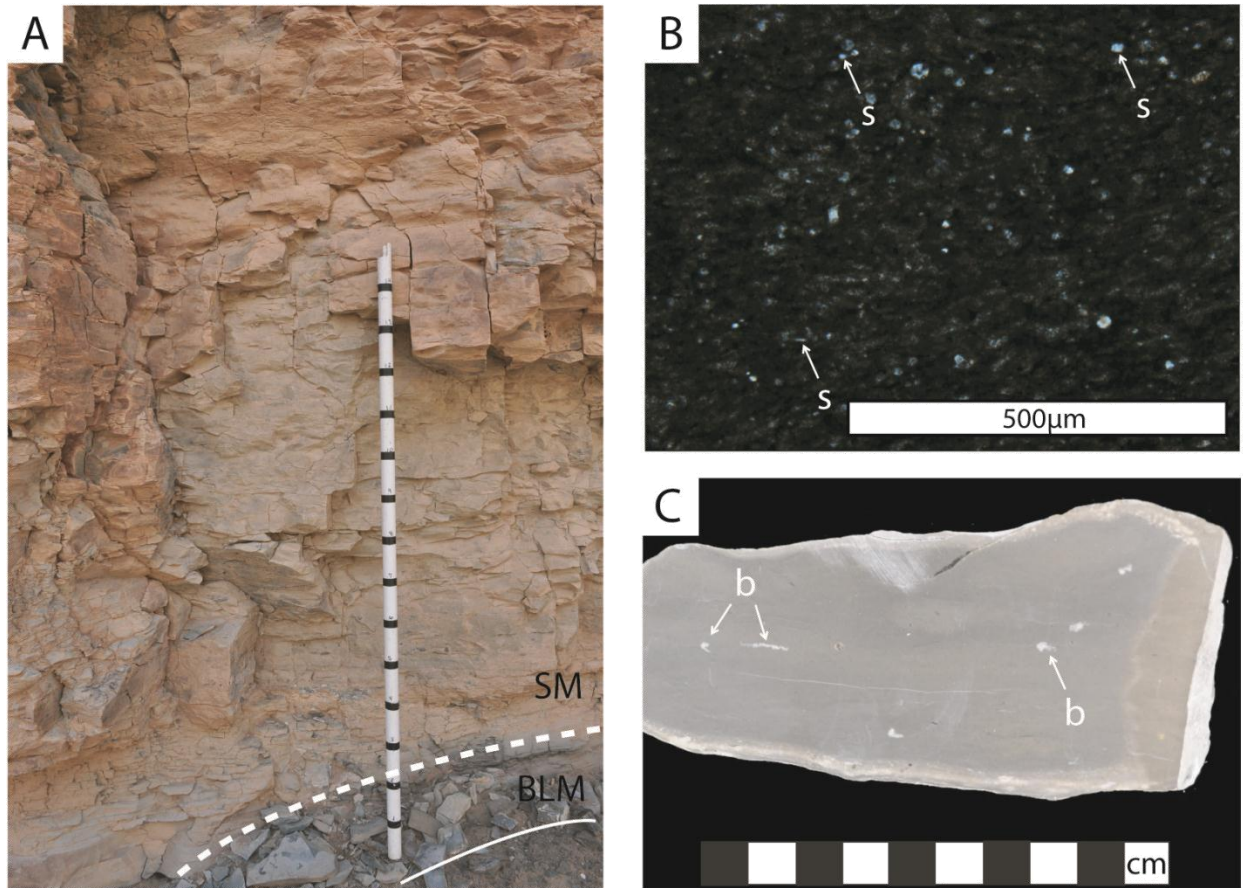
In conclusion, the Black Laminated Mudstone Facies was deposited in a low energy, anoxic environment through settling of mud, fossils, and detrital very fine-grained quartz sand below fair-weather and storm wave base. Modern analogs (Immenhauser, 2009) and examples from the rock record (Coe, 2003) place fair-weather wavebase at 5-20m deep and storm wave base up to 40m. Goldhammer et al.’s (1991) reconstructed subsurface-stratigraphic cross-sections places the water depth deeper than 30m. For the purpose of this study, the BLM was deposited at approximately 50-100m in low-energy, anoxic waters.

## **Lithofacies 2: Spicule Mudstone (SM)**

**Description** - The Spicule Mudstone is a poorly sorted lime mudstone that becomes more siliceous stratigraphically upwards and locally grades into a calcareous siltstone. It forms a recessive unit approximately 4 meters thick below the algal facies and is brownish-gray in color (weathers yellow) (Figures 12A). Petrographic analysis of sample 8FN1-1 showed (in descending volume percentages) 35% peloidal mud, 30% subangular-subrounded silt-to-very fine-grained quartz sand, 20% siliceous sponge spicules, estimated 5% clay, estimated 5% calcite pore-filling and replacement spar, estimated 1-5% marine fossils (brachiopods, crinoids, and bryozoa), and no visible porosity (Figures 12B, C). Fossils show little to moderate abrasion and are not oriented in life positions. The fossil content increases in abundance to 10% upwards. Bedding (2-15cm) is undulose to nodular with approximately 2 cm-scale vague laminations obscured by possible burrowing. Chert beds (10-20cm) are generally laterally traceable for greater than 2 river miles.

The Spicule Mudstone is in gradational contact with the underlying Black Laminated Mudstone and overlying Skeletal Wacke-Packstone (see description below).

**Interpretation** – Although not abundant, the presence of fossils and possible burrowing in the Spicule Mudstone indicates a change from anoxic conditions during underlying BLM deposition to dysaerobic conditions. The appearance of marine fossils and possible bioturbation suggests a change in available oxygen and circulation more favorable for organisms. Sponge spicules are the main fossil constituent with a low abundance and low-diversity of marine fossils. Sponges can survive in most depths and conditions, including muddy waters (Elias, 1963; West, 2011). The possible bioturbation and absence of fossilized burrowing fauna suggests soft bodied organisms were present (Grammer et al., 2000). The lack of marine fossils in the lower part of



**Figure 12.** Photos and photomicrograph of Spicule Mudstone (Lithofacies 2). A) Field photo of SM in gradational contact (dashed line) with underlying BLM. 1.5m jacob staff with 10cm markings for scale. B) Thin section of sponge spicules (s). C) Hand sample of SM showing muddy matrix with sparse marine fossils, mostly brachiopods (b).

the unit suggests low oxygen, possibly restricted, conditions (Byers, 1977; Goldhammer et al., 1991; Grammer et al., 2000). The mild abrasion of grains and the high amounts of mud suggest a low-energy depositional environment. Due to the abundance of mud, low abrasion of fossils, and the fossil assemblages, the lower SM is interpreted as being deposited in a similar depositional energy as the BLM.

An increase in abundance of marine fossils, including crinoids and brachiopods, moving stratigraphically upwards indicates that conditions continued to improve during the deposition of the Spicule Mudstone. The increase in fossil content suggests more oxygen and better circulation was introduced to the system (Goldhammer et al., 1991). Crinoids and brachiopods, similar to sponges, do not rely on sunlight and can thrive within muddy water (Elias, 1963). The fossils were moderately abraded with no indication of *in situ* position. The moderate abrasion and the organisms out of life position suggest a possible increase in energy, although no wave or current sedimentary structures were observed. Overall, these trends indicate improving conditions for marine fauna, including an increase in oxygen and circulation (Byers, 1977).

Evidence suggesting an overall shallowing can be seen within the Spicule Mudstone. The color of SM transitions from the black underlying BLM to the gray color of the SM. This may signify a decrease in organic matter caused by an overall shallowing and cutoff of organic matter being introduced into the system (Hite, 1970). The silt and very fine-grained sand of SM was likely land-sourced. The Pennsylvanian deposits to the south have been eroded away, so a direct comparison to nearby continental deposits is difficult. The silt may have had an eolian source. The percentage of detrital very fine-grained quartz sand increases upsection and could indicate shallowing events forcing progradation of nearshore sands and silt out into the basin (Van Wagoner et al., 1990). Fossil content and fossil diversity increases upsection indicating

improving conditions for marine biota. Moderate abrasion and non-life position of fossils suggest an increase in energy, possibly caused by shallowing.

Using solely the gradational boundaries as depth constraints, the Spicule Mudstone would be shallower than BLM and deeper than the overlying Crinoid Packstone. The base of the SM would be shallower than 50-100m, and the top of the unit would be deeper than 15-20m, based on evidence for water depth interpretations of the Crinoid Packstone discussed below.

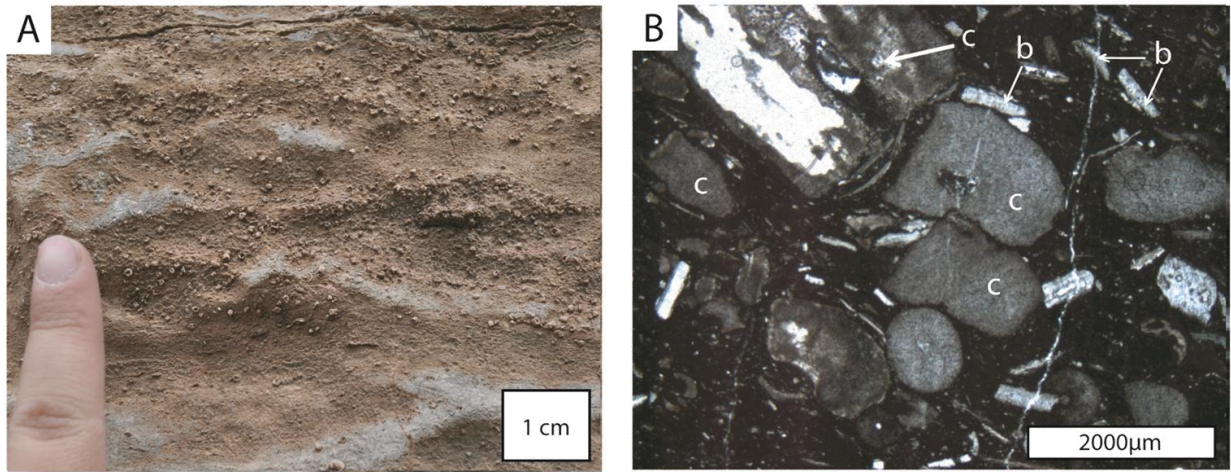
Goldhammer et al.'s (1991) paleoreconstructions from stratigraphic cross-sections (Choquette and Traut, 1963; Herrod and Gardner, 1988; Herrod et al., 1985) and his utilization of Hite's (1970) barred basin model places the SM between 15m and 30m. With the BLM interpretation developed in this study, the Spicule Mudstone is interpreted to be deposited between 50-100m (base) and 15-20m (top).

### **Lithofacies 3: Crinoid Packstone (CP)**

**Description** – The Crinoid Packstone is a yellow-brown packstone, poorly to moderately sorted, and approximately 3m thick (Figure 13A). CP contains 30% normal marine fossils (bryozoa, brachiopods, brachiopod spines, ostracods, and sponge spicules), 20-30% crinoids, 15% peloidal lime mud, 5-10% pore-filling and neomorphic spar, sparse pellets, and 0-1% visible porosity. The fossils are moderately fragmented and abraded (Figure 13B). Mud content increases to 40-50% and local phylloid algae appears (~5%) upsection. The unit is highly stylolitized near the base of the facies, indicating compaction occurred. Bioturbation is observed throughout the facies.

The Crinoid Packstone lies stratigraphically above the Spicule Mudstone in gradational contact and below the Algal Bafflestone (described below) in sharp contact.





**Figure 13.** Photo and photomicrograph of Crinoid Packstone (Lithofacies 3). A) Field photo of CP showing abundant crinoids. B) Thin section of crinoid (c) and brachiopod (b) fragments near stylolite.

**Interpretation** – The Crinoid Packstone shows a significant increase in normal marine fossil abundance and diversity as compared to the underlying SM, suggesting continued improvement of conditions for marine biota. This is further supported by the high abundance of bioturbation throughout the unit. Oxygen abundance and circulation improved from dysaerobic to aerobic conditions (Choquette and Traut, 1963; Goldhammer et al., 1991; Grammer et al., 2000). The high amount of mud and lack of current-generated sedimentary structures suggests a low-energy depositional environment.

The Crinoid Packstone represents a normal-marine environment with abundant organisms. Goldhammer et al.'s (1991) paleoreconstructions from stratigraphic cross-sections estimated the depositional depth between 5 and 15m. Grammer et al. (2000) placed the depositional depth between 5 and 10m. The amount of mud and the lack of sedimentary structures that indicate wave-sediment interaction suggest an environment near the edge of fair-weather wave base, deeper than Goldhammer et al. (1991) and Grammer et al. (2000) interpretations. Analogs place the fair-weather wave base at 5-20m deep (Immenhauser, 2009; Coe, 2003). Thus, the depositional depth for CP is interpreted at approximately 15-20m.

#### **Lithofacies 4: Algal Bafflestone (AB)**

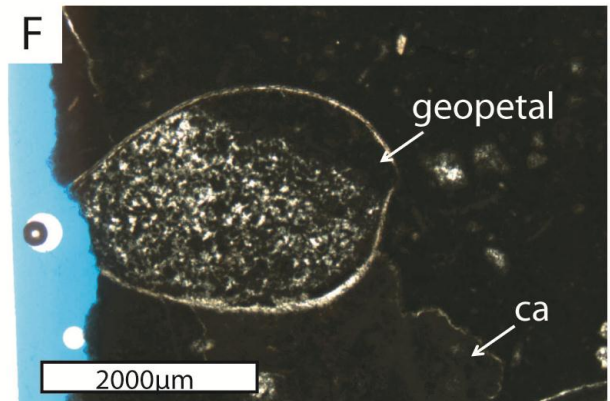
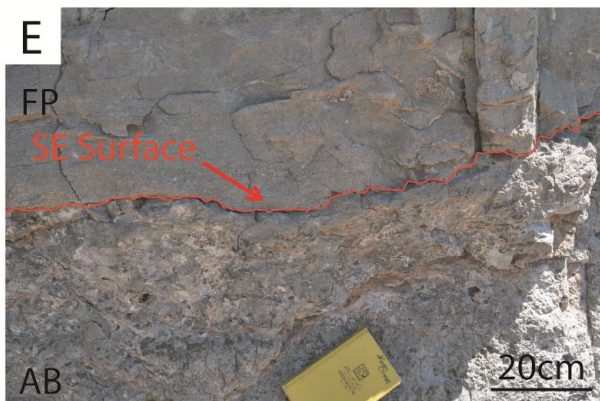
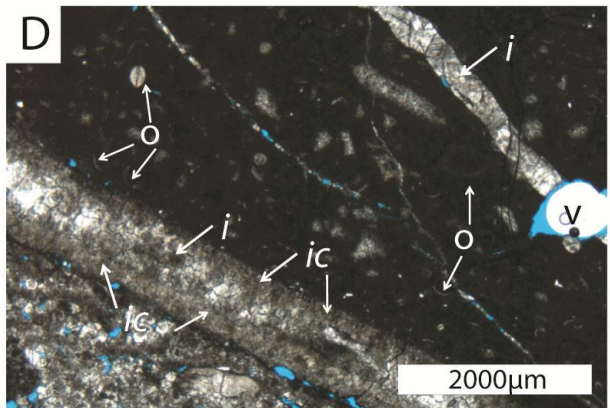
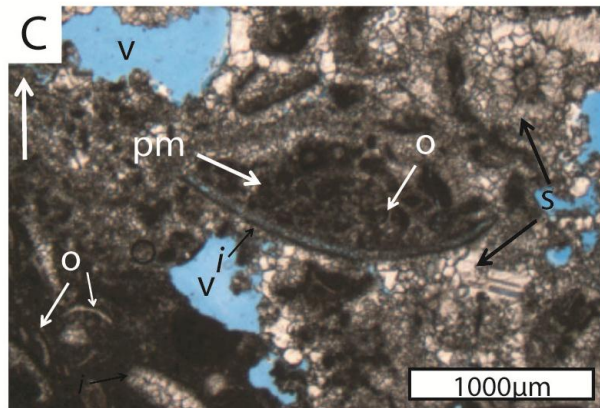
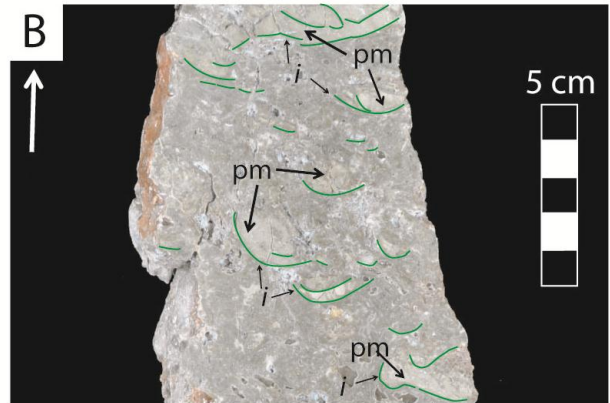
**Description** – The Algal Bafflestone is brownish gray, poorly sorted bafflestone dominated by the phylloid algae *Ivanovia*. It ranges from approximately 10cm-3m in thickness. AB and Algal Packstone (AP, see below) make up algal facies. AB appears massive due to weathering and is difficult to distinguish from AP in the field (Figures 14A). Distinguishing between AB and AP is best determined using polished slabs and thin sections, therefore, the distribution patterns of AB and AP are based on lab analysis rather than field observations (Figure 14B). AB consists of 15-30% peloidal mud, 10-30% whole phylloid algae (*Ivanovia*), 1-5% hard peloids, sparse to low

abundance of normal marine fossils (fusulinids, biserial foraminifera, encrusting foraminifera, bryozoa, brachiopods, crinoids, gastropods, and ostracods), 25-40% pore-filling dentic and equant calcite cements, 1-5% chalcedony, and 5-10% visible porosity (post-depositional vugs, with some shelter, fracture, moldic, and breccia porosity) (Figure 14C, D). AB's distinguishable characteristics are its whole phylloid-algae that formed cup-shaped plates, oriented depositionally up, that trapped sediment (Figure 14B). Autobrecciation occurred where the fragile algal plates buckled under the weight of the overlying sediment (Figure 14B, C, D). Calcite cement reduces fracture, breccia, shelter, moldic, and vuggy porosity throughout the facies. Geopetal fabrics are observed in the depositionally up position (Figure 14B, C).

The Algal Bafflestone facies predominates in the algal mounds. It forms medium, laterally continuous beds that thicken and thin laterally, ranging from approximately 10cm to 3m in thickness, and are in sharp contact with other beds. AB beds interfinger laterally with irregular patches of AP concentrated on or near topographic highs. See the Sequence Stratigraphy section for the description and interpretation of algal bed geometries.

A traceable, irregular surface tops algal facies AB and AP, and truncates algal beds within the low topography areas of the algal facies (Figure 14E). Local relief of the surface on the mounds measures up to 5.7m. Fissures and autobrecciation are observed along the surface and underlying algal facies. Overlying facies fill in fissures and vugs created by the surface. Directly below the surface, caliche nodules, red staining, and overturned geopetal fabrics are observed in a calcrete, approximately 5-27cm thick (Figure 14F).

**Interpretation** – AB has similar textures to the Type B Algal Facies of Choquette and Traut (1963) and Grammer's (2000) Incipient Mound Facies. AB's "cup-like" plates of *Ivanovia*



**Figure 14.** Photos and photomicrographs of Algal Bafflestone (Lithofacies 4). A) Hand sample of AB showing the weathered surface and the difficulty in seeing fabrics. Note the visible vuggy porosity. B) Polished slab of AB. The *Ivanovia* “cup-shaped” algal plates (green lines, labeled *i*) baffled and trapped peloidal mud and skeletal fragments (pm). The upper left white arrow designates the depositional up direction. C) Thin section showing an *Ivanovia* (*i*) leaf that baffled peloidal mud (pm) and ostracods (*o*). The vuggy porosity (*v*) is partially filled with spar (*s*). The upper left white arrow designates the depositional up direction. D) Thin section of *Ivanovia* (*i*) that baffled peloidal mud and ostracods (*o*). Note the cortex (*ic*) visible on both edges of the *Ivanovia* leaf. E) Field photo of the subaerial exposure surface (red) above the AB and below the Fusulinid Packstone. F) Thin section of AB along the subaerial exposure surface. The ostracod has an overturned geopetal fabric indicating redistribution from original orientation (present-day up towards the top of the photograph). Alteration and possible caliche pisoids are visible.

baffled currents and collected mud and grainy fossils. The fragile algal plates are mostly intact and, therefore, are commonly interpreted to be deposited in living position in a low-energy environment, most likely below fair-weather wave base (Goldhammer et al., 1991; Roylance, 1990). Roylance (1990) hypothesized that *Ivanovia* outpaced other normal marine organisms creating an overall decrease in diverse fauna in the algal facies compared to other facies. The plates commonly collapsed and created brecciated textures. Heckel and Cocke (1969) provided an alternative to typical interpretations of AB depositional environments when describing algal mound development in Kansas. Oscillatory currents of seawater across the stratigraphically lowermost, or the oldest, algal beds are responsible for the undulose geometries of algal facies (Heckel and Cocke, 1969). Algae continued to build due to the “feedback” effect described by Harbaugh (1964) where algae kept pace with water depths and continued to exaggerate the initial undulose geometries. Pray and Wray (1968) described *Ivanovia* as a photosynthetic organism analogous to the green algae *Halimeda*. Modern-day *Halimeda* habitat ranges from the shallower depths to 150m (Multer and Clavijo, 2004); therefore, *Ivanovia* was also likely living shallower than 150m.

Overall observations of the facies show a decrease in mud and increase in broken and abraded algal plates towards the tops of individual beds, suggesting that the mounds grew vertically into higher energy, or relatively shallow waters (see Algal Packstone description below). Syn- and post-depositional differential compaction may also have caused the algal beds to appear thinner and have lower relief compared to when they were originally deposited.

Goldhammer et al.'s (1991) paleoreconstructions from stratigraphic sections places the depositional environment of all algal facies at 5 to 15m depth. Algae acted as a baffling agent that baffled currents transporting mud and skeletal grains, therefore, the depositional

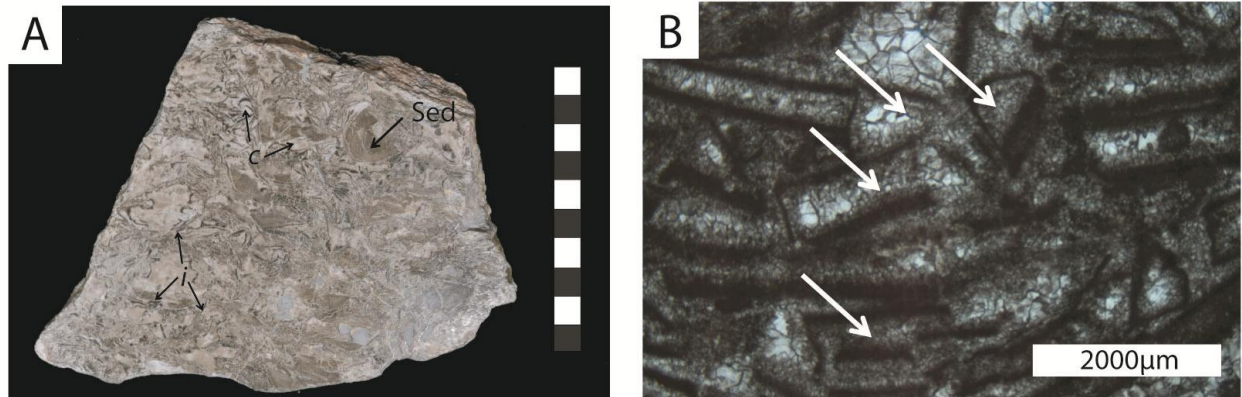
environment was within fair-weather wave base of 5-20m (Immenhauser, 2009; Coe, 2003). The amount of mud suggests that the environment was on the deeper end of the fair-weather wave base range. Thus, the Algal Bafflestone depositional environment is interpreted as between 10m and 15m water depth.

The traceable fissured surface described above is a subaerial exposure surface. The truncation of algal beds and local relief of up to 5.7m is evidence for erosion. Fissures filled with Fusulinid Packstone (described below) suggest that the timing of the subaerial exposure occurred after the deposition of the algal facies, but before the overlying FP. The FP filled in the fissures during the next transgression.

The caliche nodules, soil pisoids, and iron oxide found underlying the surface suggest chemical weathering and the beginning of soil development (Retallack, 2001). Overturned geopetal fabrics, observed directly under the surface, suggest that organisms inhabited the subaerially exposed algal facies and pedoturbation occurred.

#### **Lithofacies 5: Algal Packstone (AP)**

**Description** – The Algal Packstone is a brownish gray, moderately- to well-sorted packstone with local grainstone textures. It is difficult to distinguish from the Algal Bafflestone in the field due to its massive appearance caused by weathering (Figure 15A). AP consists of 25-40% highly fragmented phylloid algae (*Ivanovia*), 20-50% cement, 5-40% peloidal mud, sparse to low abundance of normal marine fossils (fusulinids, biserial foraminifera, encrusting foraminifera, pellets, bryozoa, brachiopods, crinoids, gastropods, and ostracods), and 5-40% visual porosity (primarily vugs, as well as moldic, fracture, and intercrystalline porosity). Fossils show fragmentation, moderate abrasion, and good sorting (Figures 15B). The lack of laminations or internal bedding suggests that bioturbation took place during deposition. Cements include pore-



**Figure 15.** Photos and photomicrographs of Algal Packstone (Lithofacies 5). A) Polished slab showing broken *Ivanovia* algal plates (*i*), sediment fills (Sed), and cement (*c*). B) Thin section of broken and sorted algal plates (white arrows).



filling calcite (dentic and equant) and altered botryoidal aragonite (Figures 15B). Spar reduces vugular porosity.

AP observed at ANB and 8-Foot localities accumulated in irregular patches less than 1m thick with approximate lateral extent of 1-2m that interfinger the Algal Bafflestone. AP is typically associated with the high topographic areas of the beds. The algal facies of the Honaker Trail locality, the most updip location of the study area, is dominantly AP.

**Interpretation** – AP and AB are commonly described as one facies in earlier literature, most likely due to their similar fossil constituents and difficulty in distinguishing them in the field (Choquette and Traut, 1963; Goldhammer et al., 1991; Grammer et al., 2000; Lehrmann and Goldhammer, 1999). AP is observed higher than AB, typically associated with topographic highs. AP and AB are interpreted as being deposited coevally because they interfinger laterally. In comparison, AP exhibits increased fragmentation, increased sorting, decrease in mud content, and higher position of AP suggesting the facies formed in shallower, higher energy waters than AB. Lack of laminations or internal bedding suggests that bioturbation may have taken place during deposition. *Ivanovia*'s thin, brittle structure made it susceptible to breakage and transport (Pray and Wray, 1963; Roylance, 1990). Ginsburg and James (1976) and Roylance (1990) suggested that pore space between the *Ivanovia* chips that was not filled with mud was quickly cemented with syndepositional aragonite botryoids.

The regional distribution of facies shows the highest abundance of AP at the Honaker Trail locality (HTF), where AP is observed throughout the algal unit. The location of the HTF locality is up depositional dip from the other sections according to the basin geometry. These observations further support that AP was created in a shallower environment that experienced higher energy conditions than the depositional environment of AB.

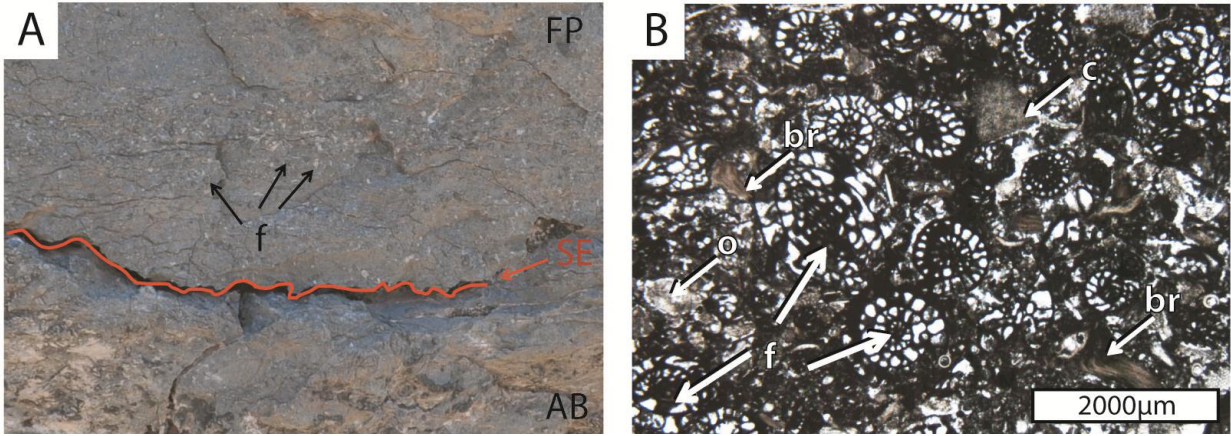
Goldhammer et al.'s (1991) paleoreconstructions places algal facies between 5 and 15m water depth. According to the observations, the AP was deposited updip in shallow water or on the highs that grew into shallower water in comparison to the AB, therefore AP is interpreted to have been deposited between 5 and 10m depth.

### **Lithofacies 6: Fusulinid Packstone (FP)**

**Description** – The Fusulinid Packstone is a gray, well-sorted packstone that overlies the subaerial exposure surface on top of AB facies. FP drapes the undulose subaerial exposure surface and fills in constructional (mound) and erosional relief on the underlying algal facies (Figure 16A). FP ranges from 5cm-1.5m thick and pinches out near 8FR locality. It consists of 45-60% fusulinids, 10-20% normal marine fossils (bryozoa, foraminifera, brachiopods, ostracods, gastropods, and crinoids), 10-20% peloidal mud, 5% pore-filling and replacement calcite spar, and no visual porosity (Figure 16B). The foraminifera show little or no abrasion. The non-foraminifera fossils are moderately to highly abraded. No crossbedding or evidence of bioturbation was observed.

The FP is thicker in the topographically low areas (fills) and thins on the higher topographic areas (drapes). It is in sharp contact with the overlying Skeletal Wacke-Packstone (see below) and underlying exposure surface.

**Interpretation** - Fusulinids make up 45-60% of FP, making it the dominant organism of the facies. Fusulinids are benthic organisms (Flügel, 2010). The fusulinids show little-to-no abrasion, so it is likely that they lived in the setting in which they are now found, and were not transported in. Fusulinid accumulations have also been reported to form down-slope from algal bioherm deposition (Flügel, 2010). This can be seen in the Sacramento Mountains and Kansas cyclothems through lateral tracing (Boardman et al., 1995; Fly, 1986). Fusulinids occupy open-

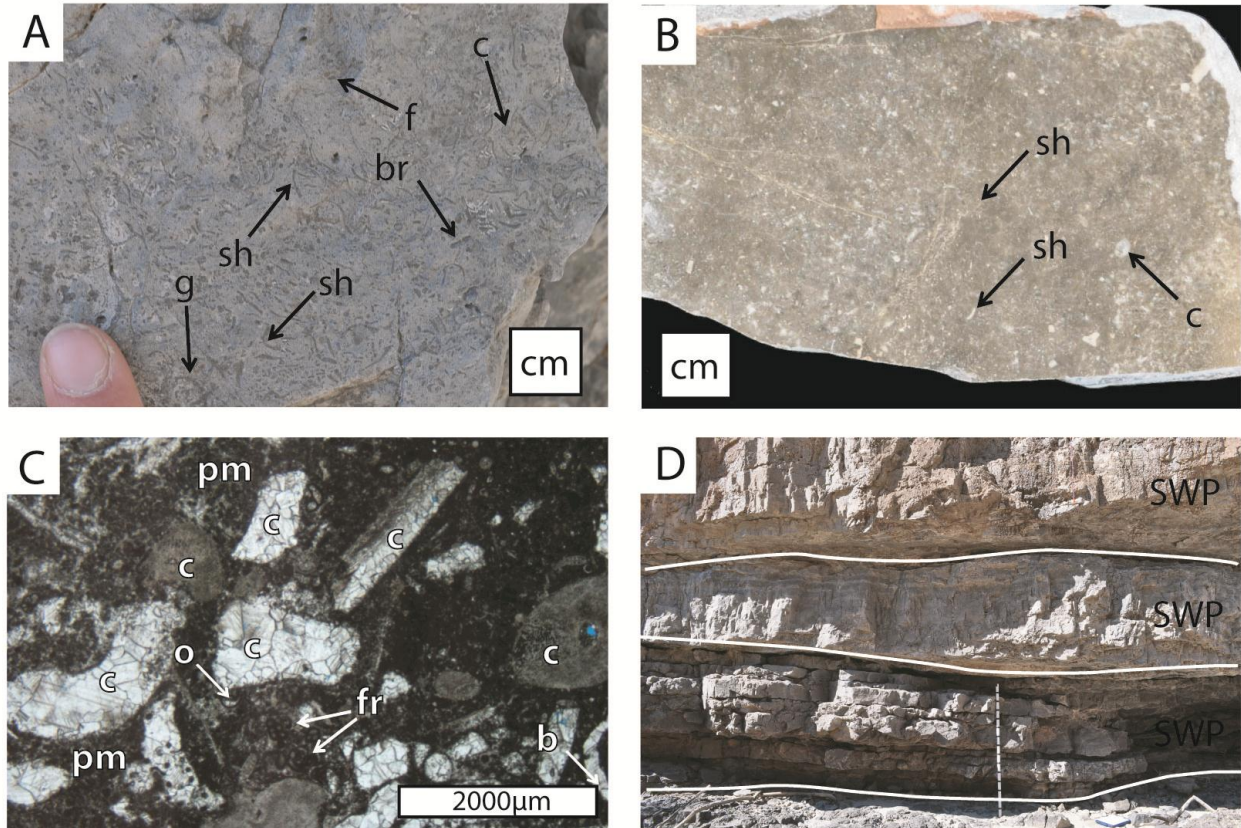


**Figure 16.** Photo and photomicrograph of Fusulinid Packstone (Lithofacies 6). A) Field photo of FP above subaerial exposure surface (SE) traced in red. Fusulinids (f) marked with black arrows. B) Thin section of FP showing high abundance of fusulinids (f). Also in thin section are ostracods (o), crinoid fragments (c), and bryozoa (br).

shelf, normal-marine environments with normal oxygen and salinity (Flügel, 2010; Boardman et al. 1995). The presence of benthic forams places the depositional environment shallower than 50m (Flügel, 2010). The low abundance of other marine fossils suggests that the environment is deeper than most organisms' habitats. Apart from the fusulinids, other fossils are moderately to highly abraded, suggesting that they were transported from upslope. No crossbeds or other physical sedimentary structures were observed, indicating that FP was deposited below fair-weather wave base of 5-20m depth (Immenhauser, 2009; Coe, 2003). The observations of FP suggest that it was deposited at a depth that was too deep for most organisms, but shallow enough for fusulinids to thrive. FP's depositional environment is thus interpreted to be 20-25m.

#### **Lithofacies 7: Skeletal Wacke-Packstone (SWP)**

**Description** – The Skeletal Wacke-Packstone is a poorly sorted (excluding matrix and cement) wackestone and packstone that varies in fossil and mud abundance locally (Figure 17A, B). It is gray to dark gray in color, burrow mottled, and is found draping and onlapping underlying facies. SWP is the dominant facies stratigraphically above the algal facies and beds range in thickness from 10cm-2m in thickness (Figure 17D). SWP consists of 20-70% highly diverse normal marine fauna (crinoids, bryozoa, brachiopods, foraminifera, ostracods, gastropods, rugose coral fragments, *Chaetetes* sponge fragments, and local phylloid algae), sparse pellets, 15-55% peloidal mud, 5-25% pore-filling and replacement spar, 1-6% chalcedony, 1-5% replacement chert, and 0-5% visual vuggy porosity (Figure 17C). Rare to abundant bioturbation is observed throughout the facies. The SWP shows 0-5% porosity, mostly as vugs. Fossils are moderately to highly abraded and commonly fragmented. Syolites and chert lenses are observed throughout the facies. Chalcedony and replacement quartz is more abundant upsection.



**Figure 17.** Photos and photomicrograph of Skeletal Wacke-Packstone (Lithofacies 7). A) Field photo of weathered SWP surface showing shell fragments (sh), crinoids (c), bryozoa (br), fusulinids (f), and a gastropod (g). B) A polished slab showing the abundance of fossils within SWP. The fossils are difficult to identify, but brachiopod shells (sh) and crinoids (c) are marked with black arrows. C) Thin section of SWP showing crinoid fragments (c), brachiopod shell (b), foraminifera (fr) surrounded by peloidal mud (pm). D) SWP makes up various beds with a range of thickness. At the Narrows (pictured), the lower beds range from 10cm-20cm thick, the middle bed is 1m thick, and the uppermost beds are 2m thick. The 1.5m jacob staff with 10cm black markings for scale.

SWP overlies the algal facies and FP, filling in relief and overlapping onto underlying mounds. SWP is in sharp contact with other facies and SWP beds.

**Interpretation** – SWP contains a highly diverse normal-marine fauna. These fossils and observed bioturbation suggest a normal marine depositional environment that was well circulated and oxygen-rich, ideal for organisms to thrive (Byers, 1977; Pray and Wray, 1963). Grammer et al. (2000) interpreted SWP as “well-washed” shoals deposited at less than 5m water depth. No current-indicating sedimentary structures were observed to suggest such a shallow environment, although the amount of burrowing could have obscured any such structures. The fossils are moderately to highly abraded indicating that the allochems were transported in a high-energy environment. The high abundance of mud, on the other hand, suggests that SWP was not “well washed” and that SWP was deposited in a low-energy environment. Goldhammer et al. (1991) placed the SWP depositional environment at 0-5m water depth, at subtidal depths near shoal environments, but not shoals themselves. Pray and Wray (1963) interpreted this facies at normal-marine depths, while Boardman et al. (1995) placed SWP fauna in open marine settings. The fossil constituents do not place depth constraints on the depositional environment with the exception of being dominantly in the photic zone.

The lack of current structures and high mud content suggests that the SWP was deposited below wavebase; however, the high degree of abrasion of skeletal grains indicates a high energy environment. This places the depositional environment deeper than subtidal depths at approximately 5-10m water depth.

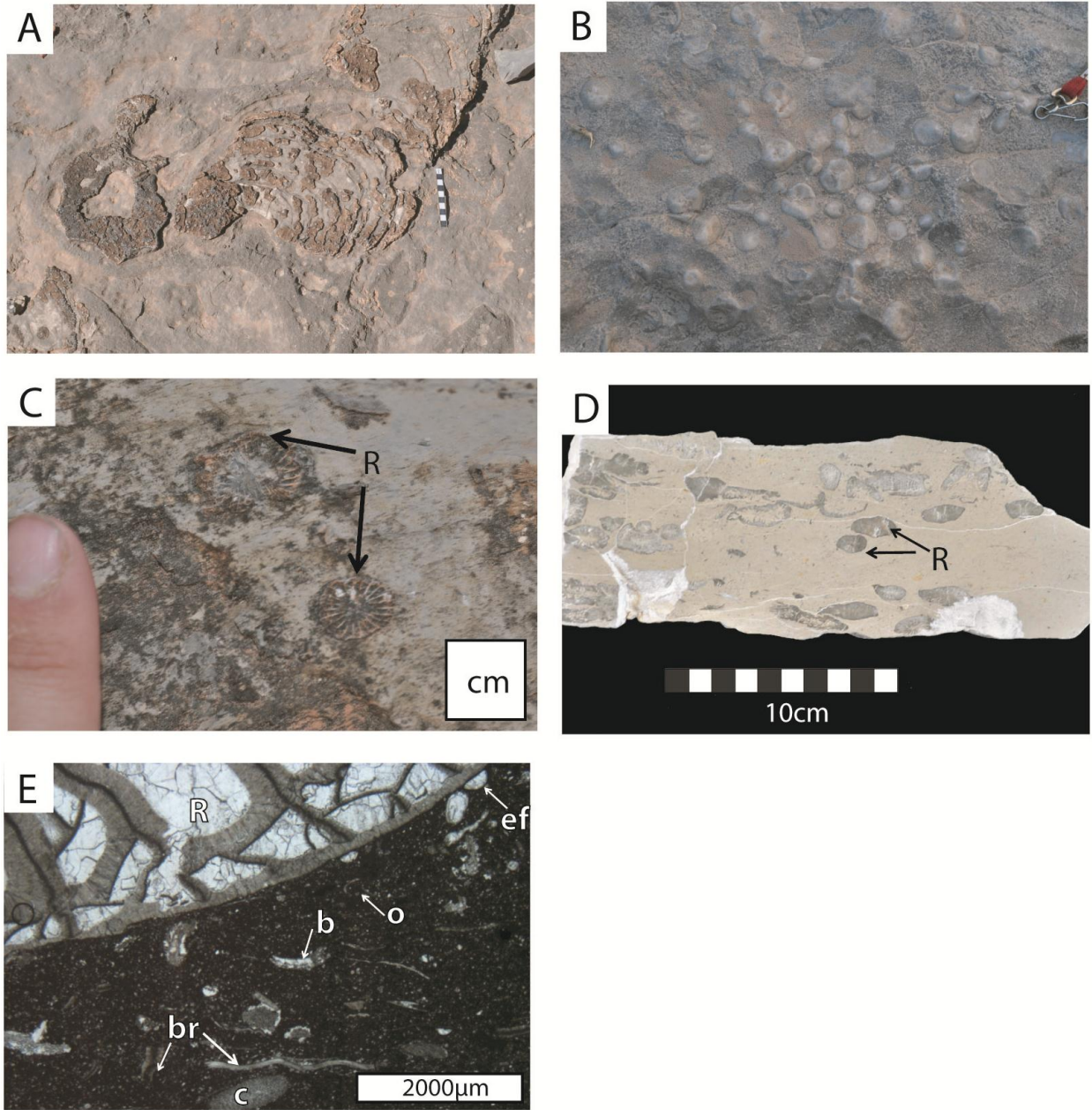
#### **Sublithofacies 7a: Skeletal Wacke-Packstone - *Chaetetes* (SWP-C)**

**Description** – The Skeletal Wacke-Packstone – *Chaetetes* is a poorly sorted (excluding matrix and cement) wacke-packstone that approximately ranges from 20cm-1m thick. It is dark gray in

color and is found above the Quartz Sandstone (see description below). It consists of 50-80% normal-marine fauna (crinoids, bryozoa, brachiopods, brachiopod spines, fusulinids, endothyrids, encrusting foraminifera, uniserial foraminifera, biserial foraminifera (possibly *Deckerella*), ostracods, gastropods, whole rugose corals, whole *Chaetetes* sponge heads, and local phylloid algae (*Ivanovia*)), sparse hard peloids, 15-30% peloidal mud, 5-40% pore-filling and replacement calcite spar, 1-5% chalcedony cement, 1-5% chert, and no visible porosity, preserved mostly as vugs (Figure 18A-E). Whole *Chaetetes* sponge heads (10-30cm long axis) are found as solitary sponges or in groups consisting of up to 6 sponges (Figure 18A). At the ANB locality, the sponge heads are observed in two heads or clusters of heads per square meter density. Rugose corals are also observed by themselves or in groups (Figure 18B, C, and D). The rugose corals are approximately 2cm in diameter (calyx). The density or distribution of the rugose corals was measured at 0 to 53 rugose corals per square meter. Large, nearly intact crinoid stems, or stalks, are observed in the SWP-C. The columnals measure up to 2cm in diameter and the stalks measure up to 25cm long. Post-depositional chert nodules (~10cm long axis) and stylolites are observed throughout the facies. SWP-C is highly bioturbated; therefore, no apparent crossbedding was seen.

SWP-C is in sharp contact with underlying Quartz Sandstone (QS) and overlying SWP. SWP-C fills in the lows and onlaps onto underlying topography.

**Interpretation** – The Skeletal Wacke-Packstone - *Chaetetes* consists of the same marine fossils and textural characteristics as the Skeletal Wacke-Packstone, with the exception of large *Chaetetes* sponge heads, crinoids, and rugose corals. The *Chaetetes* sponges and rugose corals are found in groups interpreted as small patch reefs (Grammer et al., 2000). The classification of *Chaetetes* has been debated over the years where it has been deemed a coral, demosponge, and



**Figure 18.** Photos and photomicrograph of Skeletal Wacke-Packstone – *Chaetetes* (Sublithofacies 7a). A) Field photo of SWP-C showing *Chaetetes* sponge. 10cm scale in picture. B) Field photo of SWP-C showing groups of rugose corals. Radiating septae visible in each coral. C) Field photo of rugose corals. D) Polished slab of rugose corals pictured in photo C. E) Thin section photomicrograph of rugose coral (R) and surrounding matrix. Matrix includes bryozoa (br), crinoids (c), brachiopod fragments (b), ostracods (o), encrusting foraminifera (ef), and peloidal mud.



now a sponge (Connolly et al., 1989; West, 2011). The depths at which *Chaetetes* lived have also been debated. At the time of Grammer et al. (2000), *Chaetetes* was thought to inhabit shallow water, which constrained the depth interpretation to less than 5m (Connolly et al., 1989). West (2011) discovered that *Chaetetes* can be found at various depths from shallow to deep water, therefore, *Chaetetes* is no longer a depth constraining organism. Rugose corals of the Carboniferous, on the other hand, lived in shallow and intermediate environments (Hill, 1981).

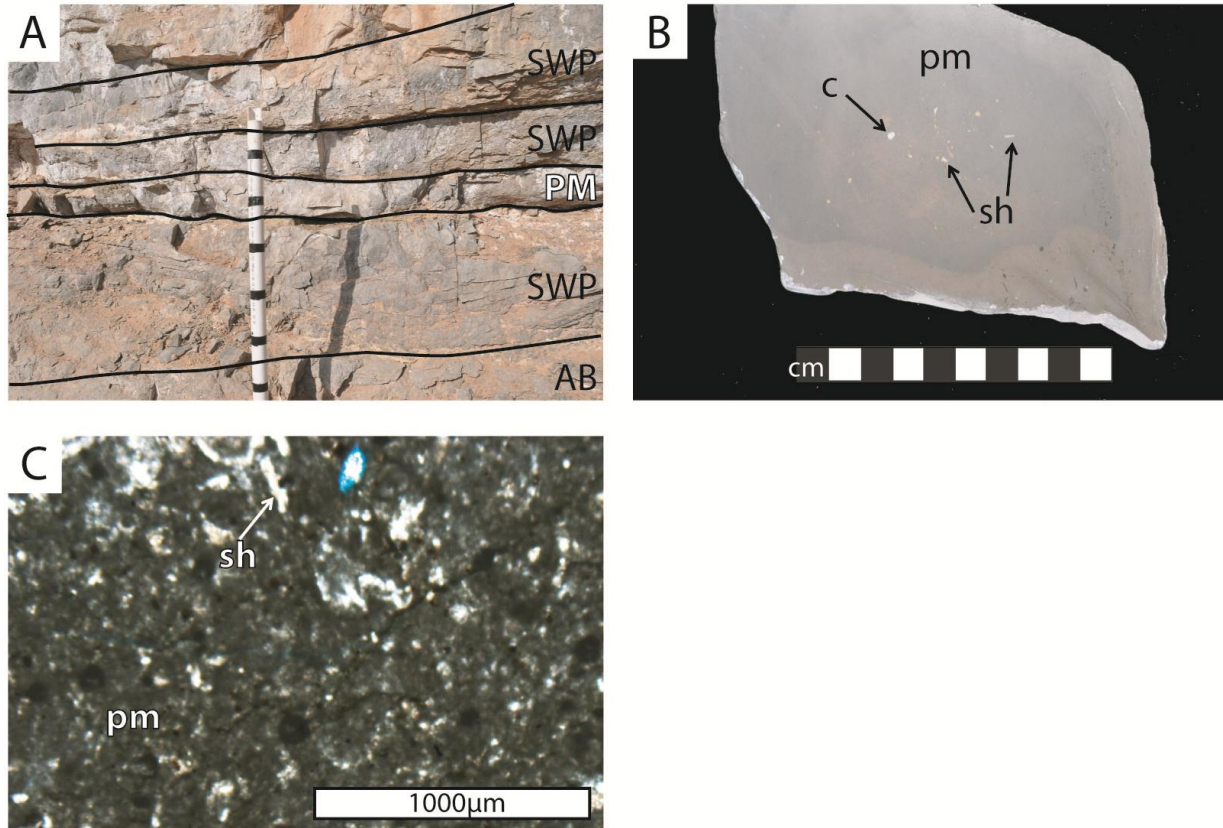
Fragmented *Chaetetes* and rugose corals present in SWP were transported to the environment through wave action. Large *Chaetetes* heads and groups of rugose corals are whole and in upright positions in SWP-C as compared to SWP. Therefore, the depositional environment is interpreted as slightly deeper than that of the SWP at approximately 10-15m depth.

#### **Lithofacies 8: Peloidal Mudstone (PM)**

**Description** – The Peloidal Mudstone is a poorly sorted mudstone that ranges 1-50cm thick and is dark gray-brown in color, but weathers gray (Figure 19A). PM consists of 80-90% soft peloids, 5% marine fossils (brachiopods, foraminifera, gastropods, and crinoids), 5% mud (indiscernible compacted peloids), 2% interparticle pore-filling calcite cement, and up to 5% visible porosity (Figure 19B, C). Peloids do not show evidence of transport; therefore, the peloids are classified as soft peloids per criteria established in the Methodology section, therefore, PM is a mudstone. Poorly sorted fossils are fragmented and moderately abraded. Mottling as evidence for bioturbation was seen throughout.

PM beds are in sharp contact with bounding beds of SWP. Beds are discontinuous and onlap onto highs of the underlying topography.

**Interpretation** – The Peloidal Mudstone contains dominantly soft peloids and unabraded, poorly



**Figure 19.** Photos and photomicrograph of Peloidal Mudstone (Lithofacies 8). A) Field photo of PM at 8FN1. Staff marked at 10cm intervals for scale. B) Polished slab of PM showing low abundance of marine fossils (crinoid (c) and shell fragments (sh)) within the peloidal mud matrix (pm). C) Thin section of PM showing high abundance of peloids. The peloids are classified as soft peloids; therefore, PM is a mudstone.

sorted marine fossils. The state of the marine fossils and the high abundance of peloids suggests a low-energy depositional environment. PM is observed in stratigraphic low areas and onlaps onto adjacent paleotopographic high areas, typically overlying SWP. Similar deposits are found in modern day Cat Cay and Joulters Cays, Bahamas (Shinn et al., 1993). Thin, 5cm beds of laminated sand-sized peloids were deposited after a hurricane (Shinn et al., 1993). Upon inspection weeks later, the mudstone was preferentially preserved in low-lying areas (Shinn et al., 1993). Burrowing organisms churned up the mud layer and erased evidence of laminations (Shinn et al., 1993). Shinn et al.'s (1993) peloidal mud deposit descriptions are a possible analogy to the PM. Shinn et al.'s (1993) peloid deposits were found in association with an ooid shoal environment in tidal channels of approximately 4m depth. The depositional environment for PM, on the other hand, lacked ooid shoals and channels. PM could have been deposited as a result of a storm, then bioturbated, and eroded leaving muddy, peloidal-rich mudstone in the troughs created by underlying topography, similar to Shinn et al. (1993). PM could have also resulted from a protected environment similar to SWP that experienced low energy and a high abundance of organisms to create a plethora of peloids. PM is interpreted to be deposited at 4-10m water depth.

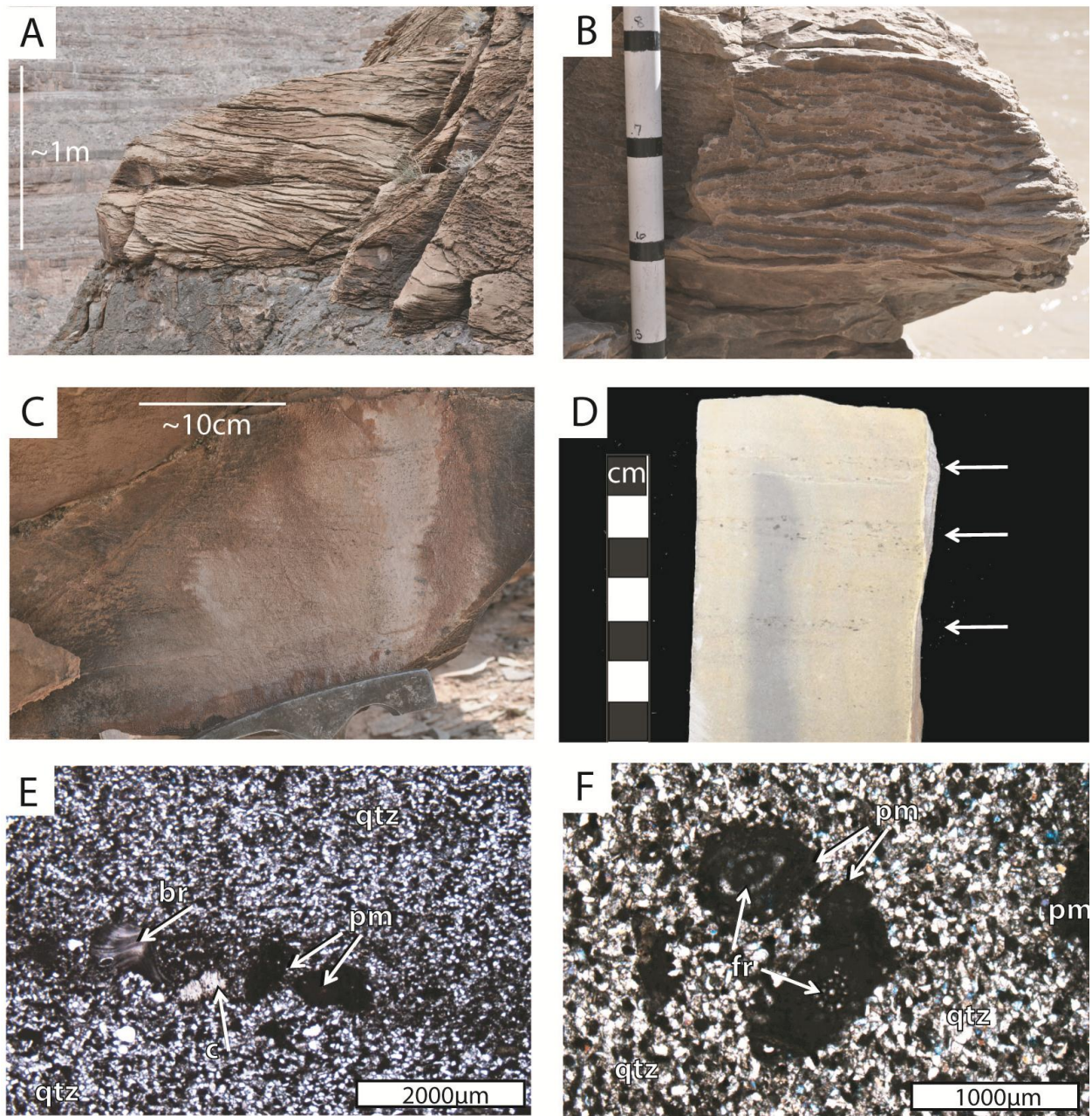
### **Lithofacies 9: Quartz Sandstone (QS)**

**Description** – The Quartz Sandstone is moderately to well-sorted siltstone-sandstone that ranges from 1.3-3.5m in thickness. It is yellow to brown in color and is easily distinguished by its well-developed low-angle trough crossbeds approximately 8cm thick at RCB and HTF localities (Figure 20A and B). Possible hummocky cross-stratification or planar bedding is observed at the base of the facies at the 8FDN locality (Figure 20C). QS forms a discontinuous wedge-shaped, bed observed from HTF to RCB localities. It consists of <70% sand -sized quartz, <5% diverse

marine fauna (brachiopods, foraminifera, crinoids, and ostracods), 1% feldspars, sparse pyrite, and 5% visible interparticle porosity (Figures 20D, E, and F). The fossils are concentrated in peloidal mud matrix on crossbed surfaces and are the same as those observed in SWP. Quartz grains are subrounded-rounded and fossils are highly abraded and fragmented. QS is in sharp contact with the underlying SWP and overlying SWP-C beds.

**Interpretation** – In previous literature, the QS has been interpreted as a complex of depositional environments (Grammer et al., 2002; Goldhammer et al., 1991). QS is similar to Goldhammer et al.'s QSF1 Facies and Grammer's (2000) Tidal Quartz Sandstone. Grammer et al. (2002) and Goldhammer et al. (1991) interpreted the well-sorted, quartz grains as eolian deposits that were carried by wind out into an exposed basin area during a sea-level lowstand. The QS was then reworked during a subsequent transgression and marine fossils were incorporated into the facies (Grammer et al., 2002; Goldhammer et al., 1991). Similar marine reworking of shallow-marine sands is observed in the sandstones of the upper Yates and lower Tansill formations of the Guadalupe Mountains (Mutti and Simo, 1993; Neese and Schwartz, 1977; Pray, 1977; Sarg, 1977). The low-angle trough crossbeds show alternating direction suggesting a tidal environment of a few meters depth (Goldhammer et al., 1991; Grammer et al., 2002).

Grammer et al. (2002) and Goldhammer et al. (1991) provided a depositional model for QS. The model requires terrigenous sand to be blown into the basin during a lowstand (Grammer et al., 2002; Goldhammer et al., 1991). With this model, an exposure surface resulting from the drop in sea level should sit below QS. No such surface was observed in the field. Also, sand-sized grains are primarily transported by saltation and are too large for wind to carry in suspension for long distances (Bagnold, 1941; Pye and Tsoar, 1987).

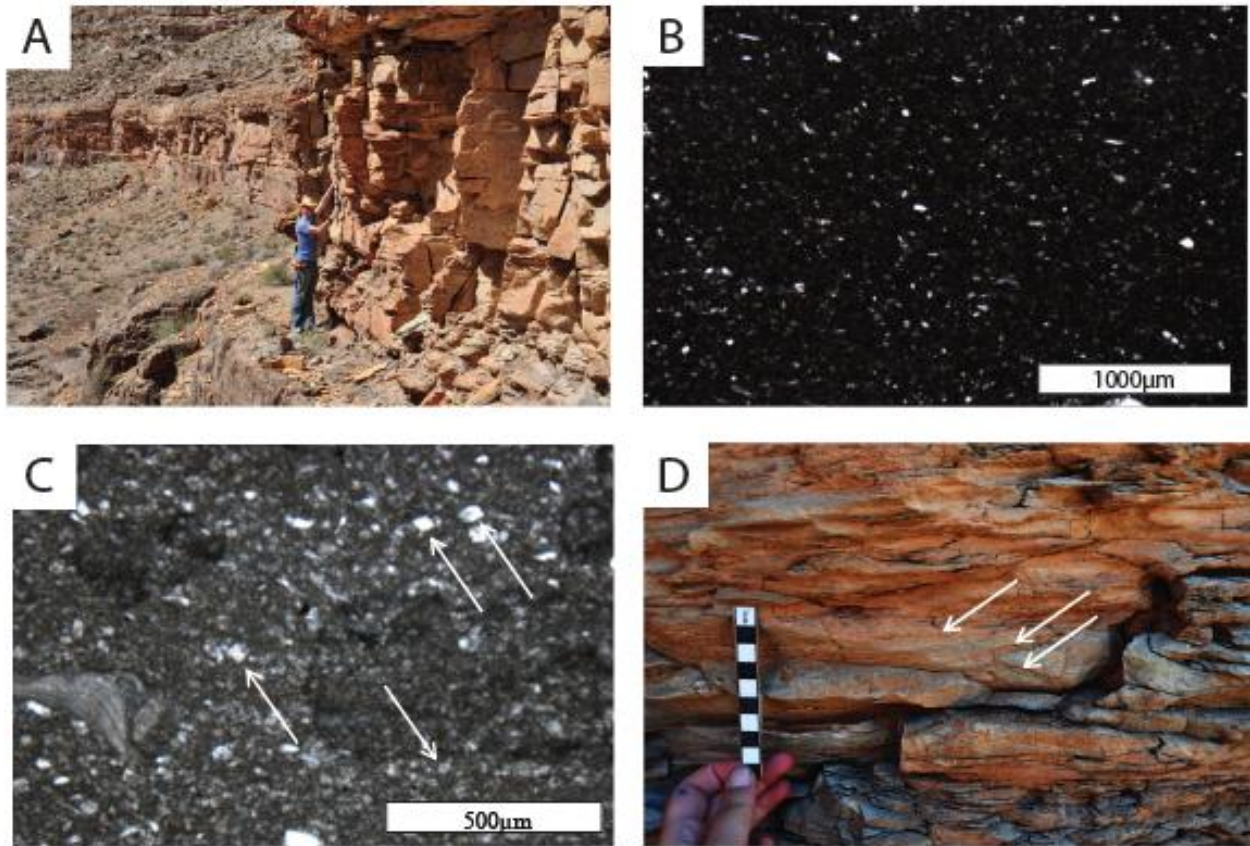


**Figure 20.** Photos and photomicrograph of Quartz Sandstone (Lithofacies 9). A) Field photo of QS showing sets of trough crossbeds (HTF). B) Close-up field photo of QS showing alternating crossbeds (RCB). C) Close-up field photo of QS showing unweathered crossbeds (8FDN). D) Polished slab of QS showing crossbeds with marine fossils concentrated on the crossbed surfaces (arrows). E) Thin section of QS in crossed polars showing fossils (bryozoan (br), crinoid (c), peloidal mud (pm)) along crossbed surface surrounded by coarse silt to fine-grained quartz sand (qtz). F) Close-up view of thin section showing fossils (foraminifera (fr)) surrounded by peloids (pm) along crossbed surfaces.

A alternative explanation attributes QS deposition to the structural uplifts to the north, south, and west of the Paradox basin during the Pennsylvanian (Baars and Stevenson, 1981). These uplifts shed siliciclastics into the basin during times of uplift (Goldhammer, 1991). The QS is thickest at 8FDN (southwest) and pinches out at RCB (northeast) (Goldhammer, 1991), therefore, it could likely have been sourced from the west. The Emery uplift was actively eroding during the Pennsylvanian (Baars and Stevenson, 1981), and could have been the source of the siliciclastics, transported into the marine environment by braided stream systems. The alternating crossbeds indicate changing current direction suggesting the sand was worked in fair-weather wave-base conditions (5-15m; Immenhauser, 2009; Coe, 2003). Shipp (1984) described a modern-day barred nearshore siliclastic environment off the coast of Long Island, NY that is controlled by shallow bathymetry where debris accumulates in the troughs of crossbeds, similar to QS, at 5-10m depth. The relief created by the underlying algal facies could have created a similar hydrodynamic environment to Shipp's (1984) description. Using field data and a modern-day analog, QS is interpreted to be deposited at 5-10m water depth.

#### **Lithofacies 10: Quartz Siltstone (QSt)**

**Description** – The Quartz Siltstone is a moderately to well-sorted siltstone that is approximately 7m thick and present throughout the study area. It has a distinct yellow color and the locals nicknamed the bed “Old Yeller” (Kearsley, 2007) (Figure 21A). Petroleum companies lump QSt into the Hovenweep Shale, a thick BLM-type shale that underlies QSt. The Hovenweep Shale is not observed in the field area. It consists of 60-80% subangular-subrounded quartz silt, 20-30% mud, 5-30% diverse marine fossils (brachiopods, foraminifera, bryozoa, and ostracods) along bedding planes, <10% calcite cement, and no visible porosity (Figure 21B). Fossils are fragmented and moderately to highly abraded. Previous studies classified this unit as cemented



**Figure 21.** Photos and photomicrographs of Quartz Siltstone (Lithofacies 10). A) Field photo of QSt or "Old Yeller" at ANB location. B) Thin section of QSt mud drape showing quartz silt (light) and mud (dark). C) Thin section of QSt showing dolomite rhombohedra (white arrows). D) Field photo of QSt flaser beds. The image was altered to create more contrast between the mud and sand colors. White arrows point at mud drapes, which appear more orange in photograph.

by dolomite (Grammer et al., 2000), but an Alizarin red test identified the cement in collected samples as calcite. Rhombohedra are observed in thin section (Figure 21C); therefore, QSt may have contained dolomite that was later replaced by calcite. Marine fauna size and abundance increases laterally towards the west (updip). Flaser bedding is observed where not obscured by bioturbation (Figure 21D). Chert nodules dominate much of the facies. Due to weathering and slumping of overlying beds, QSt is commonly poorly exposed.

The QSt observed at the HTF locality, the most updip area, looks different than downdip localities. It consists of 0.2m thick beds of less-resistant laminated siltstone alternating every 0.4m within the more resistant siltstone. Lags of whole and fragmented brachiopod valves measuring 5cm thick are observed within the siltstone.

The contact below the QSt is commonly covered due to weathering. SWP grades upward into silt-dominated QSt at the Narrows locality. The base of the QSt bed marks the top of the Lower Ismay zone (Homewood and Eberli, 2000).

**Interpretation** – The Quartz Siltstone is commonly interpreted to have been deposited similar to QS, through eolian transport during a lowstand and later reworking through marine transgression (Goldhammer et al., 1991; Grammer et al., 2000). Silt-sized grains can be transported in suspension by wind (Bagnold, 1941), which makes Goldhammer et al. (1991) and Grammer et al.'s (2002) eolian transport model more favorable for QSt than for QS. If the QSt was originally deposited during a lowstand in a subaerial environment, however, the gradational contact with the underlying SWP goes unexplained. Their hypothesis would be possible if an exposure surface is located updip of the study area; however, the silt content increases upsection within the QSt suggesting that change in environment was gradual, possibly a gradual shallowing that brought terrigenous eolian silts basinward. The flaser beds indicate that the eolian sands were



likely deposited in a tidal environment. The fossils within QSt show moderate to high abrasion, suggesting they were transported in a high-energy environment. The presence of bioturbation, indicates an environment that supported organisms. The increase in fossil size and abundance towards the west (toward interpreted paleoshoreline) could be related to storm events that brought the organisms into shallower waters. The field observations and depths of modern tidal environment analogs (Immenhauser, 2009),<sup>3</sup> places QSt depositional water depth at less than 5m.

### **STRATIGRAPHY**

Previous studies of the Paradox basin succession break the stratigraphy into genetic cycles bounded by dark “shales” that can be traced extensively throughout the basin (Hite, 1970; Peterson, 1966; Baars and Stevenson, 1981). This method was used to designate zones within the Paradox Formation and correlate basinward evaporites (Malin, 1958; Wengerd, 1962). Goldhammer et al. (1991) developed a sequence stratigraphic model for the Paradox Formation using fourth- and fifth-order depositional sequences bounded by regionally correlative surfaces that showed evidence for subaerial exposure. Sequences were typically marked by BLM facies near or at the base of sequences (Goldhammer et al., 1991). Within the sequences, Goldhammer et al. (1991) observed two types of cycles: (1) cycles bounded by marine flooding surfaces termed subtidal cycles and (2) cycles bounded by subaerial surfaces termed exposure cycles. Cycles were also documented by the transition of facies representing deepening or shallowing of depositional environments (Goldhammer et al., 1991). Grammer et al. (2000) adopted Goldhammer et al.’s (1991) classification system. The term parasequence was used interchangeably with cycle or was modified to mean “a shallowing-upward trend in facies” (Grammer et al., 2000; Goldhammer, 1991).

The goal of this study was to analyze the Lower Ismay zone of the Paradox Formation at centimeter-scale resolution to aid in correlation. Small-scale bedding features, such as thin mud-rich beds, could be traced from stratigraphic section to stratigraphic section. The features, however, could not be traced regionally. A location map documents the position of measured stratigraphic sections, locality names, and cross-sections (Figure 22). The cross-sections are drawn upstream to downstream to aid in orientation when in the field. Dip and strike directions are labeled on cross-sections. Figure 23 shows a dominantly strike-oriented cross section (A-A') through the Narrows (N) and Rock Cairn Bend (RCB) localities. Figure 24 is a cross-section (B-B') between the Alligator Nose Bend (ANB) and the 8-Foot Narrows (8FN) localities. Figure 25 is a cross-section (C-C') through 8-Foot Drainage Navajo (8FDN) section, located in an abandoned meander near 8-Foot Rapids, and the 8-Foot Narrows (8FN) localities. Figure 26 is a conceptual cross-section (D-D') connecting stratigraphic sections at 8FDN and Honaker Trail Fin (HTF) localities. The stratigraphic relationship is a hypothesis because the outcrop is not exposed between the sections. Figure 27 is a fence diagram that illustrates the 3D relationships of cross-sections A-A', B-B', and C-C'. See Figure 10 for explanation of colors and symbols.

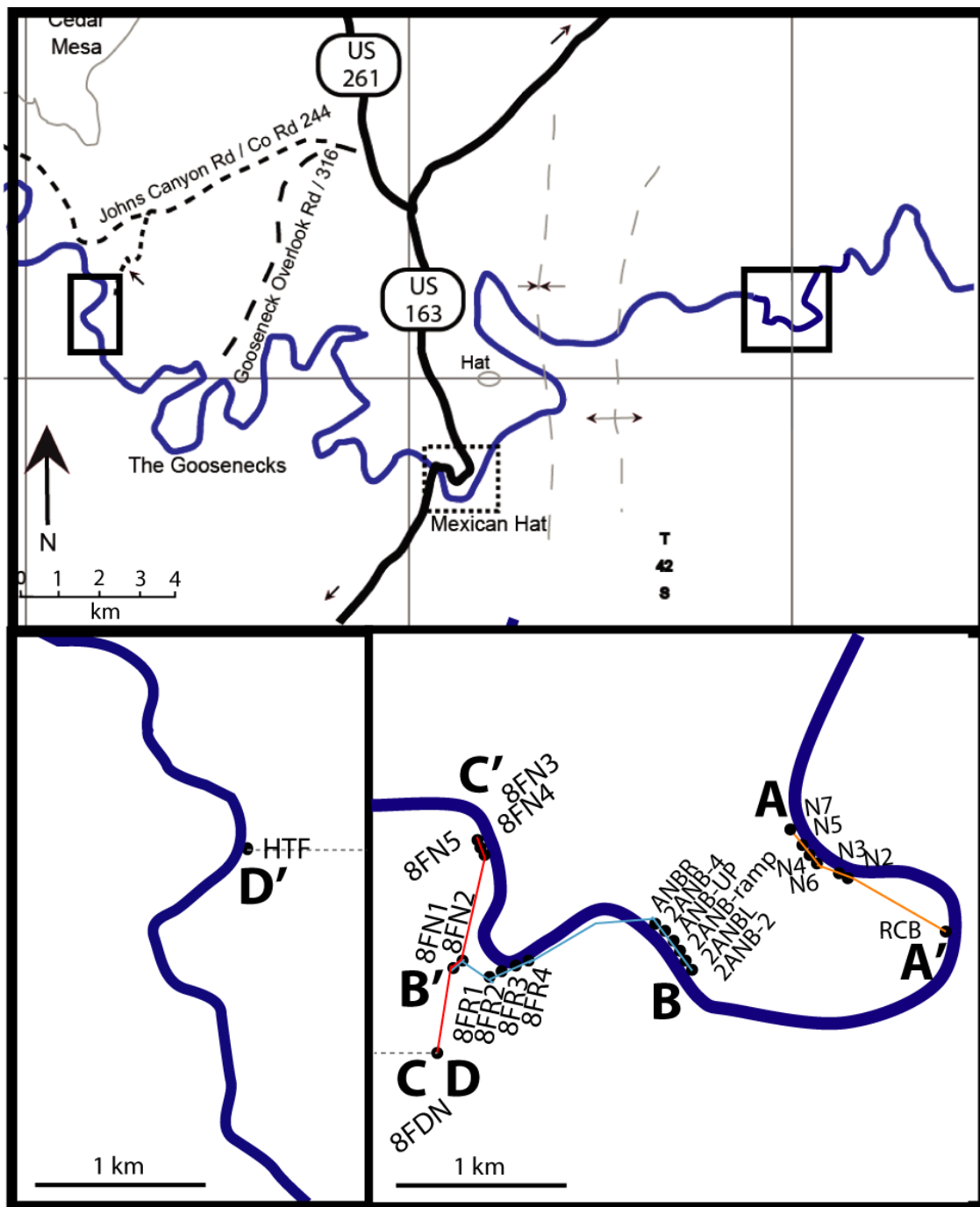
For this study, sequence boundaries (SB) indicate significant relative sea-level falls (SB1, SB2) and parasequence boundaries (PSB) indicate significant flooding events (PSB1, and PSB2). This classification system uses Van Wagoner et al.'s (1988) sequence stratigraphic definitions of parasequences, parasequence boundary, and sequence boundary and will also acknowledge shoaling upward characteristics used by Goldhammer (1991) and Grammer et al. (2002) described above. Parasequences (P) and sequences (S) are labeled P1, P2, S1, and S2. A parasequence boundary is defined as a surface that shows a significant landward shift in facies, or deepening, and is indicative of a relative rise in sea level. A parasequence is a relatively

conformable succession of shoaling-upward, genetically related beds bounded by parasequence boundaries. A sequence boundary is defined as a surface that marks a relative fall in sea level by showing evidence of exposure or a significant basinward or seaward shift in facies. For the purpose of this study, if the facies in a stratigraphic unit show evidence of a relative sea-level rise and fall, it is considered a sequence.

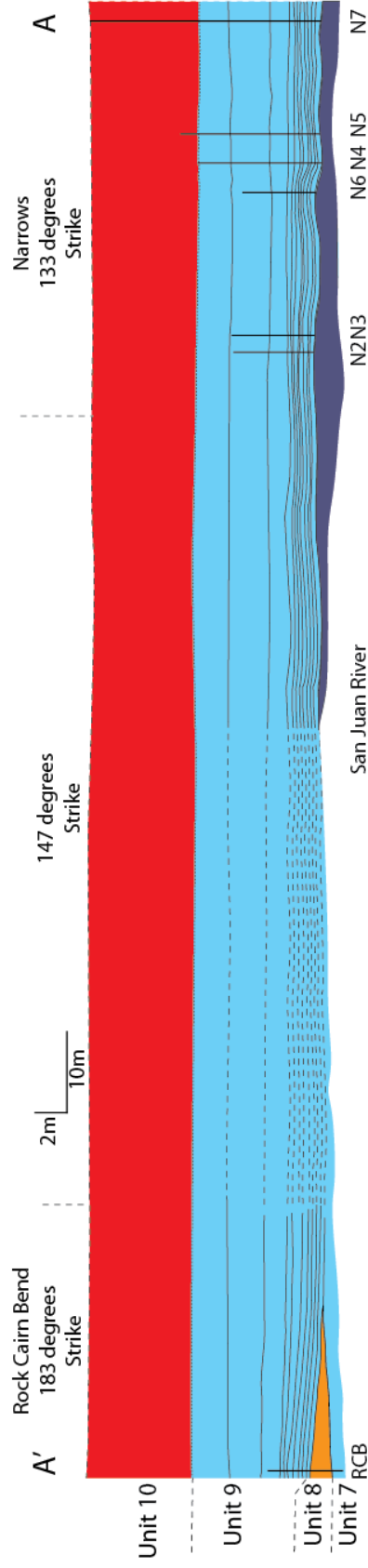
### **Paleotopographic Reconstruction**

Pre-Pennsylvanian Paradox Basin stratigraphy consisted of a broad stable shelf (Goldhammer et al., 1991). Uplift during late Mississippian created an extensive subaerial exposure surface and paleosol across the basin (Goldhammer et al., 1991; Peterson, 1966b). Initial marine transgression of the subaerial surface occurred in the Early Desmoinesian (Goldhammer, et al., 1991; Stevenson, 1984).

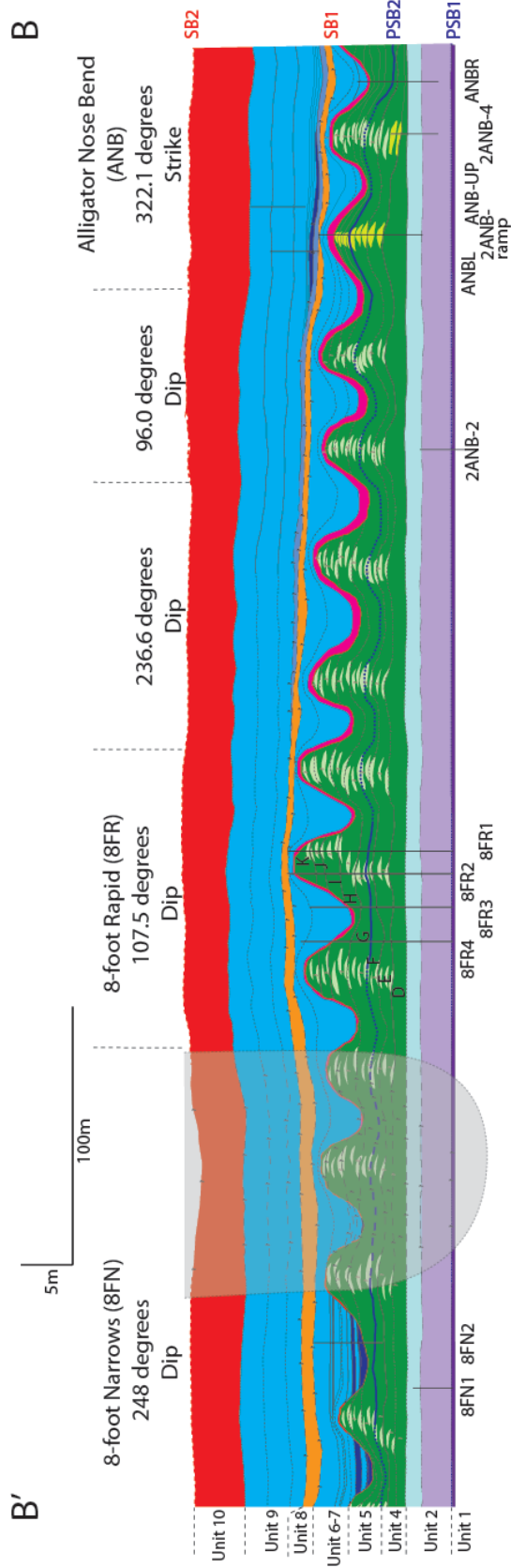
Eltson et al. (1962), Peterson and Hite (1969), Baars (1966; 1988), Baars and Stevenson (1981), Stevenson and Baars (1984), Roylance (1990), Chidsey et al. (1996a), Goldhammer et al. (1991), and Grammer et al. (2000) described evidence for increased accommodation due to continued asymmetric subsidence throughout the Desmoinesian. Subsidence and extensional faulting continued during the accumulation of distal basin evaporites (Goldhammer et al., 1991; Stevenson, 1984). The faults created subtle paleotopographic relief, which have been interpreted in previous studies, to influence the depositional distribution of algal mounds of the Paradox Formation (Goldhammer et al., 1991; Grammer et al., 2000). Dip continued to increase towards the basin throughout the Desmoinesian as the distal basin subsided. Because the topography was evolving throughout deposition of the Lower Ismay, it is difficult to confidently reconstruct paleotopography cannot be confidently reconstructed.



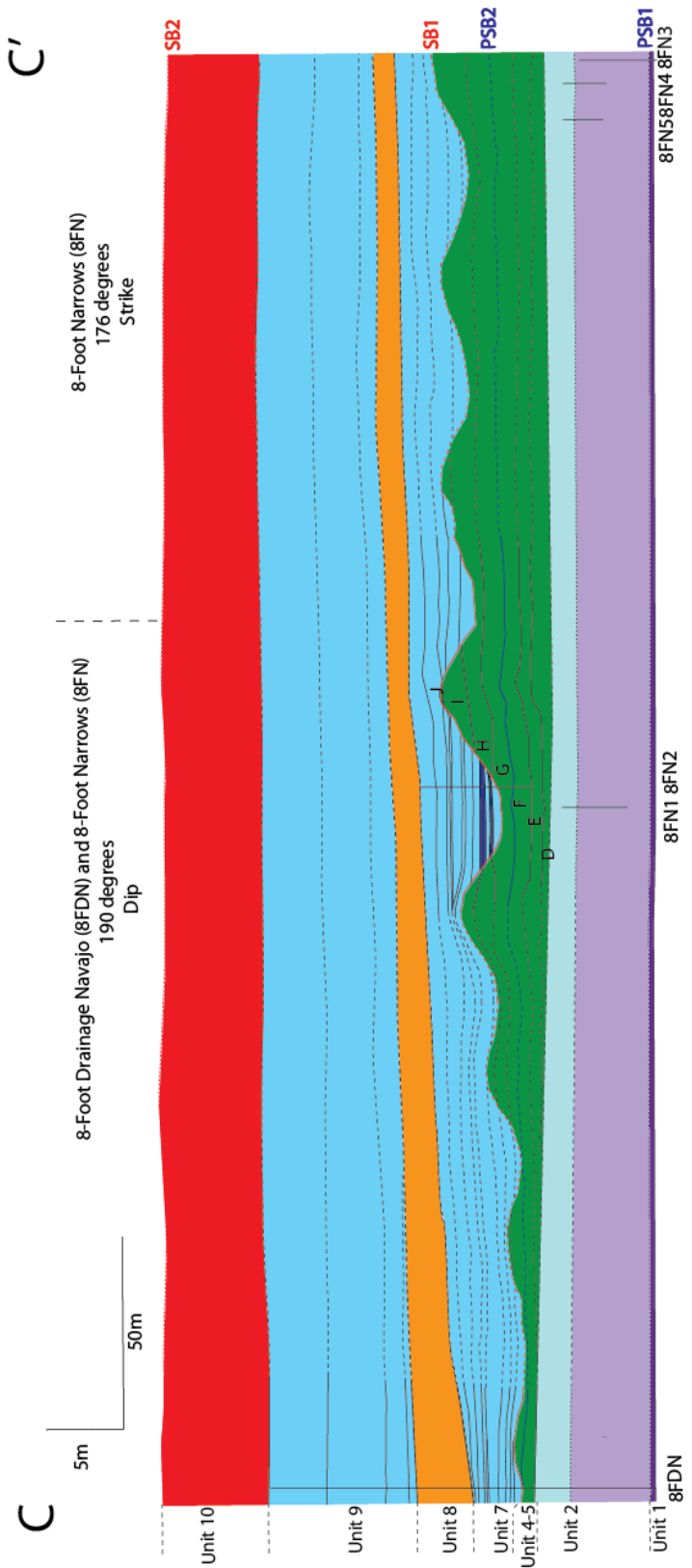
**Figure 22.** Map showing the locations of stratigraphic sections in relationship to the San Juan River (dark blue line). The cross-section locations are highlighted with the colored lines: cross-section A-A' (orange), cross-section B-B' (blue), and cross-section C-C' (red), and cross-section D-D' (dashed gray). D' is approximately 14km from D. Cross-sections are oriented from upstream to downstream.



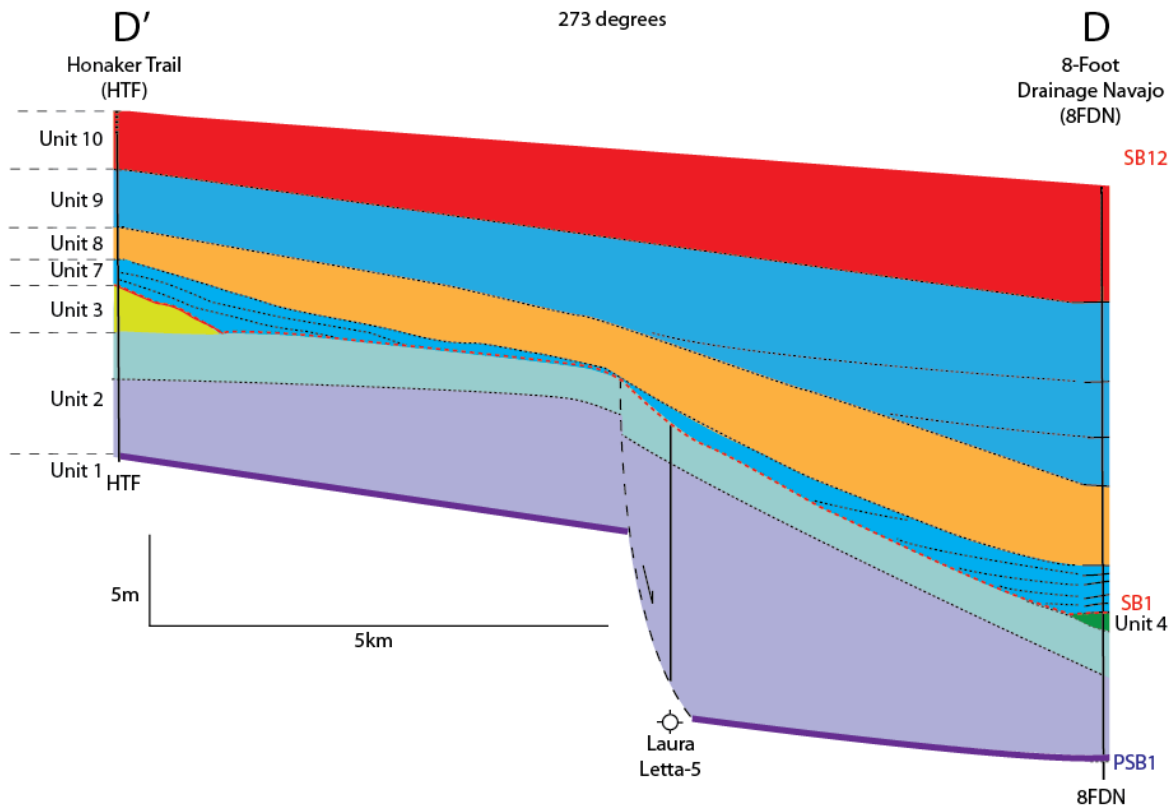
**Figure 23.** Cross-Section A-A'. Constructed from stratigraphic sections between Narrows (N) and Rock Cairn Bend (RCB) measurement sites. The section is oriented upstream (A', right) to downstream (A', left). Traveling downstream, cross-section is on the right side of the river (BLM). This is the northern strike-oriented cross-section and shows no dip component. Only the upper portion of the Lower Ismay zone is exposed by the San Juan River (Units 7-10). The Narrows stratigraphic sections were measured on rappel. Surfaces were traced using photomosaics where there was no access. Sedimentary symbols were purposely left off the cross-section to maintain a clear illustration of stratigraphic relationships. The units and sequence stratigraphic boundaries are labeled. See Figure 22 for cross-section location and Figure 10 for explanation of colors and symbols. See Appendix I for stratigraphic sections and Appendix II for annotated photomosaics.



**Figure 24.** Cross-Section B-B'. Constructed from stratigraphic sections between Alligator Nose Bend (ANB) measurement site and 8-foot Narrows (8FN) locality. The section is oriented upstream (B', right) to downstream (B', left). Traveling downstream, the ANB localities are on the right bank (BLM) and 8-Foot localities are on the left bank (Navajo). The BLM facies was used as the datum. Accessibility using ropes was limited due to overhangs. Surfaces were traced using photomosaics where there was no access (See Appendix II). Sedimentary symbols were purposely left off the cross-section to maintain a clear illustration of stratigraphic relationships. The units, algal facies beds, and sequence stratigraphic boundaries are labeled. The gray polygon indicates area of cross-section that is missing due to erosion from the modern-day San Juan River. See Figure 22 for cross-section location and Figure 10 for explanation of colors and symbols. See Appendix I for detailed stratigraphic sections.

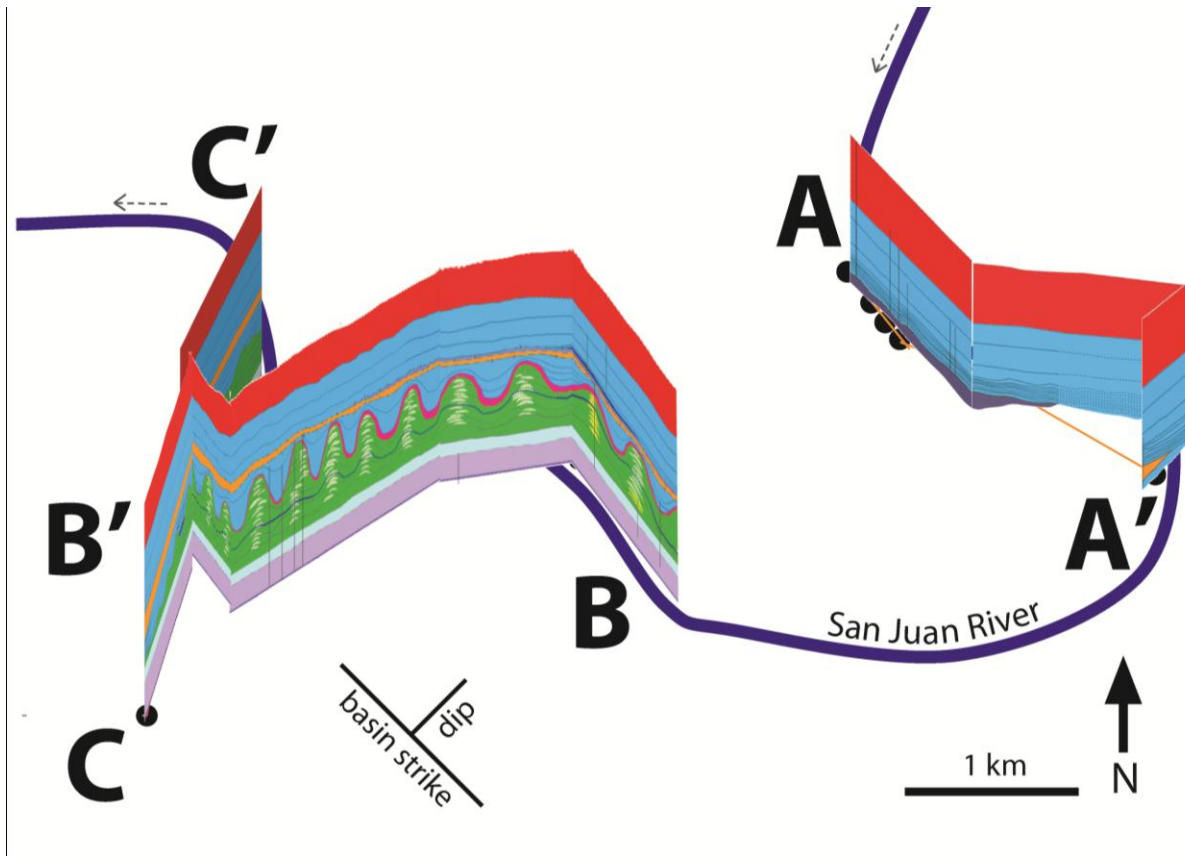


**Figure 25.** Cross-Section C-C'. Constructed from stratigraphic sections between 8-Foot Drainage Navajo (8FDN) measurement site and 8-foot Narrows (8FN) measurement site. The section is oriented upstream (C, left) to downstream (C', right). 8FDN is located in an abandoned meander on the left bank (Navajo). The 8-Foot Narrow localities are located on the left bank (Navajo). Accessibility using ropes was limited due to overlying limestone creating overhangs. Surfaces were traced using photomosaics where there was no access. Sedimentary symbols were purposely left off the cross-section to maintain a clear illustration of stratigraphic relationships. The units, algal facies beds, and sequence stratigraphic boundaries are labeled. See Figure 22 for cross-section location and Figure 10 for explanation of colors and symbols. See Appendix I for stratigraphic sections and Appendix II for annotated photomosaics.



**Figure 26.** Cross-section D-D'. Conceptual diagram constructed from stratigraphic sections at Honaker Trail Fin (HTF) and 8-Foot Drainage Navajo (8FDN) localities. The section is oriented upstream (D, right) to downstream (D', left) and hung on an interpretive structure with an overall 0.1 degree dip. The relationship between HTF and 8FDN localities is not exposed between river-miles 18 and 35. The outcrop is accessible at river mile 45 along Honaker Trail. Reported Gothic Shale top from the Laura Letta-5 well guided the interpretation of the nonoutcropping geometries between sections. All interpreted contacts are dashed. The fault direction is marked with an arrow. Sedimentary symbols were purposely left off the cross-section to maintain a clear illustration of stratigraphic relationships. The units, algal facies beds, and sequence stratigraphic boundaries are labeled. See Figure 22 for cross-section location and Figure 10 for explanation of colors and symbols. See Appendix I for stratigraphic sections and Appendix II for annotated photomosaics.





**Figure 27.** Fence diagram constructed from cross-sections A-A', B-B', and C-C'. Cross-section D-D' is purposefully not included in the fence diagram because the large distance covered by D-D' obscures the detail of the other cross-sections. The fence diagram illustrates the orientation of exposed cliff walls along the San Juan River (dark blue line) in relation to approximate basin strike (southeast) and dip (southwest). Dashed arrow indicates the flow direction of the river. The units and boundaries are illustrated in cross-section diagrams (Figures 23-26). Figure 10 for explanation of colors and symbols.

Calculations from isopach map data (Goldhammer et al., 1991) indicate a regional dip of 0.4 degrees, basinward (northeast) of Desmoinesian carbonates and siliciclastics of the Paradox Formation. Facies relationships, discussed in the Sequence Stratigraphy section, suggest a dip of approximately 0.1 degree throughout the study area. This 0.1 degree dip, was used to correlate the Honaker Trail stratigraphic sections across the outcrop gap of unexposed Lower Ismay between the Raplee anticline and Monument upwarp to the downdip sections (8-Foot through ANB).

### **Lower Ismay Zone Sequence Stratigraphy**

The generalized stratigraphy of the Lower Ismay zone was introduced in the Geological Background section. The following summarizes vertical and lateral stratigraphic relationships within the Lower Ismay zone in stratigraphic order from oldest (basal) to youngest (topmost) in the study area. The Lower Ismay zone is divided into two sequences, distinctly separated by a sequence boundary atop the algal facies. See Figure 28 for a summary of the sequence stratigraphy.

#### ***Sequence 1***

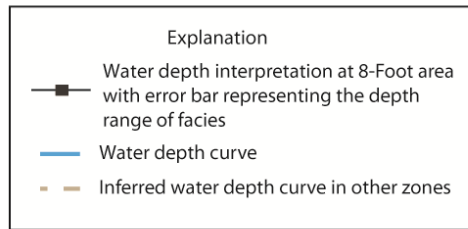
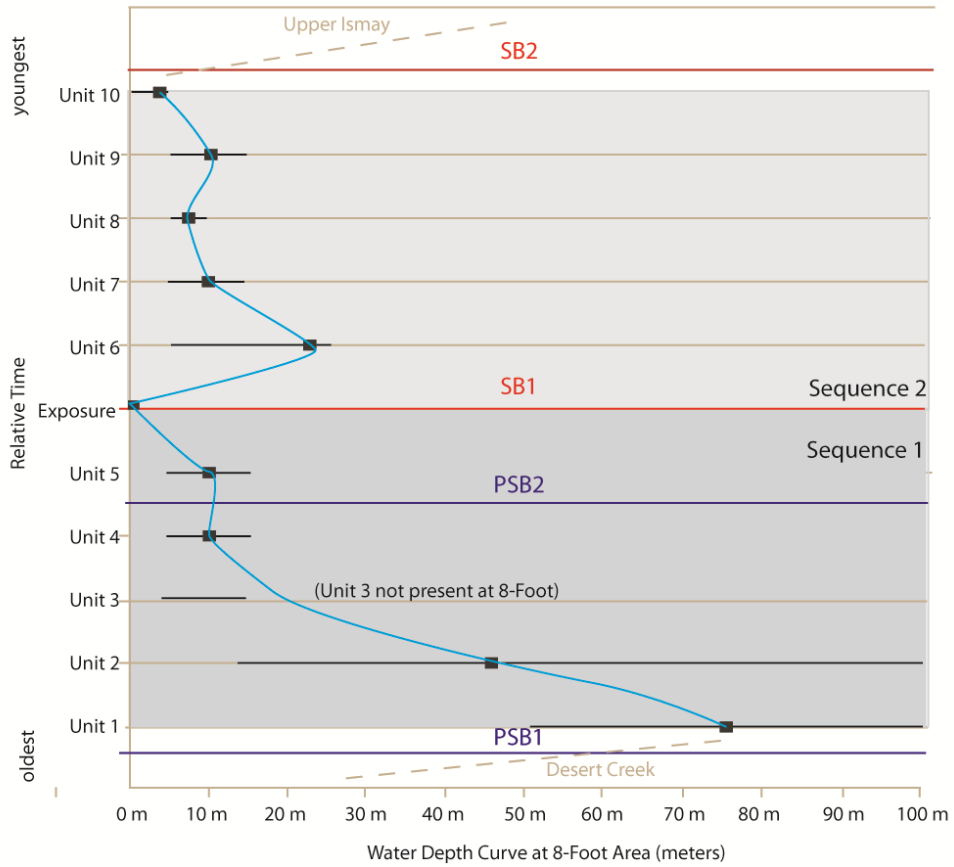
**Unit 1.** Unit 1 directly overlies, in sharp contact, the Upper Desert Creek deposits of the Honaker Trail Formation and is the oldest (basal) unit of the Lower Ismay in the Paradox Basin. Unit 1 consists of Lithofacies 1 (BLM). Lithofacies 1 is a black to dark grey, laminated mudstone that, where exposed, is consistent in thickness (10-40cm) and is present in all sections (Figures 23-26). The internal laminations parallel the underlying bedding. Unit 1 is observed throughout the basin in outcrop, core, seismic, and well logs and is used in literature as a marker bed and datum when hanging cross sections (Grammer et al., 2000).

Unit 1 was deposited in relatively deep, anoxic conditions after a relative sea-level rise and is a different sequence than the underlying Upper Desert Creek SWP facies (Lithofacies 7) (5-10m water depth). A relative sea-level rise of 45-95m occurred to deposit Unit 1 (50-100m). The sharp contact between Lithofacies 1 and 7 suggests a flooding event in which facies deposited between the depths of Lithofacies 1 and 7 were unable to accumulate. The relative sea-level rise and the landward shift in facies indicate that the surface between the Upper Desert Creek and Unit 1 is a flooding surface, likely a parasequence boundary (PSB1).

**Unit 2.** Unit 2 is approximately 5m thick throughout the study area and is in gradational contact with underlying Unit 1. Unit 2 is above river level in localities updip of RCB, including ANB, 8FR, 8FDN, 8FN, and HTF localities (Figure 23-25). It consists of Lithofacies 2 (SM) and Lithofacies 3 (CP).

Lithofacies 2 (basal facies of Unit 2) increases in thickness downdip, measuring 3m thick at the HTF locality (updip) and 4.2m at the 8FN and ANB localities (downdip) (Figures 23-25). The color of Lithofacies 2 changes from dark gray at the base to light gray at the top. The marine fossil content also increases upsection. Lithofacies 3 is in gradational contact with underlying Lithofacies 2 and also increases in thickness downdip, measuring 1m thick at the HTF locality to 1.5m at the downdip ANB locality (Figures 24-26). Lithofacies 3 consists of abundant marine fossils and represents an aerobic depositional environment.

Unsuccessful oil wells were drilled between the HTF and 8-Foot localities where the Lower Ismay is in the subsurface. Formation tops reported to the state website for the Laura-Leta 5 well indicate that the Unit 1-2 equivalent is up to 12m thick, approximately 4m thicker than outcrop measurements (Figure 29; Utah...c2014).



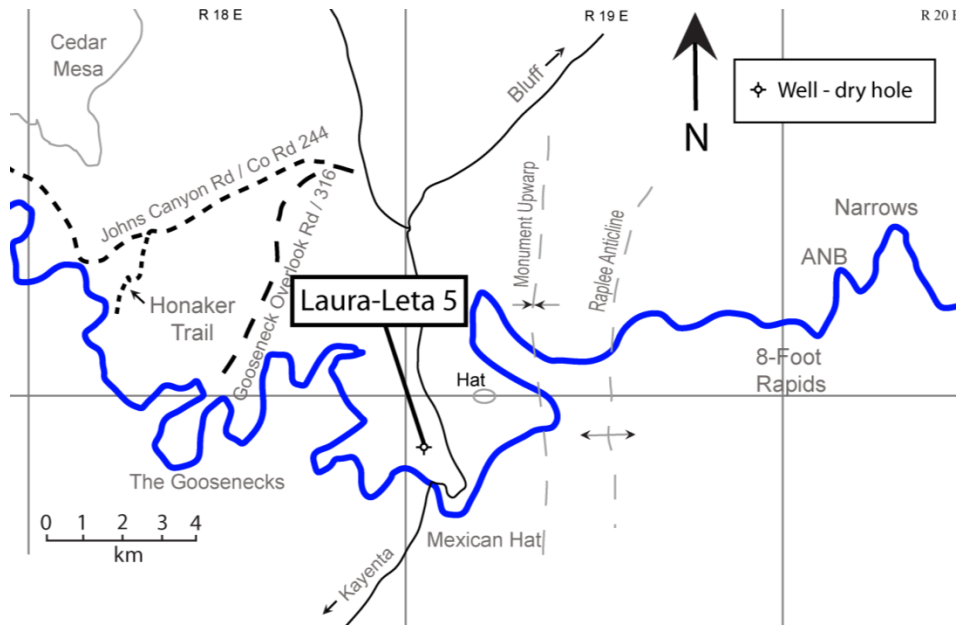
**Figure 28.** Water depth curve for Units 1-10 developed for the 8-Foot Rapids area. An interpreted water depth (black box) and water-depth range (black line) are given for each unit at 8-Foot Rapids area. Time is relative and does not represent quantitative ages. A sea-level curve could not be interpreted because paleotopography could not be reconstructed.

Goldhammer et al. (1991) and Grammer et al. (2000) suggested that basement faults were reactivated during the Pennsylvanian and created topographic relief that influenced Lower Ismay facies distribution. I speculate that a thickness change of Units 1-2 between HTF and 8-Foot localities could be attributed to syndepositional faulting as illustrated in Figure 26. Lithofacies 2 is bounded by gradational contacts and is interpreted as the transition from the dysaerobic environment of underlying Unit 1 (50-100m depth) to the aerobic environment of overlying Lithofacies 3 (15-20m depth). Thus, from the base to the top of Unit 2, there was a relative sea-level fall of 30-80m. The deposition of Unit 2 marks the beginning of facies stepping basinward during an overall relative sea-level fall.

**Units 3-5.** Units 3-5 are typically referred to as the “algal mounds” due to their mounding or undulose geometries. To reduce confusion, this study will refer to all of the algal deposits, consisting of Lithofacies 4 (AB) and Lithofacies 5 (AP), as the “algal facies.” In the literature, the algal facies in this stratigraphic unit are commonly described as one large bed, but the algal facies of Units 3-5 are made up of at least 12 beds that thin and thicken laterally, exhibit undulose geometries, and are each separated by sharp contacts.

Unit 3 crops out at the HTF locality. Units 4 and 5 crop out at 8-Foot and ANB localities. The lack of outcrop between HTF and 8-Foot localities obscures the relationship of Unit 3 to Units 4 and 5; therefore, confidence is low when correlating the algal facies across D-D' (Figure 26). The outcrops at 8-Foot and ANB localities are more accessible and laterally continuous, therefore, the algal facies relationships are analyzed in greatest detail in Unit 4 and 5.

**Unit 3.** Unit 3 is only present at the HTF locality, 10.9km (N84W) updip of 8FDN. Inaccessibility to the entire outcrop due to overhangs and poor rappelling anchors made direct



**Figure 29.** Laura Leta-5 well targeting Ismay and Desert Creek zones of the Paradox Formation near Mexican Hat, Utah. The Lower Ismay is at approximately 790ft (240.8m) true vertical depth. The well was a dry hole. The state-reported formation tops of the Laura-Leta 5 well suggests that Units 1-2 are approximately 12m thick.

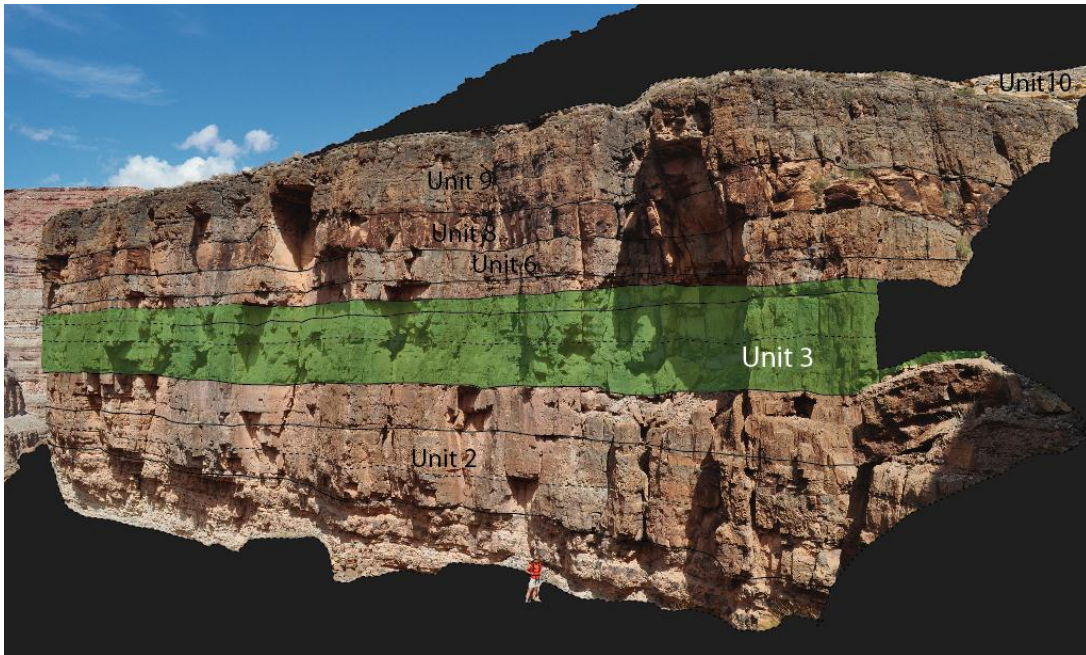
measurements difficult. Observations were made along the established hiking trail and from photomosaics.

Unit 3 consists of at least 3 beds (A-C) of Lithofacies 4 (AB) and Lithofacies 5 (AP). Lithofacies 5 is volumetrically dominant at the HTF locality. Beds A-C do not exhibit as large mound-like geometries as seen in downdip Units 4-5. Individual beds have local thickness variation, but there is no clear regular spacing of topographic highs (Figure 30). Beds are in sharp, non-erosive contact with one another. An erosional surface is observed at the top of Bed C.

The relationship between Units 3 and 4 are obscured by the structure of the Raplee anticline and Monument upwarp. Reported tops from the Laura Leta-5 well suggest a thickening of underlying Unit 1-2 (Utah...c2014). The presence of algal facies was not reported and logs were not available.

**Unit 4.** Unit 4 is present at ANB and 8-Foot localities. It is in sharp, non-erosive contact with underlying Unit 2. Unit 4 consists of Lithofacies 4 (AB) and Lithofacies 5 (AP). At ANB and 8-Foot localities, Lithofacies 4 is volumetrically dominant within Unit 4. Lithofacies 5 occurs in irregular lenses less than 1m thick with approximate lateral extent of 1-2m that interfinger with Lithofacies 4.

Unit 4 ranges in thickness from approximately 1m to 6m thick, encompassing the basal 3 beds (beds D-F) of the algal facies below PSB2. Local thickness variation of individual beds average 70cm with average spacing from crest to crest of 40.5m leading to mound-like geometries that stack vertically with an asymmetrical basinward-thickening component (Figure 31). The lateral extent of individual mound-like geometries from low to low average 38.5m in the dip direction and 39.7m in the strike direction, suggesting that there is no preferred



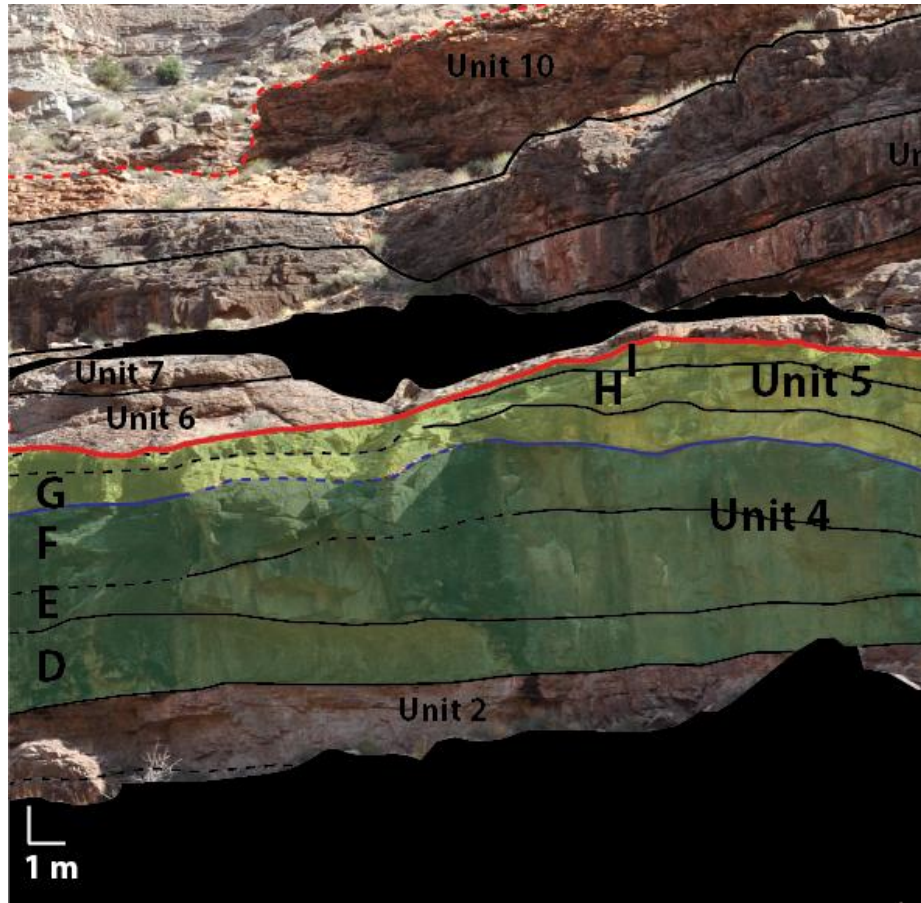
**Figure 30.** HTF locality photomosaic with Unit 3 highlighted in green. Person for scale.



orientation. These are isolated mound-shaped features rather than linear bar-shaped features. See Appendix IV for algal facies spacing and dimension measurements.

The basal bed of Unit 4 (Bed D, Figure 23) is in sharp contact with underlying Unit 2. It is dominantly Lithofacies 4 and exhibits an undulose geometry along its upper contact. Bed D is thickest at the 2ANB-ramp locality and thins laterally in all observable directions. Moving updip from 2ANB-ramp to the 8FR sections respectively, Bed D measures 2.1m thick and thins to less than 1m continuing updip to the 8FR sections, approximately 300m away (N83W direction; Figure 24). Continuing updip to the 8FDN locality, Bed D appears to pinch out and is not present at the 8FDN locality (Figure 25). The confidence of correlation of Bed D from 8FR locality to 8FDN is low due to poor exposure between localities. Moving southeast along strike from 2ANB-ramp to ANBR, Bed D measures 2.1m thick and thins to 0.5m (Figure 24). The bed thins 1.6m in approximately 40m along strike (N51W direction; Figure 24).

Beds E and F of Unit 4 consist of Lithofacies 4 and Lithofacies 5 and are in sharp, non-erosive contact with underlying and overlying beds. Beds E and F consist of Lithofacies 4 and 5, with Lithofacies 5 preferentially on paleotopographic highs and Lithofacies 4 in adjacent lows. Bed E appears to pinch out updip and is not present at 8FDN locality. Bed E is approximately 3m thick at its thickest at the 2ANB-4 stratigraphic section. Approximately 0.5km updip (N80W direction) at 8FN1, it thins to approximately 1m thick. Moving 23.5m along strike (S67E direction) at ANBR, it thins to 17cm thick (Figure 26). Bed F's thickest area is at the 2ANB-ramp stratigraphic section location, measuring 1.5m thick. Approximately 0.5km updip (N80W direction) near 8FN1, the bed thins to approximately 1m thick and pinches out at 8FDN locality (Figure 32); 60m along strike (S66E) at ANBR, it thins to 0.7m (Figure 26). Poor exposure

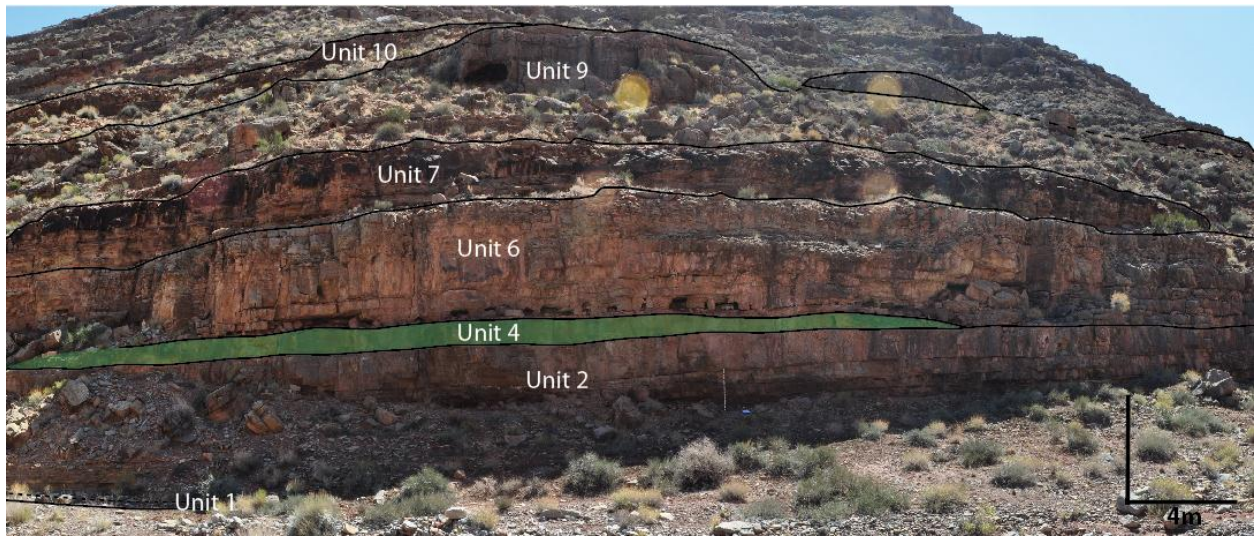


**Figure 31.** Annotated photomosaic at the ANB locality illustrating the thinning and thickening of individual algal beds. The thick areas are also staggered moving stratigraphically upwards. Unit 4 (Beds D-G) and Unit 5 (Beds H-I) are highlighted in different shades of green and labeled accordingly. Approximate bed contacts are dashed, whereas known contacts are solid. Sequence boundaries are colored red and parasequence boundaries are blue.

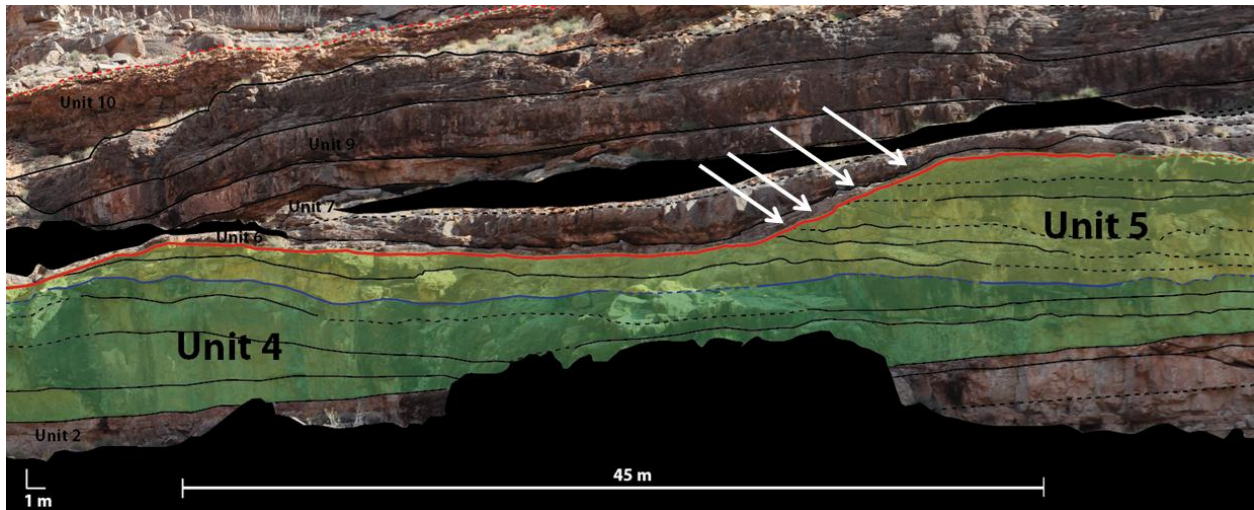
between 8FN and 8FDN localities limits the confidence by which Unit 4 bed is interpreted to pinch out at 8FDN. Unit 4's thickest areas are located at the ANB locality.

**Unit 5.** Unit 5 is exposed at ANB and 8-Foot localities. It is made up of 5 beds (Beds G-K) that are in sharp, non-erosive contact with one another. Local thickness variation of beds average 61cm with the average spacing from crest to crest of 40.2m. These mound-like geometries stack vertically with an asymmetrical basinward component. The lateral extent of individual mounds from low to low within Unit 5 average 38.7m in the dip direction and 39.1m in the strike direction, suggesting near symmetrical geometries. Unit 5's bed geometries, stacking patterns, and facies distribution of Lithofacies 5 concentrated on local highs and Lithofacies 4 concentrated in the lows are identical to those observed in Beds E and F of Unit 4. The basal bed of Unit 5 (Bed G, Figure 23) is mostly laterally continuous. Local thickness variation of Bed G averages 50cm with an average spacing of 40.3m between highs and lows giving rise to mound-like geometries. The four overlying beds (Beds H-K), however, are erosionally truncated along an undulose surface with an approximate wavelength of 40m and relief of 2-5m (Figure 33). The local minimum depositional thickness variation of Beds H-K averages 62cm. The average spacing is similar to Bed G with preferential thickening on the underlying highs.

Bed G is thickest at the 8FR4 locality, measuring 2.6m thick, 300m updip (S68W direction) from Bed F's thickest area. Approximately 30m updip (N87E direction) at 8FR1, Beds H and I have maximum thicknesses of 2.7m and 2.2m thick respectively. Approximately 12m downdip (S81W) at 8FR2, Bed J has its maximum thickness of 1.3m. Approximately 12m updip (N81E direction) at 8FR1, Bed K has its maximum observable thickness of 2.5m. Overall,



**Figure 32.** Unit 4 (green) pinches out at the 8FDN locality. Jacob staff (1.5m) for scale as well as scale bar.



**Figure 33.** Annotated photomosaic at the ANB locality illustrating truncation of beds in Unit 5 (white arrows). The typical length between crests of the highs of the algal facies is approximately 40m. Units 4 and 5 are separated by a parasequence boundary and highlighted by different shades of green. Approximate bed contacts are dashed, whereas known contacts are solid. Sequence boundaries are colored red and parasequence boundaries are blue.

Unit 5's thickest area is at the 8FR locality. The beds of Unit 5 are not present at the updip 8FDN locality.

**Relative Sea-Level Interpretation of Units 3-5.** The interpreted water depths for Units 1 through 5, and interpreted subaerial exposure just after Unit 5 deposition, indicate Units 1 through 5 were deposited during an overall relative sea-level fall. Unit 3 is the most updip of the algal facies and is interpreted to have been deposited before Units 4-5. During the deposition of Unit 3 (5-15m depth at HTF), downdip locations were still depositing Unit 2 facies (15-50m depth). As relative sea-level continued to fall, facies deposition migrated basinward. Units 4-5 were deposited 10.9km downdip of Unit 3, resulting in 19m of relief between Unit 3 and Unit 4 at 8-Foot localities. Taking into consideration the range of water depths of Units 3 and 4 (5-15m water depth), a relative sea-level fall of at least 4m is required to deposit Unit 4. During deposition of Unit 4, Unit 3 would have been subaerially exposed and susceptible to erosion during the deposition of Unit 4-5, therefore Unit 3 originally may have been thicker and exhibited greater relief.

A thick algal deposit occurs in each bed of Units 4-5. If the thick area of each bed indicates a depositional environment for optimum algal accumulation at a specific depth, a significant shift in the location of the thick area along dip indicates a relative sea-level change. In Unit 4, the thickest areas are located at the ANB locality. After the deposition of Unit 4, the thickest accumulations (optimal area deposited at the same depth as the optimal area of Unit 4) shifted approximately 1km updip to deposit Unit 5. This would require a relative sea-level rise of approximately 1.8m (using a 0.1 degree depositional dip). The algal facies in Units 3 through 5 are interpreted to have built relief during minor rises or stillstands during an overall relative sea-level fall.

Prior to subaerial exposure and erosional modification (SB1), the algal facies built 0.4-2.1m of local depositional relief. The lateral extent of individual mound geometries of each bed average 38.6m in the dip direction and 39.4m in the strike direction, suggesting that the individual mounds are nearly circular. This observation is also supported by the digital outcrop model produced using LIDAR surveys of the study area by Goodrich (2013) and field measurements by Reed (2014). The asymmetrical stacking of the mounds downdip, however, suggests a current influence oriented normal to the depositional strike.

Although obscured by the regional structure, other algal facies complexes may be present between HTF and 8-Foot. Observations of that Unit 4-5 pinch out updip near the 8FDN locality demonstrates that the complexes at HTF and 8-Foot are isolated from one another. Outcrop studies do not give us an idea of the full extent of the algal facies, however, subsurface studies have documented algal complexes up 5 km along strike and 1.6km in the dip direction (Chidsey and Eby, 1999). State-reported formation tops in oil wells drilled between HTF and 8-Foot localities do not confirm the presence or absence of algal facies between outcrop localities. Reported formation tops in the Laura Letta-5 well (Utah...c2014) suggest that combined Units 1 and 2 are 12m thick, approximately 7m thicker than seen in outcrop. These observations could be due to different stratigraphic classifications or an error in reporting. Coalson and DuChene (2009) and Loudon et al. (1999) observed algal facies preferentially deposited on the flanks of underlying thick mud accumulations as seen in seismic surveys of the subsurface. If the top measurements are correct, the algal facies present at 8-Foot may have grown on the flank of the underlying thick of Units 1-2.

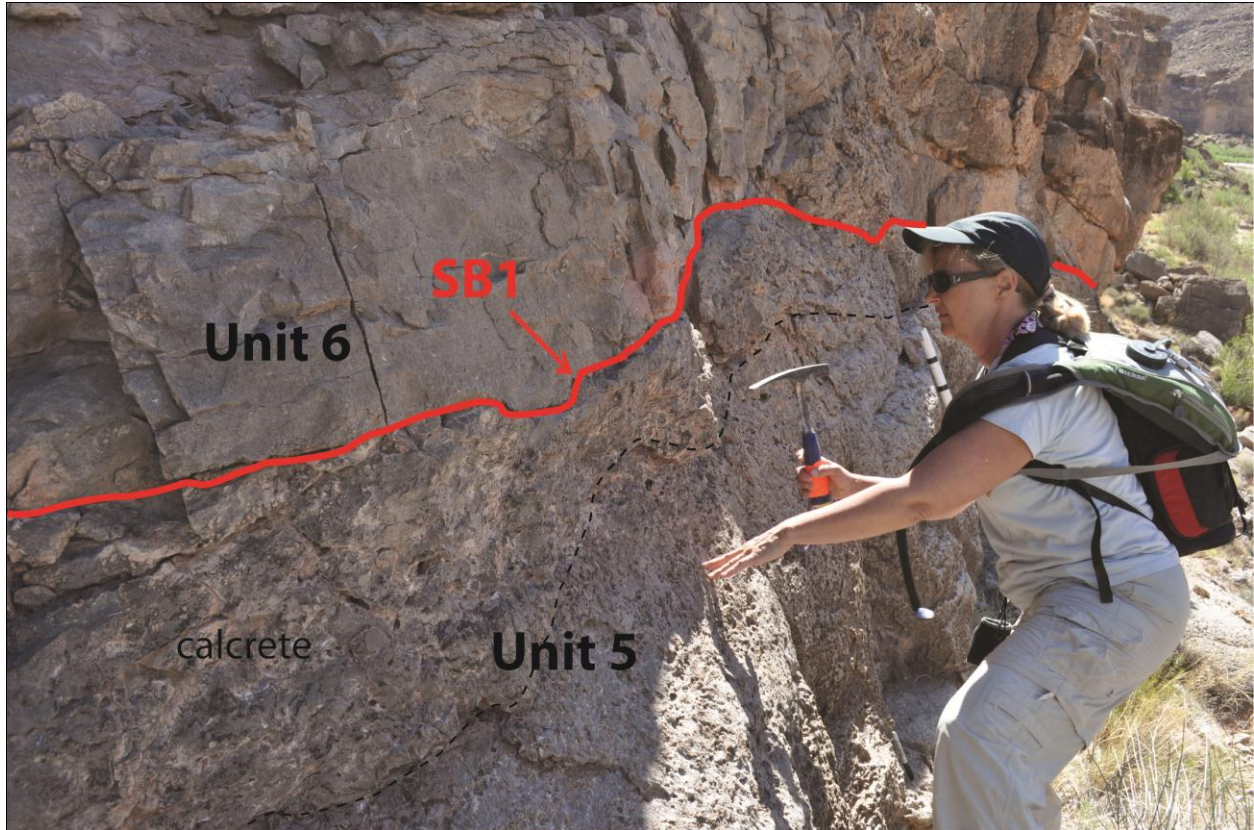
**Sequence Boundary 1.** A laterally extensive erosion surface truncates beds of Units 3-5 and is visible at HTF, ANB, and 8-Foot locations, but disappears under the modern-day river

level near the downdip RCB locality (Figures 23 and 25). At downdip localities, the surface has an average relief of 4m with an average spacing of erosional incisions of 39.5m the dip direction. In the strike direction, the surface created an average relief of 3.4m with average spacing of 41m. With the limited data set, the surface exhibits an undulose geometry along strike and dip, suggesting the underlying algal facies were eroded in a circular pattern to enhance the near-circular mounds. See Appendix IV for SB1 measurements.

Karst features, including fissures with brecciated infill penetrate up to 0.5m into underlying beds. A 5-27cm thick calcrete is present just below the surface. The calcrete is typically thicker in the underlying lows (10-27cm) compared to the highs (5-12cm). Grammer et al. (2000) observed calcrete measuring up to 1.5m thick. Geopetal fabrics are overturned and caliche pisoids are observed in thin-section samples collected directly underneath the surface in the lows. Overturned geopetals in the calcrete suggest pedoturbation occurred during the exposure (Grammer et al., 2000). Figure 34 shows the surface in outcrop.

The surface is interpreted as a subaerial exposure surface caused by a relative drop in sea level that exposed the algal facies (Goldhammer et al., 1991; Grammer et al., 2000; Pray and Wray, 1963; Choquette and Traut, 1963; and Roylance, 1990). It, therefore, is designated as Sequence Boundary 1 (SB1). The subaerial exposure surface and calcrete are traceable throughout the study area, attesting to its regional significance.

The karst landscape created by subaerial exposure was accentuated through erosion in low areas between the mounds that increased the original relief built by the underlying algal facies from 0.4-2.1m to 2.9-5.7m (Figure 32). This accentuation of topography was through surface erosion rather than cave collapse and creation of a doline landscape (Sauro, 2003). An overall 12.9-37.9m sea-level fall is calculated by adding the relative sea-level fall required to



**Figure 34.** Field view of Sequence Boundary 1 (SB1) highlighted in red. Karstic features and fissures are observed along surface. A calcrete is present directly under the sequence boundary. Erosional relief along the surface measures approximately 2.9-5.7m (person for scale).



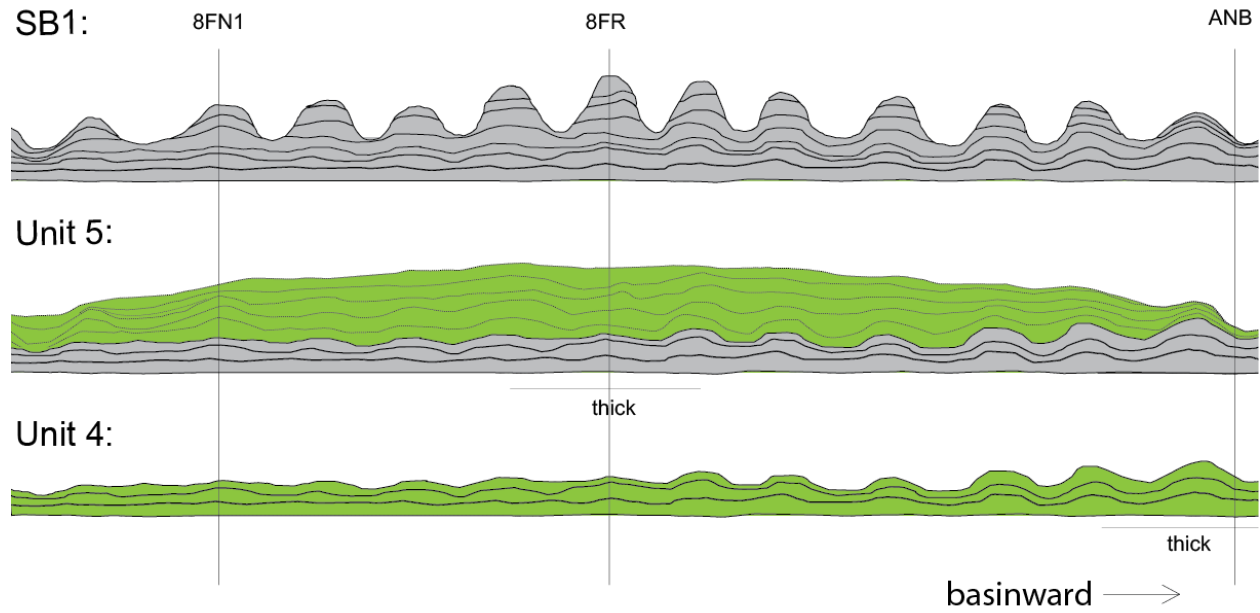
deposit Unit 4 after Unit 3 (4-19m), the relative rise in sea level between Unit 4 and 5 (1.8m), the relative-drop in sea level to expose Unit 5 (5-15m), and 5.7m of erosion.

Figure 35 illustrates the sequence of events of deposition of algal facies, exposure, and erosion.

### *Sequence 2*

**Unit 6.** Unit 6 directly overlies SB1 and is observed along the dip section from ANB to 8FR localities. It is not observed updip of the 8FR locality. Unit 6 consists of Lithofacies 6 (FP), Lithofacies 7 (SWP), and Lithofacies 8 (PM). It locally drapes the relief of the undulose sequence boundary, but thins on the highs and thickens in the lows (Figure 23). Regionally, Lithofacies 6 thins updip, measuring approximately 0.9m thick at ANB-ramp and 0.2m thick at 8FR2. Between 8FR and 8FN localities, Lithofacies 6 transitions into Lithofacies 7 and 8. The exact location where the transition occurs was removed by modern-day San Juan River erosion. Lithofacies 7 and 8 are discontinuous and onlap onto underlying topographic highs. This relationship is illustrated in cross-section B-B' (Figure 23). Lithofacies 7 directly overlies SB1 at updip HTF locality.

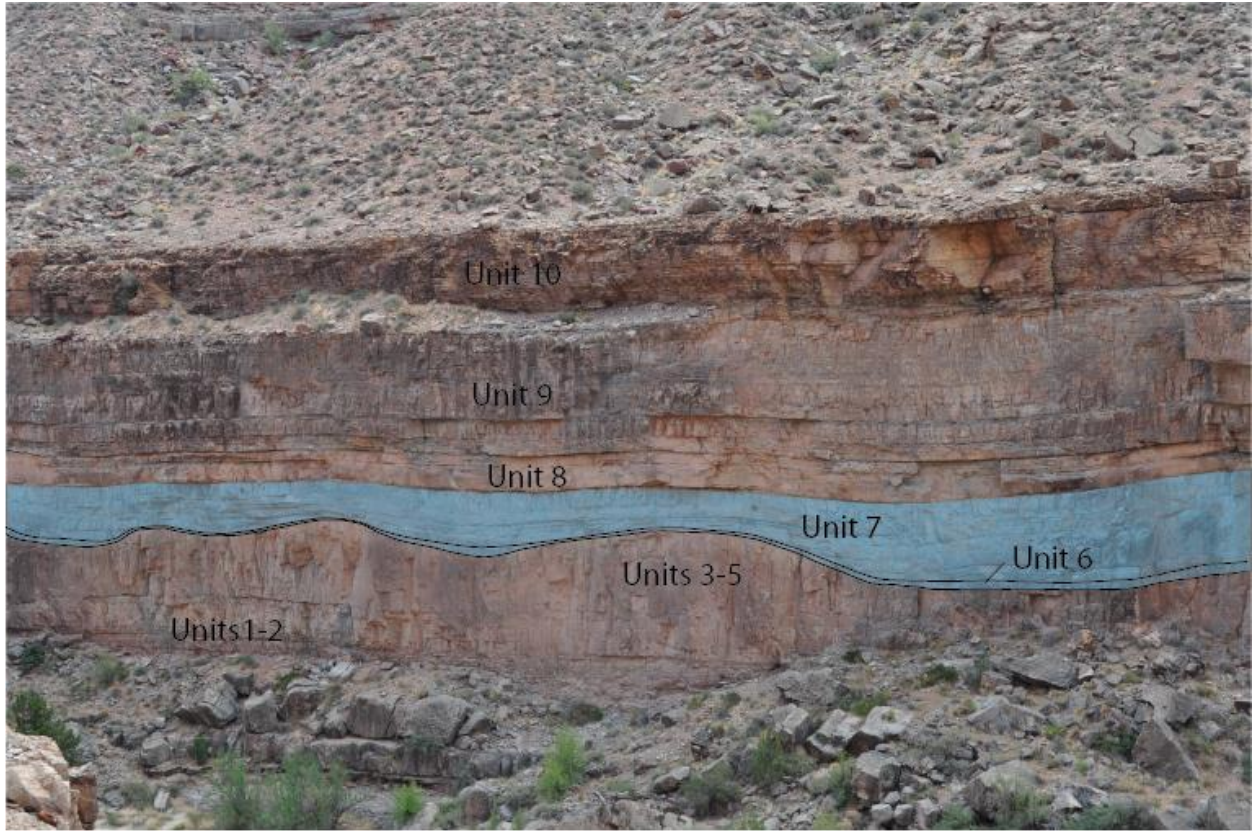
Lithofacies 7 is interpreted to be deposited at 20-25m depth. Unit 6 overlies a subaerial exposure surface that created approximately 2.9-5.7m relief, therefore, Unit 6 was deposited after a relative sea-level rise of 25.7-30.7m. The rise may have occurred rapidly, not depositing shallower-waterfacies stratigraphically below Lithofacies 6 at 8-Foot and ANB localities. Updip at the HTF location, Lithofacies 7 or Lithofacies 8 directly overlies SB1. This suggests that during the deposition of Lithofacies 6 (20-25m water depth) at 8-Foot and ANB localities, Lithofacies 7 and 8 (4-10m water depth) was being deposited updip.



**Figure 35.** Illustration of the geometries of Units 4 and 5 and resulting erosion during subaerial exposure. Individual units are highlighted in green and thick areas (optimum accumulation) are labeled. Solid lines are preserved contacts. Dotted lines are interpreted contacts spanning erosionally truncated gaps. The red line marks Sequence Boundary 1 (SB1). Measurement localities are labeled at the top of the figure.

**Unit 7.** Unit 7 consists of Lithofacies 7 (SWP) and Lithofacies 8 (PM). The base of Unit 7 is in sharp contact with underlying Unit 6. Lithofacies 7 beds are approximately 1m thick, and onlap onto the Unit 6-draped highs of the underlying sequence boundary (Figure 36). The discontinuous Lithofacies 7 beds cannot be confidently correlated, as they are limited to local paleotopographic lows. Lithofacies 7 beds show evidence of bioturbation and overturned geopetals; therefore, no internal bedding features can be used for correlation. Lithofacies 8 beds are observed only in the topographic lows where they onlap onto the highs. They typically are bounded above and below by Lithofacies 7 beds. Lithofacies 8 beds range in thickness from 1cm-50cm. Bed thicknesses, number of beds, and facies distribution of Lithofacies 7 and 8 are updip of 8-Foot and ANB localities, Unit 7 beds thin significantly at the 8FDN locality (Figure 24). Although the beds cannot be confidently traced due to cover, the number of beds present is consistent with beds observed at the nearby 8FN locality. The unit thicknesses change from approximately 5m (8FN) to 3.1m (8FDN). Overall, in this locality, the top of Unit 7 also shows 1.1m of erosional truncation. The underlying algal facies of Unit 4 also thins approximately 6m from 8FN to 8FDN. Throughout the study area, Unit 7 seems to be thickest where the algal facies of Units 3-5 are at their thickest.

The depositional depths of Lithofacies 7 and 8 are interpreted as 5-15m and 4-10m respectively. Unit 7 overlies Unit 6, suggesting a relative sea-level turnaround and fall of 10-21m. Reed (2014) documented increased diversity of foraminifera upsection, also indicating shallowing of relative sea-level. As sea level fell, Unit 7 likely filled the lows starting at the most updip locations and stepped basinward. Lithofacies 7 constituents were washed into topographic lows, suggested by the onlapping geometries and overturned geopetal fabrics. Lithofacies 8 beds were deposited in a depositional environment similar to Lithofacies 7 as



**Figure 36.** Annotated photomosaic near ANB locality illustrating Units 6 and 7 (blue) filling and smoothing underlying topography. Note that Units 6 and 7 thicken in the underlying topographic lows and thin on the topographic highs.

remnants of storm deposits or in locally protected or isolated areas occupied by few marine organisms where peloids collected over time.

Lithofacies 7 and 8 of Unit 7 appear to accumulate preferentially where the underlying algal facies is regionally thicker, providing a shallower environment for deposition.

Alternatively, Unit 7 may also appear to be thinning, but is actually eroded by the overlying Unit 8.

**Unit 8.** Unit 8 consists of Lithofacies 9 (QS), and is in sharp erosional contact with Unit 7. Local erosional relief of Unit 7 is greatest at 8FDN locality where underlying units are particularly thin measuring 3.5m thick at 8FDN, 1.3m thick at RCB, and 2.0m at HTF (Figure 24-26). Unit 8 fills and smoothes relief of underlying topography. Unit 8 is covered at ANB and 8FR localities. It pinches out on a paleotopographic high at the RCB locality (downdip) (Figure 37).

Goldhammer et al. (1991) and Grammer et al. (2000) interpreted Lithofacies 9 in Unit 8 as an eolian sandstone deposited after a relative sea-level fall. The sand was subsequently reworked during a transgression (Goldhammer et al., 1991; Grammer et al., 2000). In contrast to this interpretation, no moldic porosity, vugs, paleokarst, caliches, or diagenetic alteration indicative of exposure was observed beneath Unit 8 despite careful cm-scale stratigraphic sections and analysis in thin section.

The basinward thinning and pinching out of Lithofacies 9 supports the idea that the sand was land-sourced. The Paradox Basin was undergoing structural uplifts to the north, south, and west during the Pennsylvanian (Baars and Stevenson, 1981), and these uplifts could be sources for clastics for Lithofacies 9. The unit exhibits possible hummocky cross-stratification or planar bedding at the base that changes vertically to trough crossbedding, most notable at 8FDN.



**Figure 37.** Annotated photomosaic illustrating the pinch out of Unit 8 (orange) onto Unit 7 at the RCB locality.

Unit 8 is thickest at 8FDN immediately above an area where underlying units have thinned depositionally and through post depositional erosion. The lack of paleosols and paleokarst and the interpreted water depths for Unit 7 (4-10m) and Unit 8 (5-10m) suggests the erosion surface marking the contact between the units was likely marine in origin. The transition from Unit 7 to Unit 8 can be explained by a static or minor relative sea-level fall of less than 5m. Thickness variations were controlled by proximity to landward source and local paleotopography.

**Unit 9.** Unit 9 consists of Lithofacies 7 (SWP), Sublithofacies 7a (SWP-C), and Lithofacies 8 (PM) and is in sharp contact with underlying Unit 8. At ANB and Narrows localities, the 1m-thick basal bed consists of Sublithofacies 7a. The bed is not observed updip of ANB locality. Lithofacies 7 and 8 were deposited updip where Sublithofacies 7a is not present.

Moving stratigraphically upwards, beds of Lithofacies 7 and 8 overlie the basal bed. At the Narrows, RCB, and ANB localities, the lower portion of Unit 9 is dominated by thin beds (10-50cm thick) and the upper portion is dominated by thick beds (1-2m thick). Ten thin beds are present at the Narrows locality (downdip) and 3 beds are present at ANB locality (updip) (Figures 23 and 24). These beds are dominantly Lithofacies 7 exhibiting faint crossbedding. Discontinuous Lithofacies 8 beds, measuring 1-60cm thick, are typically bounded above and below by Lithofacies 7 and onlapping onto subtle underlying topographic highs. The thin beds pinch out and are absent updip of the ANB locality.

A laterally continuous 1m-thick bed consisting of Lithofacies 7 overlies the thin beds downdip. It is consistent in thickness and traceable from the Narrows to 8-Foot sections (Figures 23-25). It is not present at the HTF locality. The bed consists of 55% mud, significantly higher than other Lithofacies 7 beds in the study area, and is highly burrowed.

Overlying the 1m-thick bed in sharp contact, are 2 beds of Lithofacies 7, each measuring 2m thick. These beds are consistent in thickness and are present throughout the Narrows locality (downdip) and laterally continuous through 8-Foot localities (updip). One 2m-thick bed is present at HTF, although it is not clear if it is equivalent to downdip localities.

The 1m-thick bed, overlying the thin beds, is significantly muddier than the other beds consisting of Lithofacies 7, and laterally continuous throughout the 8-Foot and Narrows localities. Thus, this bed was likely deposited in comparatively calmer conditions, possibly due to minor relative sea-level rise within the depositional depth range of 5-10m. The bed is not present at the HTF locality and likely onlaps updip of the 8-Foot localities.

The two beds overlying the 1m-thick bed have comparatively less mud content. The cleaner facies suggests a slightly higher energy environment, possibly due to a minor relative sea-level fall within Lithofacies 7's depositional depth of 5-10m. One 2m bed is present in the most updip HTF locality. To correlate the bed present at HTF to a 2m bed present downdip, a relative sea-level change between HTF and the Narrows is greater than the constraints of the depositional environment's depth range. Therefore, the two beds at downdip localities likely onlap underlying beds and are not time correlative to the 2m-thick bed at HTF. Confidence in correlation from HTF to 8-Foot localities is low due to exposure limitations.

Considering the depositional depths of Unit 9 at downdip localities, the updip deposits of Unit 8 were likely exposed subaerially. Evidence of exposure was not directly observed at HTF, but this may have been due to inaccessibility.

**Unit 10.** Unit 10 consists of Lithofacies 10 (QSt), an eolian-sourced calcitic siltstone commonly referred to as "Old Yeller" due to its recognizable yellow color. Unit 10 is laterally



continuous throughout all localities, and measures approximately 7m thick at the Narrows locality to 6.8m at the HTF locality.

Unit 10 is in gradational contact with underlying Unit 9, and represents a transition from Lithofacies 7 (10-15m depth) to Lithofacies 10 (<5m depth). Relative sea level fell approximately 5-10m to deposit Unit 10. Units 9-10 in total, are less than 15m thick, therefore, sediments may have simply filled the remaining accommodation after the deposition of Lithofacies 7a (10-15m depth), with minor sea-level fluctuations. The upper contact of Lithofacies 10 (< 5m depth) is interpreted as Sequence Boundary 2 (SB2).

### *Summary*

Pennsylvanian paleotopography cannot be fully reconstructed due to differential subsidence of the Paradox basin during deposition. A quantitative sea-level curve cannot be established without an accurate paleotopographic reconstruction. A constant regional dip of 0.4 degrees calculated from Pennsylvanian isopachs (Goldhammer et al., 1991) produces unrealistic geometries and facies relationships. A dip of 0.1 was used to calculate relative sea-level changes. Relative sea-level changes were identified according to sequence stratigraphic relationships of depositional environments and their interpreted water depths.

The Lower Ismay zone of the Paradox Formation was deposited as two sequences. The basal sequence (S1) is composed of Units 1-5, showing evidence of a relative sea-level rise and fall with an internal flooding event. The sea level fell from a 50-100m depth to subaerial exposure and erosion of approximately 5.7m.

Unit 1 of S1 was deposited after a relative sea-level rise of 45-95m (PS1) resulting in an anoxic environment. Unit 2 represents a change in conditions from an anoxic to an aerobic

depositional environment during a relative sea-level fall of 30-80m. The relative sea level fell 0-15m to deposit Units 3-5.

Units 3-5 were deposited during an overall sea-level fall. Unit 3 is the most updip of the algal facies and was deposited first, relative to Units 4-5. A relative sea-level fall of 4-19m was required to deposit Unit 4, 10.9km downdip of Unit 3. An observable shift in the location of thick algal accumulations suggests a minor relative sea-level rise of approximately 1.8m occurred after Unit 4 to deposit Unit 5. Relative-sea level then continued to fall 10.7-20.7m to regionally expose and erode the algal facies up to 5.7m deep (SB1).

Sequence 2 (S2) consists of Units 6-10, showing evidence of an overall relative sea-level rise and fall. A flooding event of 25.7-30.7m occurred to deposit Unit 6, which draped and onlapped underlying relief. Relative sea level continued to fall 10-21m and deposited Unit 7. Unit 7 filled in the relief created by the erosion of underlying algal facies and draping of Unit 7. Individual beds of Unit 7 onlapped onto underlying topographic highs. Unit 8, a sand sourced from the southeast, was then deposited after a relative sea-level fall of less than 5m. It is underlain by an erosion surface. Unit 8 filled in the local lows in topography from the erosion and from underlying underlying units. Units 9-10 were deposited either by filling the remaining accommodation or through an overall sea-level fall of 10-15m.

Throughout the deposition of the Lower Ismay, building of depositional relief occurred during minor rises or stillstands during an overall relative sea-level fall (Units 3-5). Exposure and erosion (SB1) increased relief from 0.4-2.1m (built by algal facies) to 2.9-5.7m (erosional). The relief was then draped after a rise (Unit 6) and later filled and smoothed in by facies (Unit 7-8) deposited during a subsequent relative sea-level fall.

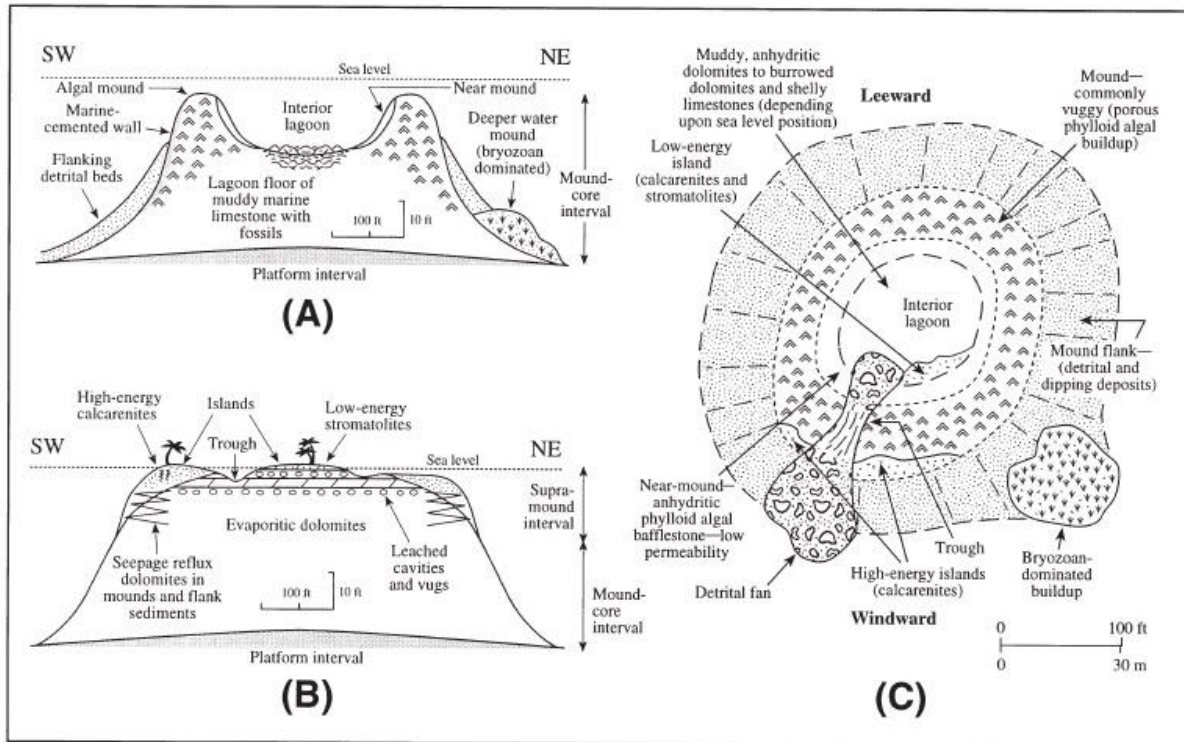
## DISCUSSION

### Algal Facies Development

The algal facies of the Lower Ismay consists of approximately 12 individual beds (A-L) that created puzzling geometries of regular thickening and thinning, resulting in undulose or mounded character. Lithofacies 4 (AB) and Lithofacies 5 (AP) make up the algal facies, with Lithofacies 5 typically associated with the topographic highs and Lithofacies 4 associated with the lows. The mechanism responsible for the algal growth or accumulation have been debated throughout the literature.

Montgomery et al. (1999) suggested the algal facies developed as circular mound accumulations with interior lagoons, similar to modern atolls (Figure 38A and C). Mud accumulated within the lagoons while algal and skeletal debris was deposited on the flanks of the mounds (Montgomery et al., 1999). Nearby mounds converge during late stages of mound building (Montgomery et al., 1999). During lowstands, the mounds were subaerially exposed and non-marine water modified mound porosity (Montgomery et al., 1999) (Figure 38B). Montgomery et al.'s (1999) model attempted to account for the appearance of muddier algal deposits in the lows between the mound crests. The mound morphology, however, seems unlike what the exposures show. The algae do not appear to preferentially make a ring geometry instead of a mound. Also, if mounds were to coalesce during late stages of mound-building, the internal bedding of the mounds would show downlapping and onlapping geometries within meters of topographic highs. The model also suggests that the packstone lithofacies would be found on the flanks, whereas the muddier bafflestone facies would be observed in the center of the mounds.

The algal facies in this study area show the opposite relationship. Overall, field observations do not support Montgomery et al.'s (1999) model of mounds with interior lagoons.



**Figure 38.** Depositional model for algal mounds suggested by Montgomery et al. (1999). A) Cross-section illustrating depositional setting during sea-level highstand during active building phase. B) Cross section showing processes affecting the mound during sea level lowstand. C) Plan view of idealized circular buildup with interior lagoon. (Montgomery et al., 1999).

Heckel and Cocke (1969) described the algal buildups of Kansas to have developed because of the baffling effect described by Harbaugh (1964). The algae kept pace with accommodation and continued to thrive into shallow water. They baffled currents, which allowed accumulation of high amounts of mud seen in Kansas algal buildups. In Kansas, the growth into shallow water was interpreted to have reduced nutrient replenishment, resulting in lower diversity of organisms, leaving mostly gastropods (Heckel and Cocke, 1969). The algal facies of the Lower Ismay zone must have undergone different conditions during deposition. The Lower Ismay zone algae likely continued to thrive into shallow water. The amount of mud observed in the stratigraphically higher areas is much less than that of the Kansas buildups.

Lithofacies 5, interpreted to be the shallowest of the algal facies, deposited in 5-10m water depth, has as little as 5% peloidal mud (samples show 5-40% peloidal mud). The algal facies in the study area also differ from those in Kansas in that they maintain a highly diverse invertebrate fauna. The Lower Ismay zone algal facies did not cause restriction of water circulation. Instead, the currents fragmented and sorted the *Ivanovia* leaves at the tops of the mounds and were associated with normal marine waters producing diverse invertebrate faunas.

The Lower Ismay algal facies is made up of at least 12 beds (beds A-L). Beds exhibit an undulose geometry where the algal facies created highs and lows with an average spacing of approximately 40m.

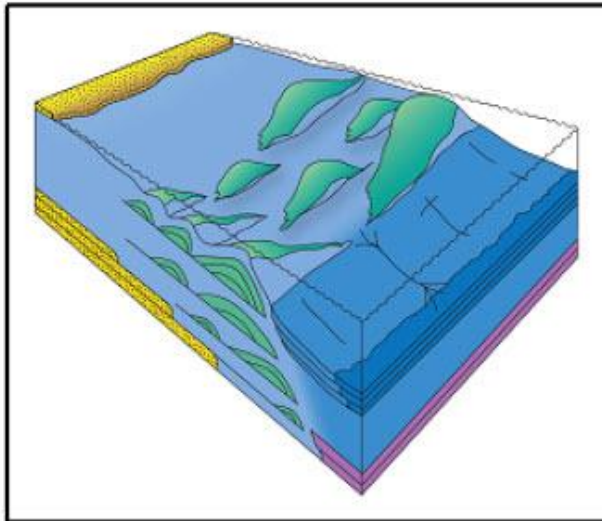
Heckel and Cocke (1969) attributed the near-sinusoidal geometries of the algal beds in Kansas to *oscillation of water* across algae that *at least perpetuated such structure originating from irregularities beneath the mound*. The troughs, or lows, were thought to have become minor channels that allowed water to move across the algal fields. The troughs accumulated sorted skeletal debris from the channels. In contrast, sorted skeletal debris in the Lower Ismay

algal facies is found on the highs. Thus, the interpretation of lows as the focus of currents is not applicable to the Lower Ismay zone.

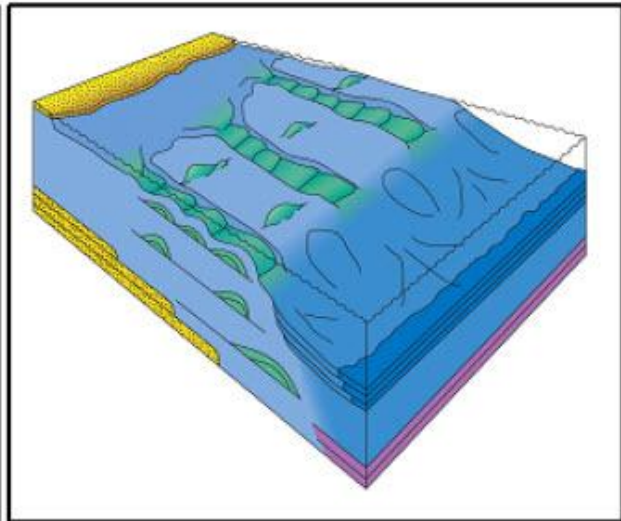
The Lower Ismay algal beds' undulose geometry appears too regular to have developed on random irregularities of the underlying topography. The beds also stack asymmetrically on the downdip, or northwest side, of the underlying highs. This stacking pattern suggests that the algal facies reacted to a current. Perhaps, after the algal growth initiated and began to build local topography, the local highs created backflows or eddies behind them, discouraging bafflestone deposition in the immediate lee of highs. The best sorting (Lithofacies 5) is observed on the local highs and is largely absent in the local lows (Lithofacies 4). The asymmetrical current could account for the regular spacing of the local highs and the basinward stacking geometries, but it does not account for the apparent circular morphologies of the mounds. Given a unidirectional current, one would expect mounds to have the geometry of bedforms.

Grammer and Ritter (2008) suggested that the algal facies are large "wave bedforms," or large dunes that accumulated in elongate narrow tidal channels that run perpendicular to strike. In the study area, the Lower Ismay algal facies pinches out at the 8FDN locality. The algal facies pinch out was previously interpreted as a strike-oriented pinch out, leading to the interpretation of the onlap of the algal facies against a tidal channel margin (Figure 39; Grammer and Ritter, 2008). Outcrop studies are inconclusive to determine if the algal facies were deposited in a tidal channel, due to the inability to trace the algal facies laterally because of restrictions of outcrop in the canyon. SB1 enhanced relief of the algal facies, which makes the mounds look like large bedforms, however, the algal facies lack crossbedding and other sedimentary structures to support the dune hypothesis. In addition, an analysis of mounds and troughs along strike and dip suggests that mounds were mostly circular in form, rather than

**Algal Mound – Patch Reefs**



**Algal Dunes/Sandwaves**



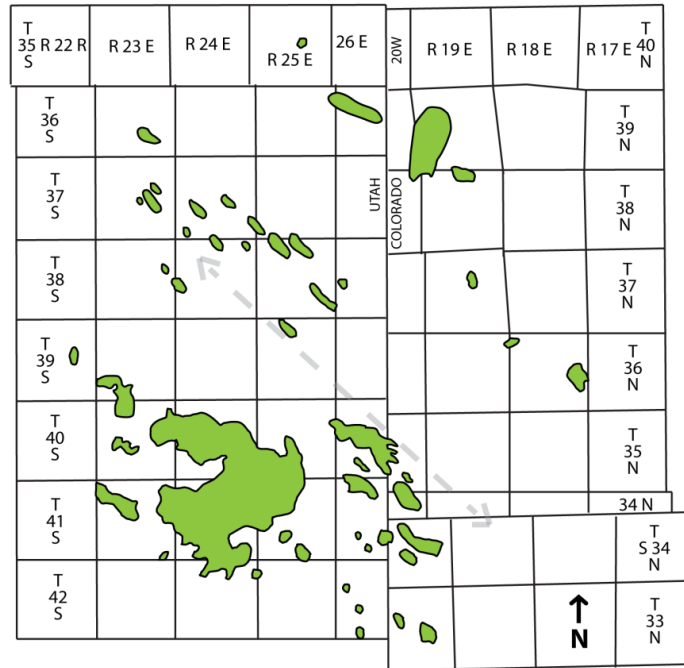
**Figure 39.** (Left) Typical mound depositional model compared to (right) algal dunes deposited in tidal channels model (Grammer and Ritter, 2008).

linear. The distribution of subsurface algal facies was documented through 3D seismic and well logs for hydrocarbon exploration in the Ismay and Desert Creek zones (McBride and Rebne, 1997; Chidsey and Eby, 2009; Weber et al., 2012). Isolated reservoirs are controlled by the northwest to southeast trending algal accumulations (Figure 40; Chidsey and Eby, 2009). Only the presence of the algal reservoirs was documented, not the orientation of mound crests. If the basin dip is true northeast, then the identified 8FDN algal facies pinch out occurred in the updip direction, not laterally against a tidal channel margin. These observations are inconsistent with Grammer and Ritter's (2008) tidal channel model.

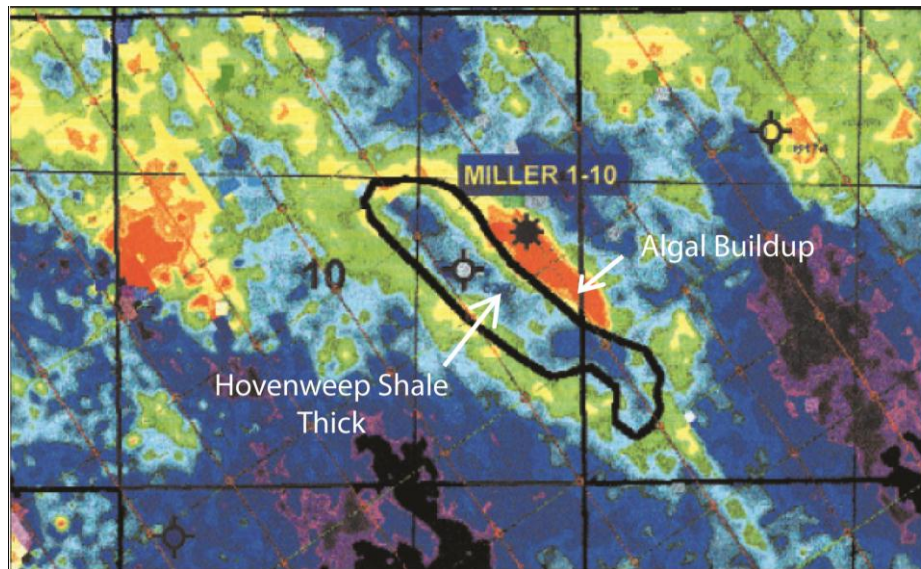
Chidsey and Eby (2009) suggest that the algal facies geometries are associated with dominantly northwest to southeast underlying local highs. Algal initiation was thought to occur on paleotopographic highs where sunlight was more favorable for algal growth. Possible hypotheses for the origin of paleotopographic highs include local mud bars (Goldhammer et al., 1991; Harbaugh, 1964), shallow-water deltaic deposits (Crowley, 1966), or other irregularities on the sea floor (Heckel and Cocke, 1969). More recent subsurface examples in Upper Ismay zone reservoirs show that algal buildups developed on the flanks of underlying thick mud accumulations (Figure 41; Coalson and DuChene, 2009; Loudon et al., 1999).

In summary, the algal facies of the Lower Ismay near the 8-Foot area developed in a paleotopographic low, overlapping on the flank of a thick mud accumulation. The 8FDN local algal facies pinch out is an example of an updip onlap onto the underlying accumulation. Although not extensively measured in this study, the updip algal facies at the Honaker Trail locality is isolated from downdip 8-Foot deposits, and could have developed in a similar environment. A dominantly landward current encouraged localized algal building resulting in organized undulose geometries and asymmetrical stacking of algal beds.





**Figure 40.** Distribution of algal facies reservoirs (green) in the Ismay and Desert Creek Formations (modified from Weber et al., 1995). The gray dashed arrow notes the northwest-southeast trend of the reservoirs.



**Figure 41.** Isochron of Upper Ismay. The thick Hovenweep Shale is outlined in black (approximately 14m thick). The position of the thick (red) algal buildup is on the flank of the underlying Hovenweep buildup. A dry hole was drilled off the structure of the thick algal buildup. A successful oil well was drilled through the thick algal buildup. Sections outlined for scale. Modified from Loudon et al., 1999.

### **Build-and-Fill Model of the Lower Ismay Zone**

Build-and-fill geometries have been identified in icehouse conditions of the Pennsylvanian, Permian, and Miocene (Mckirahan et al., 2003; Washburn and Franseen, 2003; Franseen and Goldstein, 2004; Emry et al., 2006; Franseen et al, 2007; Fairchild et al, 2008; Lipinski et al, 2008; Goldstein et al., 2013;). The systems exhibit thin carbonate or carbonate-siliciclastic sequences that maintain a consistent thickness over a significant lateral extent regardless of a complex internal architecture. These build-and-fill sequences occur in medial positions on broad shelves or ramps and in inner platform or lagoon positions. Each system consists of a relief-building phase, typically during a relative rise in sea level, and a relief-filling phase, typically during a relative fall in sea level.

The Lower Ismay aligns with many of the build-and-fill characteristics. The Lower Ismay is a zone within the Paradox Formation that consists of thin mixed carbonate-siliciclastic sequences that maintain consistent thicknesses despite complex geometries within individual sequences. The building and filling geometries within the sequences are observed at the intermediate position within the shelfal carbonates. The sequences significantly thicken basinward, off the shelf, due to halite formation deep within the basin.

At the outcrop scale, the Lower Ismay exhibits building and filling geometries. The build-and-fill model attributes much of the building-phase deposition to relative rise in sea level and a filling phase to a relative sea-level fall (McKirahan et al., 2003; Franseen et al., 2007a; Franseen and Goldstein, 2004; and Franseen and Goldstein, 2012). The Lower Ismay algal facies also build relief during small-scale relative sea-level rises and stillstands. These, however, occur during an overall relative sea-level fall. Algal facies also fill relief during relative sea-level falls. Unit 3 (updip) and Unit 4 (downdip) likely fill relief created by underlying highs during

the relative sea-level fall. Unit 5 builds relief during or after a rise. The algal facies built 0.4-2.1m of relief. After further sea-level fall, erosion during subaerial exposure increased relief up to 5.7m. After the next relative sea-level rise, Unit 6 draped and filled the erosional relief of the underlying algal facies. As sea level fell again, Unit 7 and 8 filled and smoothed the remaining relief.

The deposition of the Lower Ismay's building phase occurred during the transition from highstand (Unit 1) to lowstand (SB1), typical of the build-and-fill model's filling phase. The small-scale sea-level rise occurred during the longer term sea-level fall to allow mounds to build relief. This shows that small-scale sea-level changes superimposed on longer term trends add complexity to the build-and-fill model. The Lower Ismay demonstrates that the building phase is not constrained to long-term relative rise in sea level. A short-term relative rise in sea level during long term forced regression can also lead to building of relief.

The filling phase of Sequence 2 of the Lower Ismay was initiated after a relative sea-level rise of approximately 25-27m and deposition of Unit 6 on top of SB1. Reed (2014) suggested that the filling phase began after relative sea level fell to depths too shallow for algal development, and that shallower-water organisms filled in the lows with no exposure event between the two phases. SB1 is regionally extensive and truncates beds of Units 3-5, most notably in the lows. For SB1 to be continuous, the underlying facies had to have been subaerially exposed before the filling phase began, and thus, the Reed (2014) hypothesis is incorrect. Relative sea level then retreated, focusing currents and depositing Unit 7 in the lows. Beds of Unit 7 onlapped onto underlying highs and eventually filled in and smoothed the topography created earlier. Unit 8, a localized siliciclastic deposit sourced from the southwest, filled, eroded, and smoothed any remaining topographic disparities.

The exposed Lower Ismay zone along the modern-day San Juan River is another example of a build-and-fill sequence within the rock record. The Lower Ismay provides a complex depositional history that adds to our understanding of build-and-fill and shows that small-scale sea-level changes superimposed on longer term trends can lead to building and filling geometries. A short term relative rise in sea level can build relief during long-term forced regression.

### **Application**

The Lower Ismay zone not only furthers our understanding of build-and-fill models, it also provides an outcrop analog to nearby hydrocarbon reservoirs. The algal facies is a known reservoir in the Desert Creek and Ismay formations sourced by BLM-type shales (Grammer et al., 2000; Goldhammer et al., 1991; Chidsey et al., 1996a; Chidsey et al., 1996b; Choquette and Traut, 1963; Grammer and Ritter, 2008; Herrod et al., 1985; Montgomery et al., 1999; Peterson, 1966a; Peterson, 1966b; Peterson and Hite, 1969; McBride and Rebne, 1997). This study has shown that the reservoirs are laterally and vertically heterogeneous, as well as isolated. The previously discovered fields are conventional reservoirs with stratigraphic traps (Coalson and DeChene, 2009).

Identifying the location and extent of the algal facies is crucial for a successful well. McBride and Rebne (1997) attributed many exploration failures to “near misses” by drilling off structure. Offset well logs may aid in mapping, but would not be sufficient for mapping reservoirs. This study has shown that the algal facies can pinch out abruptly in the updip and downdip direction. A well may be drilled within meters of the reservoir. Since algal facies typically develop on the flanks of strike-oriented mud accumulations, successive wells should explore the flanks for a high chance of hydrocarbon production.

The best practice for identifying and mapping the location of a reservoir would be through the use of seismic. The lithologic contrast of the algal facies and overlying facies is enough to identify and algal complex on seismic lines. 2D seismic can identify reservoirs, but will not render the extent and shape of the complex.

Because the facies has high porosity and acts as a conventional reservoir, wells should be drilled in the thickest accumulation that is structurally higher than rest of the facies. Due to the lateral heterogeneity of the reservoirs, vertical wells would be the most appropriate exploitation method. Algal complexes are vertically stacked in other zones of the Paradox Formation, including Upper Ismay, Lower Desert Creek, and Upper Desert Creek. To maximize production potential, a wellbore could penetrate more than one algal complex if present.

## **CONCLUSIONS**

1. The Pennsylvanian (Desmoinesian) Lower Ismay zone of the Paradox Formation measures approximately 30m thick and consists of 10 lithofacies and 1 sublithofacies. The Lower Ismay is divided into 10 units.
2. Due to inconsistent asymmetrical basinward subsidence rates throughout the Pennsylvanian, the paleotopography could not be quantitatively reconstructed. A depositional dip of 0.1 degree was calculated based on observed facies relationships.
3. Two sequences are documented within the Lower Ismay zone. The lower sequence (Sequence 1) consists of Units 1-5. Units 1-2 represent a transition from a deep water, anoxic environment (50-100m depth) to an oxic, organism-rich environment (15-20m depth). Units 3-5 consist of algal facies deposited in 5-15m depth. Relative sea level fell 10.7-20.7m to expose and erode Sequence 1 (SB1).

4. Within the algal facies, an optimal accumulation zone that produced thicker areas within each bed is a marker that represents a specific depositional depth. A significant lateral shift in the optimal zone was used to identify relative sea-level changes within the algal facies. Unit 3 and 4 filled relief during relative sea-level fall. Unit 5 built relief after a minor sea-level rise.
5. Algal facies developed isolated complexes in subtle lows, possibly on flanks of underlying thick mud accumulations.
6. Algal beds alone created 0.4-2.1m of relief. Erosion during subaerial exposure truncated underlying algal beds and created up to 5.7m of relief.
7. The upper sequence (Sequence 2) consists of Units 6-10. A relative sea-level rise of 25.7m-30.7m deposited Unit 6, which draped the underlying erosional relief of SB1. During a relative sea-level fall, Unit 7 and 8 filled and smoothed the underlying topography. Units 9 and 10 represent the continued relative sea-level fall, or filling remaining accommodation to subaerial exposure (SB2).
8. The Lower Ismay zone exhibits characteristics of build-and-fill sequences. Thin, mixed carbonate-siliciclastic sequences maintain thickness laterally despite complex internal architecture that demonstrates a building phase and filling phase.
9. The Lower Ismay zone demonstrates that the building phase is not constrained to long-term relative rise in sea level. Building observed in Unit 5 occurred during a minor relative rise or standstill in sea level during a relative sea-level fall.
10. Filling occurred during Units 3 and 4 as relative sea level fell. Units 7 and 8 also filled relief during a relative sea-level fall.

11. The success of hydrocarbon exploitation of the algal facies reservoirs is dependent on drilling on the flank of underlying thicks or structure structure and in the thickest algal accumulations. This study has shown that the algal facies is vertically and horizontally heterogeneous. Algal facies can pinch out abruptly as seen at 8FDN.

## REFERENCES

- AMATEIS, L.J., and HALL, S., 2005, Drilling multilaterals in a complex carbonate reservoir, Aneth Field, Utah, *in* Coalson, E.B., Osmond, J.C., and Williams, E.T., eds., Innovative applications of petroleum technology in the Rocky Mountain area: Denver, Colorado, Rocky Mountain Association of Geologists, p. 125-136.
- BAARS, D.L., 1966, Pre-Pennsylvanian paleotectonics; key to basin evolution and petroleum occurrences in Paradox Basin, Utah and Colorado: AAPG Bulletin, v. 50, p. 2082-2111.
- BAARS, D.L., and STEVENSON, G.M., 1981, Tectonic evolution of the Paradox basin, Utah and Colorado, *in* Wiegand, D.L., ed., Geology of the Paradox Basin, Rocky Mountain Association of Geologists, 1981 Field Conference, p. 23-31.
- BAARS, D.L., and STEVENSON, G.M., 1982, Subtle stratigraphic traps in Paleozoic rocks of Paradox Basin, *in* Halbouty, M.T., ed., The Deliberate Search for the Subtle Trap, American Association of Petroleum Geologists, p. 131-158.
- BACCELLE, L., and BOSELLINI, A., 1965, Diagrammi per la stima visiva della composizione percentuale nelle rocce sedimentaire, Universita degli studi di Ferrara.
- BAGNOLD, R.A., 1941, The Physics of Blown Sand and Desert Dunes: London, Methuen and Company, 265 p.
- BOARDMAN, D.R., NESTELL, M.K., and KNOX, L.W., 1995, Depth-related microfaunal biofacies model for Late Carboniferous and Early Permian cyclothemic sedimentary sequences in Mid-Continent North America: Sequence Stratigraphy of the Mid-Continent, p. 93-118.
- BUSHINSKI, G.I., 1964, On shallow water origin of phosphorite sediments, Developments in Sedimentology: New York, Elsevier, p. 62-70.
- BUZAS, M.A., and GIBSON, T.G., 1969, Species diversity: benthonic Foraminifera in western North Atlantic: Science, v. 163, p. 72-75.
- BYERS, C.W., 1977, Biofacies patterns in euxinic basins: a general model, *in* Cook, H.E., and Enos, P., eds., Deep Water Carbonate Environments, Society of Economic Paleontologists and Mineralogists, Special Publication, p. 198-201.
- CHIDSEY, T.C. and EBY, D.E., 2009. Regional lithofacies trends in the Upper Ismay and Lower Desert Creek zones in the Blanding sub-basin of the Paradox Basin, Utah: Rocky Mountain Association of Geologists Special Publication, p. 436-470.
- CHIDSEY, T.C., EBY, D.E., and LORENZ, D.M., 1996a, Geological and reservoir characterization of small shallow-shelf fields, southern Paradox basin, Utah, *in* Huffman, A.C.J., Lund, W.R., and Godwin, L.H., eds., Geology and resources of the Paradox basin, Utah Geological Association Publication 25, p. 39-56.
- CHIDSEY, T.C., MORGAN, C., EBY, D.E., BRINTON, L., and HARTMAN, K., 1996b, Carbonate mound reservoirs in the Paradox Formation; an outcrop analogue along the San Juan River, southeastern Utah: AAPG Bulletin, v. 80, no. 6, p. 968.
- CHOQUETTE, P.W., and TRAUT, J.D., 1963, Pennsylvanian carbonate reservoirs, Ismay field, Utah and Colorado, *in* Bass, R.O., ed., Shelf Carbonates of the Paradox Basin, Four Corners Geological Society, 4th Field Conference Guidebook, p. 157-184.
- COALSON, E.B., and DUCHENE, H.R., 2009, Deposition of upper Ismay carbonate mounds, Blanding sub-basin of the Paradox Basin, Utah *in* Houston, et al., The Paradox Basin Revisited – New Developments in Petroleum Systems and Basin Analysis: RMAG Special Publication, p. 471-495.



- COE, A.L., 2003, The sedimentary record of sea-level change: Cambridge University Press, p. 1-288.
- CONNOLLY, W., LAMBERT, L., and STANTON, R., 1989, Paleocology of lower and middle Pennsylvanian (Middle Carboniferous) Chaetetes in North America: *Facies*, v. 20, p. 139-167.
- CROWLEY, D.J., 1996, Paleocology of an algal carbonate bank complex in the Late Pennsylvanian Wyandotte Formation of eastern Kansas: Unpub. Ph.D. dissert., Brown University, p. 1-182.
- DUNHAM, R.J., 1962, in *Classification of carbonate rocks according to depositional texture, Classification of carbonate rocks - a symposium*, American Association of Petroleum Geologists, *Memoir 1*, p. 108-121.
- EBERLI, G.P., SCHWAB, A.M., AND GRAMMER, G.M., 2000, Anatomy of Ismay algal fields; a comparison of outcrop and 3-D seismic data, in Homewood PW, E.G., ed., *Genetic stratigraphy on the exploration and production scales; case studies from the Upper Devonian of Alberta and the Pennsylvanian of the Paradox Basin*, Elf Exploration Production, p. 93-107.
- ELIAS, G.K., 1963, Habitat of Pennsylvanian algal bioherms, Four Corners area, in Bass, R.O., ed., *Shelf Carbonates of the Paradox Basin*, Four Corners Geological Society, 4th Field Conference Guidebook, p. 185-203.
- ELSTON, D.P., SHOEMAKER, E.M., and LANDIS, E.R., 1962, Uncompahgre front and salt anticline region of Paradox Basin, Colorado and Utah: *AAPG Bulletin*, v. 46, p. 1857-1878.
- FISCHER, A.G., 1961, Stratigraphic record of transgressing seas in light of sedimentation on Atlantic Coast of New Jersey: *AAPG Bulletin*, v. 45, p. 1656-1666.
- FLÜGEL, E., 2010, *Microfacies of carbonate rocks analysis, interpretation and application*: New York, Heidelberg.
- FLY, S.H.I., 1986, Depositional environments of Laborcita Formation (Wolfcampian), northern Sacramento Mountains, New Mexico: *American Association of Petroleum Geologists Bulletin*, v. 70, p. 344.
- FRANSEEN, E.K., and GOLDSTEIN, R.H., 2004, Build-and-fill sequences: Predictable patterns of creation and destruction of paleotopography in small-scale sequences, *Kansas Geological Survey Open-file Report 2004-16*, <http://www.kgs.ku.edu/PRS/publication/2004/AAPG/Build-and-Fill/index.html>.
- FRANSEEN, E., GOLDSTEIN, R., and MINZONI, M., 2007a, Build-and-fill sequences in carbonate systems: An emerging picture: *AAPG Annual Convention*, Long Beach, CA.
- FRANSEEN, E.K., GOLDSTEIN, R.H., and MINZONI, M., 2007b, Build-and-fill sequences in carbonate systems: An emerging picture: *AAPG Annual Convention*, Long Beach, CA.
- FRANSEEN, E.K., and GOLDSTEIN, R.H., 2012, Build-and-fill sequences in carbonate-dominated systems: Towards predictive models from global examples throughout the rock record: *KICC 2012 Annual Convention Abstracts Volume*, p. 23-28.
- GOLDHAMMER, R.K., OSWALD, E.J., and DUNN, P.A., 1991, Hierarchy of stratigraphic forcing; example from Middle Pennsylvanian shelf carbonates of the Paradox Basin, in Franseen, E.K., Watney, W.L., Kendall, G.C.St.C., and Ross, W., ed., *Sedimentary Modeling: Computer Simulations and Methods for Improved Parameter Definition*, *Kansas Geological Survey Bulletin*, p. 361-413.

- GOLDSTEIN, R.H., FRANSEEN, E.K., AND LIPINSKI, C.J., 2013. Topographic and sea level controls on oolite-microbialite-coralgal reef sequences: The terminal carbonate complex of southeast Spain: AAPG Bulletin, v. 97, no. 11, p. 1997-2034.
- GOODRICH, C.L., 2013. Digital Outcrop Model and Paleocology of the Eight-Foot Rapid Algal Field (Middle Pennsylvanian Lower Ismay Sequence), Paradox Basin, Utah: All Theses and Dissertations, Brigham Young University, paper 3830.
- GRAMMER, G.M., EBERLI, G.P., VAN BUCHEM, F.S.P., STEVENSON, G.M., and HOMEWOOD, P.W., 2000, Application of high resolution sequence stratigraphy in developing an exploration and production strategy for a mixed carbonate/siliciclastic system (Carboniferous) Paradox Basin, Utah, USA, *in* P.W., H., and G.P., E., eds., Genetic stratigraphy on the exploration and production scales; case studies from the Upper Devonian of Alberta and the Pennsylvanian of the Paradox Basin, Elf Exploration Production, Memoir 24, p. 30-69.
- GRAMMER, G.M., and RITTER, A.L., 2008, Phylloid algal mounds in the Paradox Basin U.S.A. - an alternative to the in situ constructional growth model?, *in* Swart, P.K., McKenzie, J., and Eberli, G.P., eds., Perspectives in Sedimentary Geology: A Tribute to the Career of Robert Nathan Ginsburg, International Association of Sedimentologists Special Publication 40, p. 239-254.
- HARBAUGH, J.W., 1959, Marine bank development in Plattsburg Limestone (Pennsylvanian), Neodesha-Fredonia area, Kansas: Kansas Geological Survey Bulletin 134, pt. 8, p. 289-331.
- HECKEL, P.H., 1977, Origin of phosphatic black shale facies in Pennsylvanian cyclothem of mid-continent North America: AAPG Bulletin, v. 61, p. 1045-1068.
- HECKEL, P.H., 1986, Sea-level curve for Pennsylvanian eustatic marine transgressive-regressive depositional cycles along midcontinent outcrop belt, North-America: Geology, v. 14, p. 330-334.
- HECKEL, P.H., and BAESEMANN, J.F., 1975, Environmental interpretation of conodont distribution in upper Pennsylvanian (Missourian) megacyclothem in eastern Kansas: American Association of Petroleum Geologists Bulletin, v. 59, no. 3, p. 486-509.
- HERROD, P.H., and GARDNER, P.S., 1988, Upper Ismay reservoir at Tin Cup Mesa field: Rocky Mountain Association of Geologists, 1988 Carbonate Symposium, p. 175-192.
- HERROD, P.H., ROYLANCE, M.H., and STRATHOUSE, E.C., 1985, Pennsylvanian phylloid algal mound production at Tin Cup Mesa field, Paradox Basin, Utah, *in* Longman, M.W., Shanley, K.W., Lindsay, R.F., and Eby, D.E., eds., Rocky Mountain Carbonate Reservoirs, Society of Economic Paleontologists and Mineralogists, Core Workshop 7, p. 409-446.
- HESSLER, R.R., and SANDERS, H.L., 1967, Faunal diversity in the deep-sea: Deep Sea Research, v. 14, p. 65-78.
- HILL, D., 1981, Coelenterata, Anthozoa, Subclass Rugosa and Tabulata, *in* Teichert, C., ed., Treatise on Invertebrate Paleontology, Coelenterata, Supplement 1 (Rugose and Tabulata), Part F: Boulder, Colorado and Lawrence, Kansas, Geological Society of America and the University of Kansas, p. 762.
- HITE, R.J., 1970, Shelf carbonate sedimentation controlled by salinity in the Paradox basin, southeast Utah, *in* Ron, J.L., and Dellwig, L.F., eds., Third Symposium on Salt, Northern Ohio Geologic Society, p. 48-66.

- IMMENHAUSER, A., 2009, Estimating palaeo-water depth from the physical rock record: *Earth-Science Reviews*, v. 96, p. 107-139.
- KAZAKOV, A.V., 1937, The phosphorite facies and the genesis of phosphorites, *Geological investigations of agricultural ores: Leningrad Science Institute, Fertilizers and Insecto-Fungicides Trans.*, no. 14, p. 95-113.
- KEARSLEY, L., 2014. *San Juan River Guide: Shiva Press.*, p. 1-96.
- LEHRMANN, D.J., and GOLDHAMMER, R.K., 1999, Secular variation in parasequence and facies stacking patterns of platform carbonates: A guide to application of stacking-patterns analysis in strata of diverse ages and settings, *in* Haris, P.M., Saller, A.H., and Simo, J.A., eds., *Advances in Sequence Stratigraphy: Application to Reservoirs, Outcrops and Models*, Special Publishers SEPM, 63, p. 187-225.
- LERAT, O., VAN BUCHEM, F.S.P., ESCHARD, R., GRAMMER, G.M., and HOMEWOOD, P.W., 2000, Facies distribution and control by accommodation within high-frequency cycles of the upper Ismay interval (Pennsylvanian, Paradox Basin, Utah), *in* Homewood, P.W.a.E., G.P., ed., *Genetic stratigraphy on the exploration and production scales; case studies from the Upper Devonian of Alberta and the Pennsylvanian of the Paradox Basin*, *Elf Exploration Production*, p. 71-91.
- LONGIARU, S., 1987, Visual comparators for estimating the degree of sorting from plane and thin sections: *Journal of Sedimentary Petrology*, v. 57, p. 792-794.
- LOUDEN, R.O., LEHMAN, D.D., JOHNSON, W.E., and EDWARDS, D.L., 1999, 3-D Seismic Data in Delineating Productive Ismay Algal Mounds in Southern Paradox Basin, Utah, *AAPG Explorer*.
- MCBRIDE, B, and REBNE, C.A., 2005. Use of 2-D and 3-D seismic data to reduce drilling risk, Ismay algal-mound play, Southern Paradox Basin: *Rocky Mountain Association of Geologists*, p. 93-100.
- MCKIRAHAN, J.R., GOLDSTEIN, R.H., and FRANSEEN, E.K., 2003, Build-and-fill sequence; how subtle paleotopography affects 3-D heterogeneity of potential reservoir facies, *in* Ahr, W.M., Harris, P.M., Morgan, W.A., Somerville, I.D., and Stanton, R.J.J., eds., *Permo-Carboniferous Carbonate Platforms and Reefs*, SEPM Special Publication No. 78 and AAPG Memoir 83, p. 95-114.
- MONTGOMERY, S.L., CHIDSEY, T.C., EBY, D.E., LORENZ, D.M., and CULHAM, W.E., 1999, Pennsylvanian carbonate buildups, paradox basin: Increasing reserves in heterogeneous, shallow-shelf reservoirs: *Aapg Bulletin-American Association of Petroleum Geologists*, v. 83, p. 193-210.
- OHLEN, H.R., and MCINTYRE, L.B., 1965, Stratigraphy and tectonic features of Paradox Basin, Four Corners area: *AAPG Bulletin*, v. 49, p. 2020-2040.
- PETERSON, J.A., 1966a, Genesis and diagenesis of Paradox Basin carbonate moiund reservoirs, *in* Symposium on recently developed geologic principles and sedimentation of the Permo-Pennsylvanian of the Rocky Mountains: Casper, Wyoming Geological Association, 20th Annual Conference, p. 67-86.
- PETERSON, J.A., 1966b, Stratigraphic vs. structural controls on carbonate-mound hydrocarbon accumulation, Aneth area, Paradox Basin: *AAPG Bulletin*, v. 50, p. 2068-2081.
- PETERSON, J.A., and HITE, R.J., 1969, Pennsylvanian evaporite-carbonate cycles and their relation to petroleum occurrence, southern Rocky Mountains: *AAPG Bulletin*, v. 53, p. 884-908.

- PICARD, M.D., and BROWN, B.R., 1961, Revised lower Paradox member (Pennsylvanian) cross section in Four Corners region; correction to 'Geology of Pennsylvanian gas in Four Corners region' by B. R. Brown and others (1960): AAPG Bulletin, v. 45, p. 1578-1579.
- PRAY, L.C., and WRAY, J.L., 1963, Shelf Carbonates of the Paradox Basin, *in* Bass, R.O., ed., 4th Field Conference Guidebook, Four Corners Geological Society, p. 204-234
- PYE, K., and TSOAR, H., 1987, The mechanics and geological implications of dust transport and deposition in deserts, with particular reference to loess formation and dune sand diagenesis in the northern Negev, Israel, *in* Rostick, L.E., and Reid, I., eds., Desert Sediments; Ancient and Modern, Geological Society of London, Special Publication 35, p. 139-156.
- REED, L.H., 2014, Build-and-fill development of Lower Ismay (Middle Pennsylvanian Paradox Formation) Phylloid-Algal Mounds of the Paradox Basin, Southeastern Utah: All Theses and Dissertations, Brigham Young University, paper 5569.
- RETALLACK, G.J., 2001, Soils of the Past: An Introduction to Paleopedology, Wiley-Blackwell, 512 p.
- RITTER, S.M., BARRICK, J.E., and SKINNER, M.R., 2002, Conodont sequence biostratigraphy of the hermosa group (Pennsylvanian) at Honaker Trail, Paradox basin, Utah: Journal of Paleontology, v. 76, p. 495-517.
- ROYLANCE, M.H., 1990, Depositional and diagenetic history of a Pennsylvanian algal-mound complex: Bug and Papoose Canyone fields, Paradox Basin, Utah and Colorado: American Association of Petroleum Geologists Bulletin, v. 74, no. 7, p. 1087-1099.
- SARG, J.F., 1988, Carbonate sequence stratigraphy, sea-level changes - an integrated approach, The Society of Economic Paleontologists and Mineralogists, p. 155-189.
- SAURO, U., 2003. Doline and sinkholes: Aspects of evolution and problems of classification: Università degli studi di Padova, p. 41-52.
- SCHLAGER, W., 2005, Carbonate sedimentology and sequence stratigraphy: Society for Sedimentary Geology, no. 8, p. 83-145.
- SCHOLLE, P.A., and ULMER-SCHOLLE, D.S., 2003, A color guide to the petrography of carbonate rocks: grains, textures, porosity, diagenesis, v. 77, American Association of Petroleum Geologists, 474 p.
- SHINN, E.A., STEINEN, R.P., DILL, R.F., and MAJOR, R., 1993, Lime-mud layers in high-energy tidal channels: A record of hurricane deposition: Geology, v. 21, p. 603-606.
- SHIPP, C.R., 1984, Lime-Bedforms and depositional sedimentary structures of a barred nearshore system, Eastern Long Island, New York: Developments in Sedimentology, v. 39, p. 235-259.
- SOREGHAN, G.S., KELLER, G.R., GILBERT, M.C., CHASE, C.G., and SWEET, D.E., 2012, Load-induced subsidence of the Ancestral Rocky Mountains recorded by preservation of Permian landscapes: Geosphere, v. 8, p. 654-668.
- STEVENSON, G.M., AND BAARS, D.L., 1984, Paradox Basin; a model pull-apart basin of Pennsylvanian age: AAPG Bulletin, v. 7, p. 950-951.
- TUCKER, M.E., 2009. Sedimentary petrology: An introduction to the origin of sedimentary rocks: John Wiley & Sons, 272 p.
- UTAH OIL AND GAS., c2014. Utah: State of Utah; [Accessed 2015 Jan 20]. <http://oilgas.ogm.utah.gov/>.

- VAN WAGONER, J.C., MITCHUM, R.M., CAMPION, K.M., and RAHMANIAN, V.D., 1990, Siliciclastic sequence stratigraphy in well logs, cores, and outcrops: Tulsa, American Association of Petroleum Geologists.
- VON BITTER, P.H., 1972, Environmental control of conodont distribution in the Shawnee Group (Upper Pennsylvanian) of eastern Kansas: The University of Kansas Paleontological Contributions: Article 59, p. 105.
- WEBER, L.J., SARG, J.F., AND WRIGHT, F.M., 1995. Sequence stratigraphy and reservoir delineation of the middle Pennsylvanian (Desmoinesian), Paradox Basin and Aneth Field, Southwestern USA: Society for Sedimentary Geology, p. 1-16.
- WEST, R.R., 2011, Hypercalcified Chaetetid-type porifera (Demospongiae): Treatise on Invertebrate Paleontology, Part E, Revised, p. 1-24.
- WRAY, J.L., 1964, Archaeolithophyllum, an abundant calcareous algae in limestones of the Lansing Group (Pennsylvanian), southeastern Kansas: Kansas Geological Survey Bulletin 170, part 1, p. 1-13.

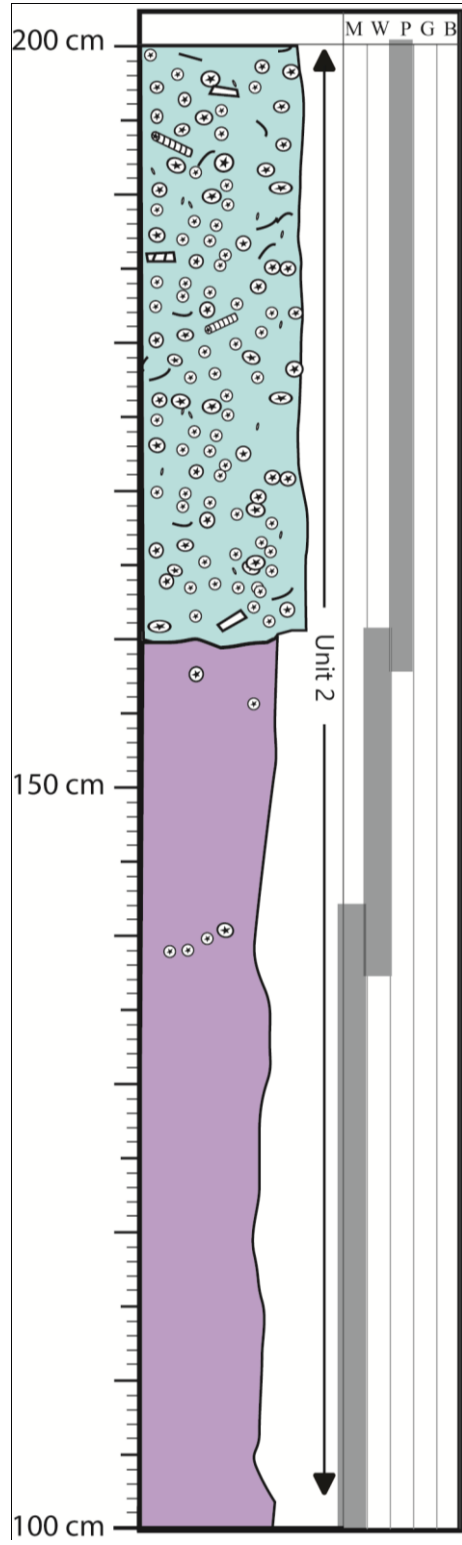
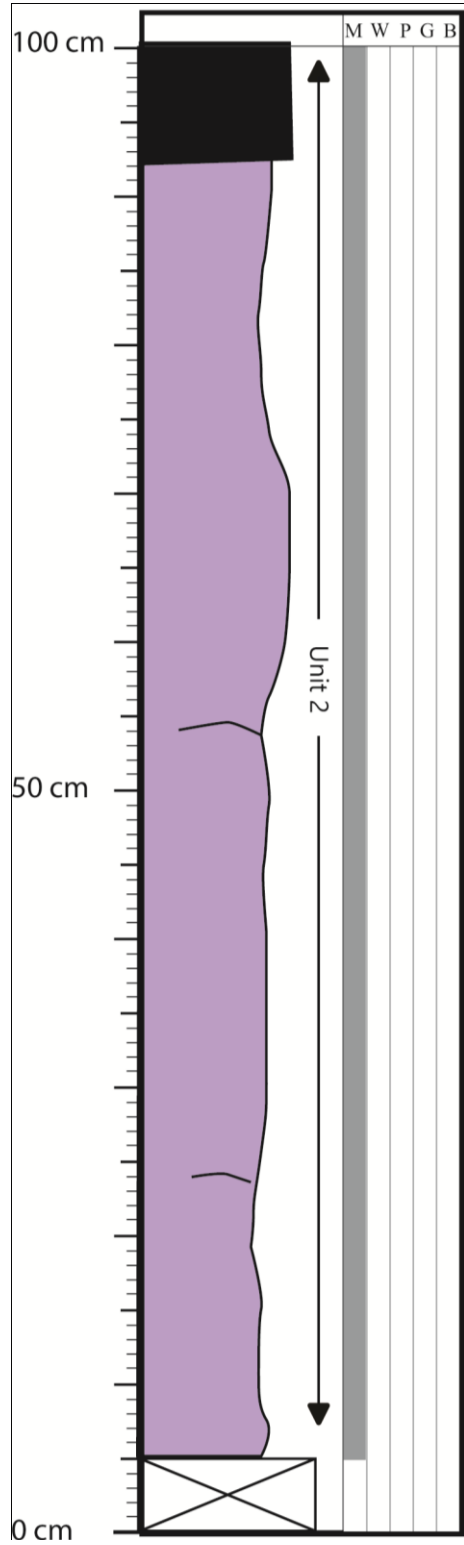
## **Appendix I**

### **Stratigraphic Sections**

Stratigraphic sections used to construct cross-sections shown in Figures 23-27, ordered alphabetically. See Figure 22 for map of stratigraphic section locations. See the following table for detailed locations. Sample names and locations are noted on the sections.

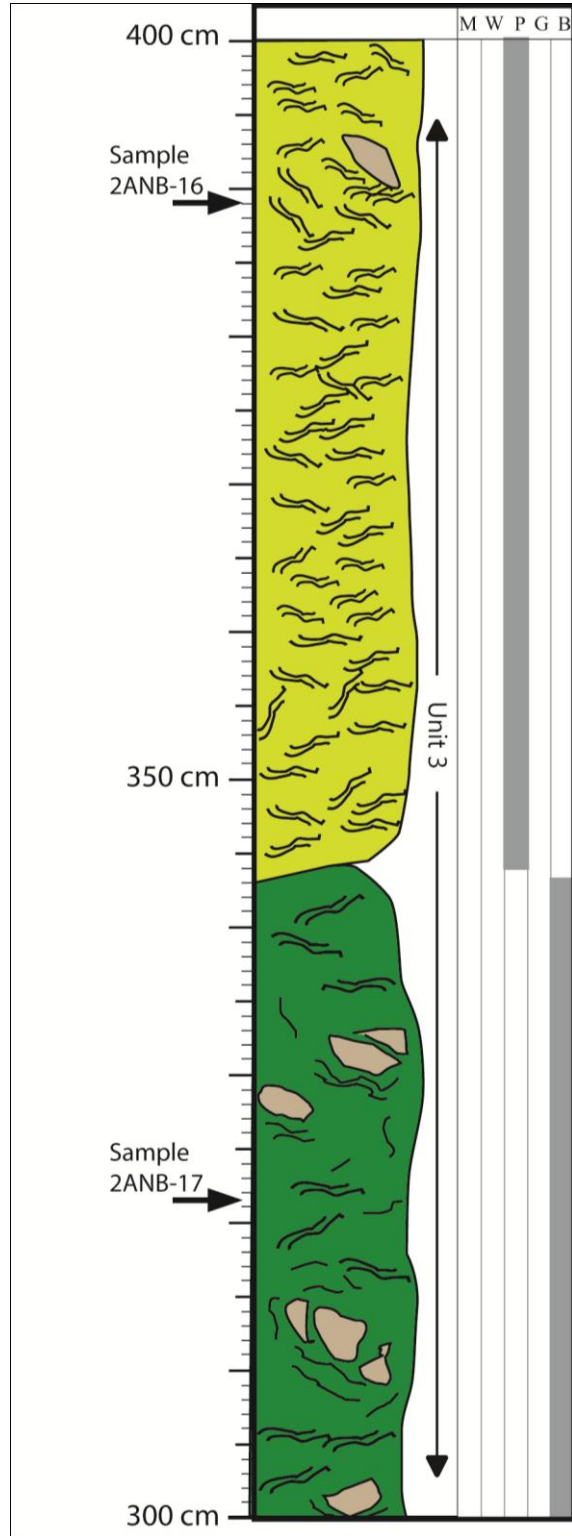
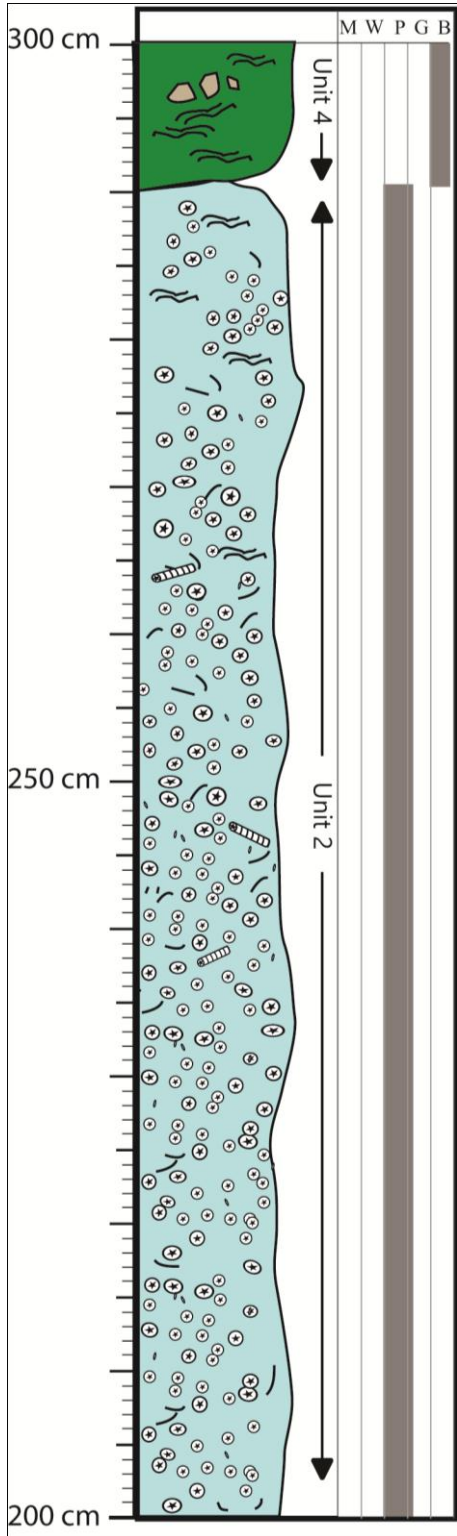
Stratigraphic Section	Latitude	Longitude	Elevation	River Mile*	Comment
<i>8-Foot Rappel</i>					
8FR1	37°10'58.64"N	109°47'04.77"W	4177 ft	17.25	Thicknesses only
8FR2	37°10'58.48"N	109°47'05.24"W	4186 ft	17.25	Thicknesses only
8FR3	37°10'58.34"N	109°47'04.90"W	4181 ft	17.25	Thicknesses only
8FR4	37°10'58.24"N	109°47'06.35"W	4185 ft	17.25	Thicknesses only
<i>8-Foot Drainage Navajo</i>					
8FDN	37°10'48.34"N	109°47'14.72"W	4423 ft	17.25	
<i>8-Foot Narrows</i>					
8FN1	37°11'00.25"N	109°47'12.33"W	4247 ft	17.25	
8FN2	37°11'01.30"N	109°47'12.55"W	4256 ft	17.25	
8FN3	37°11'13.24"N	109°47'8.76"W	4216 ft	17.5	
8FN4	37°11'12.07"N	109°47'8.69"W	4216 ft	17.5	
8FN5	37°11'10.63"N	109°47'8.49"W	4214 ft	17.5	
<i>Alligator Nose Bend</i>					
ANBR	37°10'56.93"N	109°46'31.82"W	4182 ft	16.75	
ANBL	37°10'58.52"N	109°46'34.09"W	4919 ft	16.75	
ANB-Up	37°10'57.93"N	109°46'33.36"W	4194 ft	16.75	
ANB-Ramp	37°10'57.84"N	109°46'33.68"W	4170 ft	16.75	
ANB-yeller	37°11'00.04"N	109°46'33.36"W	4212 ft	16.75	Thicknesses only
2ANB1	37°11'2.68"N	109°46'38.60"W	4182 ft	16.75	
2ANB2	37°10'58.23"N	109°46'34.49"W	4182 ft	16.75	
2ANB3	37°11'7.03"N	109°46'43.02"W	4182 ft	16.75	
2ANB4	37°10'57.03"N	109°46'32.44"W	4167 ft	16.75	
<i>Honaker Trail Fin</i>					
HTF	37°11'15.35"N	109°57'29.09"W	4444 ft	45	
<i>Narrows</i>					
N2	37°11'13.44"N	109°46'9.01"W	4166 ft	14.5	
N3	37°11'14.12"N	109°46'11.09"W	4166 ft	14.5	
N4	37°11'17.65"N	109°46'15.89"W	4167 ft	14	
N5	37°11'18.06"N	109°46'16.26"W	4167 ft	14	
N6	37°11'17.19"N	109°46'15.42"W	4167 ft	14	
N7	37°11'23.35"N	109°46'17.80"W	4190 ft	13.5	
<i>Rock Cairn Bend</i>					
RCB	37°11'17.65"N	109°46'54.63"W	4167 ft	16	
*River miles were approximated to the quarter mile using Kearsley (2014) river guide maps.					

Stratigraphic Section 2ANB2  
 Location: N37°10'58.23" W109°46'34.49"



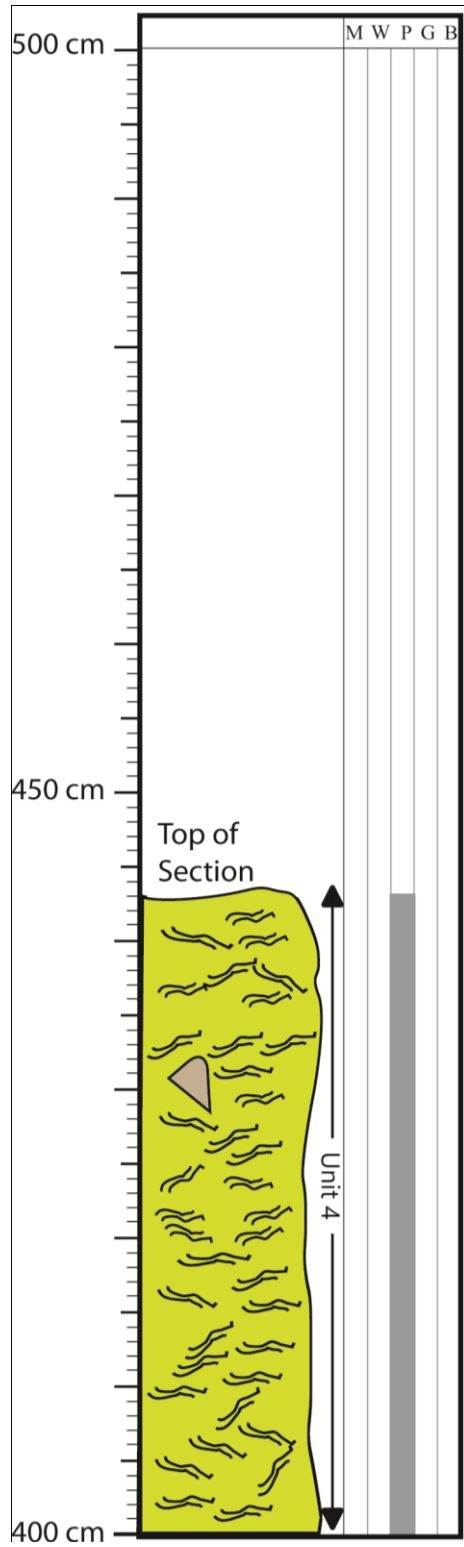


Stratigraphic Section 2ANB2 Continued  
Location: N37°10'58.23" W109°46'34.49"

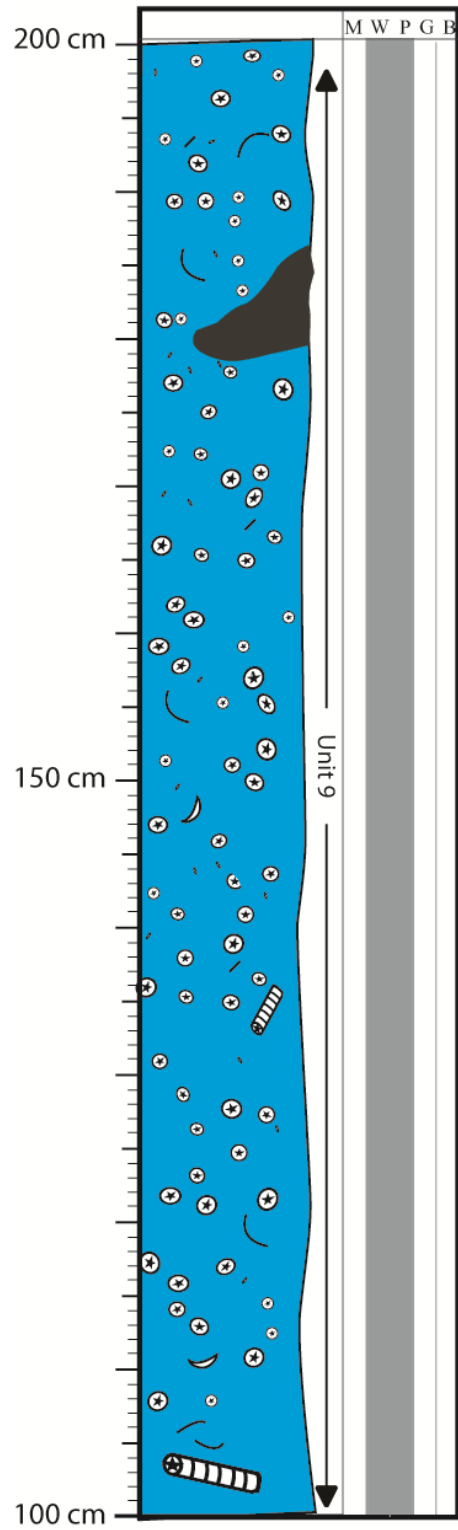
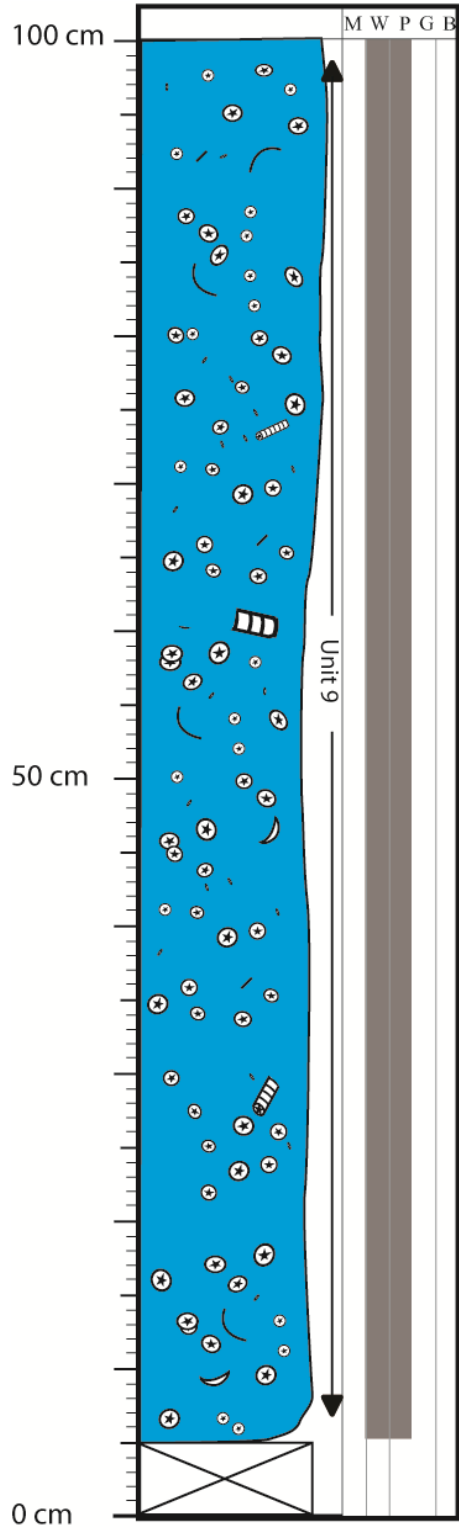


# Stratigraphic Section 2ANB2 Continued

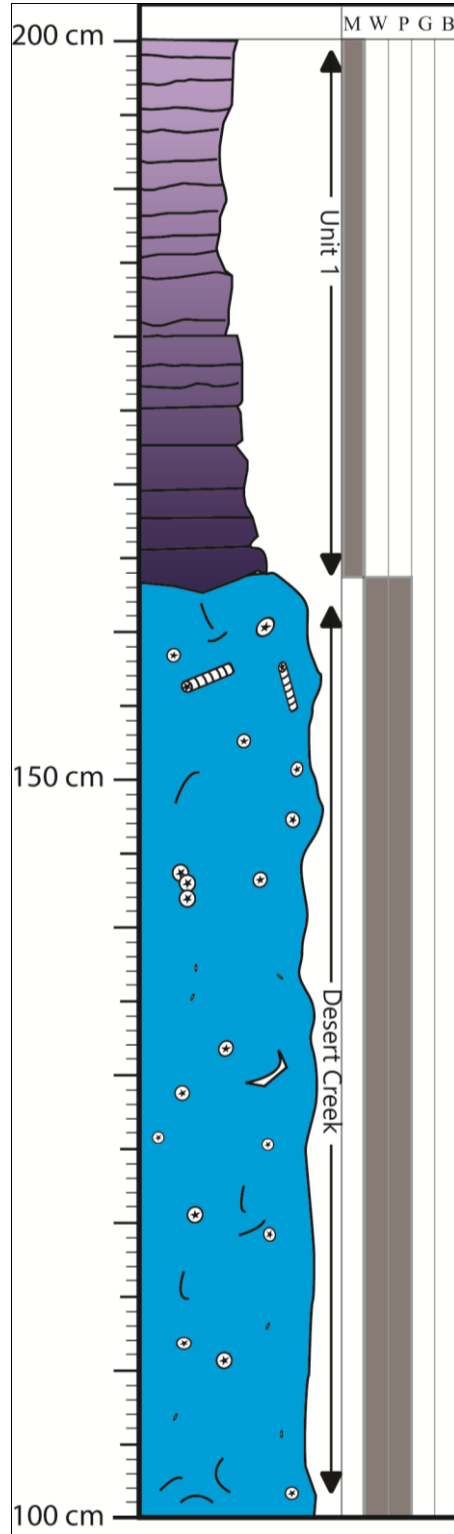
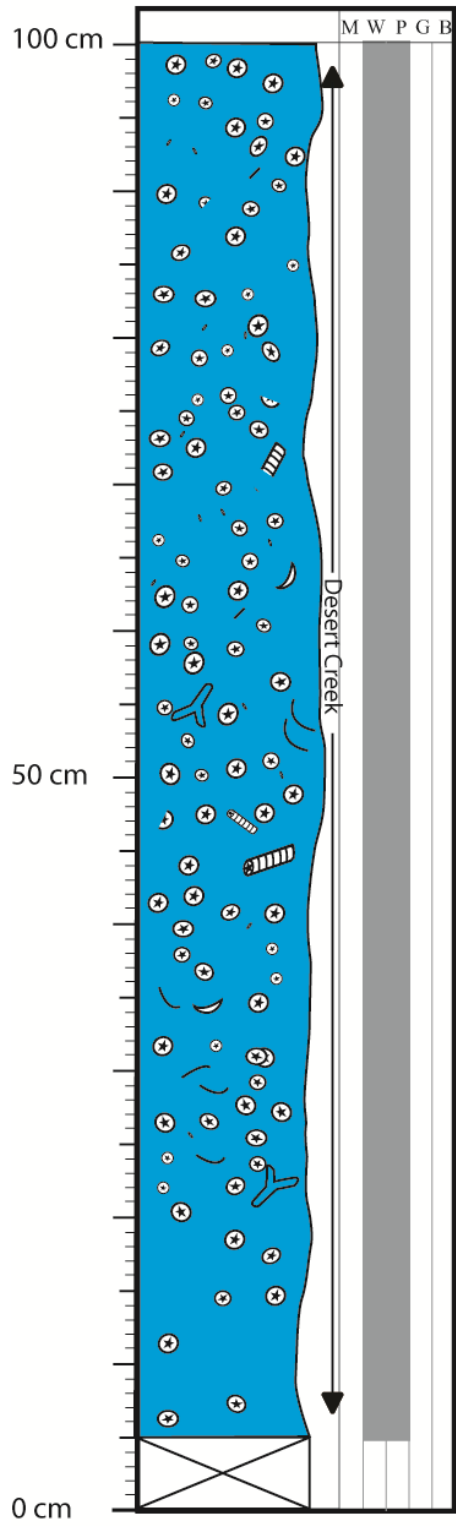
Location: N37°10'58.23" W109°46'34.49"



Stratigraphic Section 2ANB3  
Location: N37°11'7.03" W109°46'43.02"

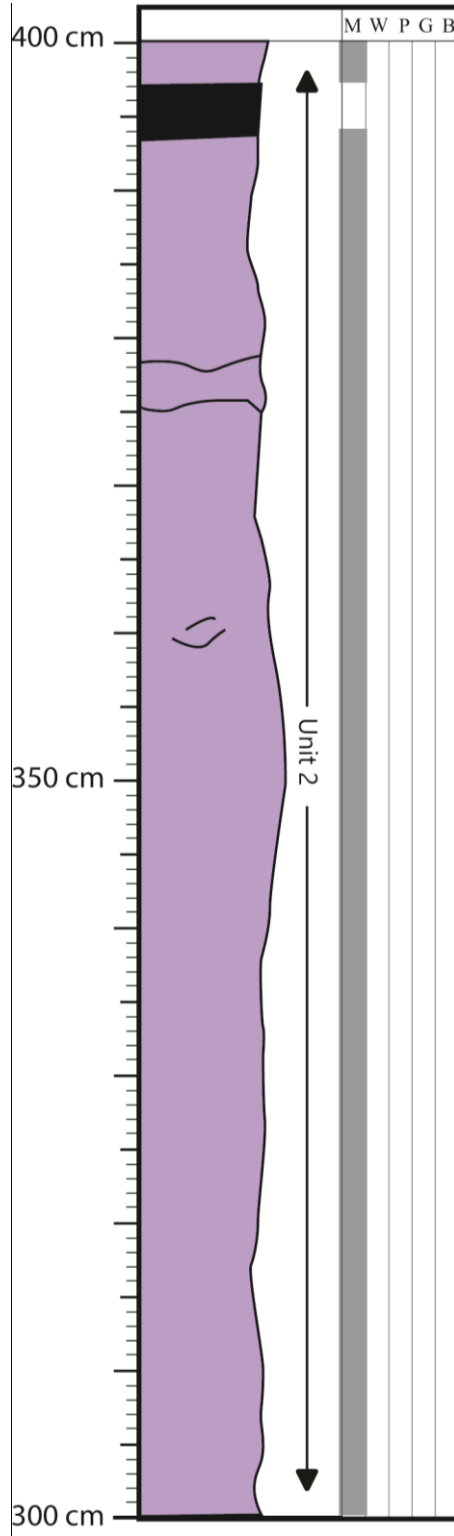
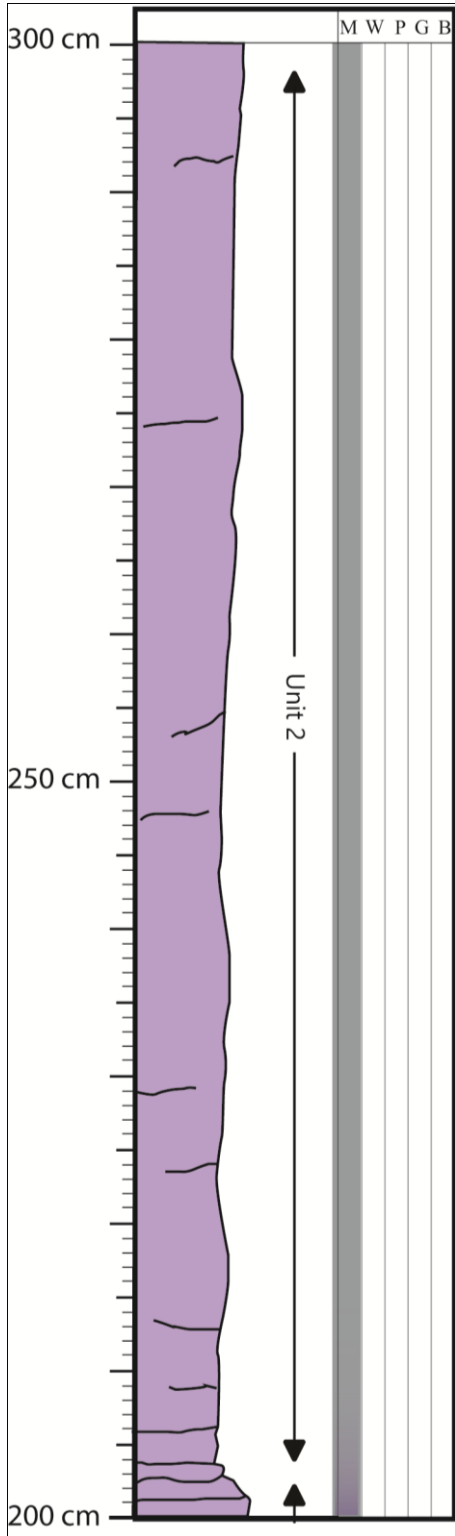


Stratigraphic Section 2ANB4  
Location: N37°10'57.03" W109°46'32.44"



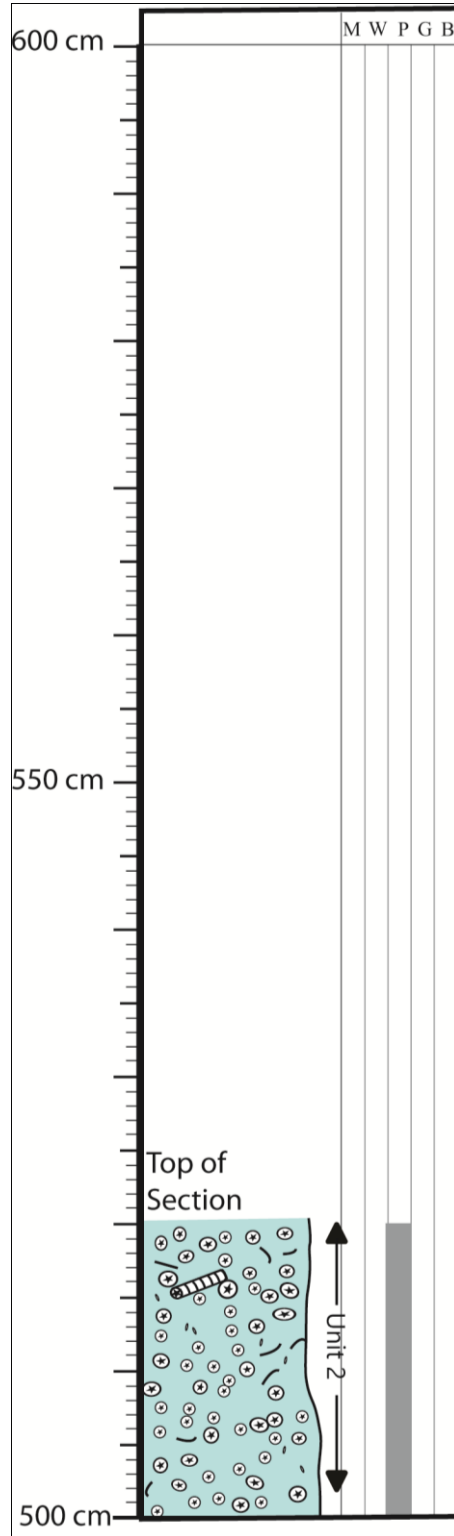
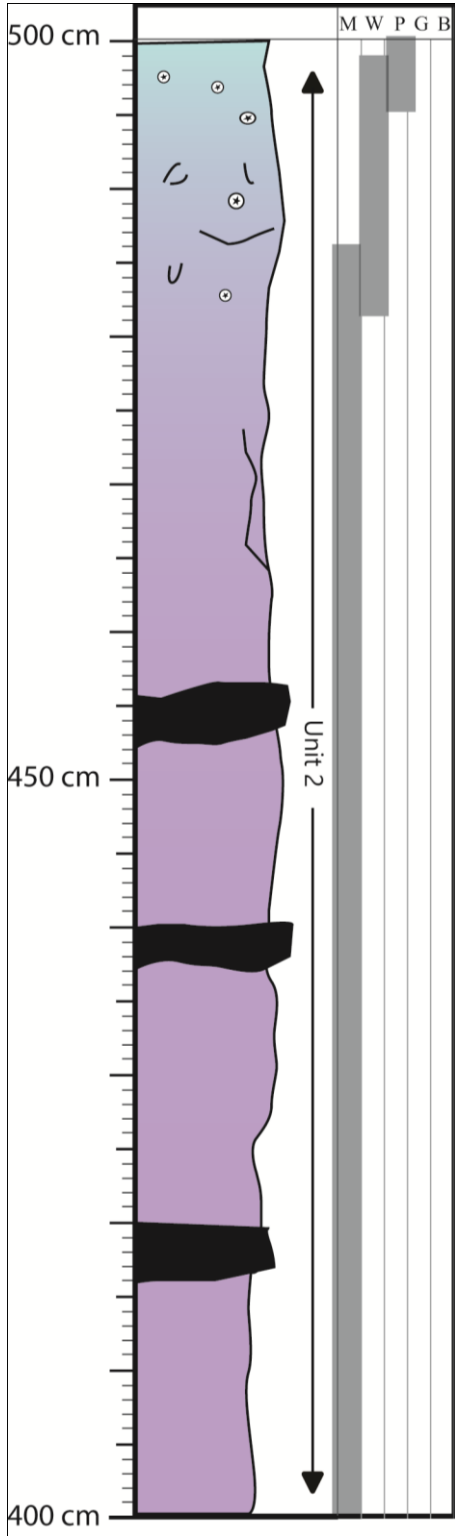
# Stratigraphic Section 2ANB4 Continued

Location: N37°10'57.03" W109°46'32.44"



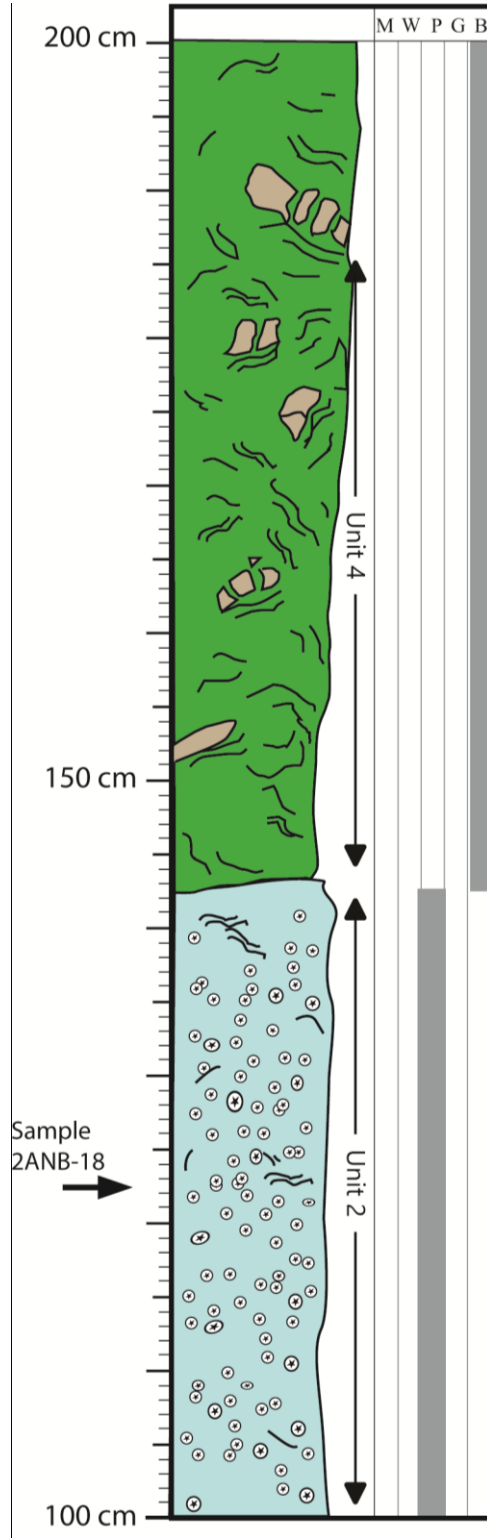
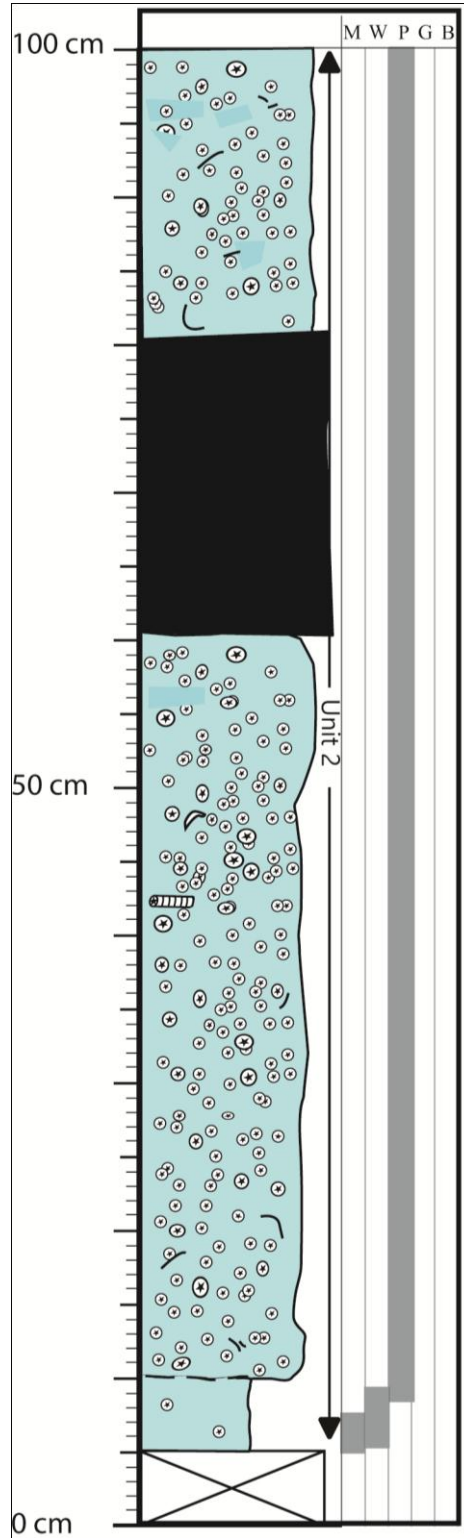
# Stratigraphic Section 2ANB4 Continued

Location: N37°10'57.03" W109°46'32.44"



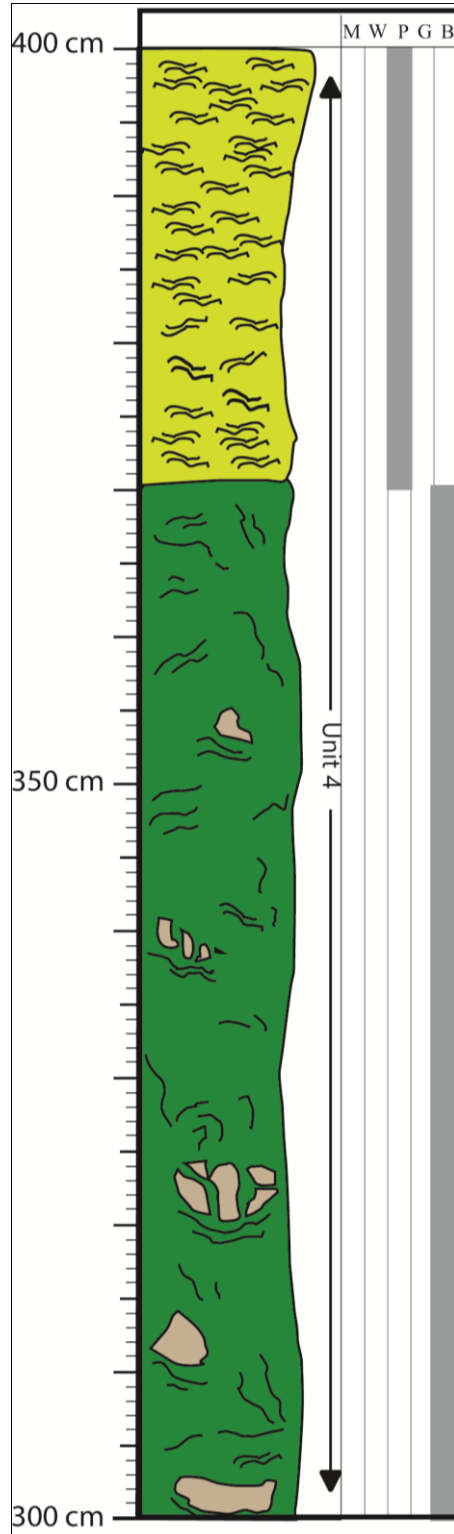
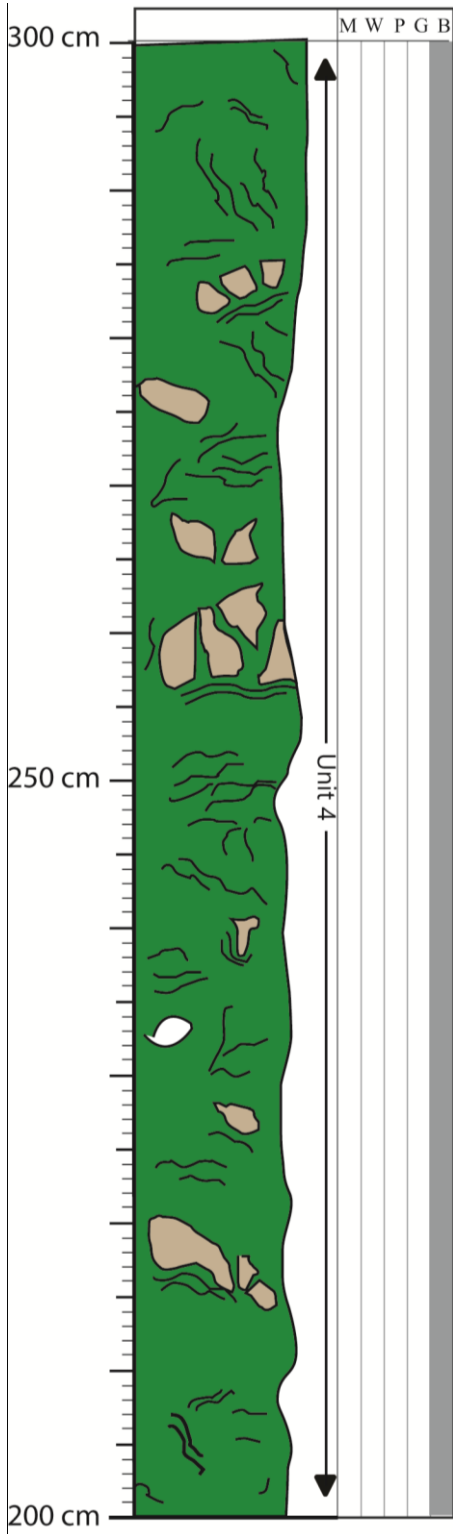
# Stratigraphic Section 2ANB-Ramp

Location: N37°10'57.84" W109°46'33.68"



# Stratigraphic Section 2ANB-Ramp Continued

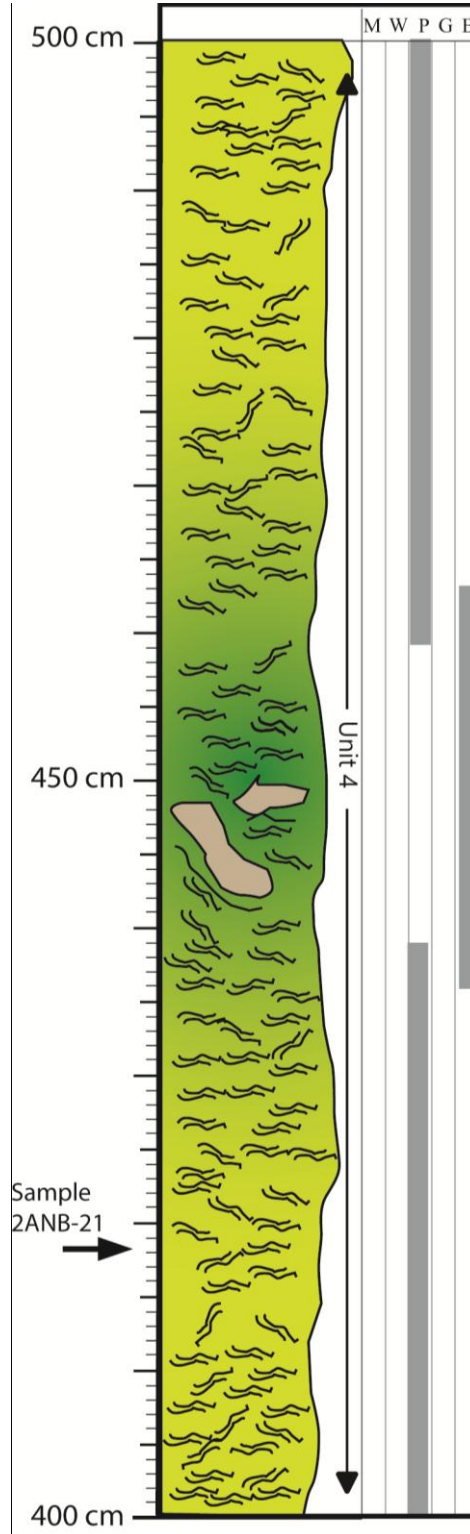
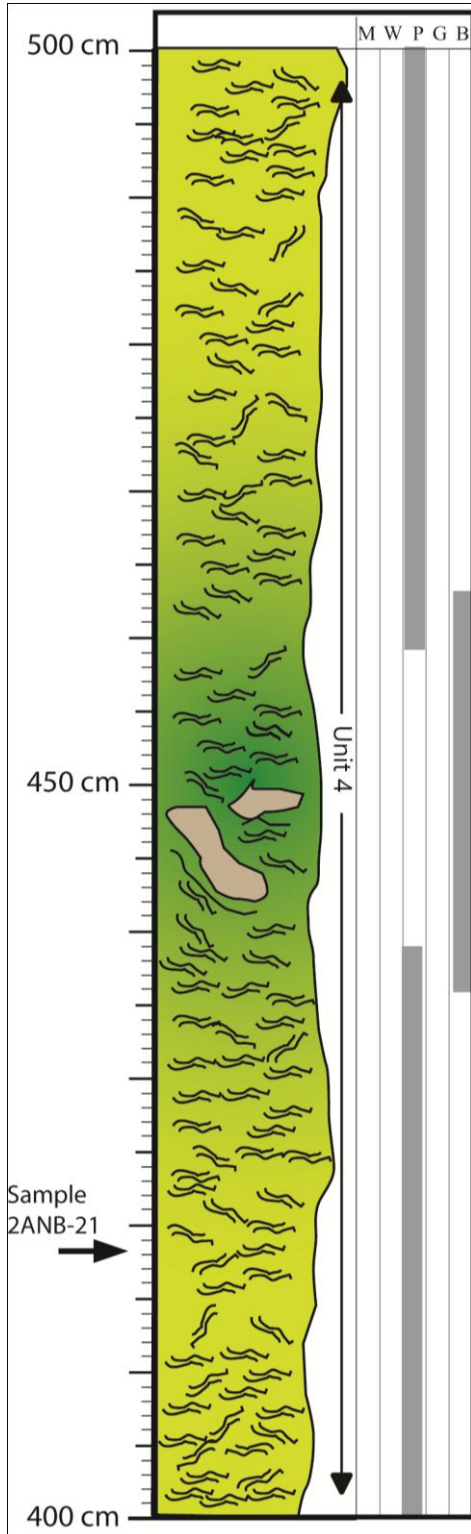
Location: N37°10'57.84" W109°46'33.68"





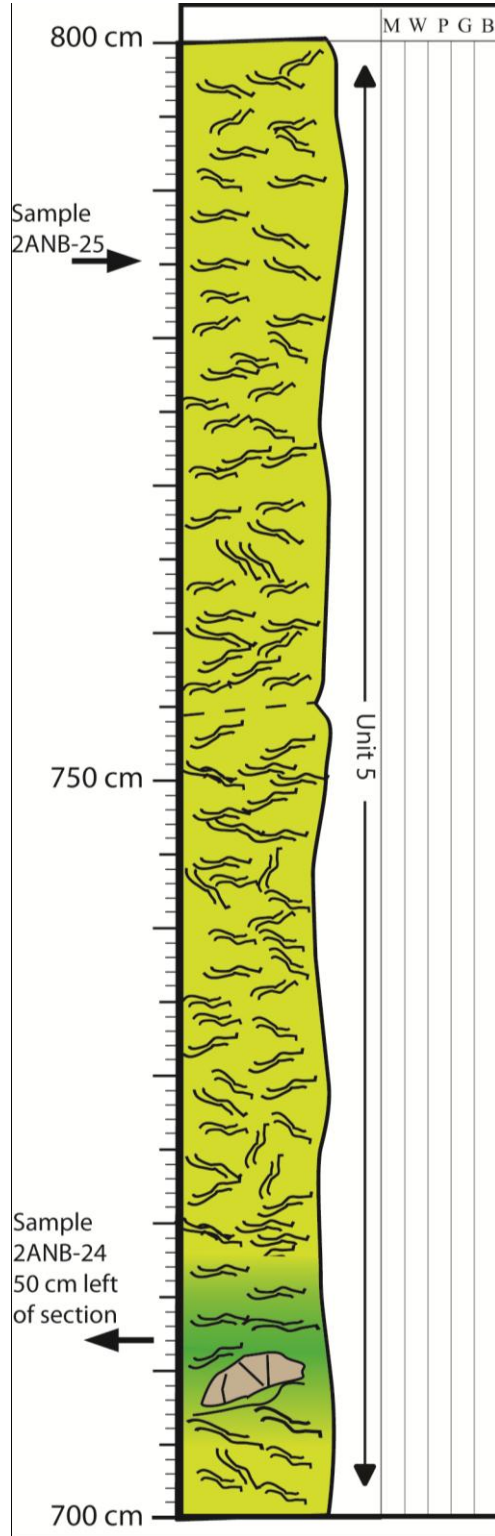
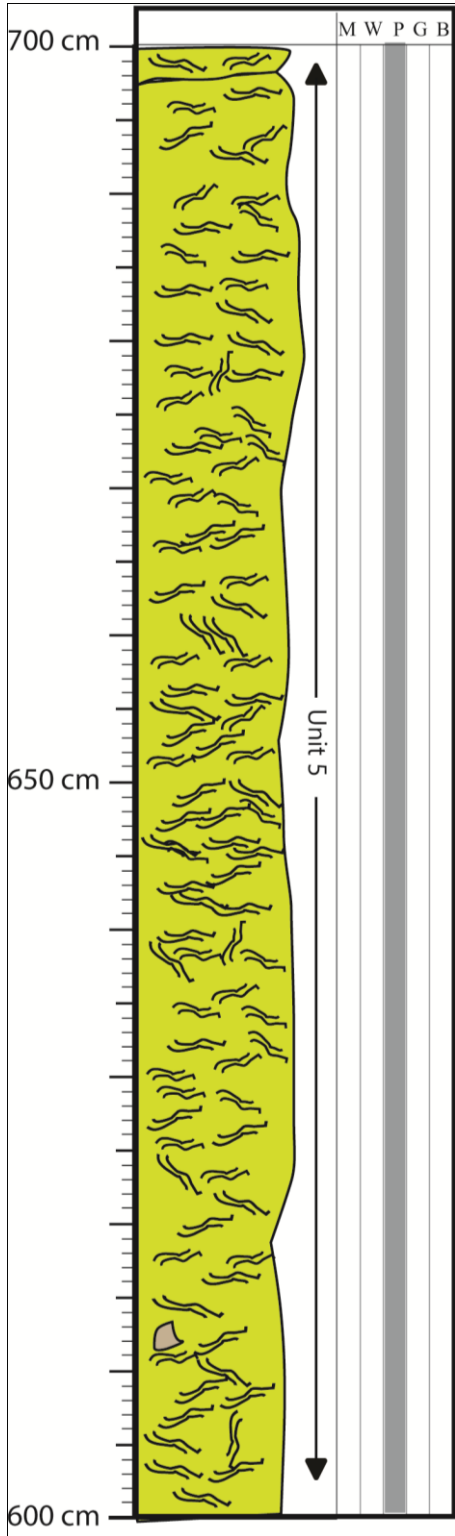
# Stratigraphic Section 2ANB-Ramp Continued

Location: N37°10'57.84" W109°46'33.68"



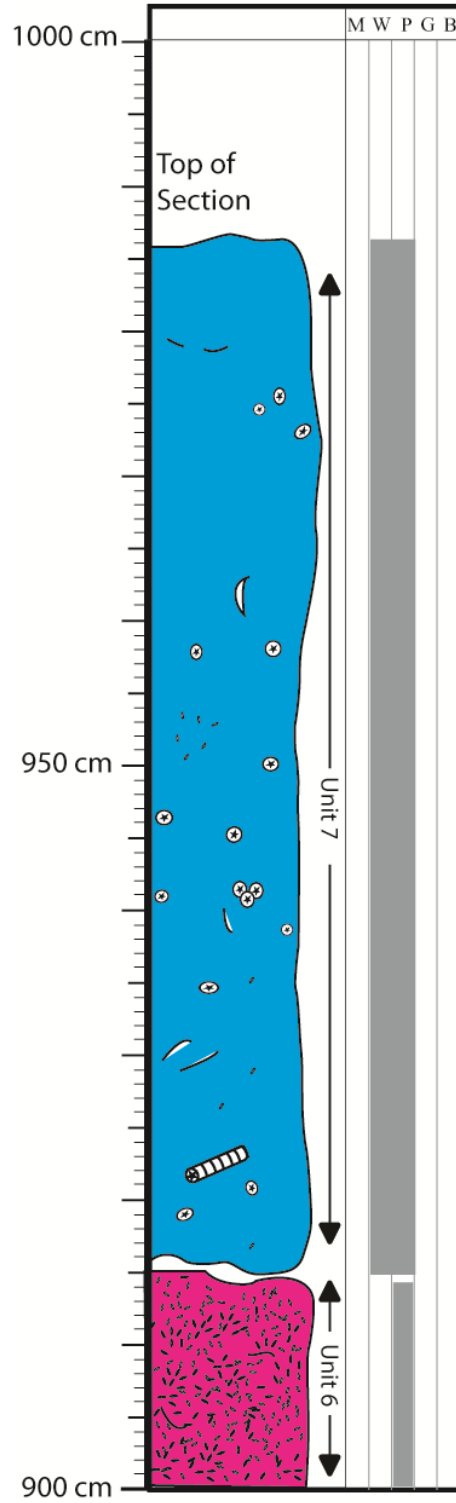
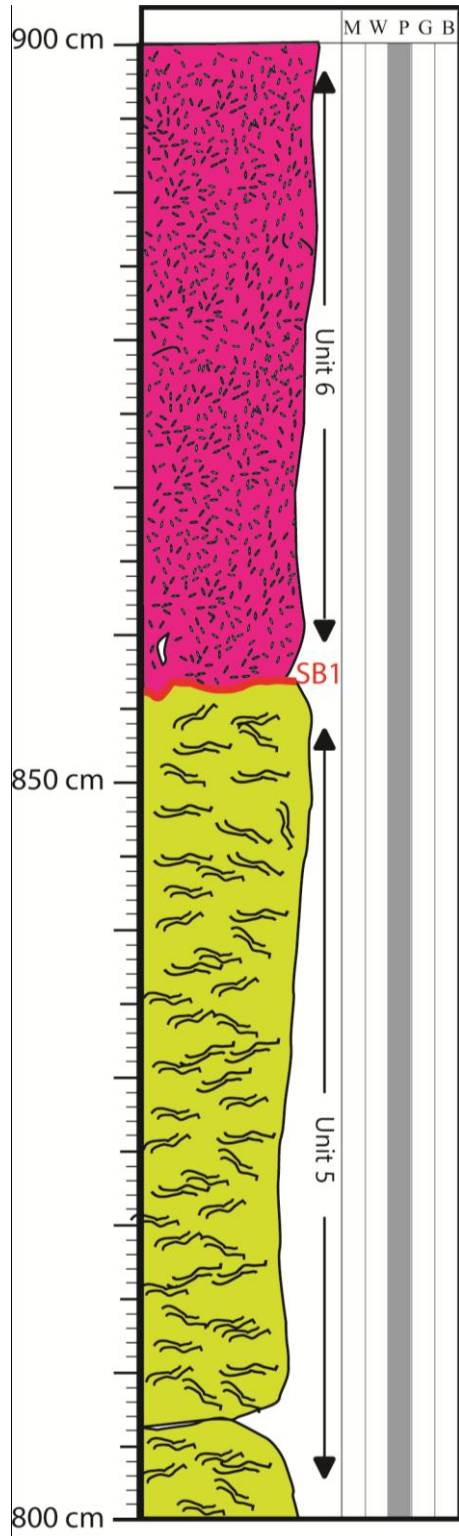
# Stratigraphic Section 2ANB-Ramp Continued

Location: N37°10'57.84" W109°46'33.68"



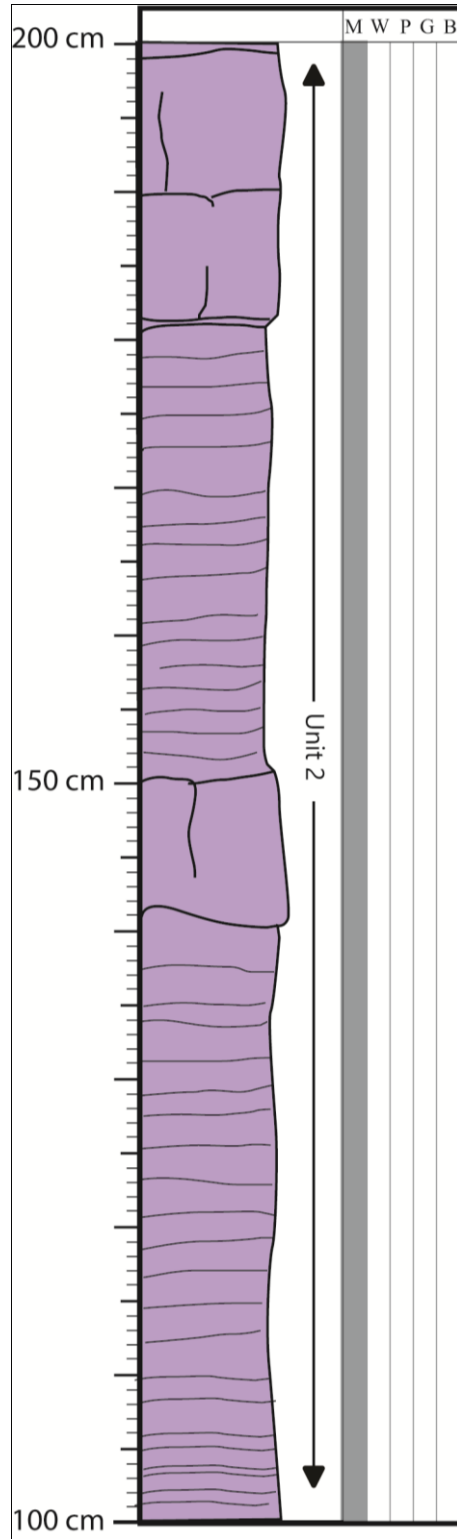
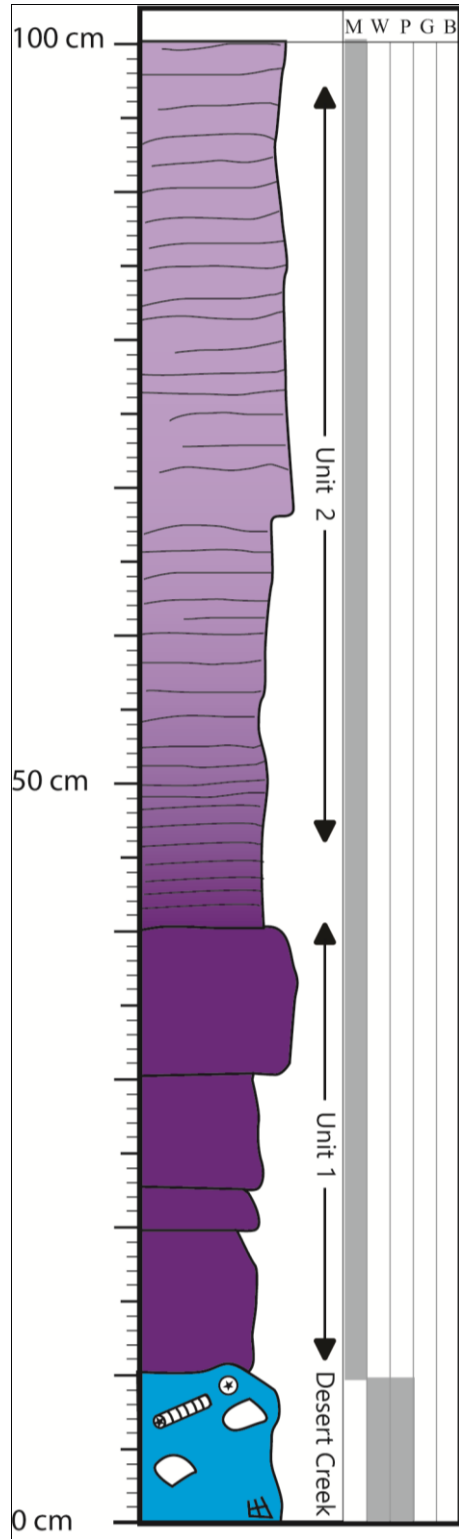
# Stratigraphic Section 2ANB-Ramp Continued

Location: N37°10'57.84" W109°46'33.68"



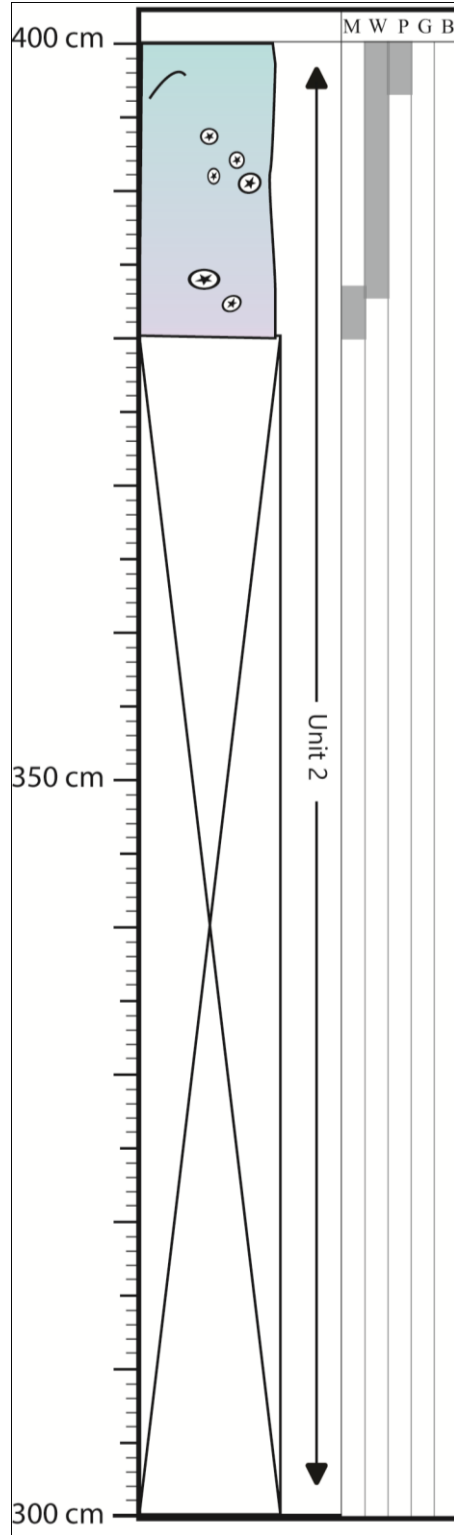
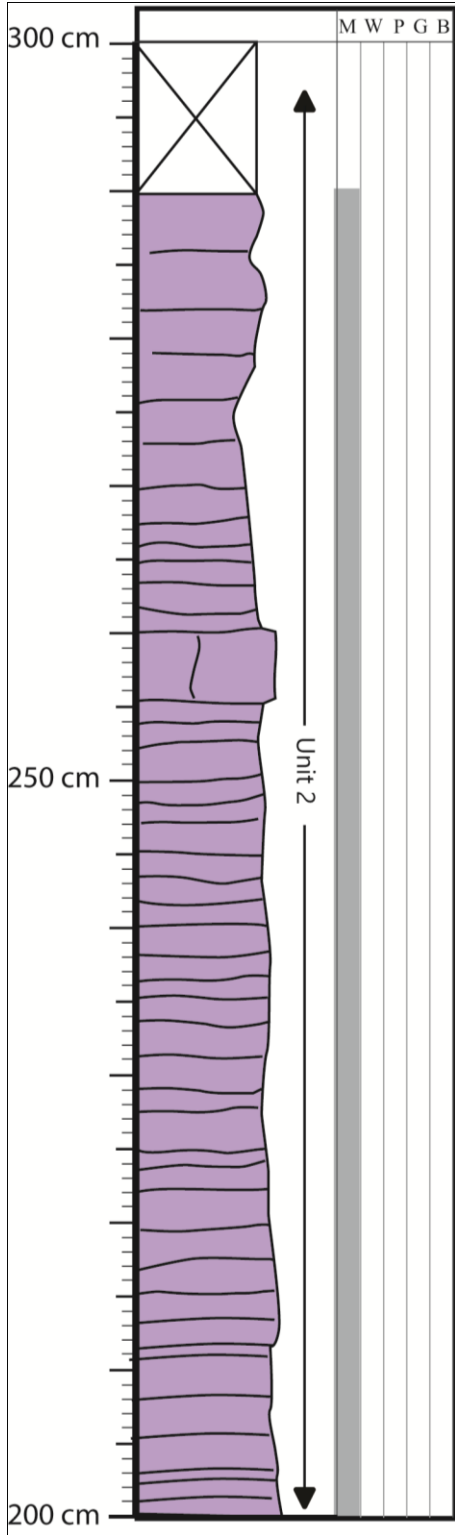
# Stratigraphic Section 8FDN

Location: N37°10'48.34" W109°47'14.72"



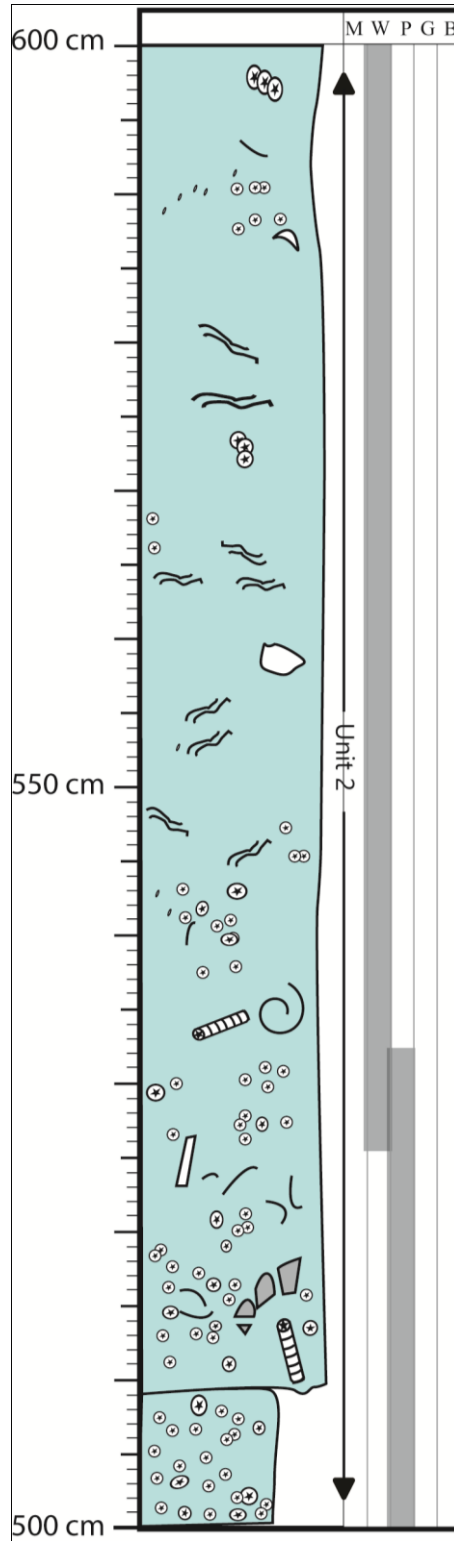
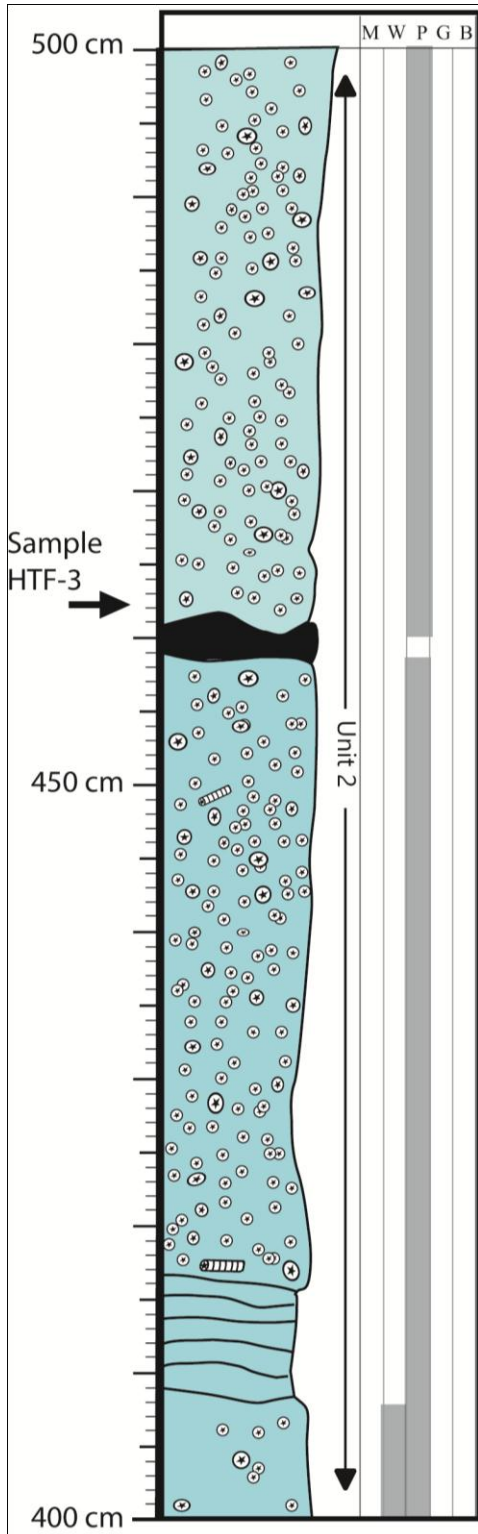
# Stratigraphic Section 8FDN Continued

Location: N37°10'48.34" W109°47'14.72"



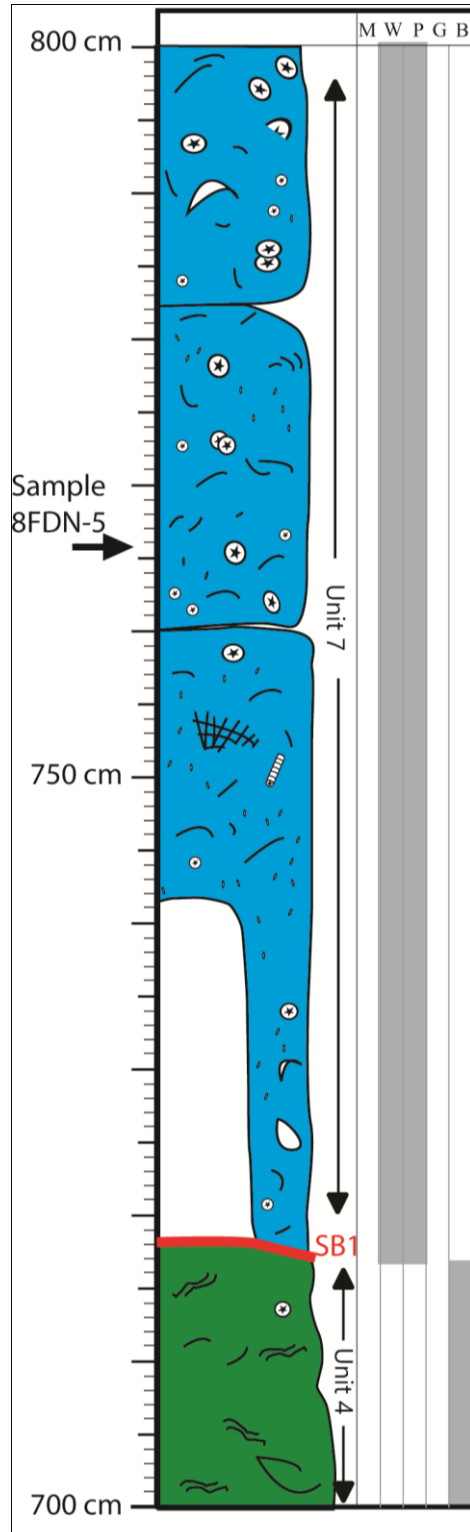
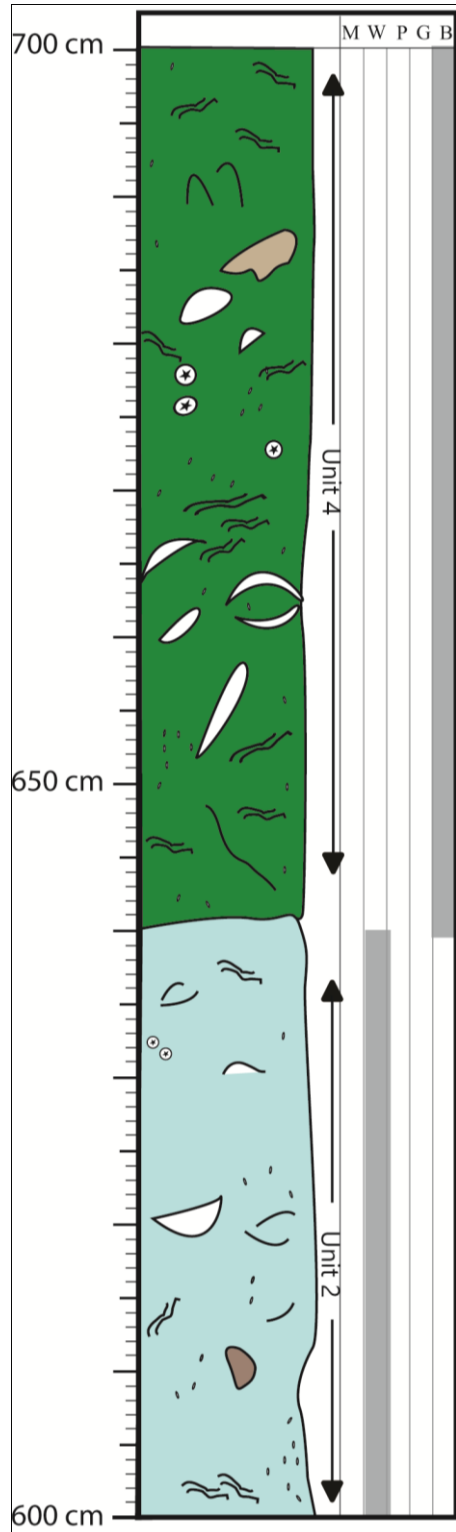
# Stratigraphic Section 8FDN Continued

Location: N37°10'48.34" W109°47'14.72"



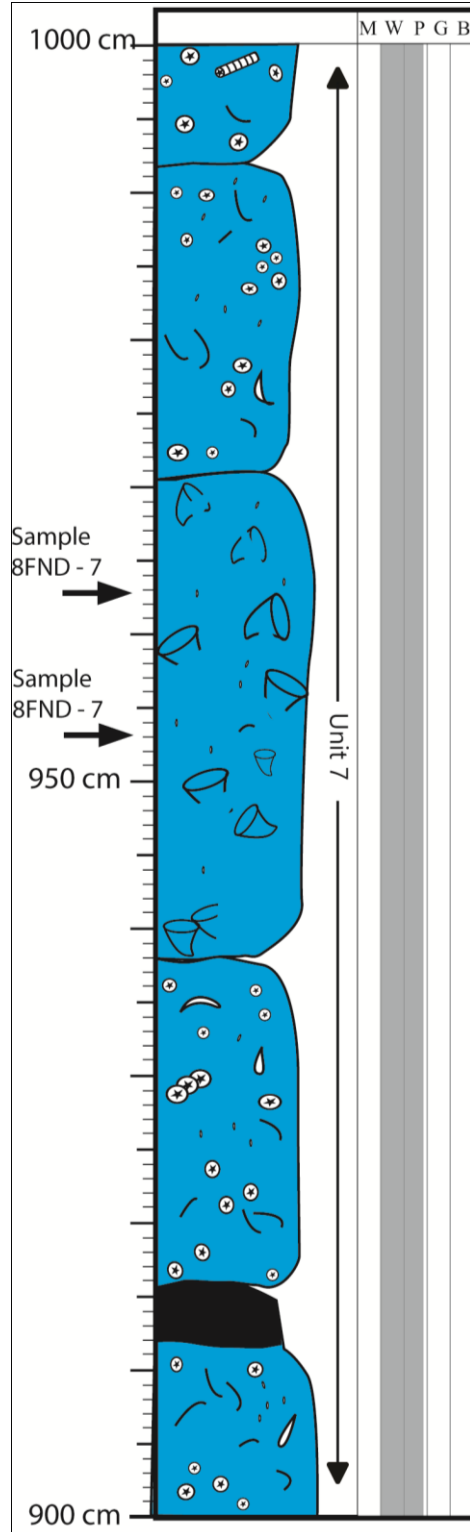
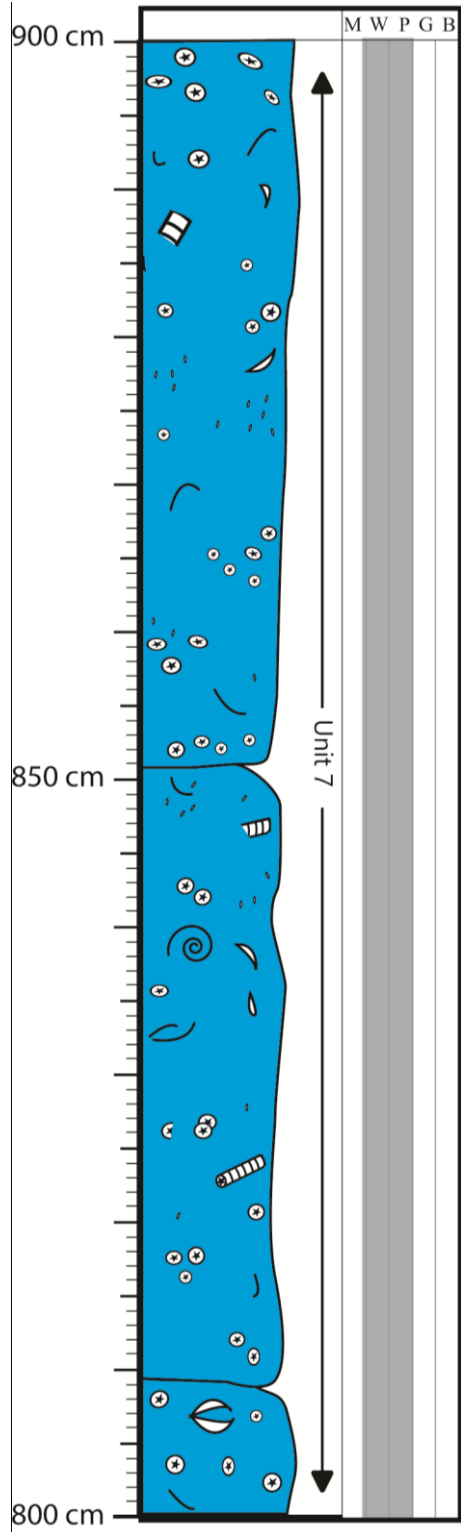
# Stratigraphic Section 8FDN Continued

Location: N37°10'48.34" W109°47'14.72"



# Stratigraphic Section 8FDN Continued

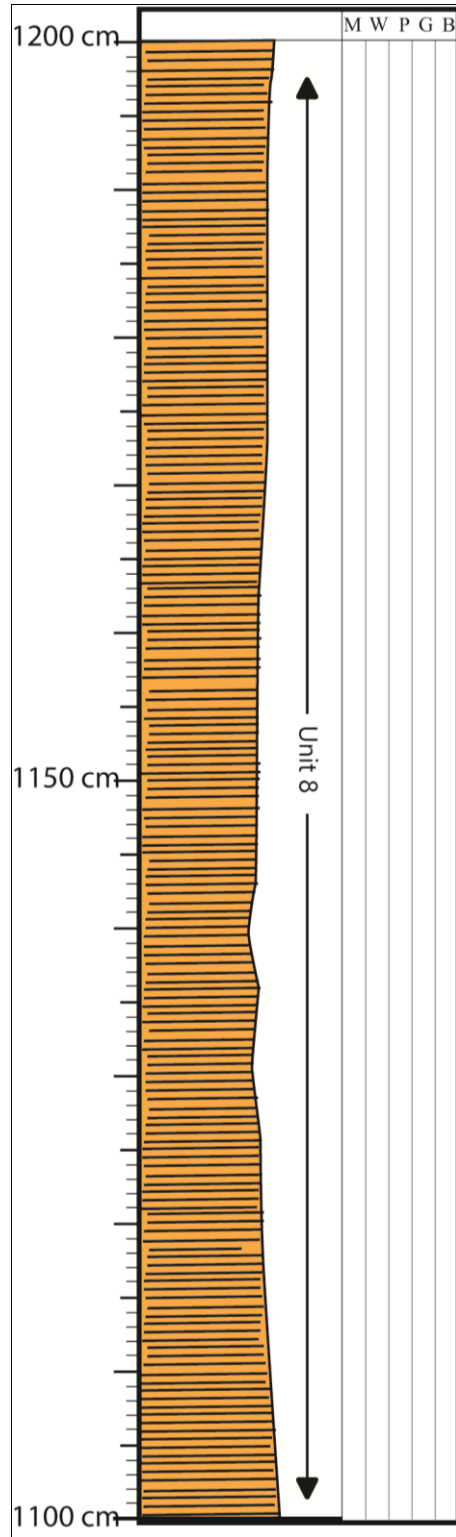
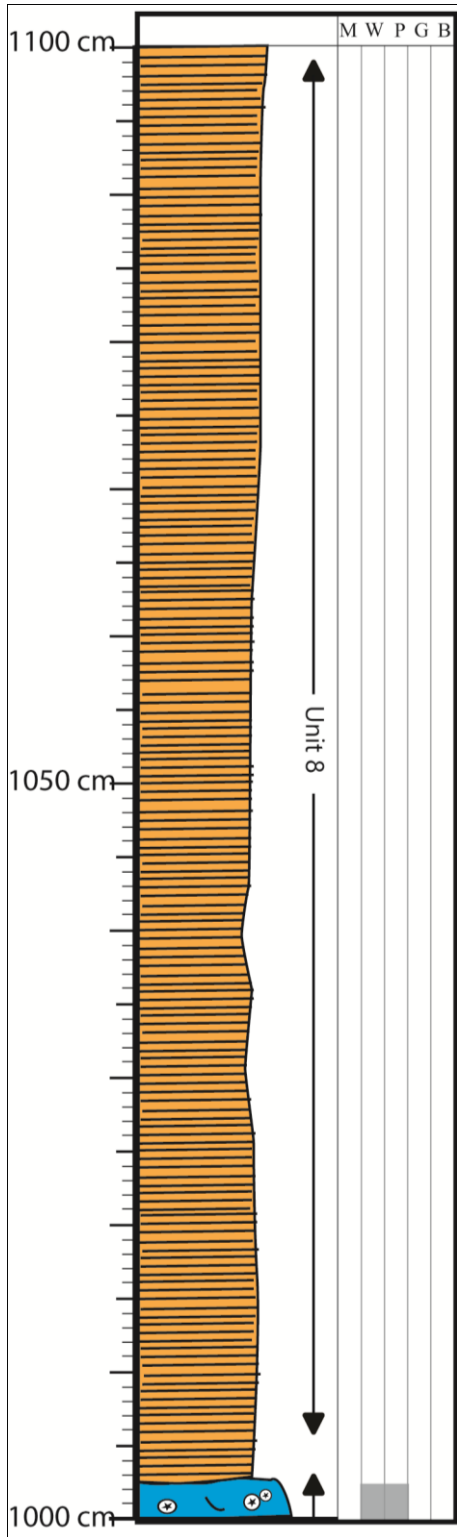
Location: N37°10'48.34" W109°47'14.72"





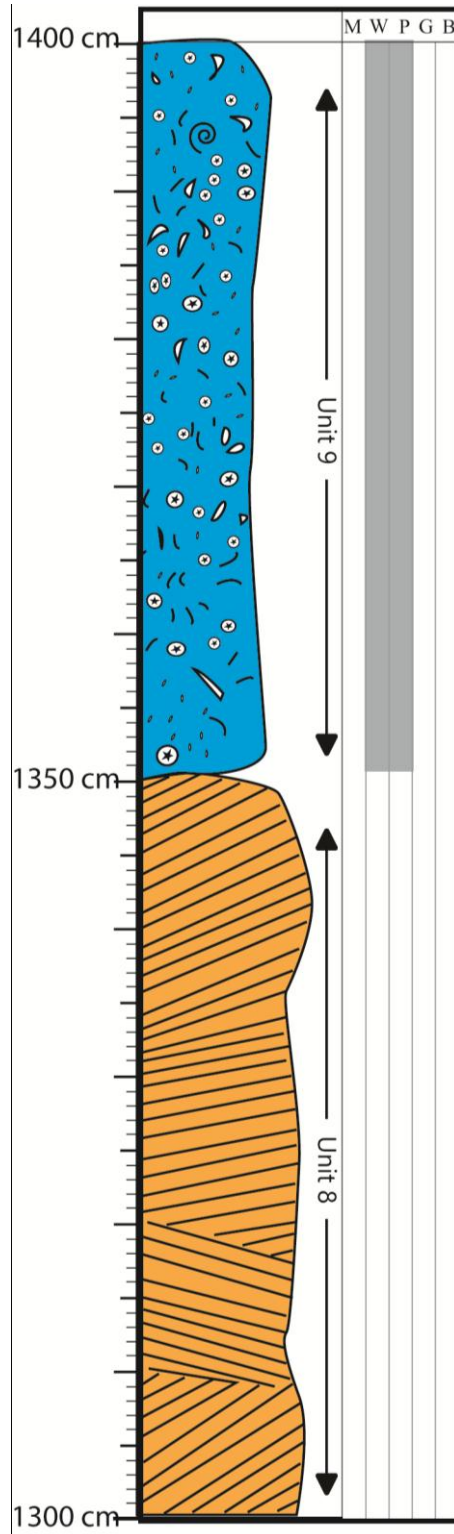
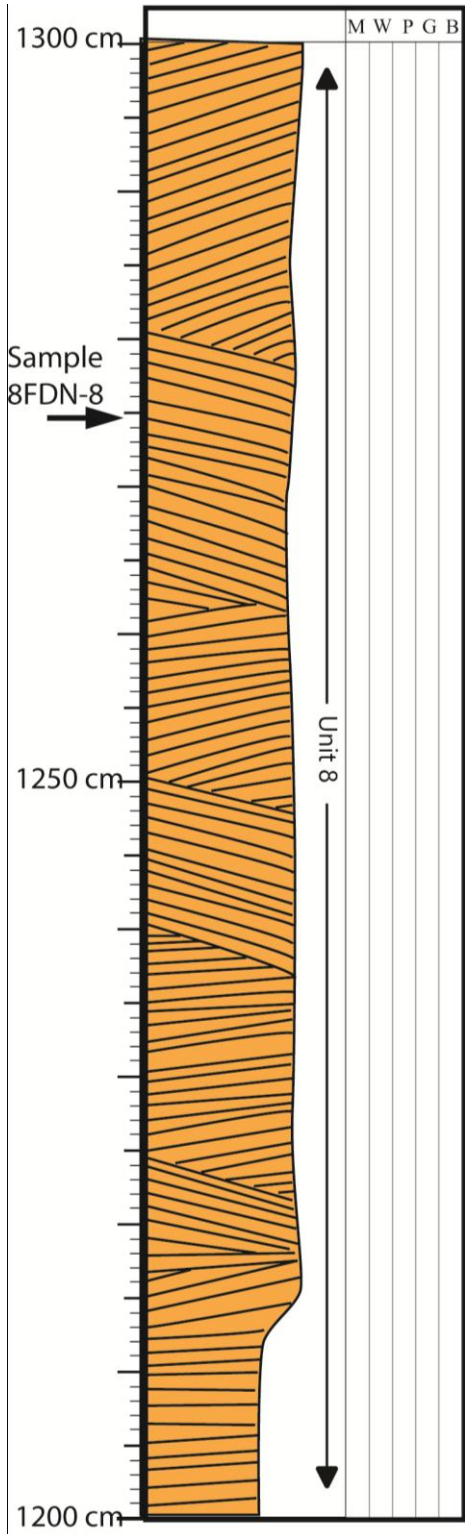
# Stratigraphic Section 8FDN Continued

Location: N37°10'48.34" W109°47'14.72"



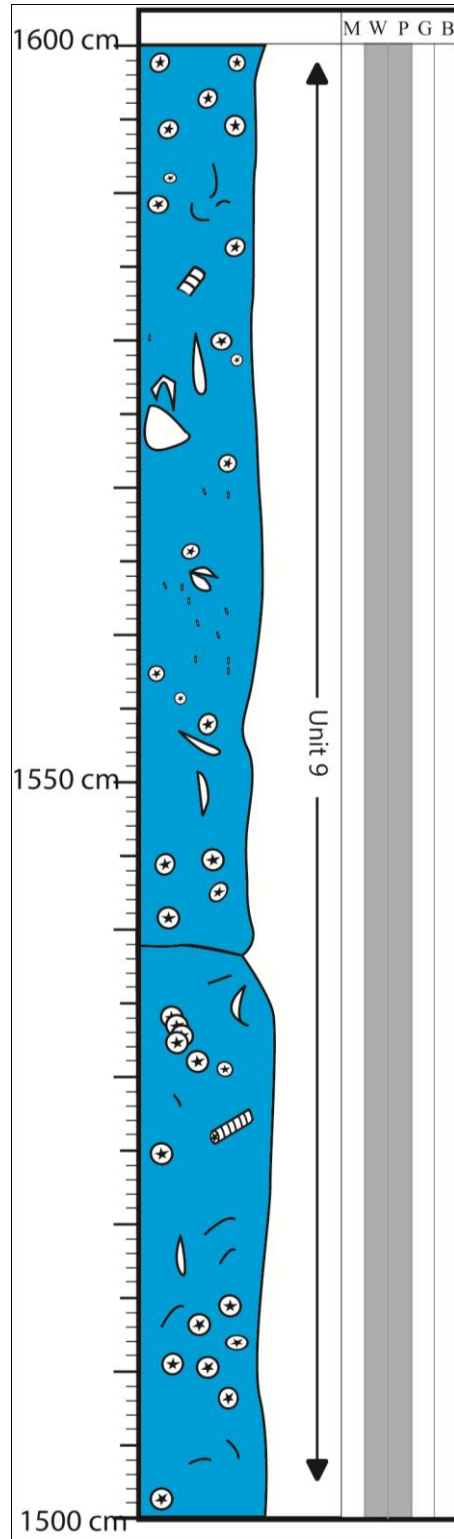
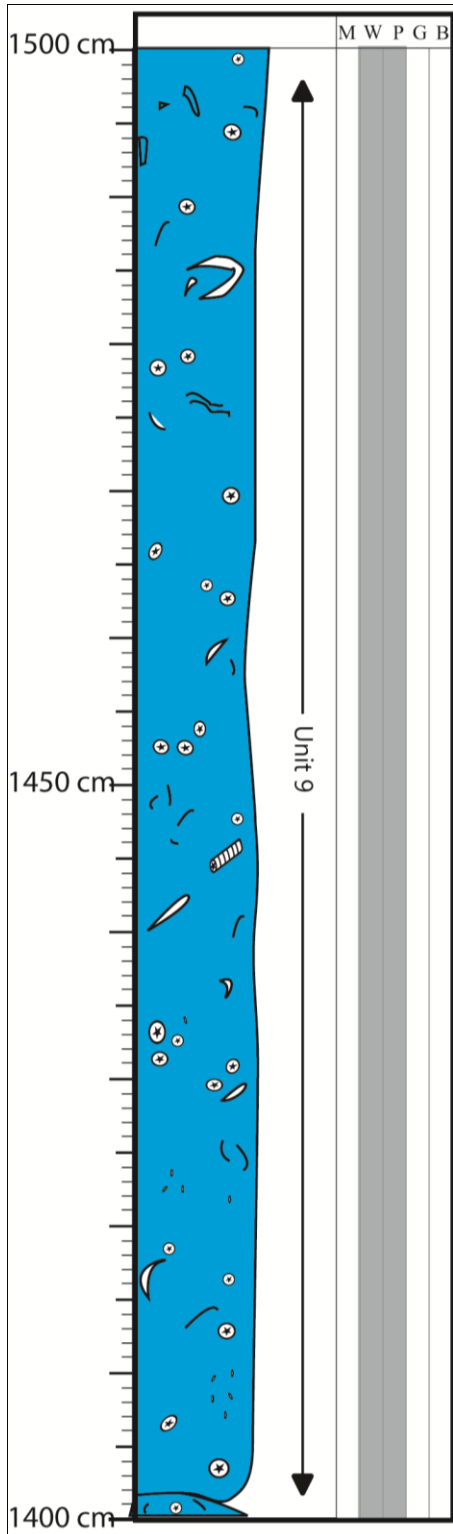
# Stratigraphic Section 8FDN Continued

Location: N37°10'48.34" W109°47'14.72"



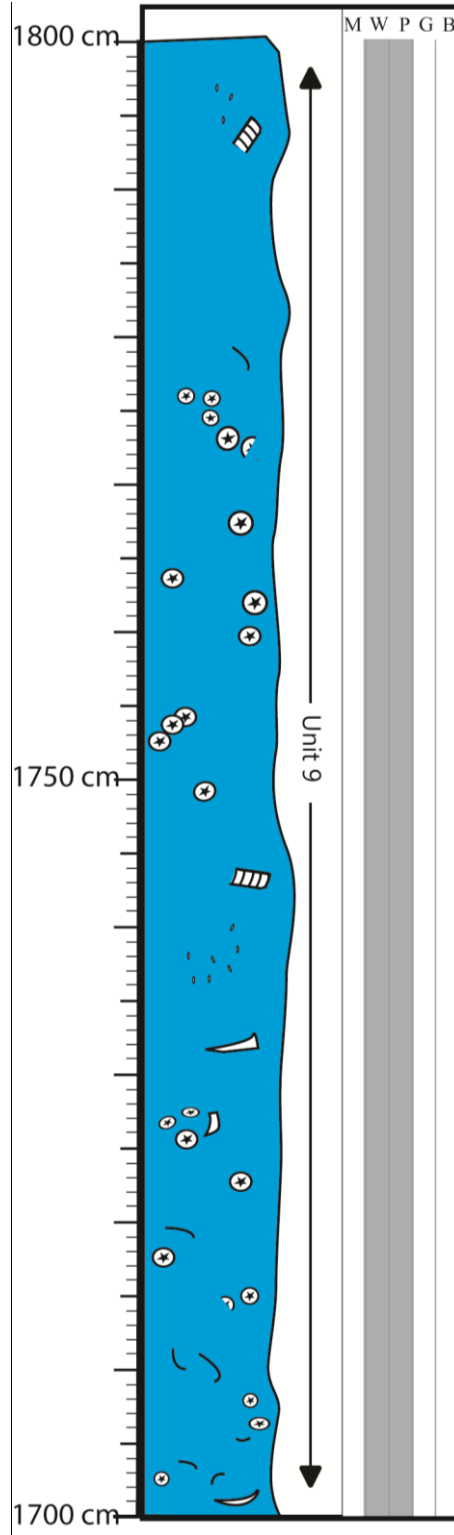
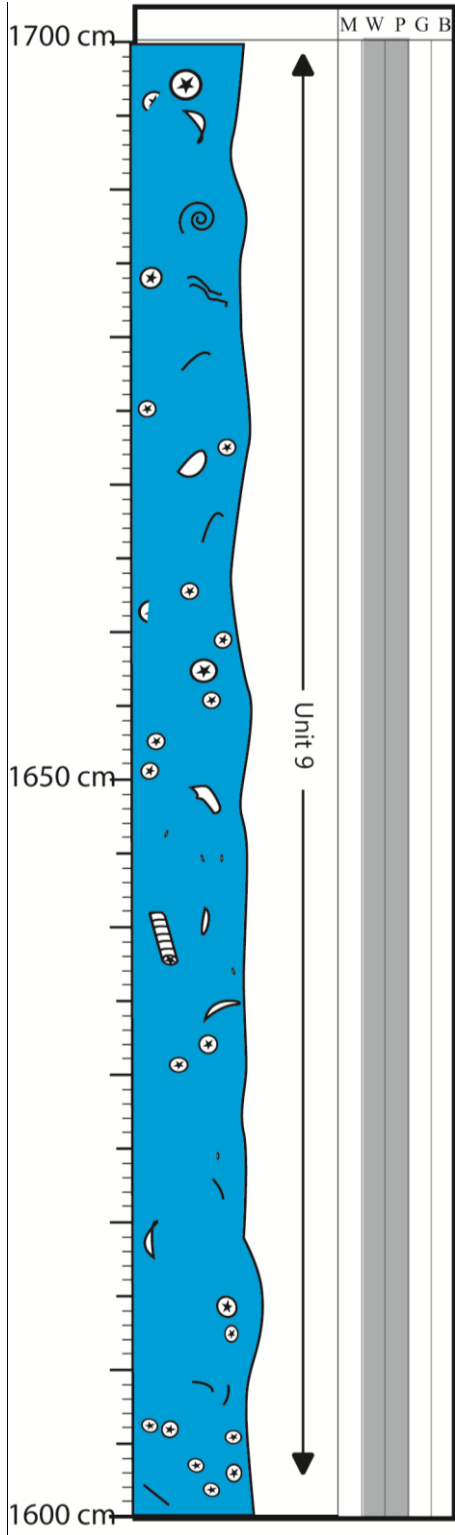
# Stratigraphic Section 8FDN Continued

Location: N37°10'48.34" W109°47'14.72"



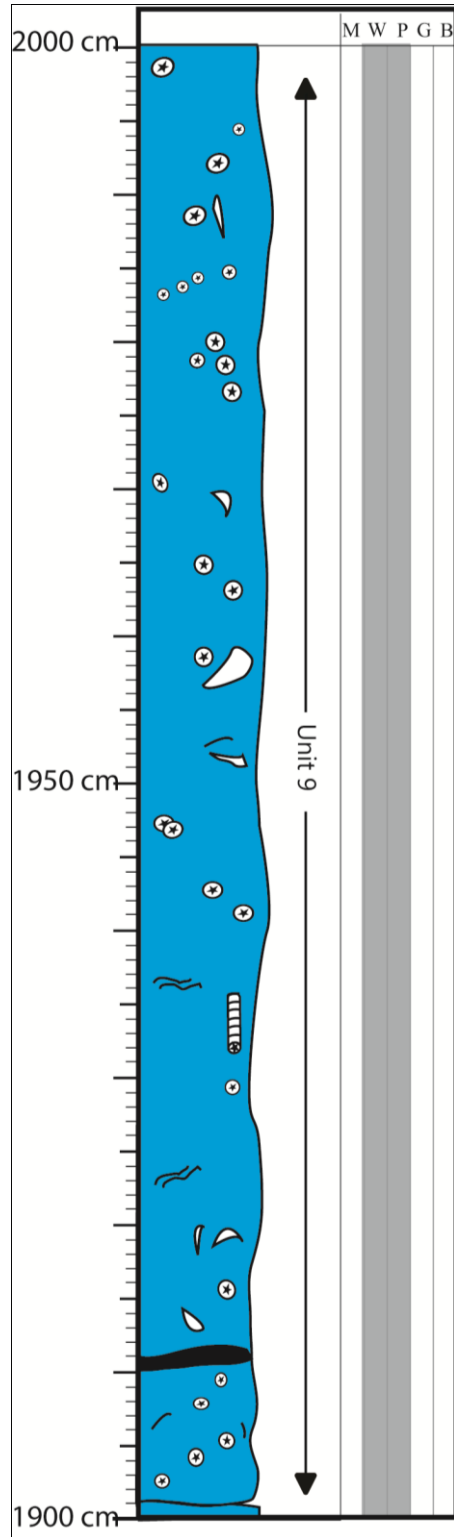
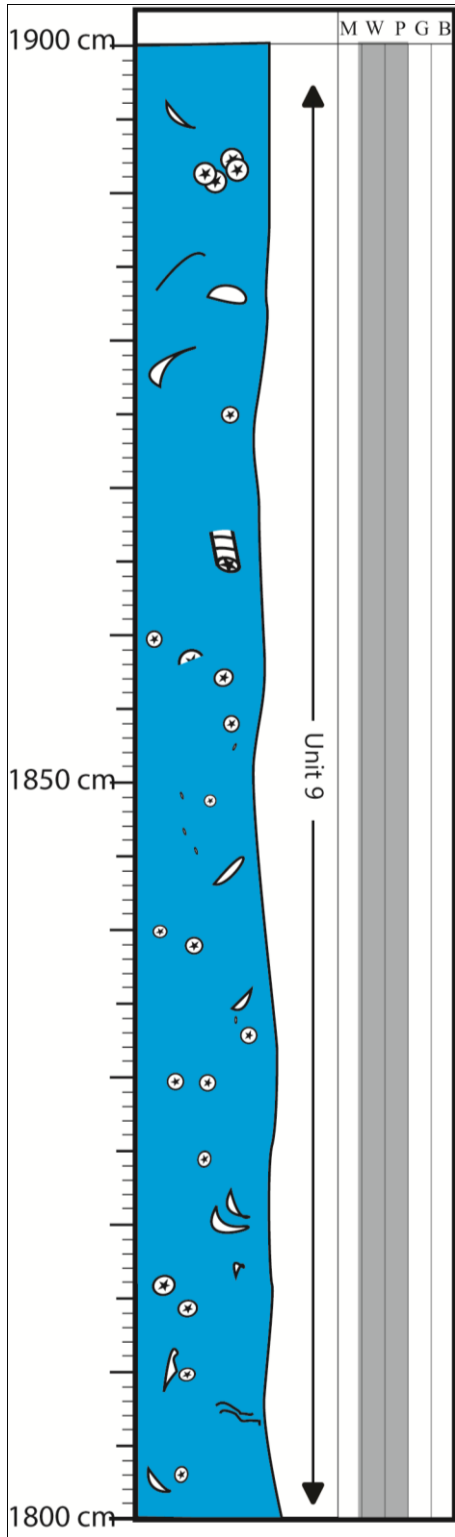
# Stratigraphic Section 8FDN Continued

Location: N37°10'48.34" W109°47'14.72"



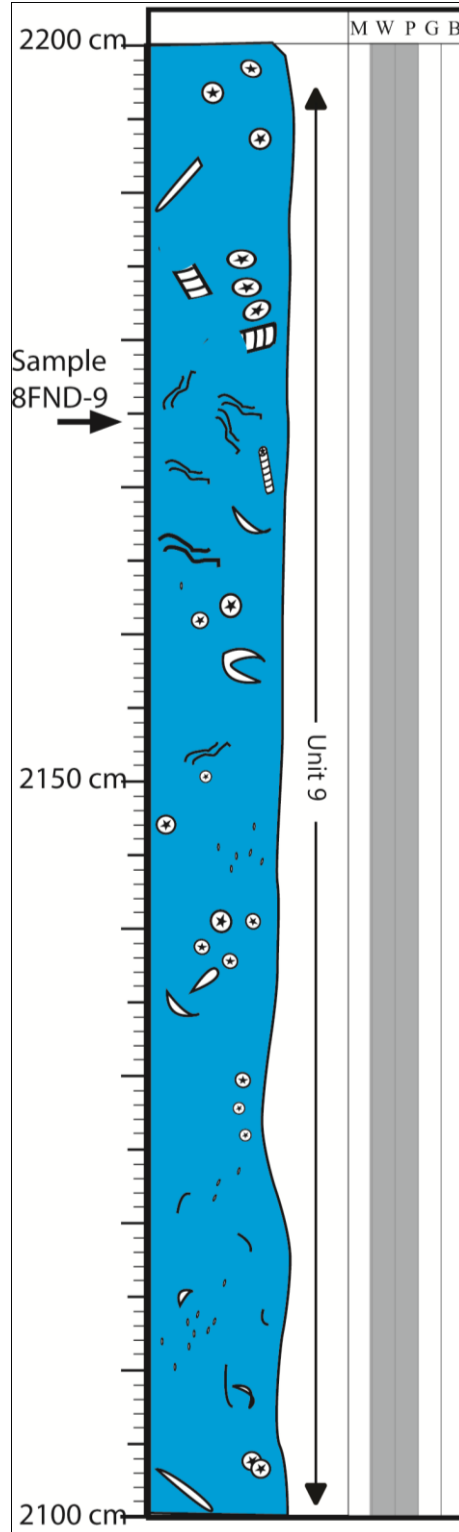
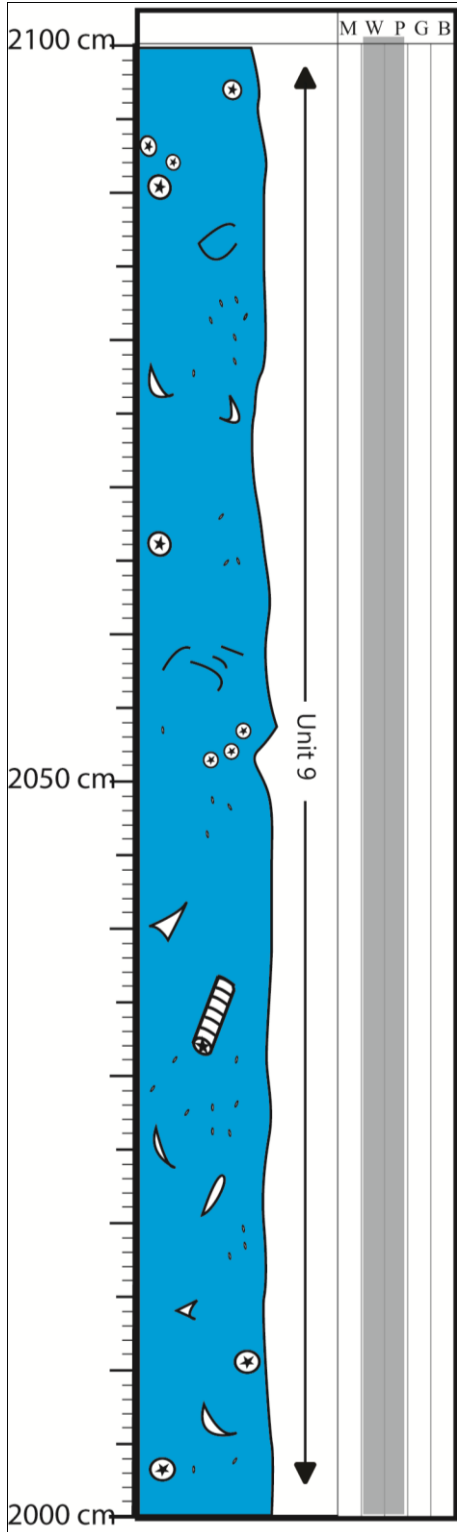
# Stratigraphic Section 8FDN Continued

Location: N37°10'48.34" W109°47'14.72"



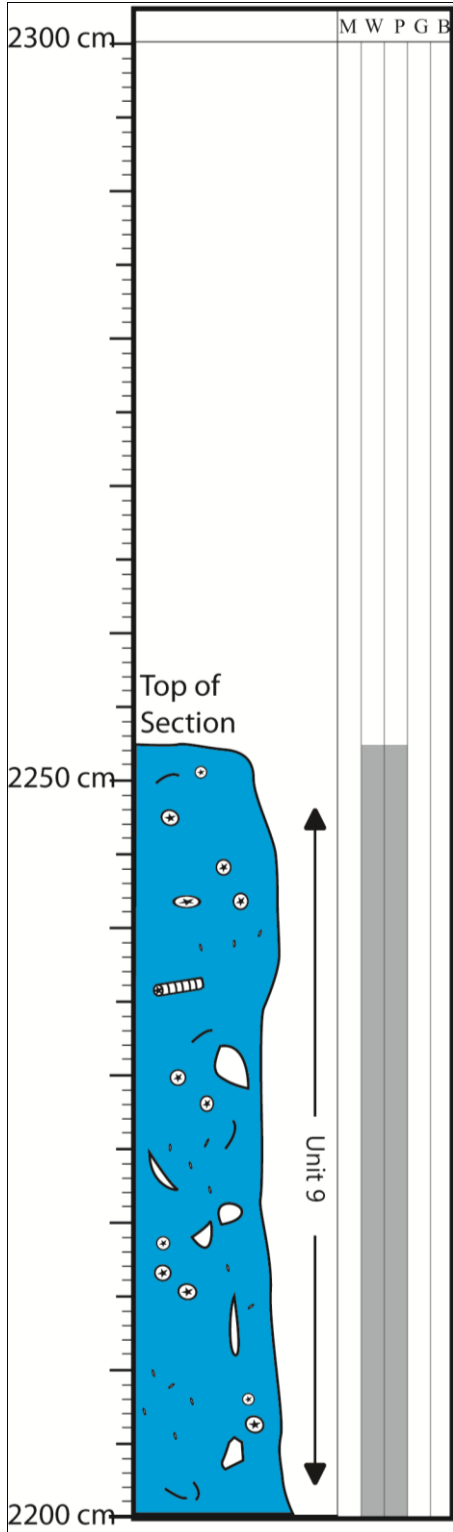
# Stratigraphic Section 8FDN Continued

Location: N37°10'48.34" W109°47'14.72"



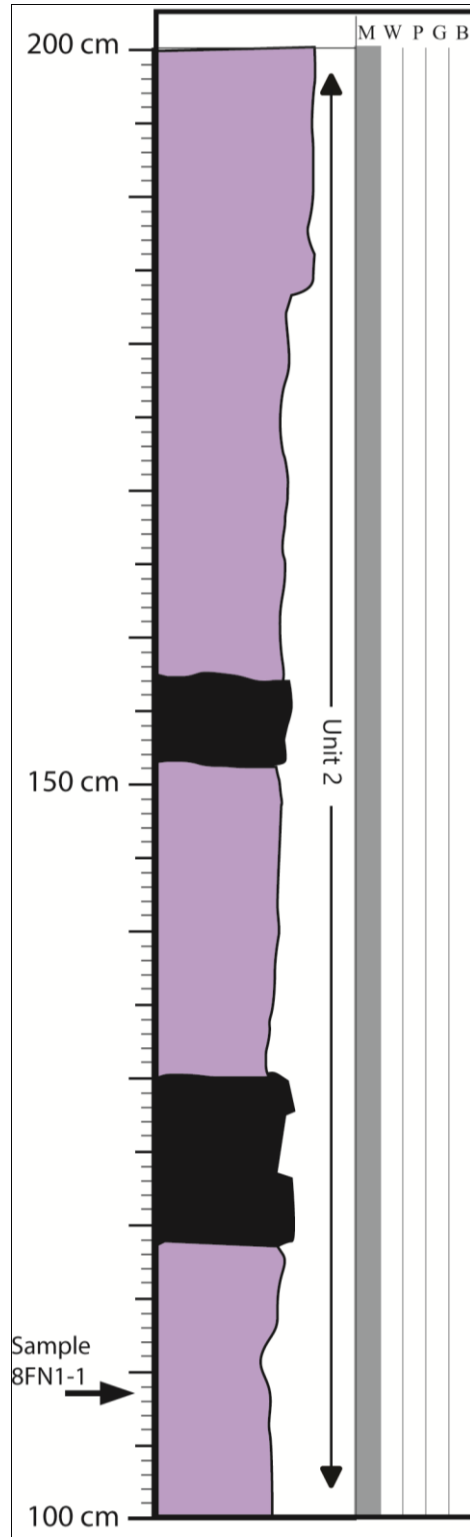
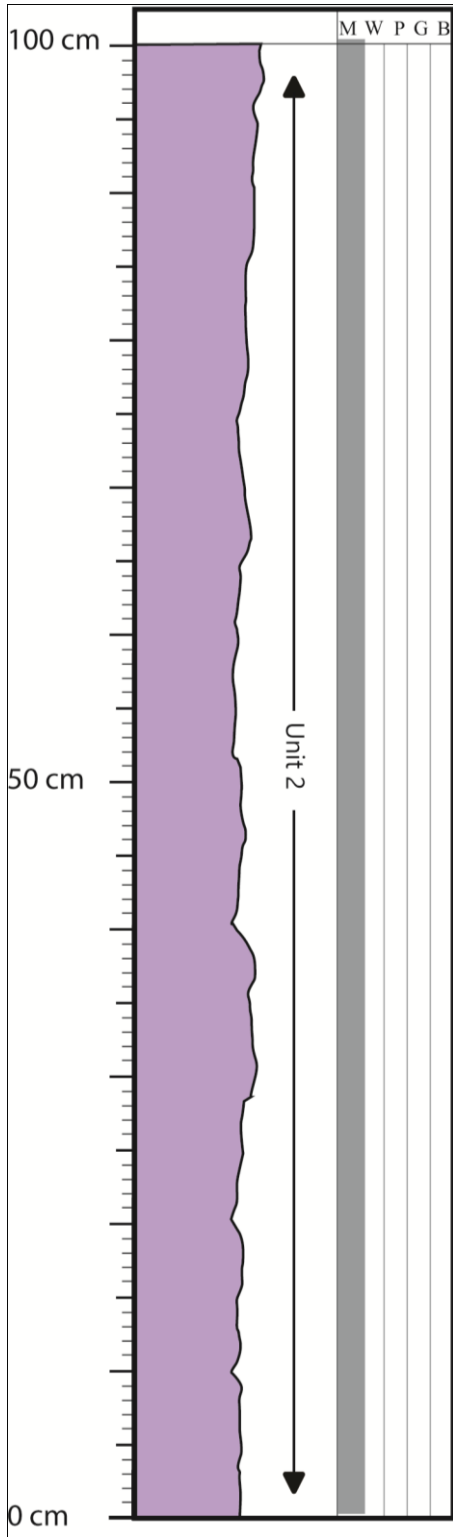
# Stratigraphic Section 8FDN Continued

Location: N37°10'48.34" W109°47'14.72"



# Stratigraphic Section 8FN1

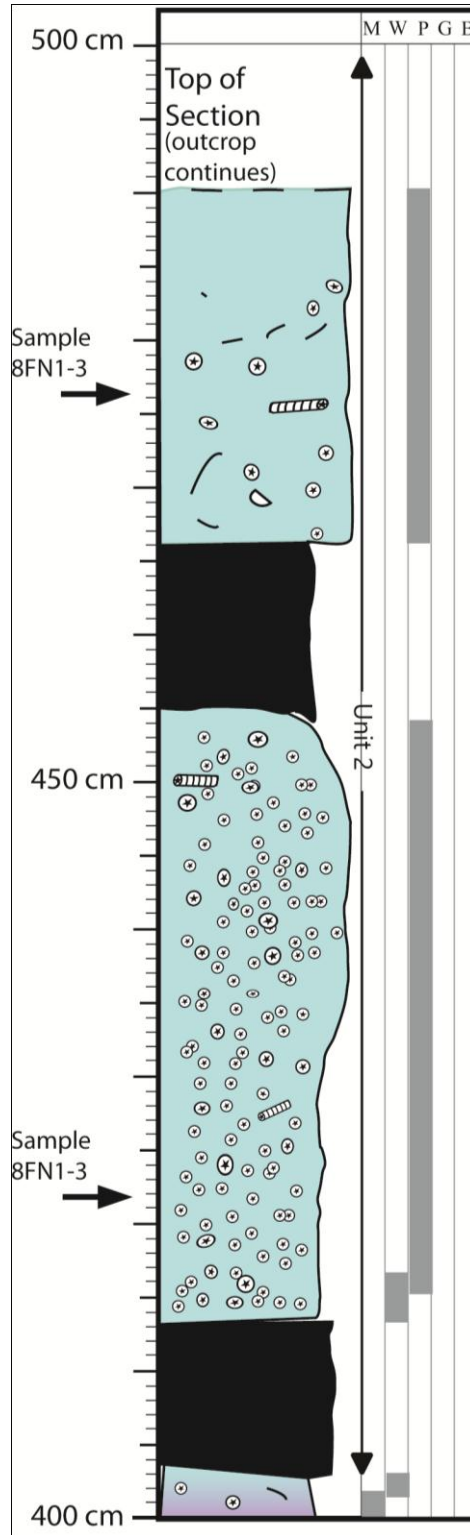
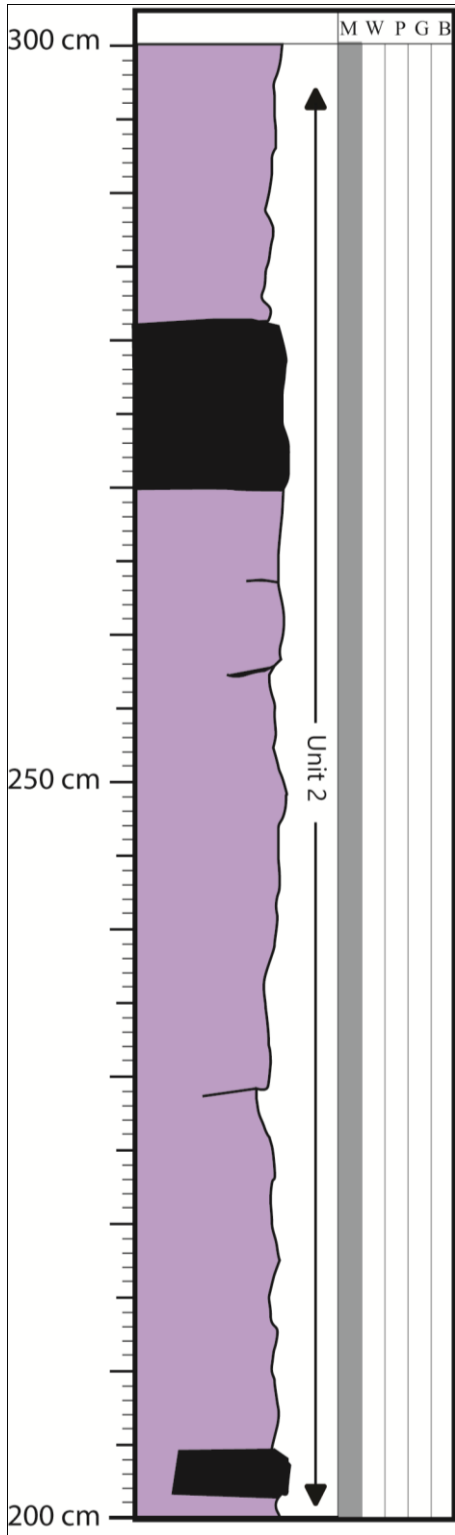
Location: N37°11'00.25" W109°47'12.33"





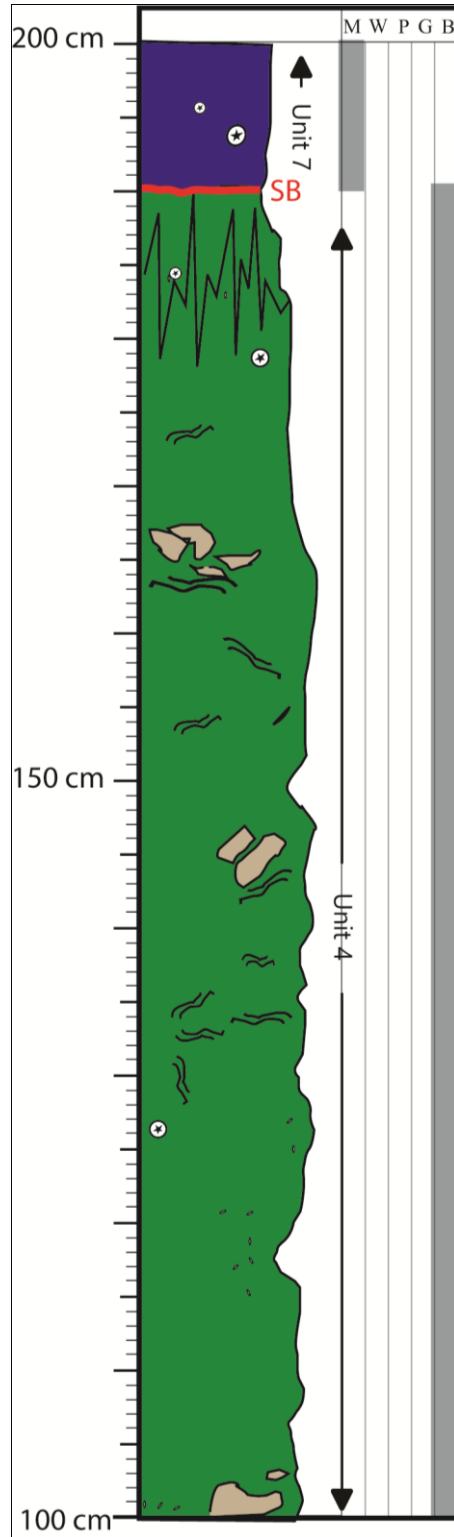
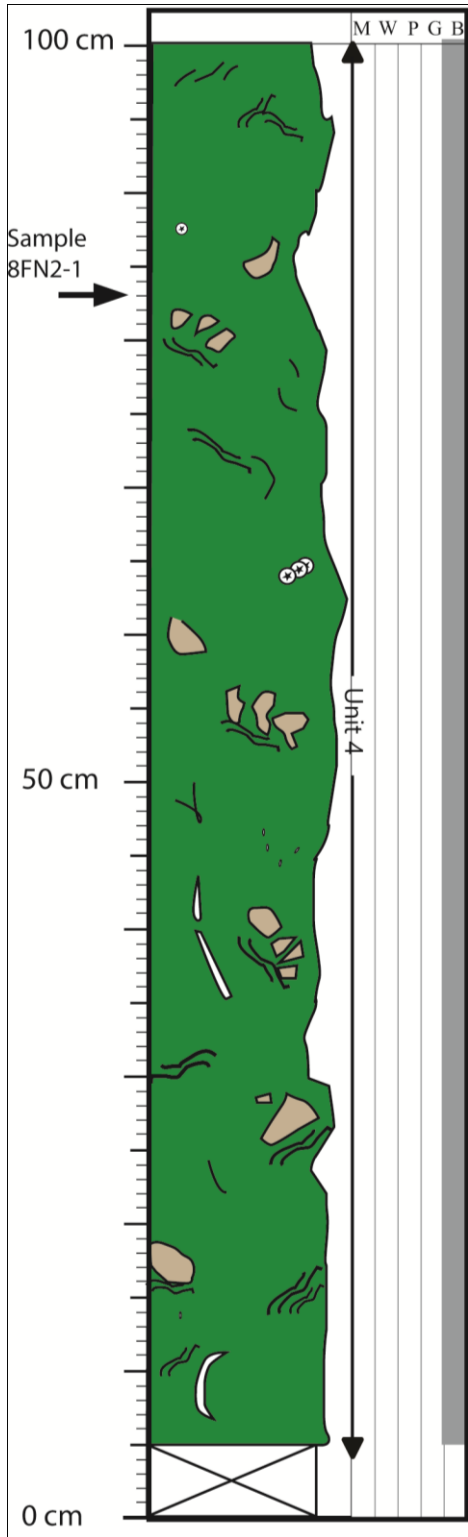
# Stratigraphic Section 8FN1Continued

Location: N37°11'00.25" W109°47'12.33"

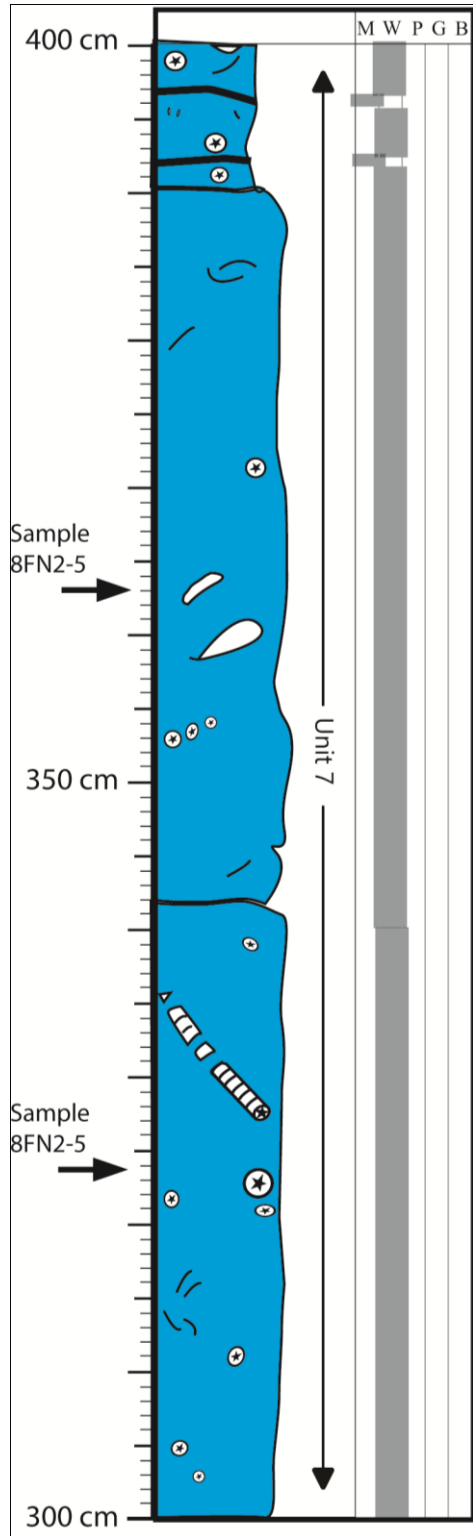
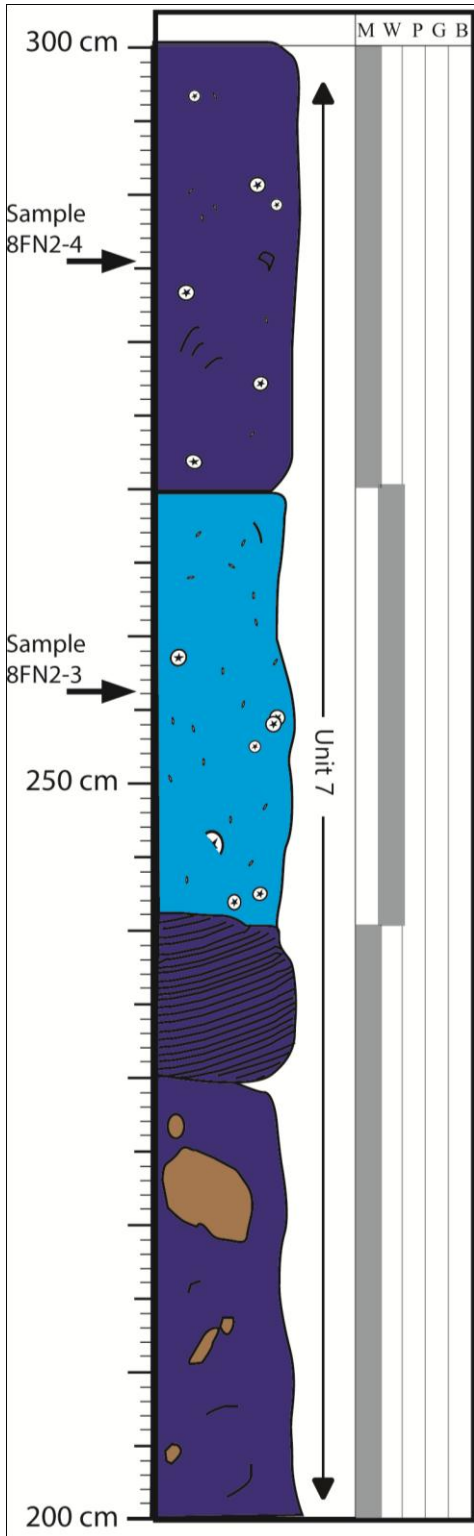


# Stratigraphic Section 8FN2

Location: N37°11'01.30" W109°47'12.55"

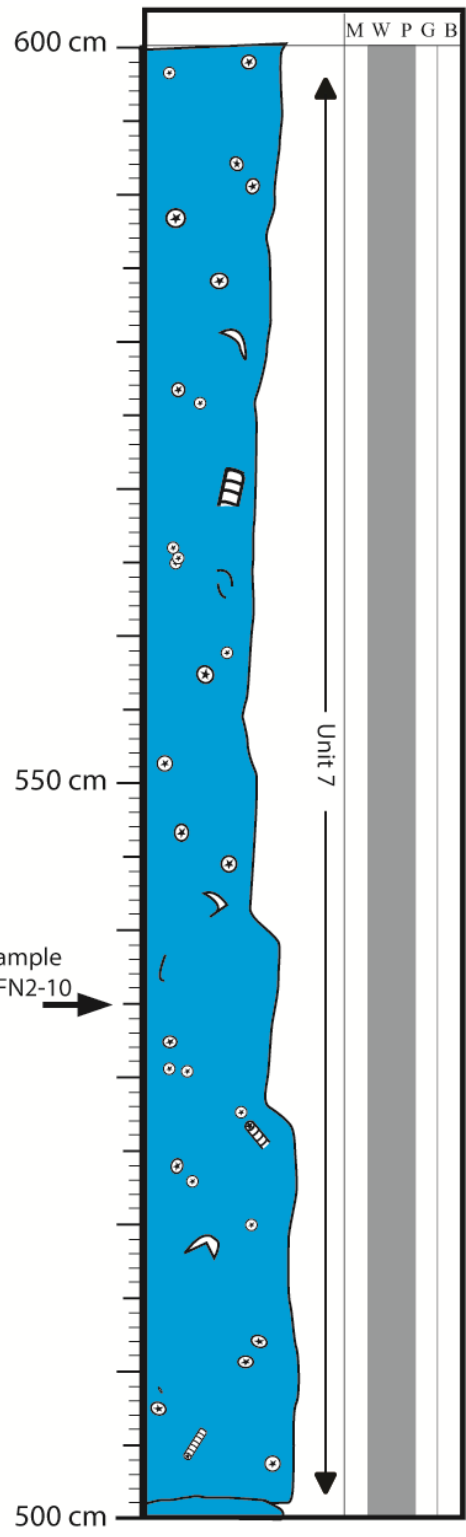
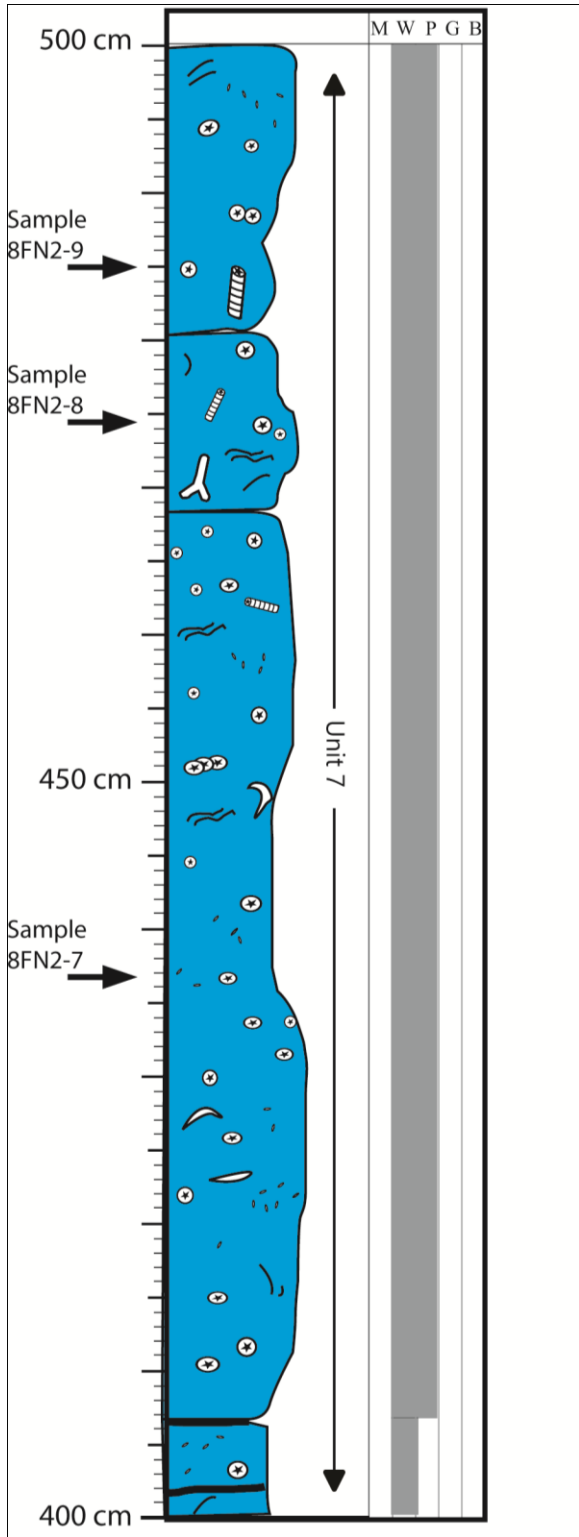


Stratigraphic Section 8FN2 Continued  
 Location: N37°11'01.30" W109°47'12.55"



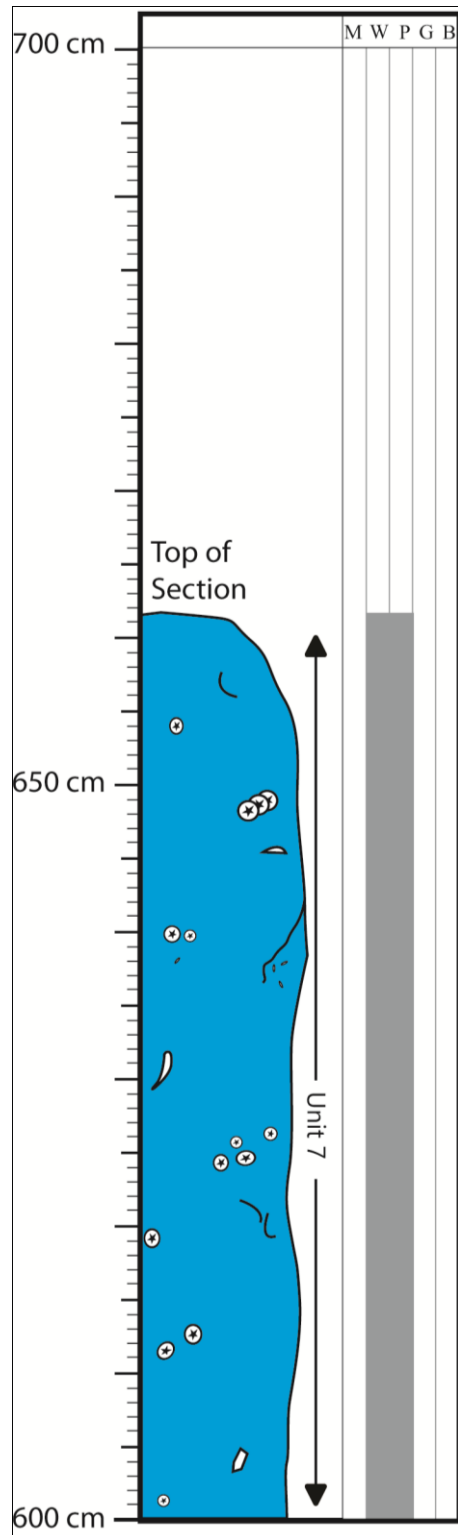
# Stratigraphic Section 8FN2 Continued

Location: N37°11'01.30" W109°47'12.55"



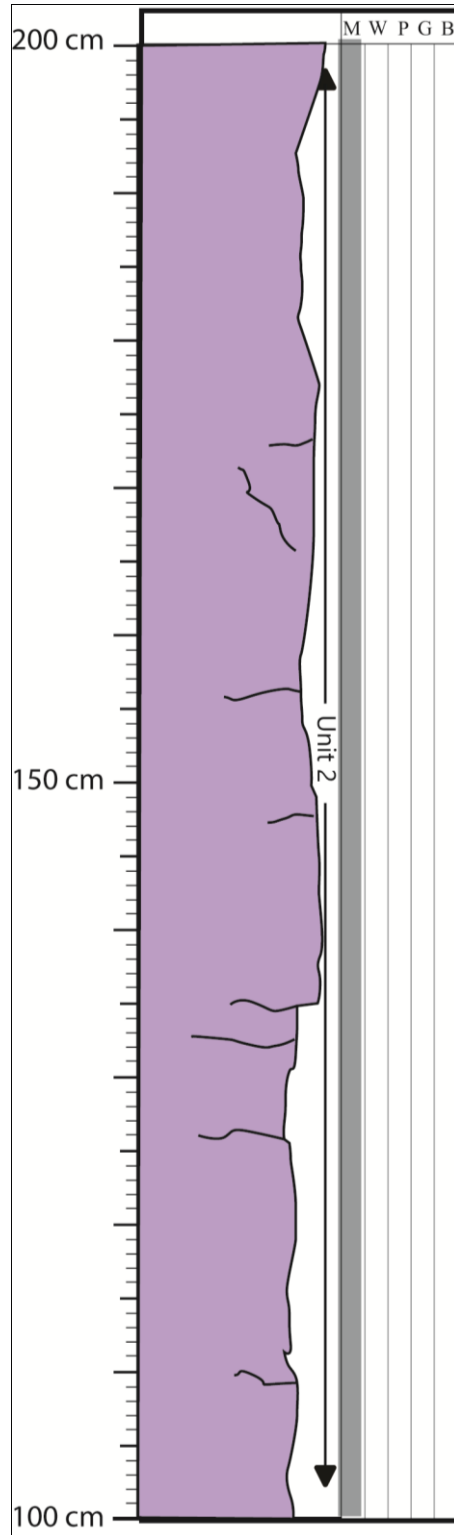
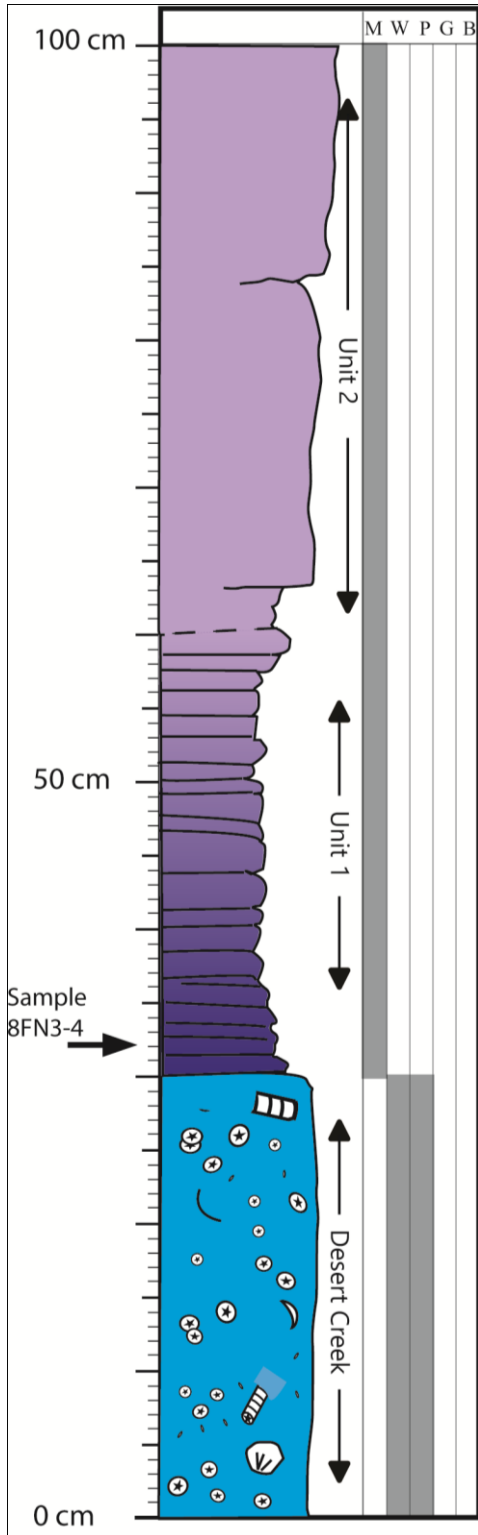
# Stratigraphic Section 8FN2 Continued

Location: N37°11'01.30" W109°47'12.55"



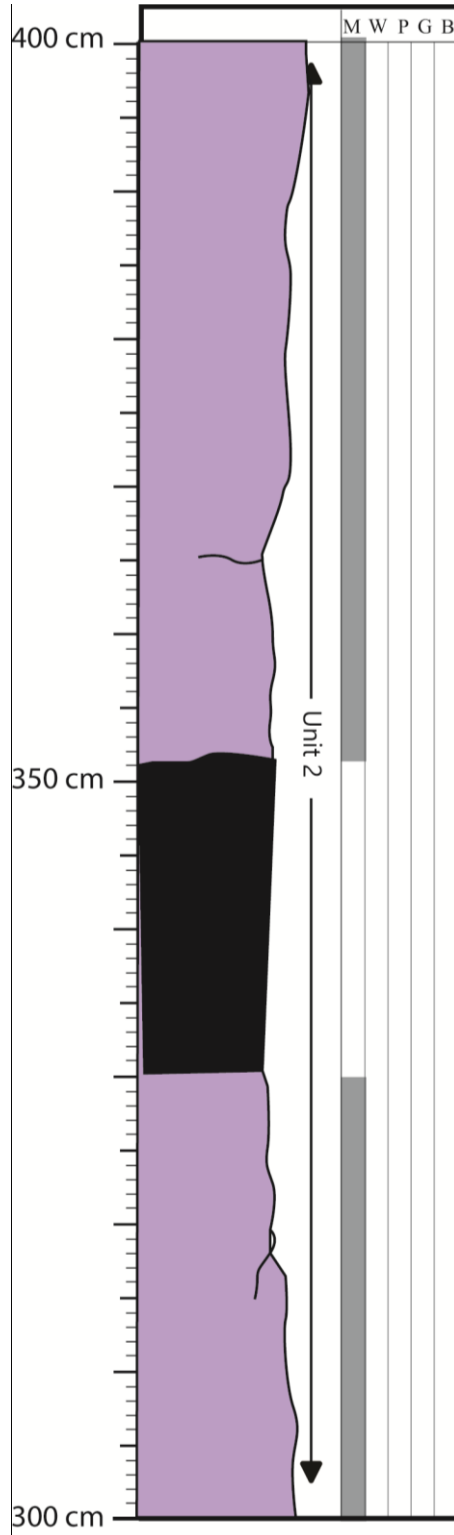
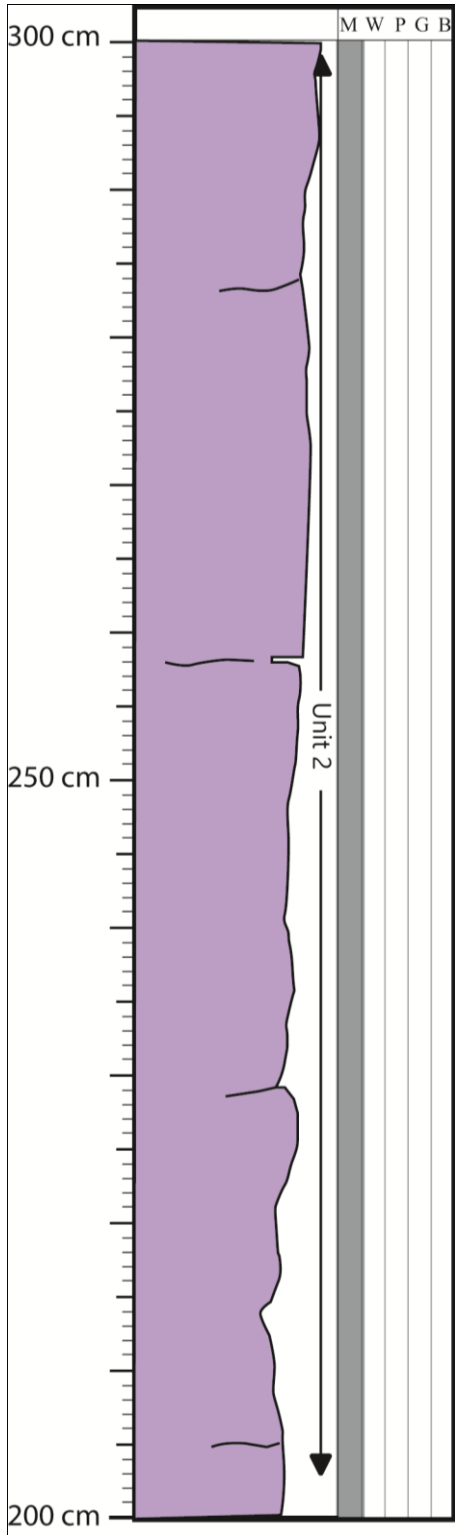
# Stratigraphic Section 8FN3

Location: N37°11'13.24" W109°47'8.76"



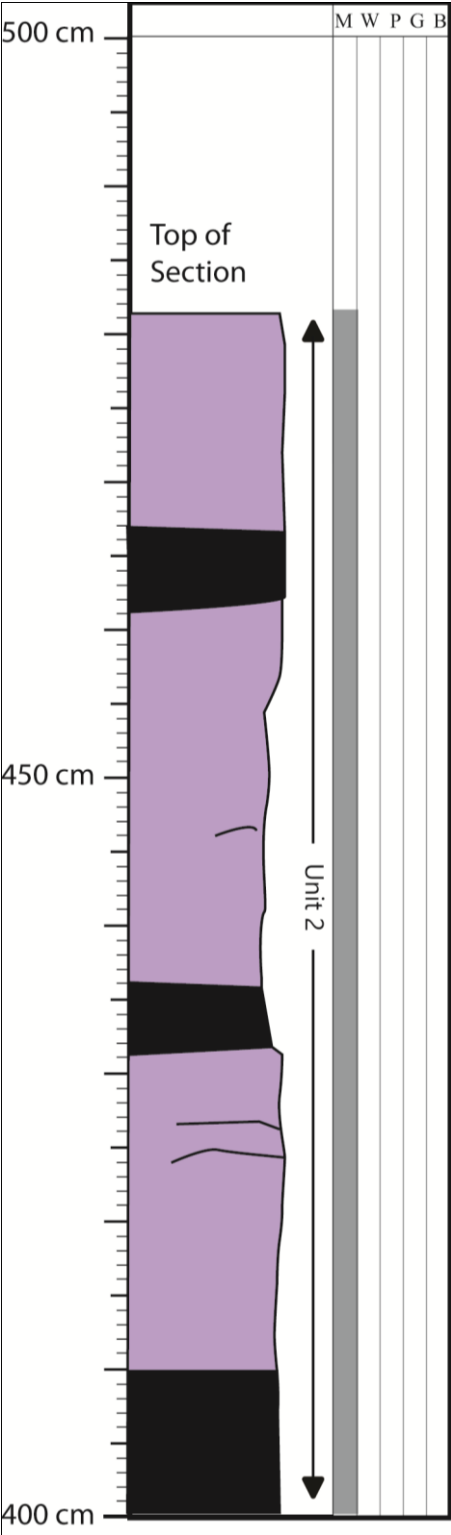
# Stratigraphic Section 8FN3 Continued

Location: N37°11'13.24" W109°47'8.76"



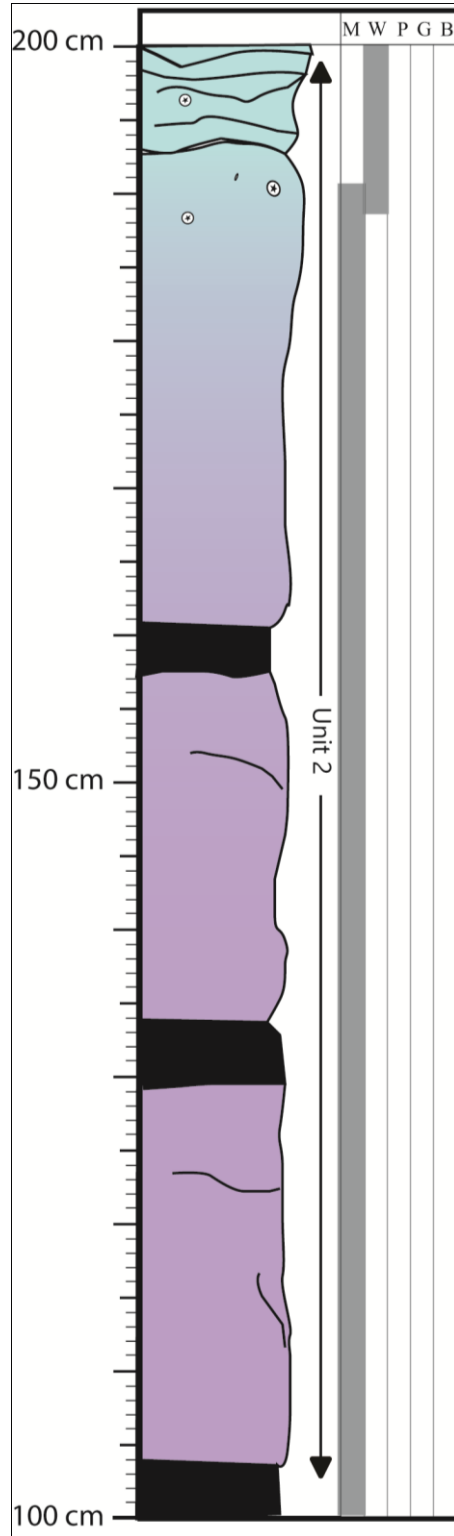
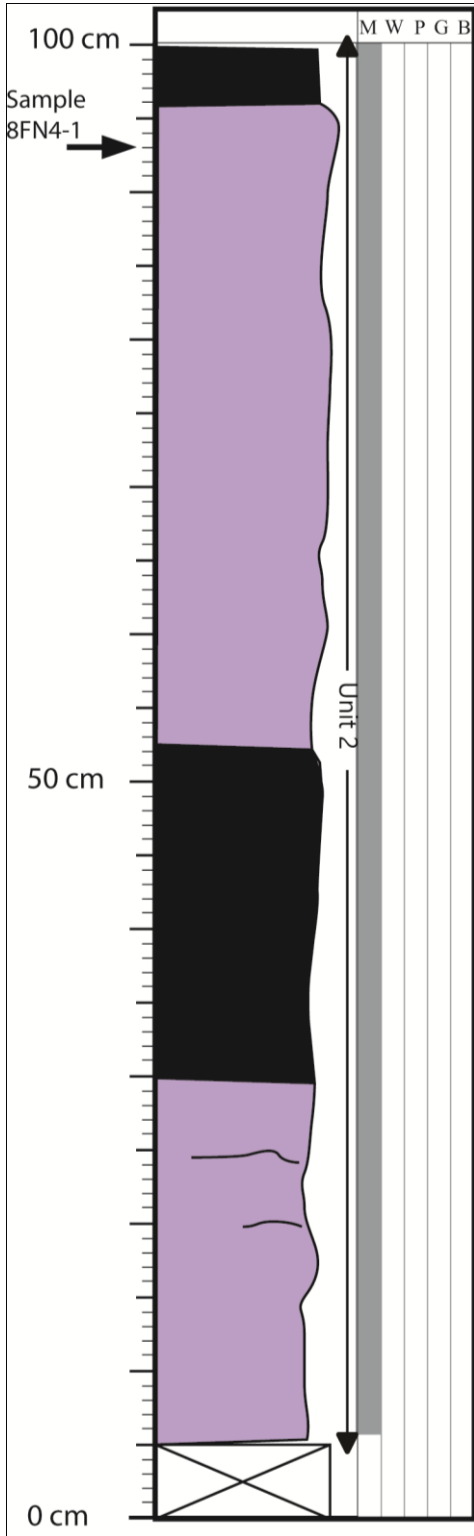
**Stratigraphic Section 8FN3 Continued**

Location: N37°11'13.24" W109°47'8.76"

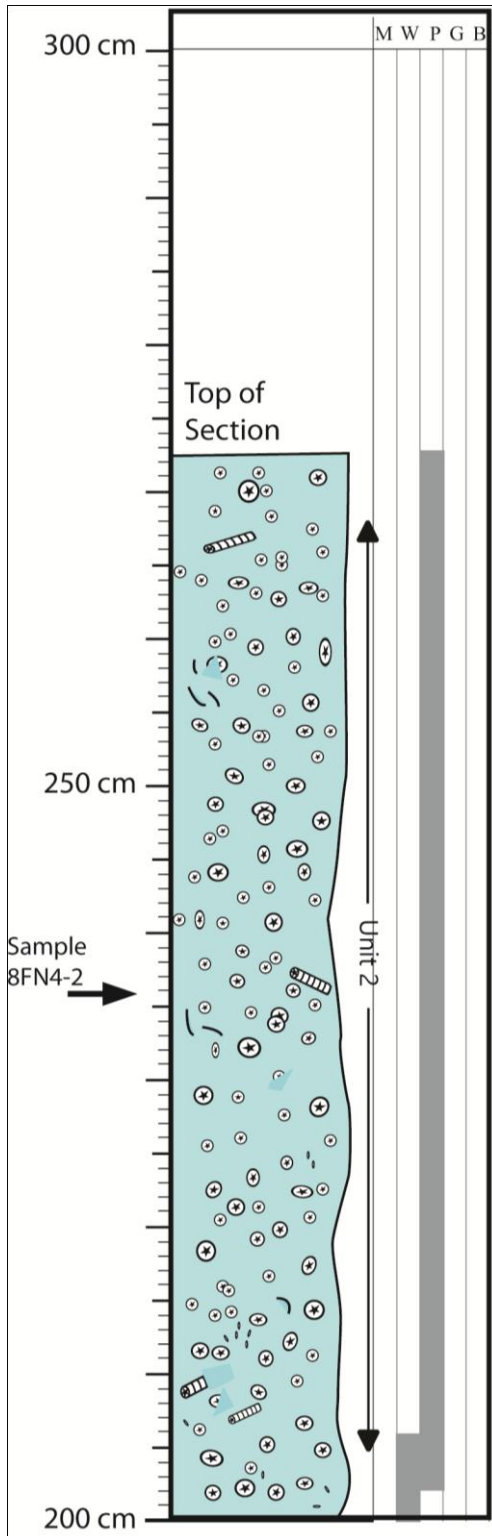




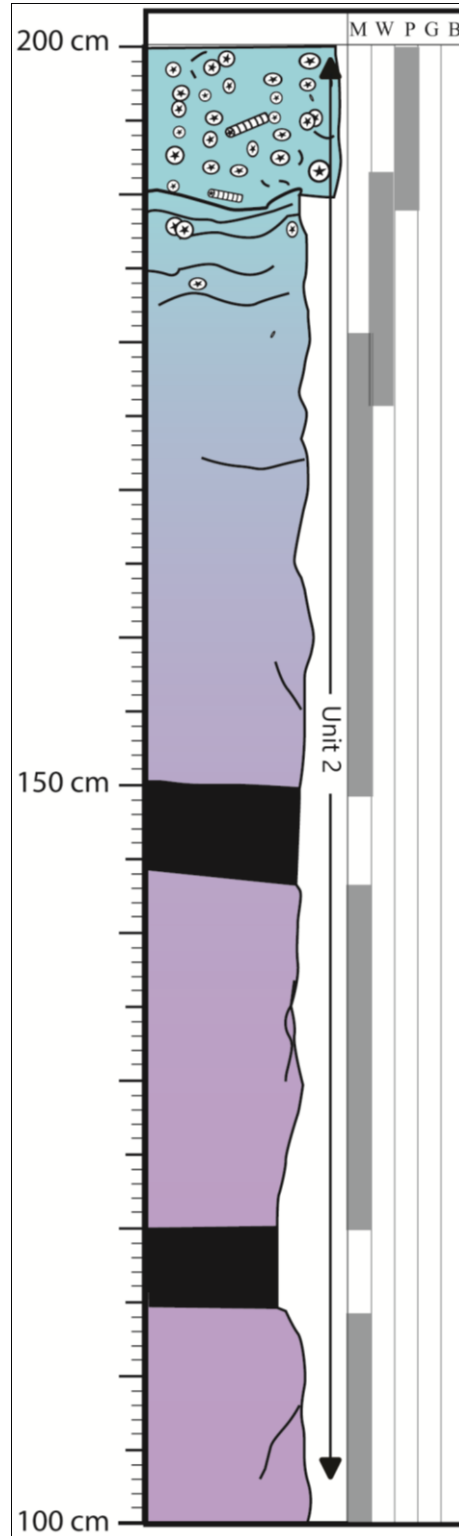
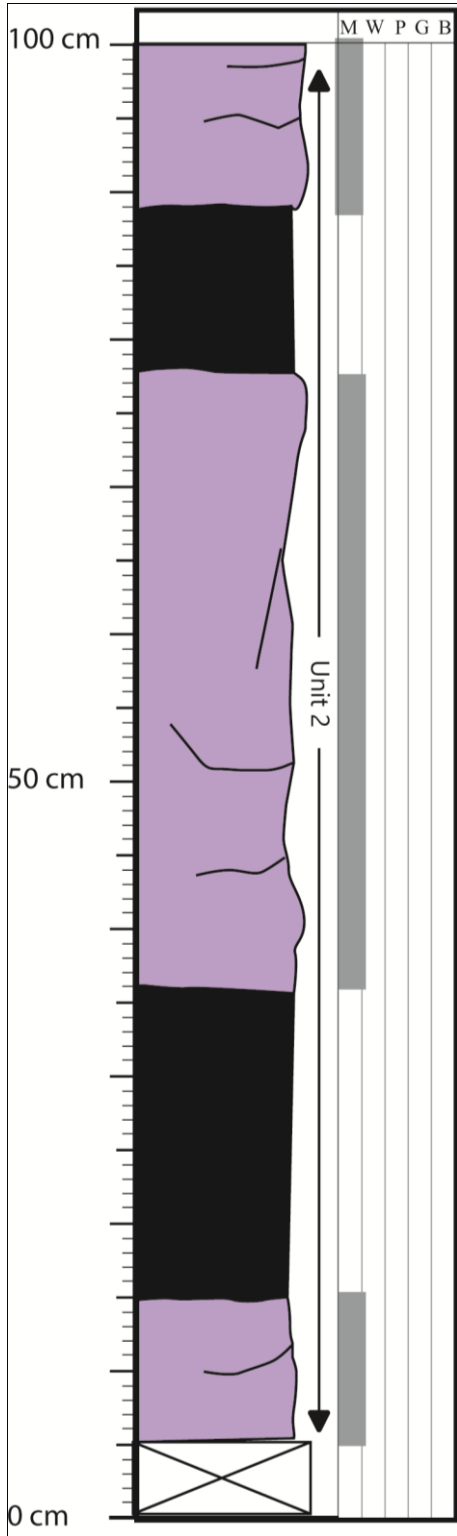
Stratigraphic Section 8FN4  
Location: N37°11'12.07" W109°47'8.69"



Stratigraphic Section 8FN4  
Location: N37°11'12.07" W109°47'8.69"

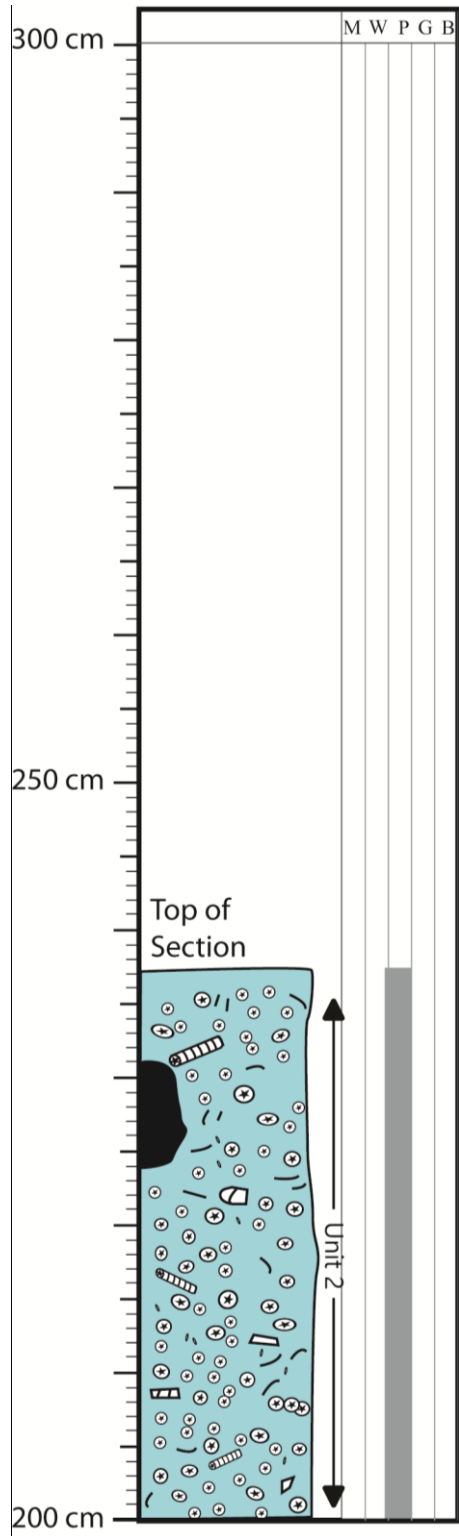


Stratigraphic Section 8FN5  
Location: N37°11'10.63" W109°47'8.49"

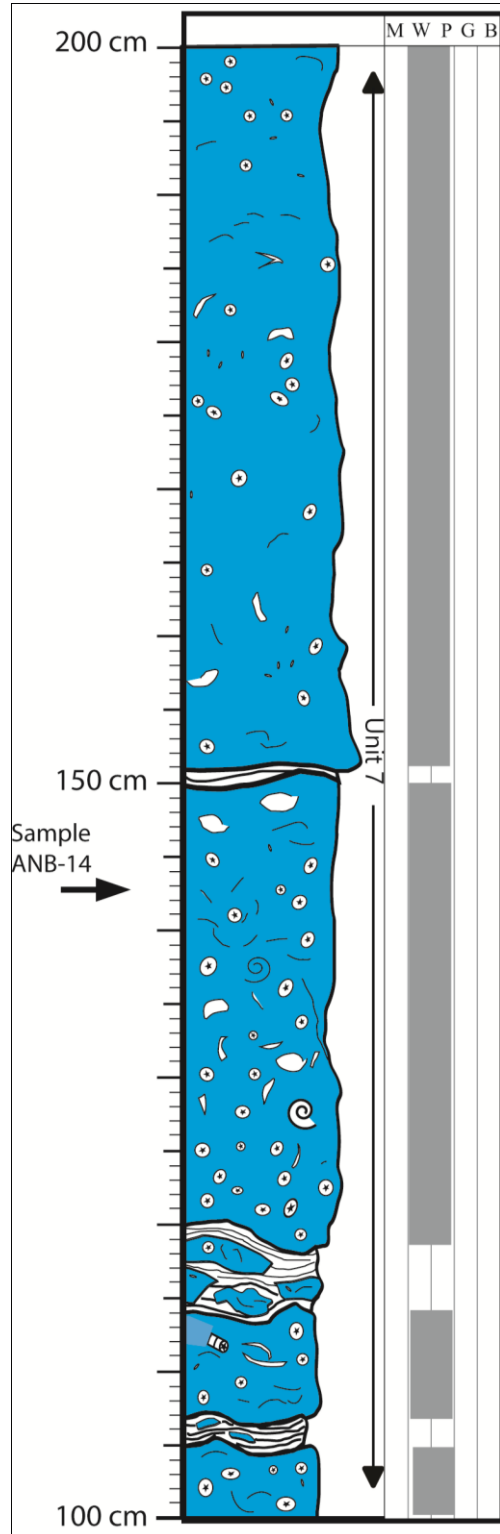
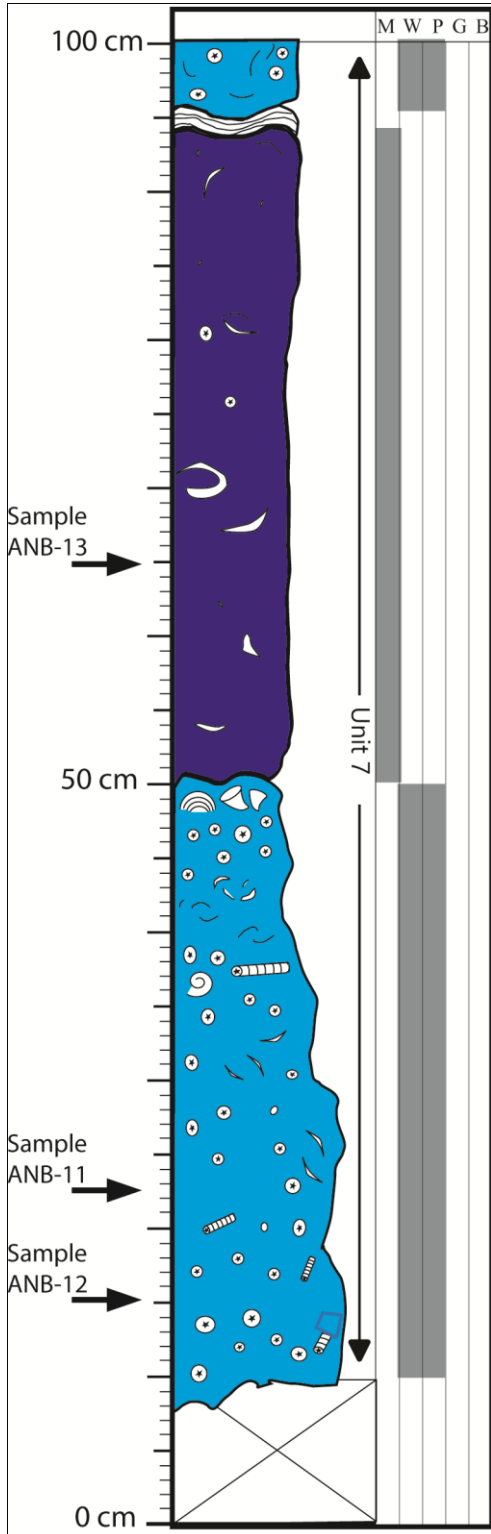


# Stratigraphic Section 8FN5 Continued

Location: N37°11'10.63" W109°47'8.49"

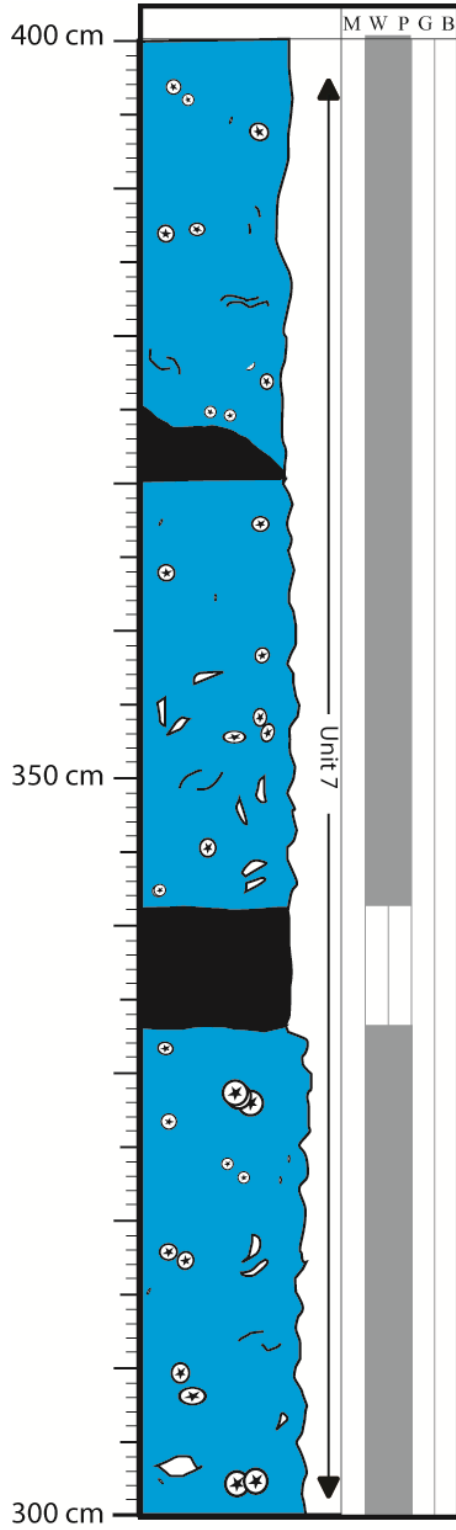
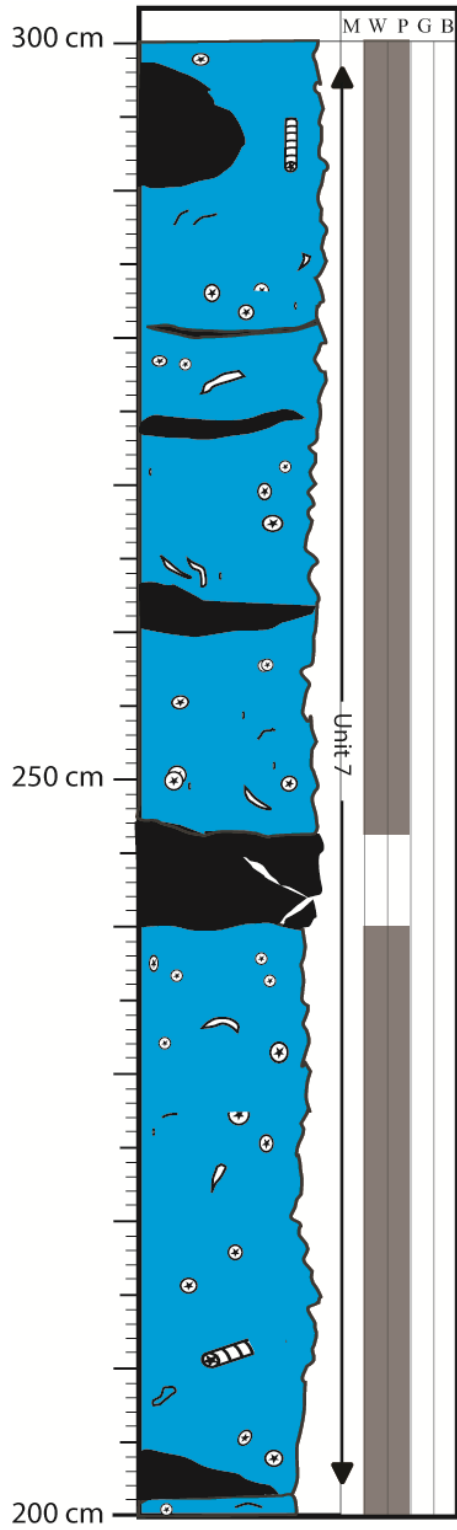


Stratigraphic Section ANBL  
Location: N37°10'58.52" W109°46'34.09"



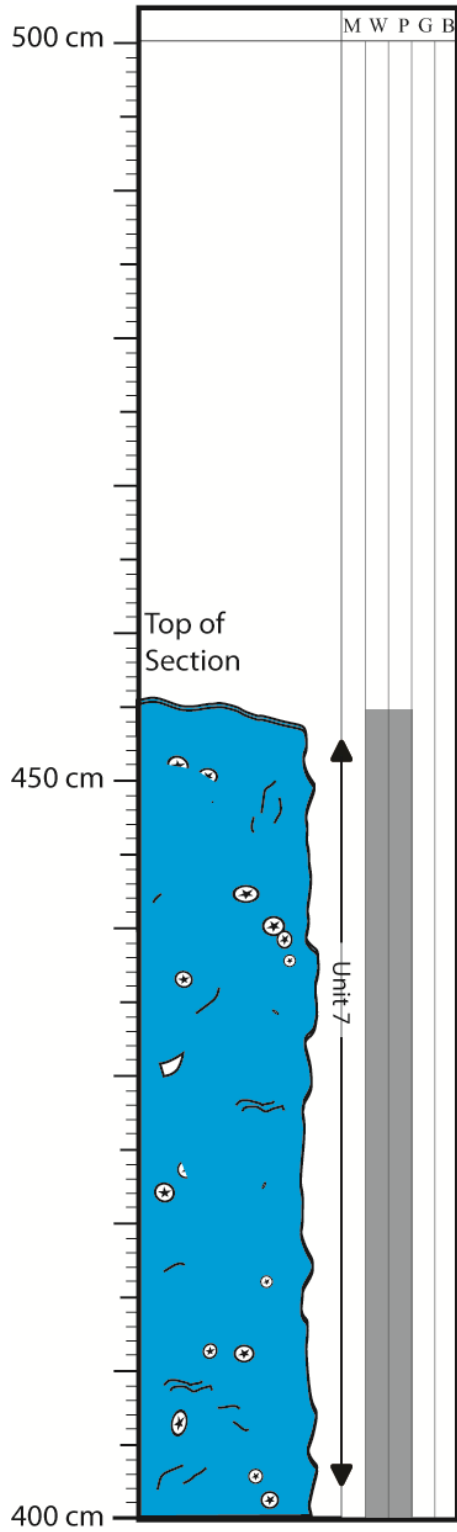
# Stratigraphic Section ANBL Continued

Location: N37°10'58.52" W109°46'34.09"

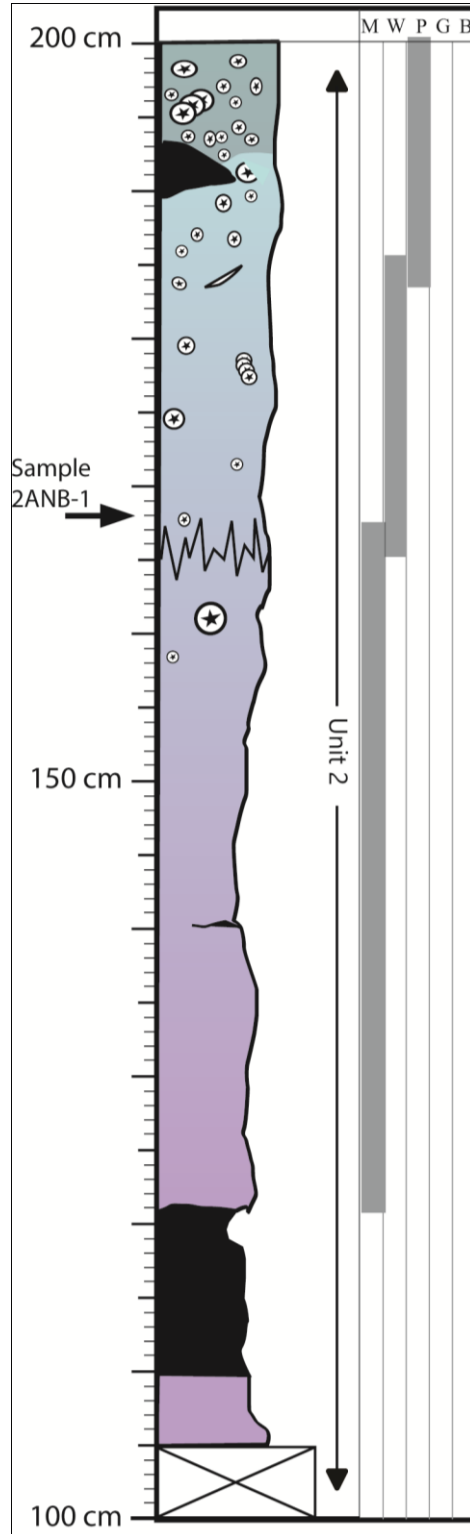
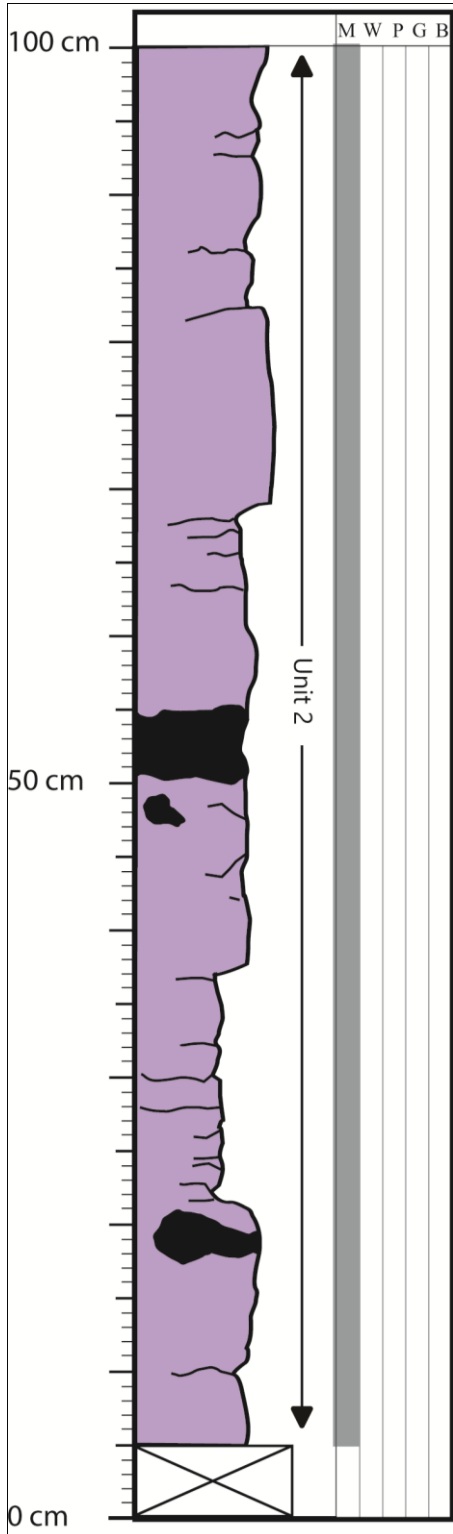


# Stratigraphic Section ANBL Continued

Location: N37°10'58.52" W109°46'34.09"

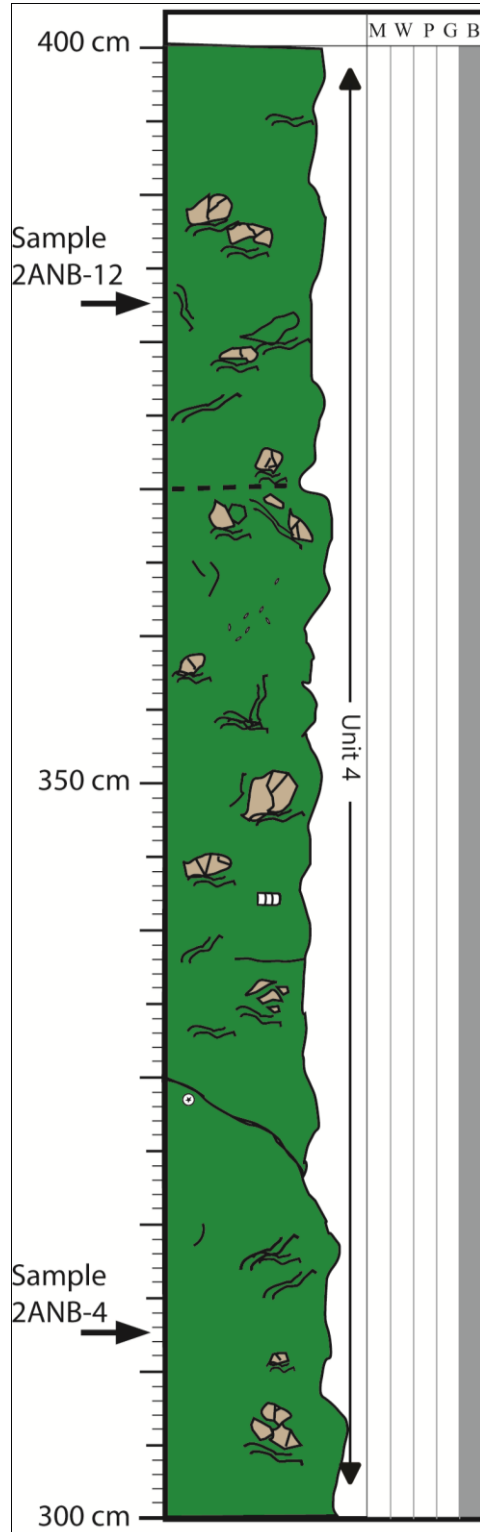
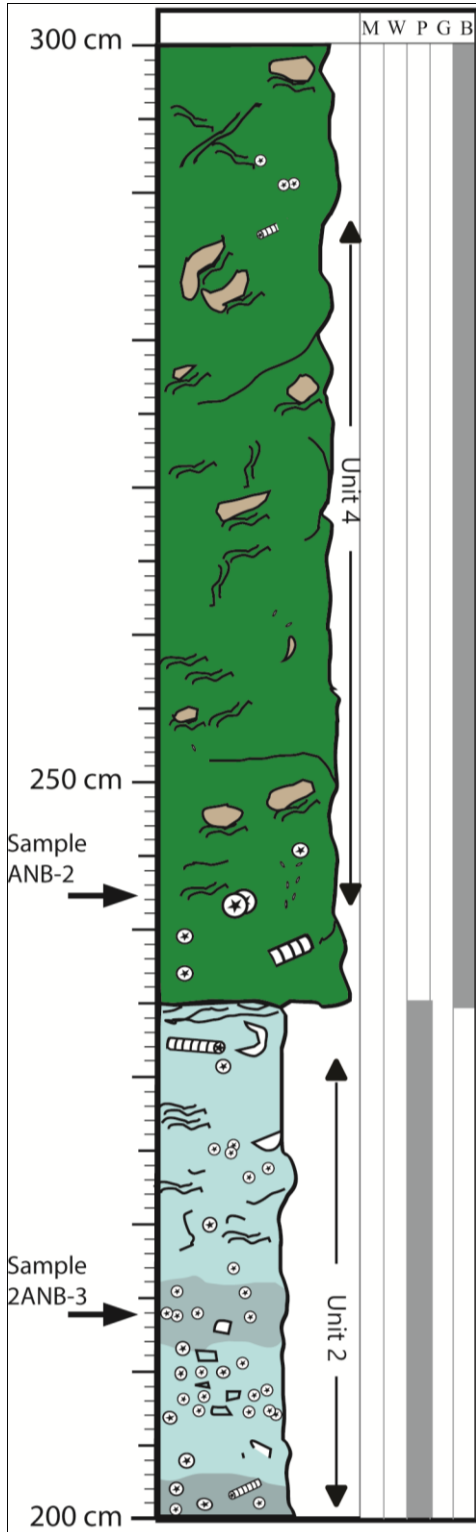


Stratigraphic Section ANBR  
 Location: N37°10'56.93" W109°46'31.82"



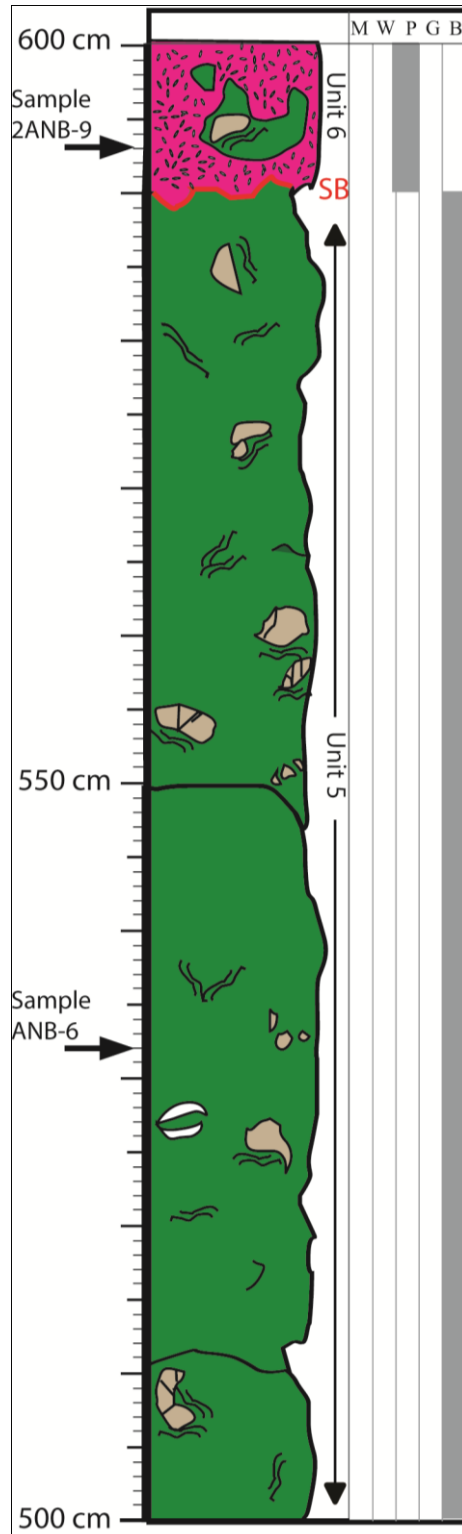
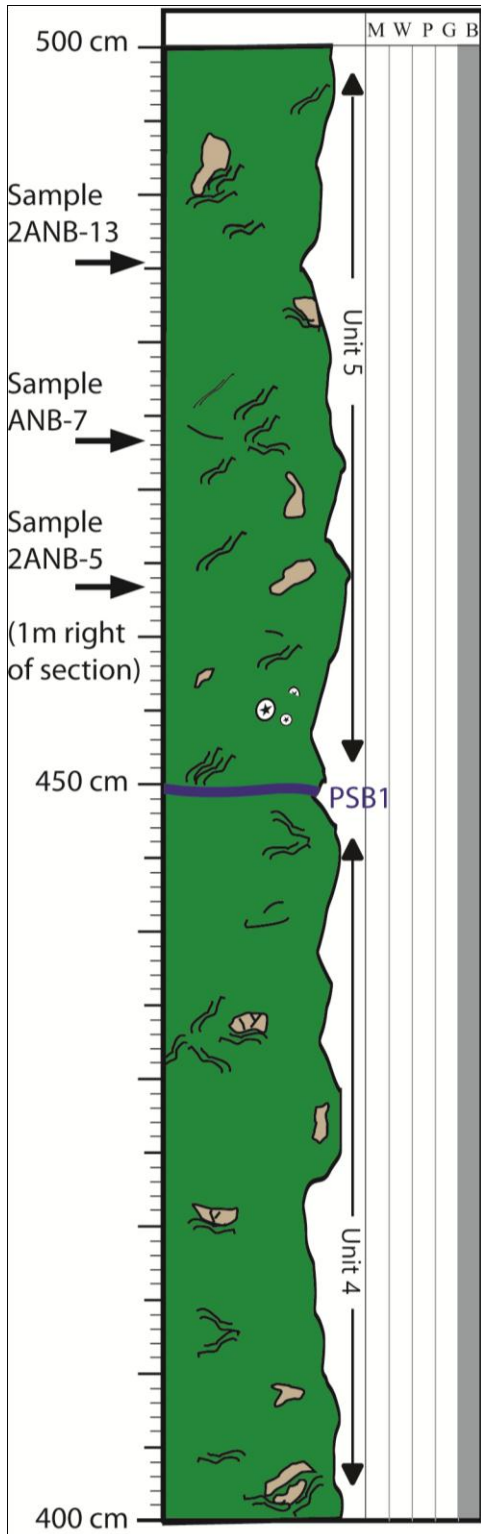


Stratigraphic Section ANBR Continued  
 Location: N37°10'56.93" W109°46'31.82"



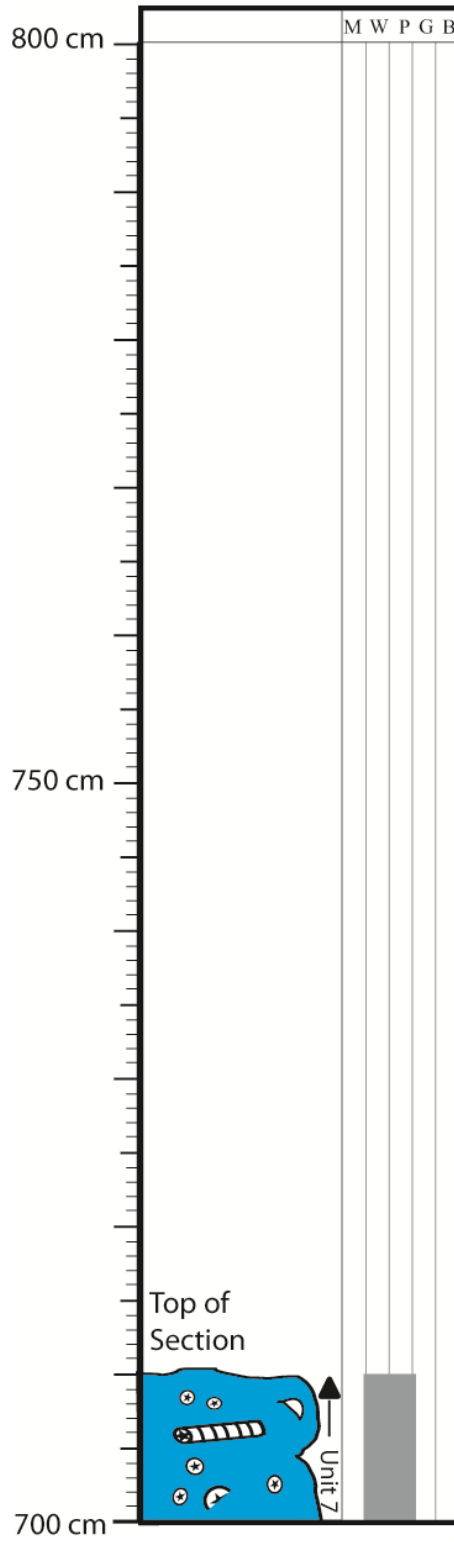
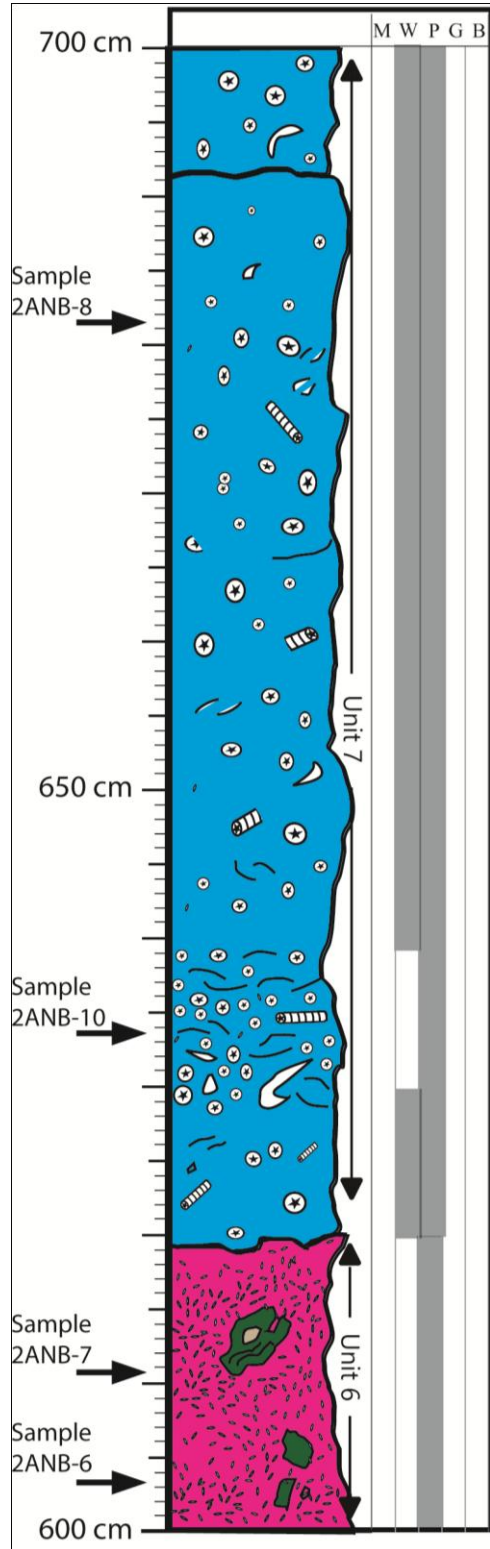
# Stratigraphic Section ANBR Continued

Location: N37°10'56.93" W109°46'31.82"

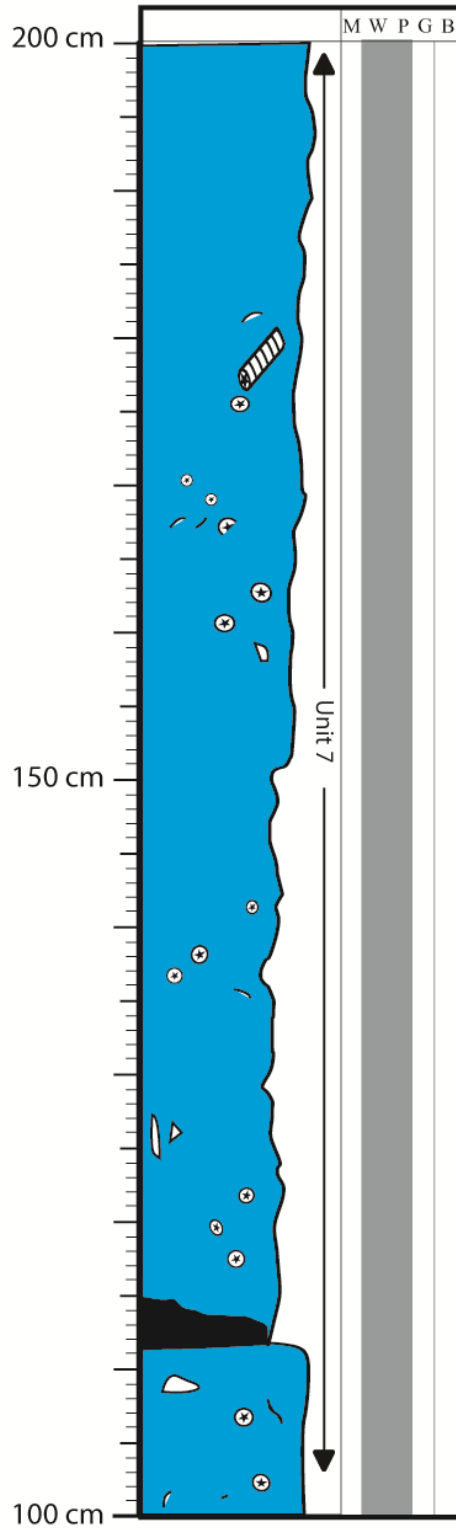
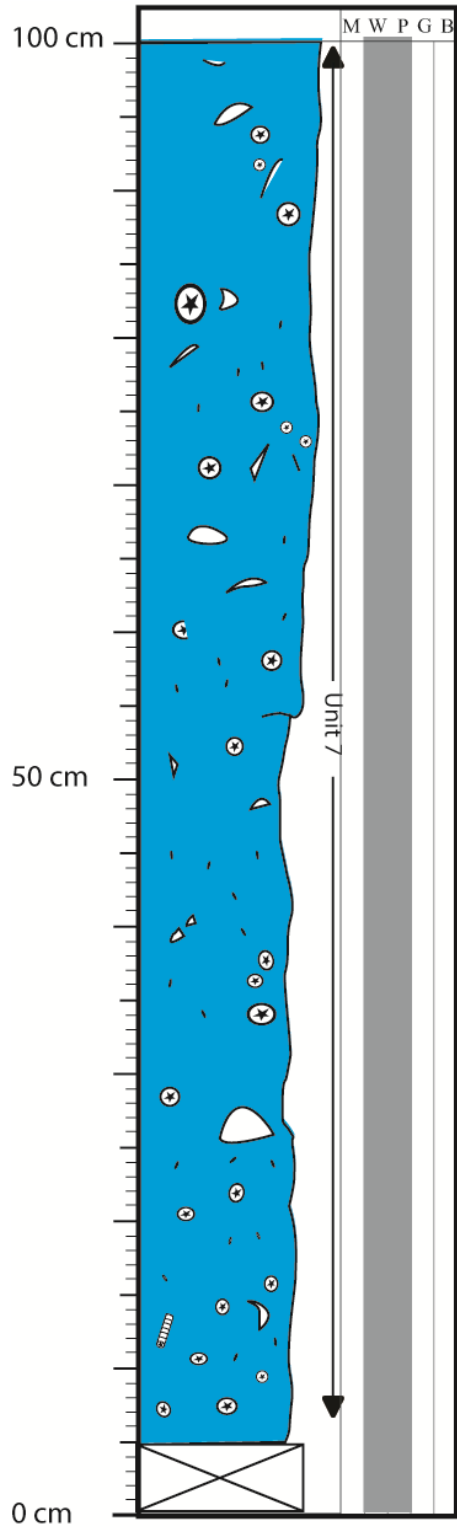


# Stratigraphic Section ANBR Continued

Location: N37°10'56.93" W109°46'31.82"

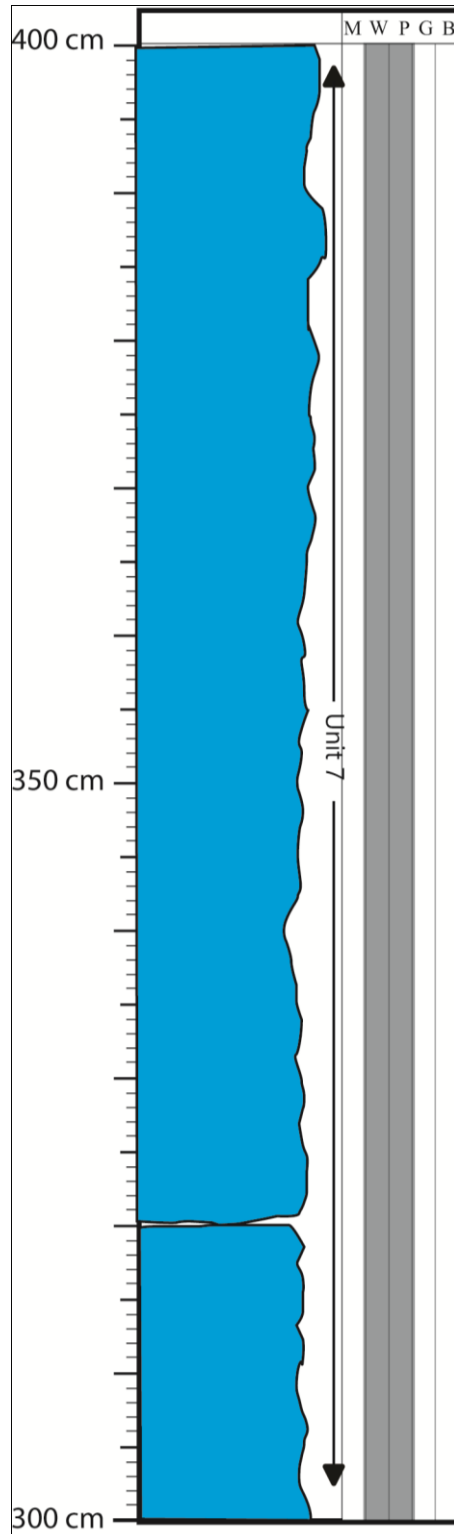
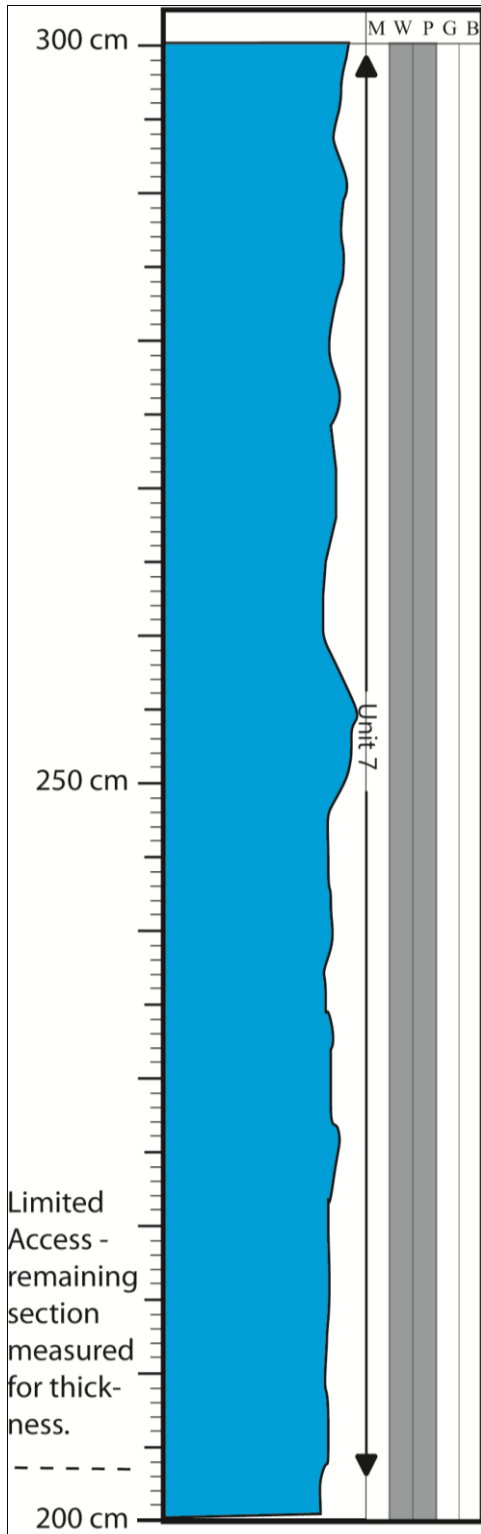


Stratigraphic Section ANB-Up  
Location: N37°10'57.93" W109°46'33.36"



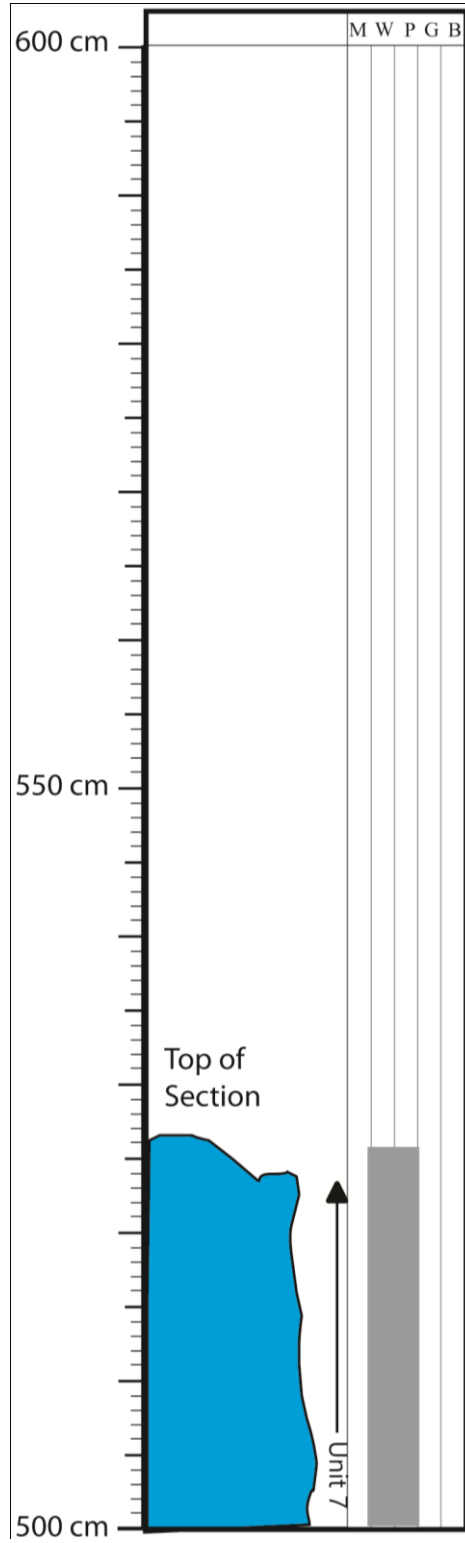
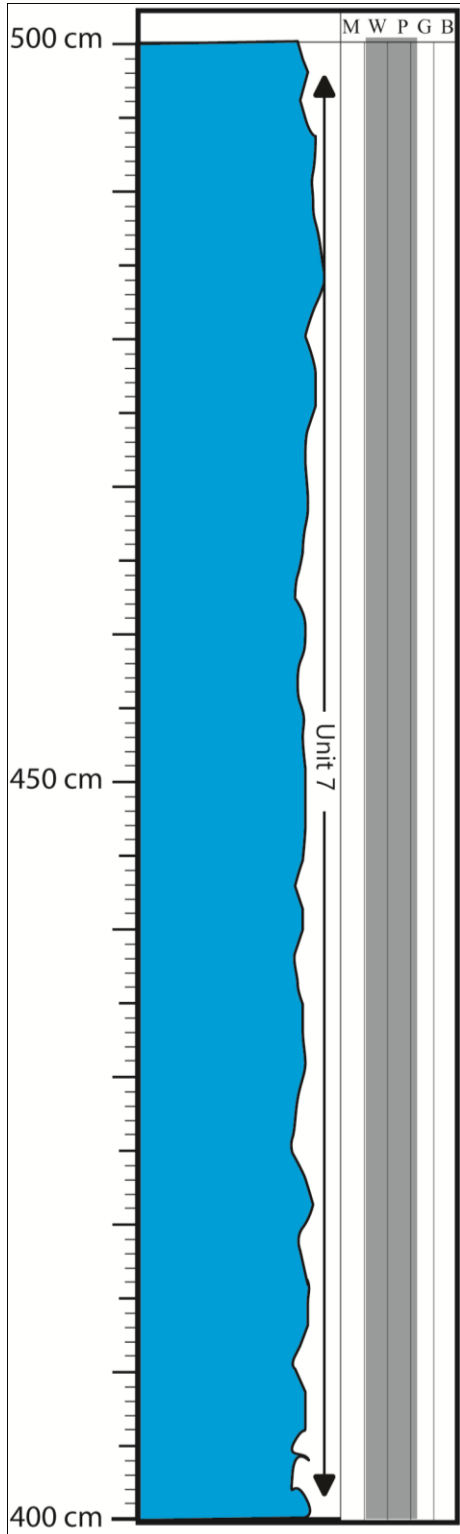
# Stratigraphic Section ANB-Up Continued

Location: N37°10'57.93" W109°46'33.36"

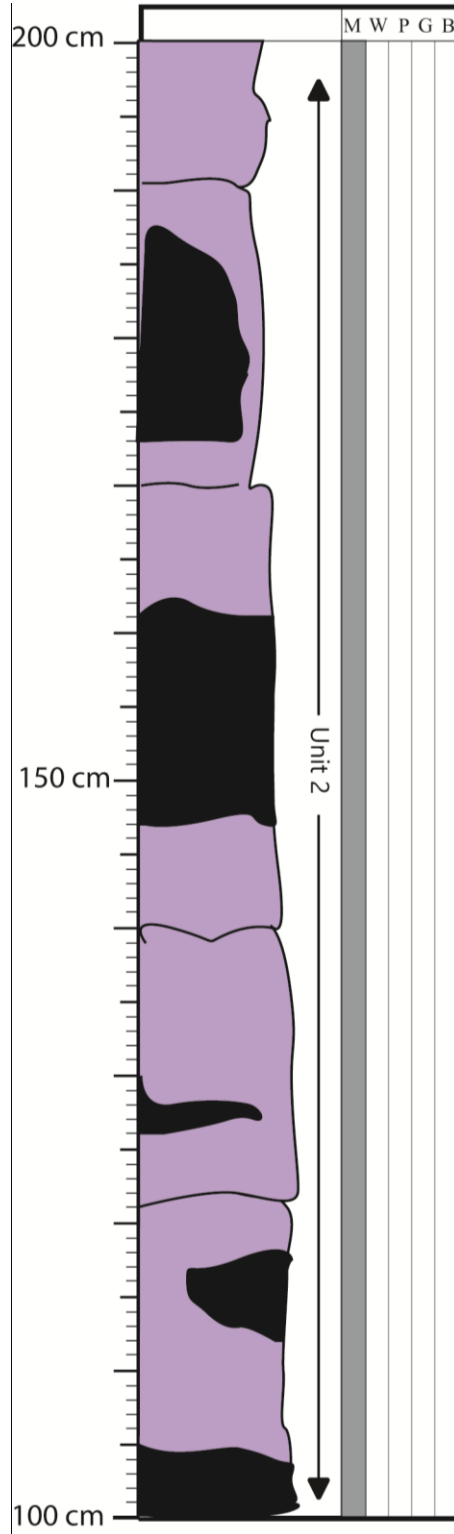
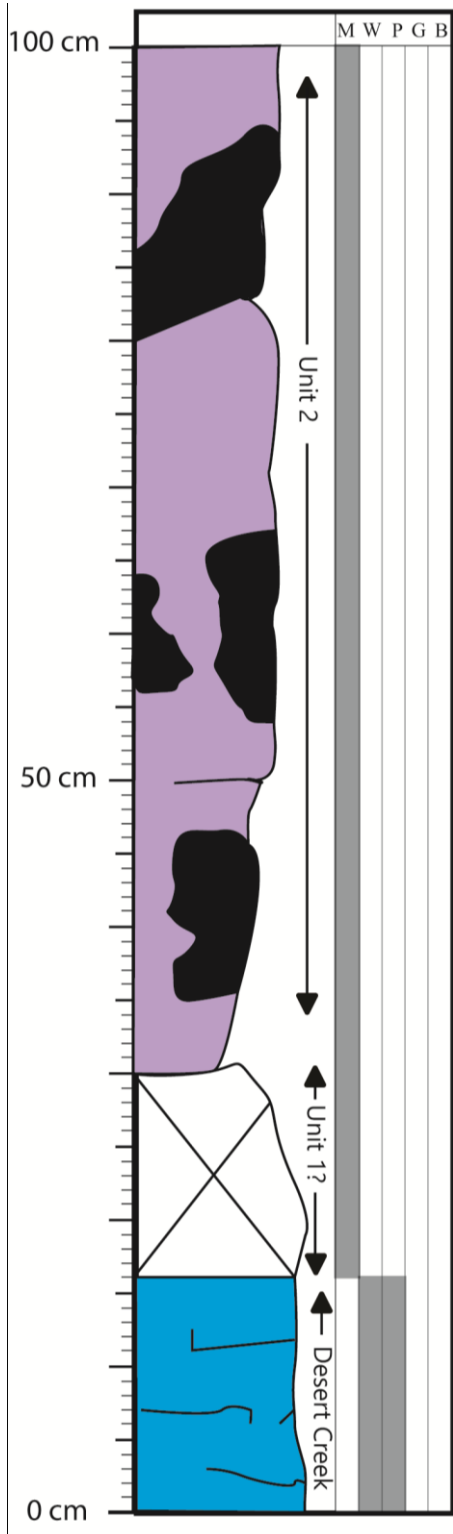


# Stratigraphic Section ANB-Up Continued

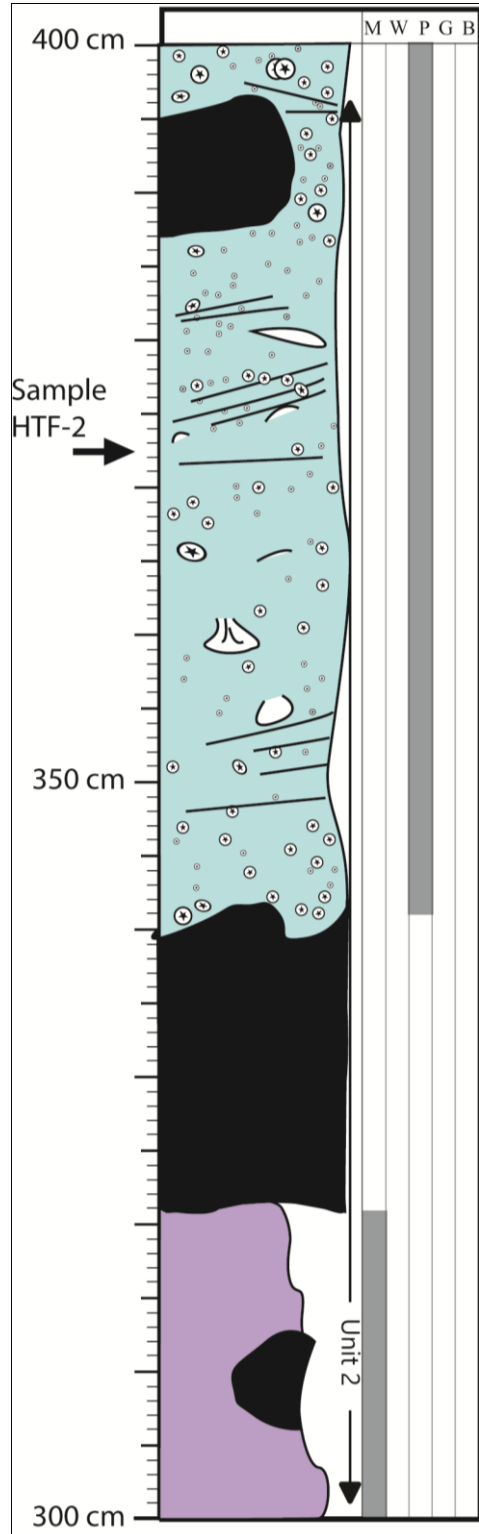
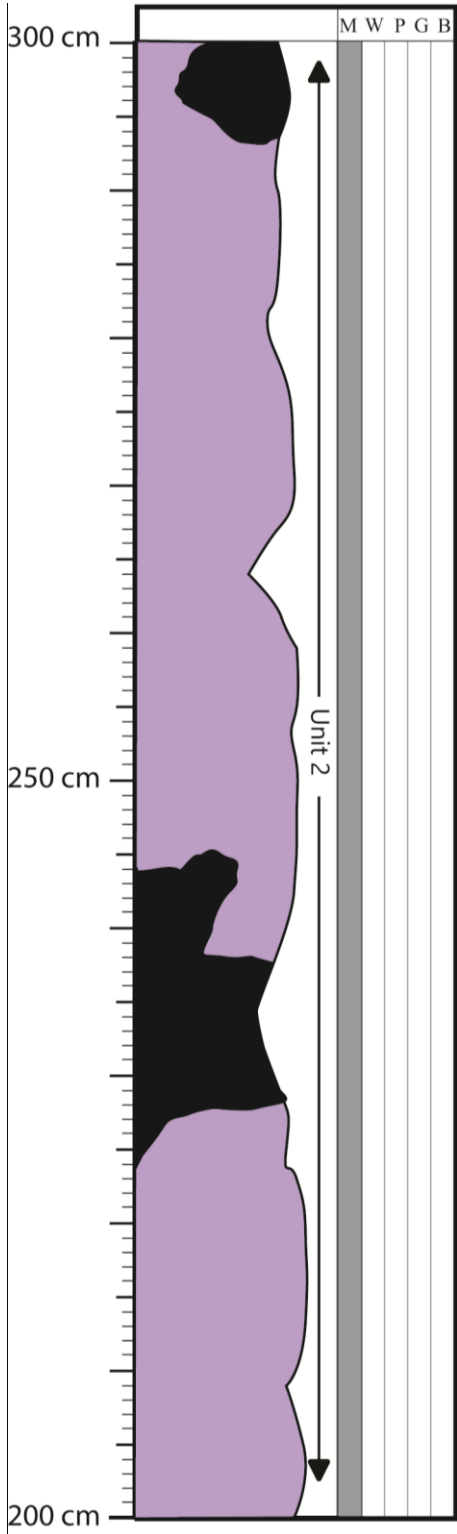
Location: N37°10'57.93" W109°46'33.36"



Stratigraphic Section HTF  
Location: N37°11'15.35" W109°57'29.09"



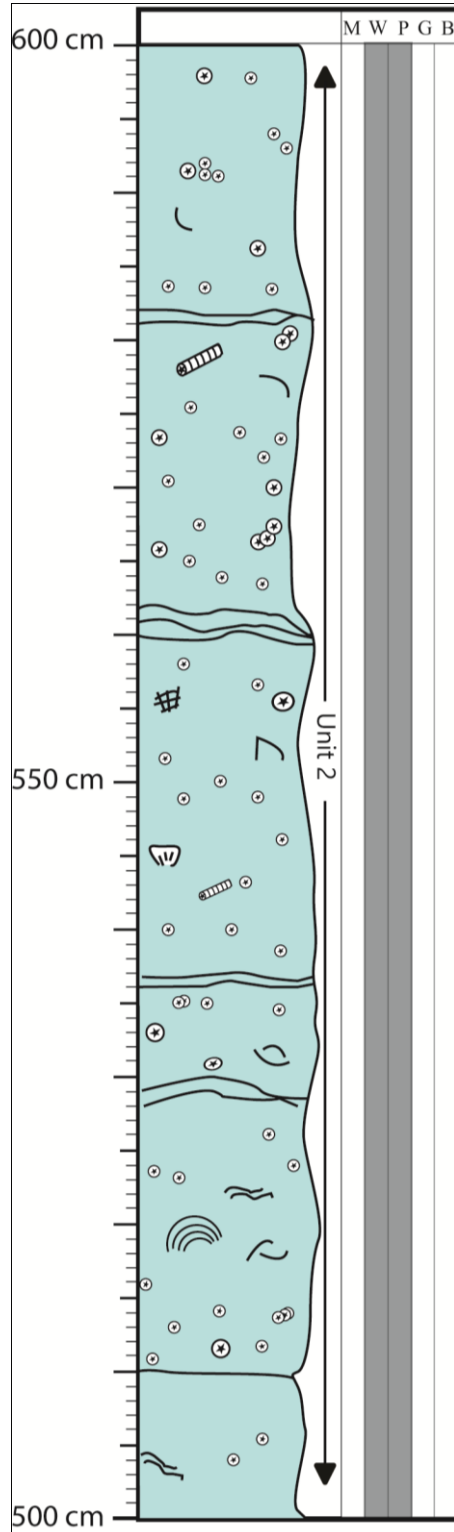
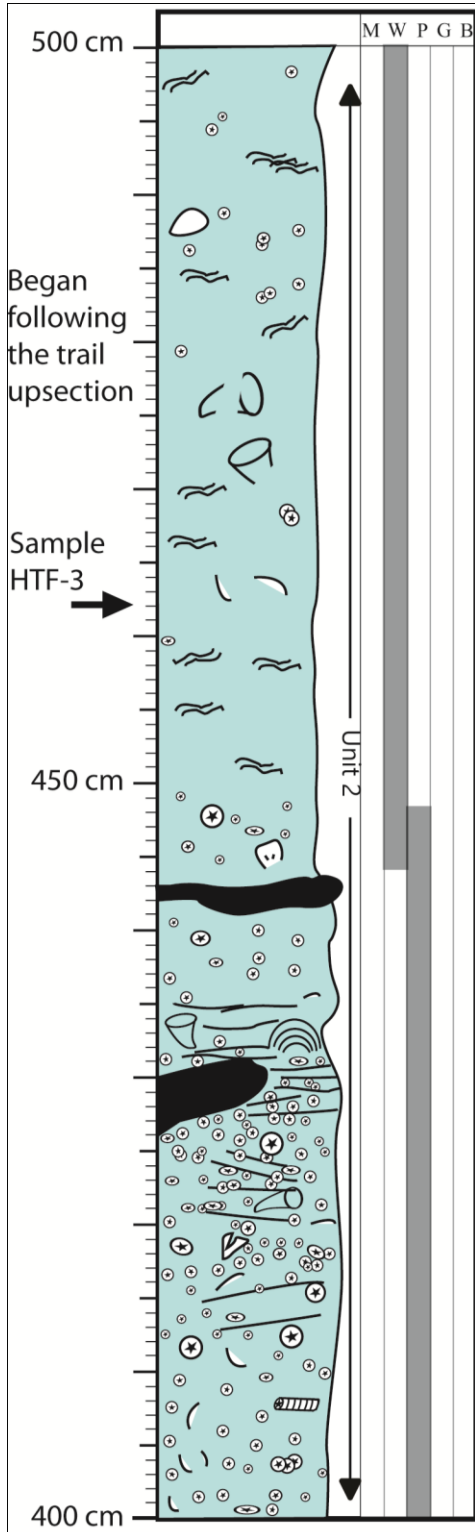
Stratigraphic Section HTF Continued  
Location: N37°11'15.35" W109°57'29.09"





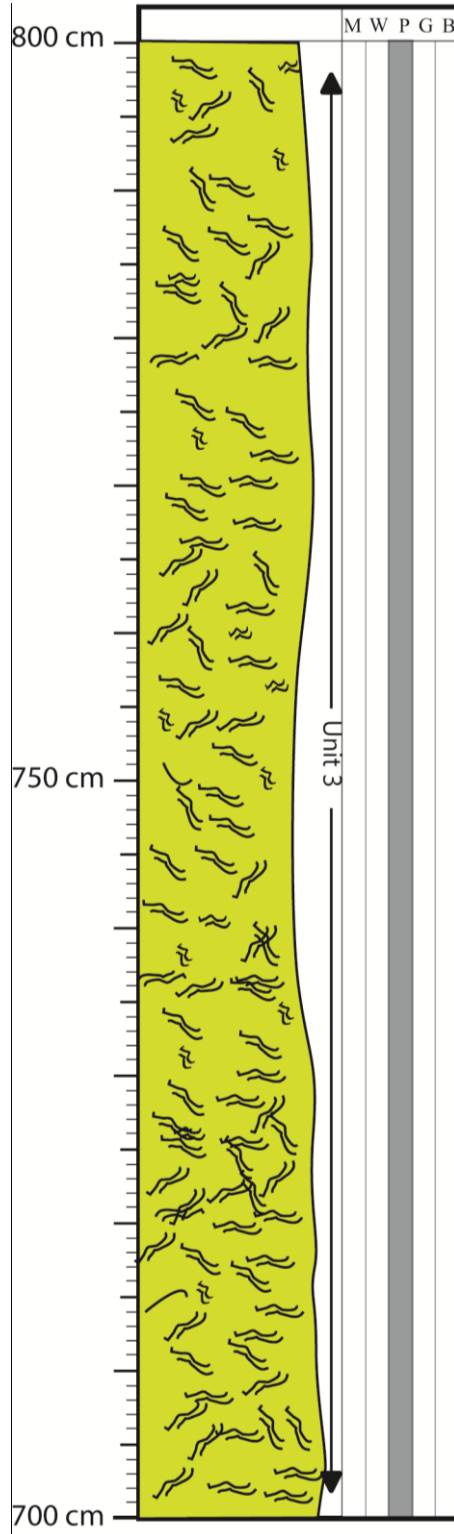
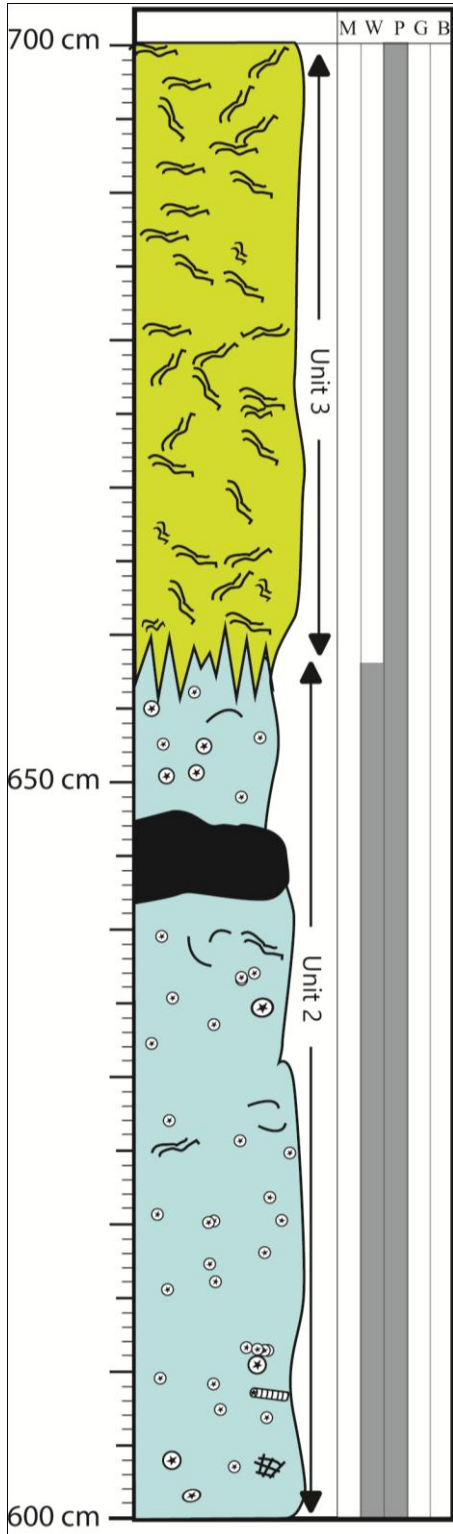
# Stratigraphic Section HTF Continued

Location: N37°11'15.35" W109°57'29.09"



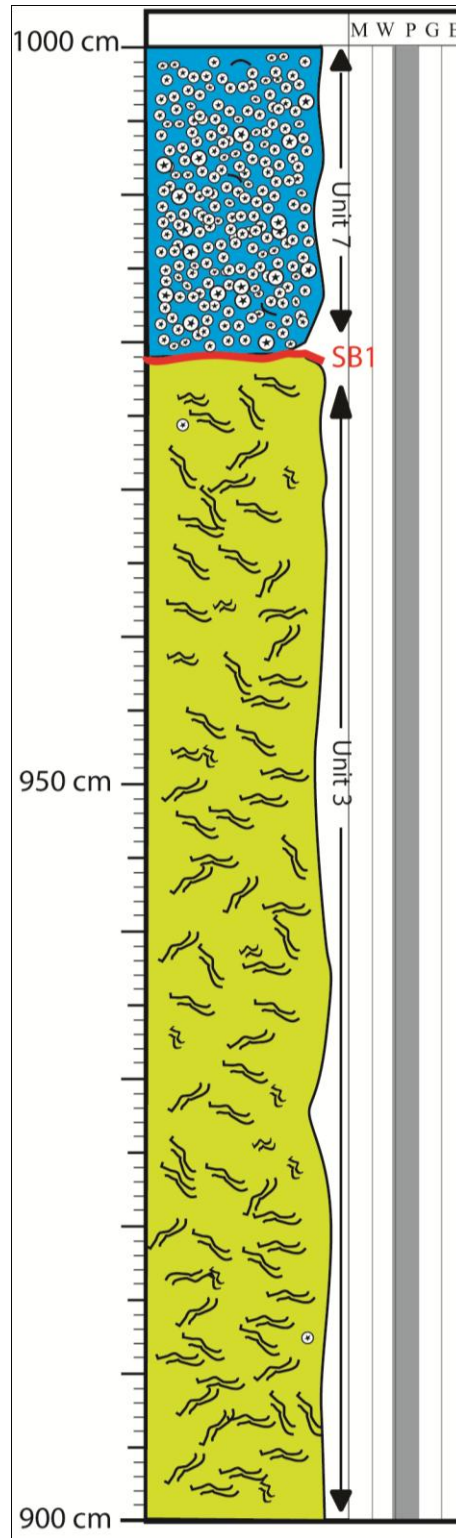
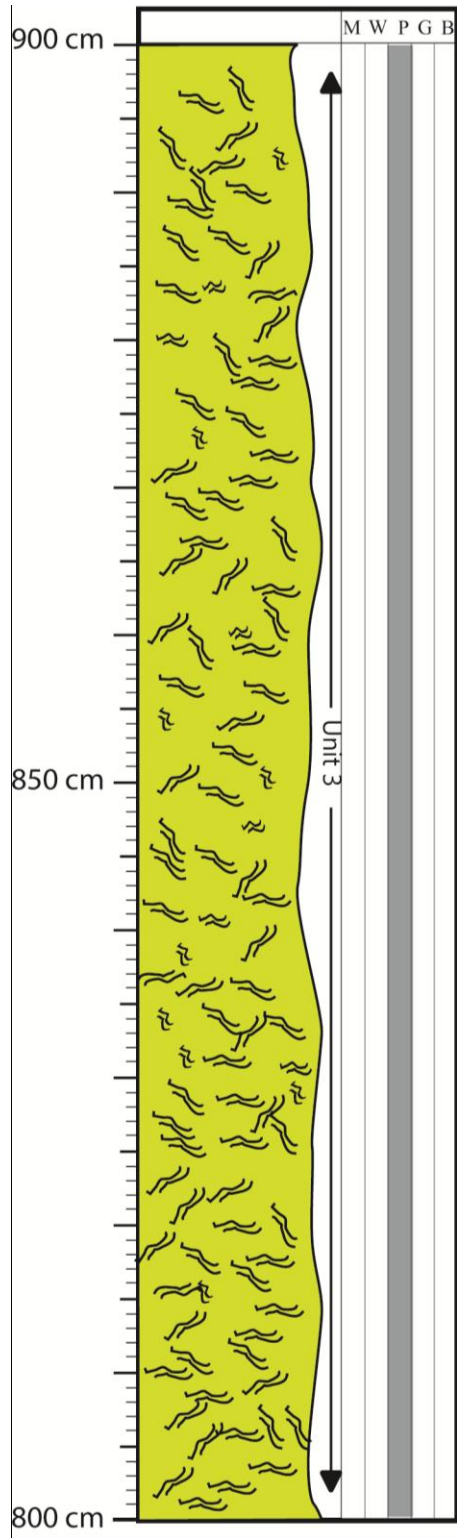
# Stratigraphic Section HTF Continued

Location: N37°11'15.35" W109°57'29.09"



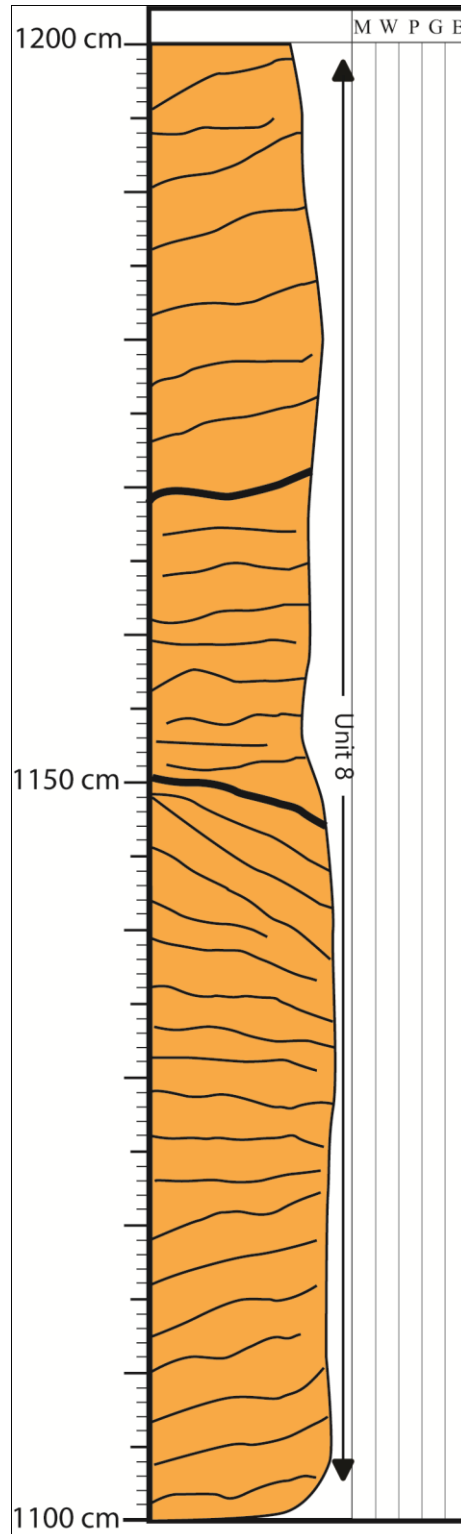
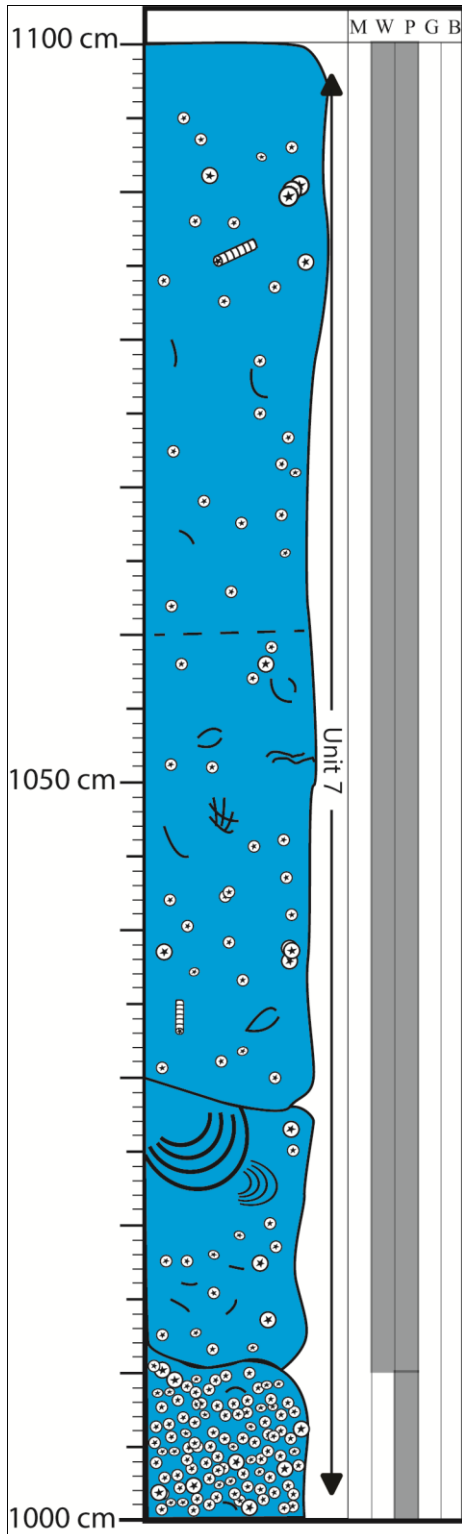
# Stratigraphic Section HTF Continued

Location: N37°11'15.35" W109°57'29.09"



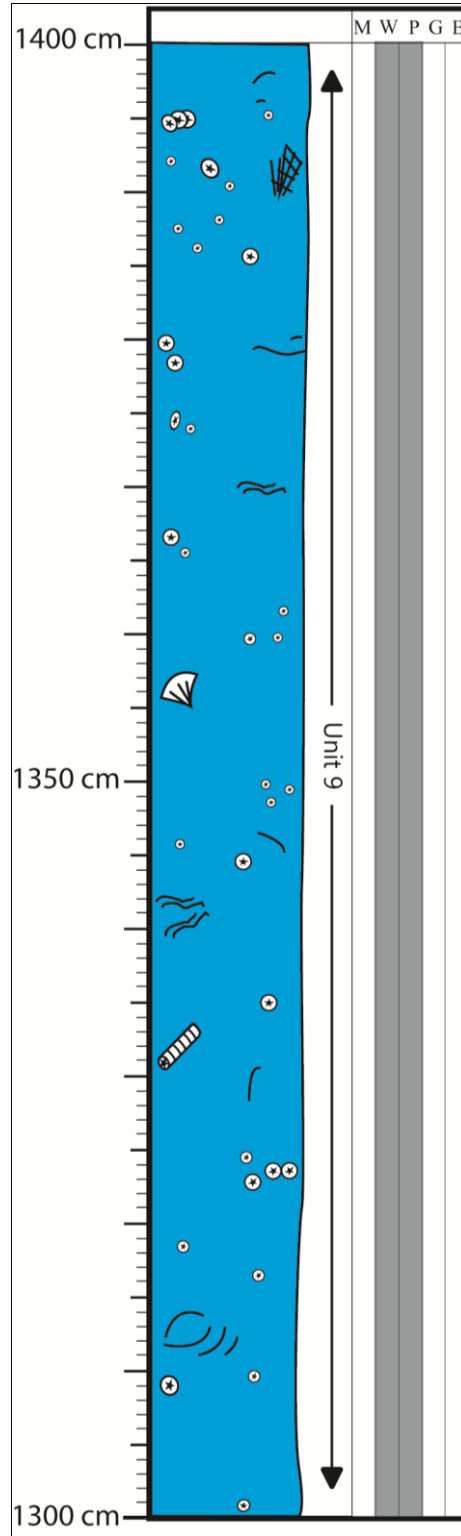
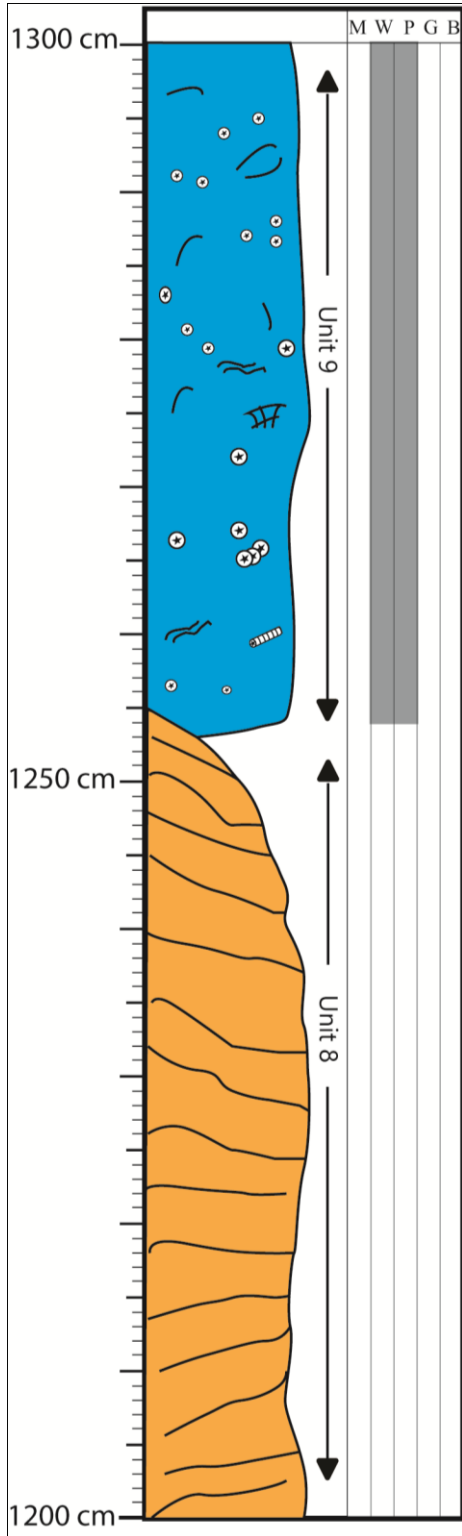
# Stratigraphic Section HTF Continued

Location: N37°11'15.35" W109°57'29.09"

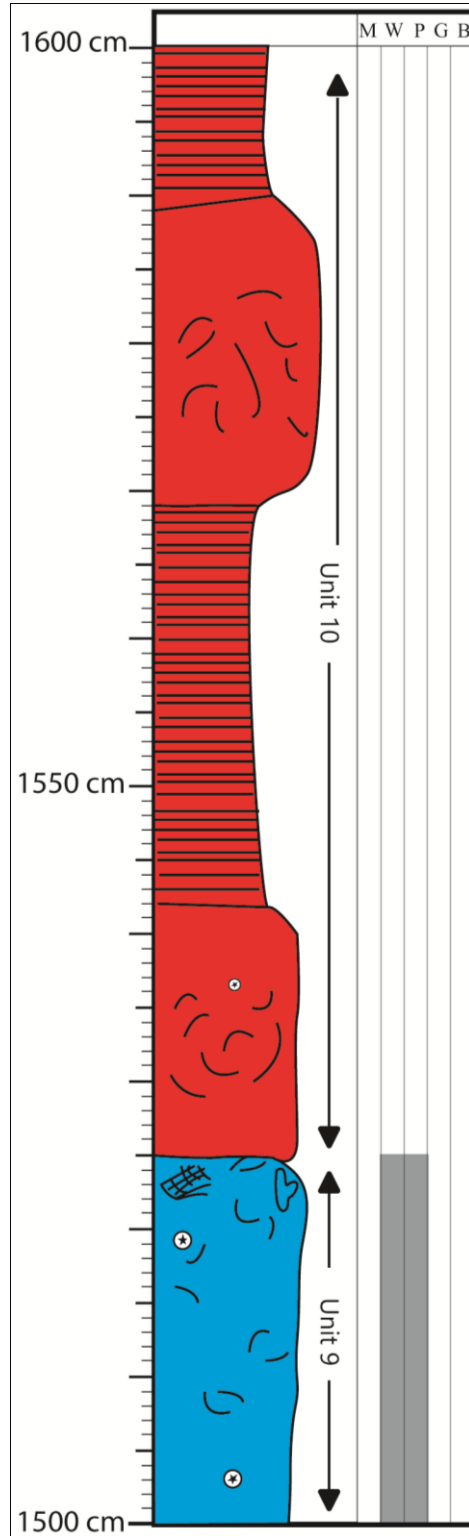
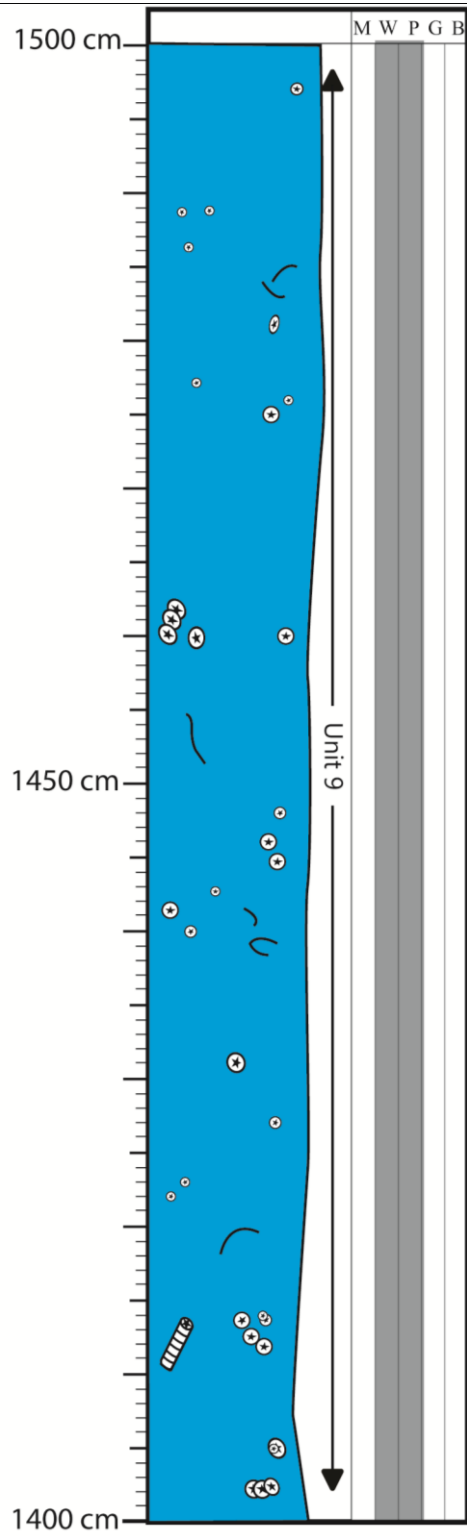


# Stratigraphic Section HTF Continued

Location: N37°11'15.35" W109°57'29.09"

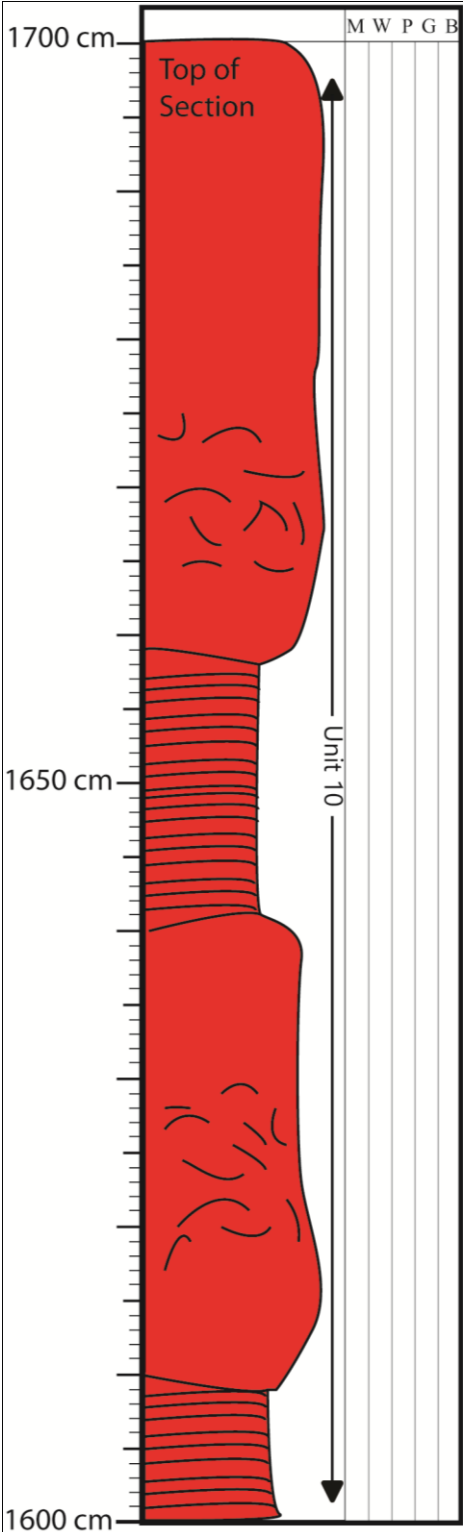


Stratigraphic Section HTF Continued  
Location: N37°11'15.35" W109°57'29.09"



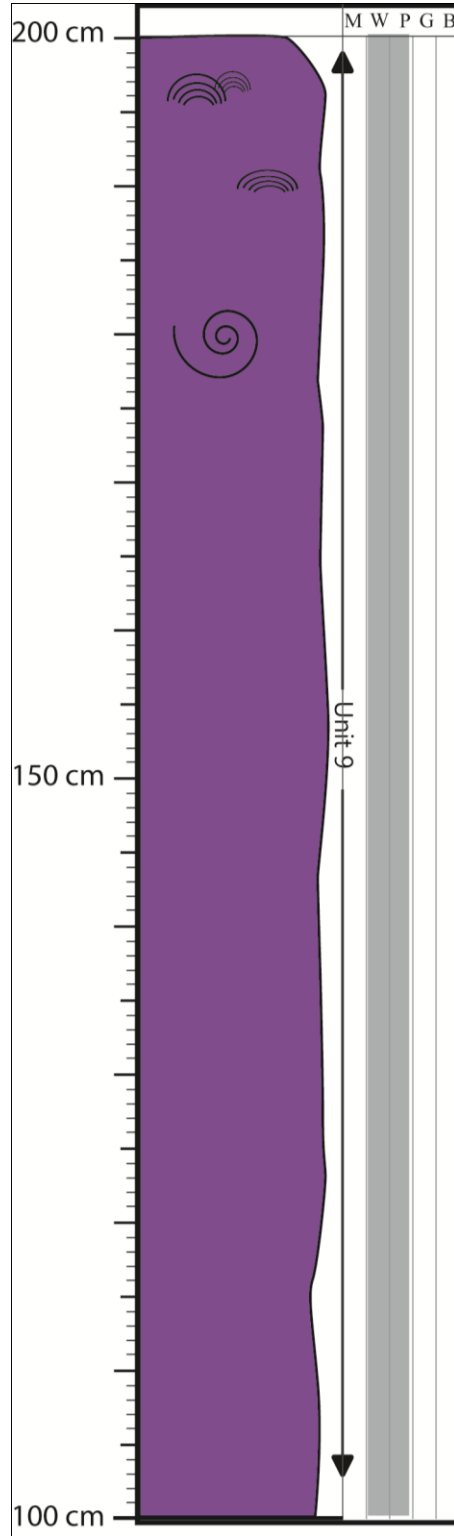
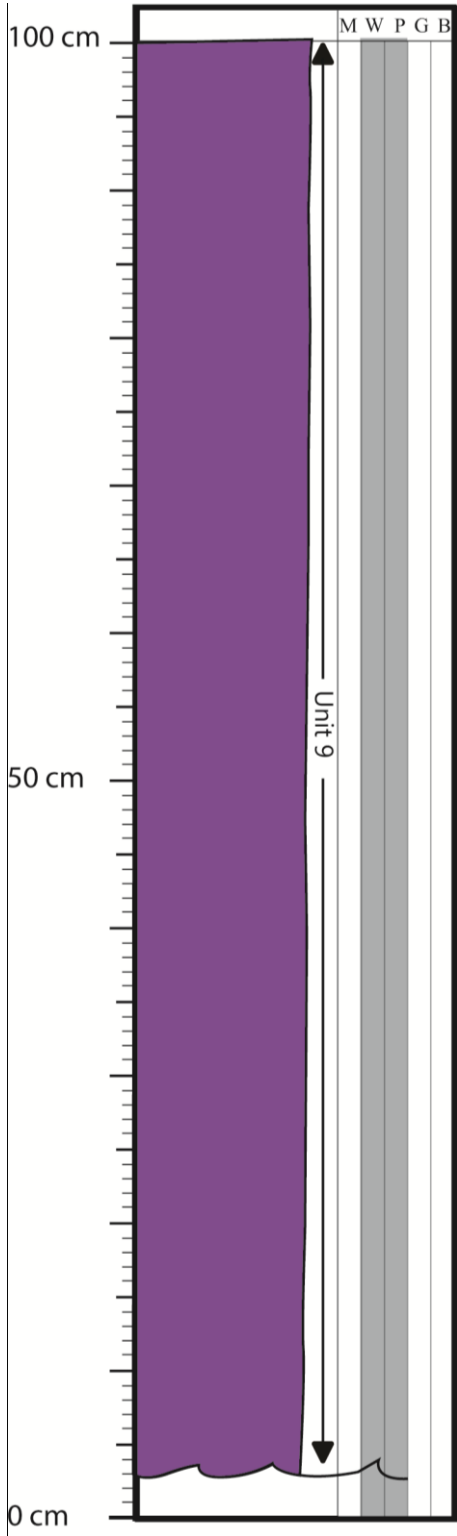
# Stratigraphic Section HTF Continued

Location: N37°11'15.35" W109°57'29.09"



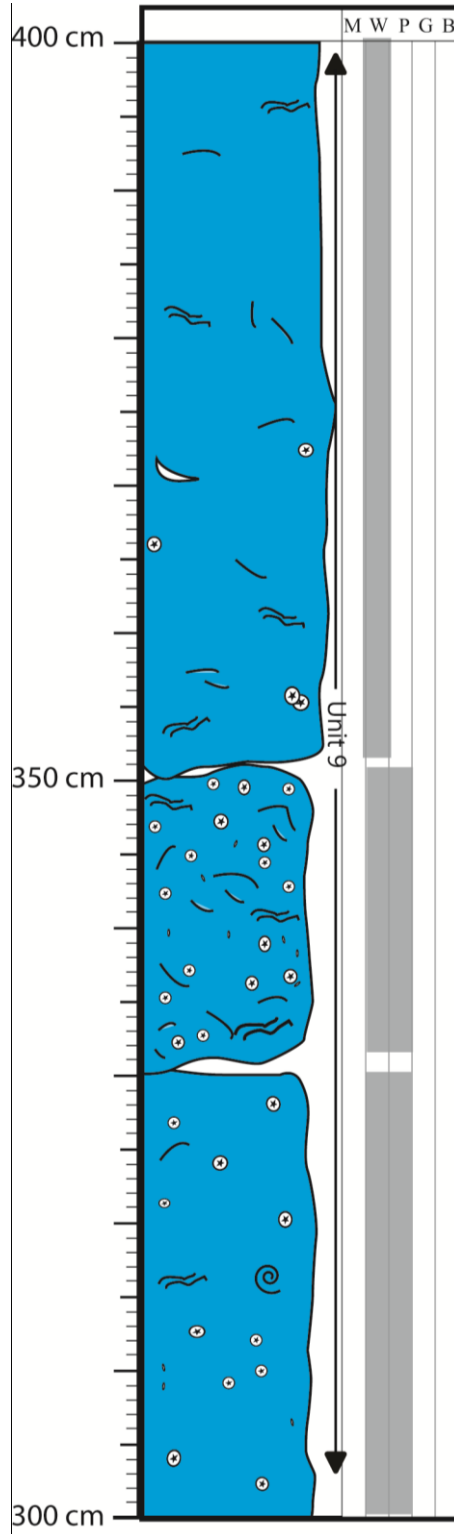
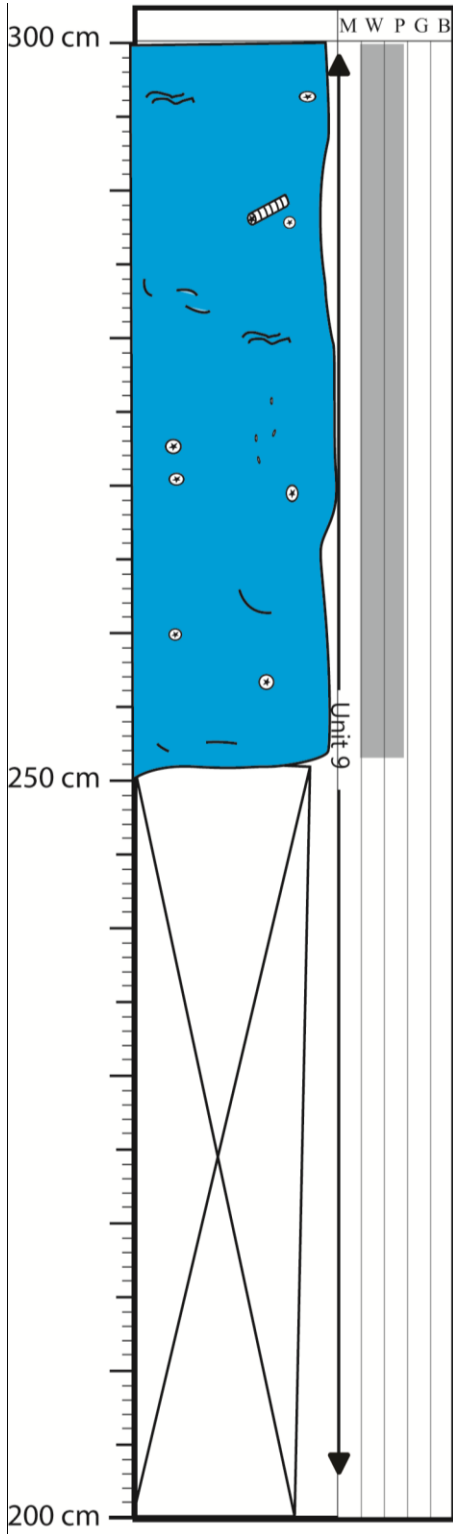
# Stratigraphic Section N2

Location: N37°11'13.44" W109°46'9.01"

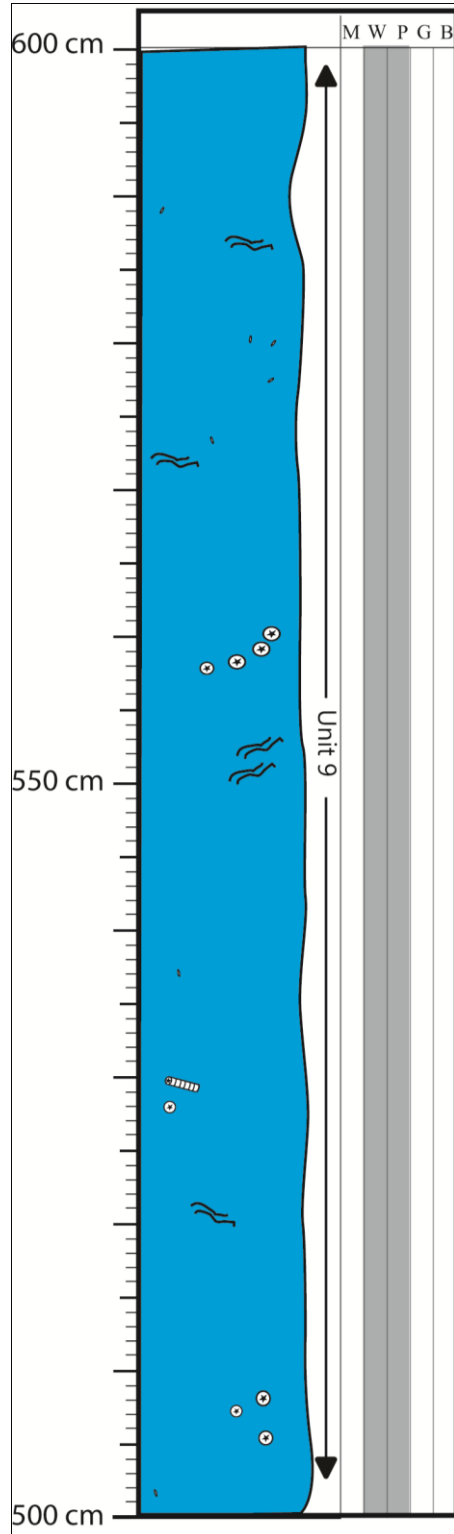
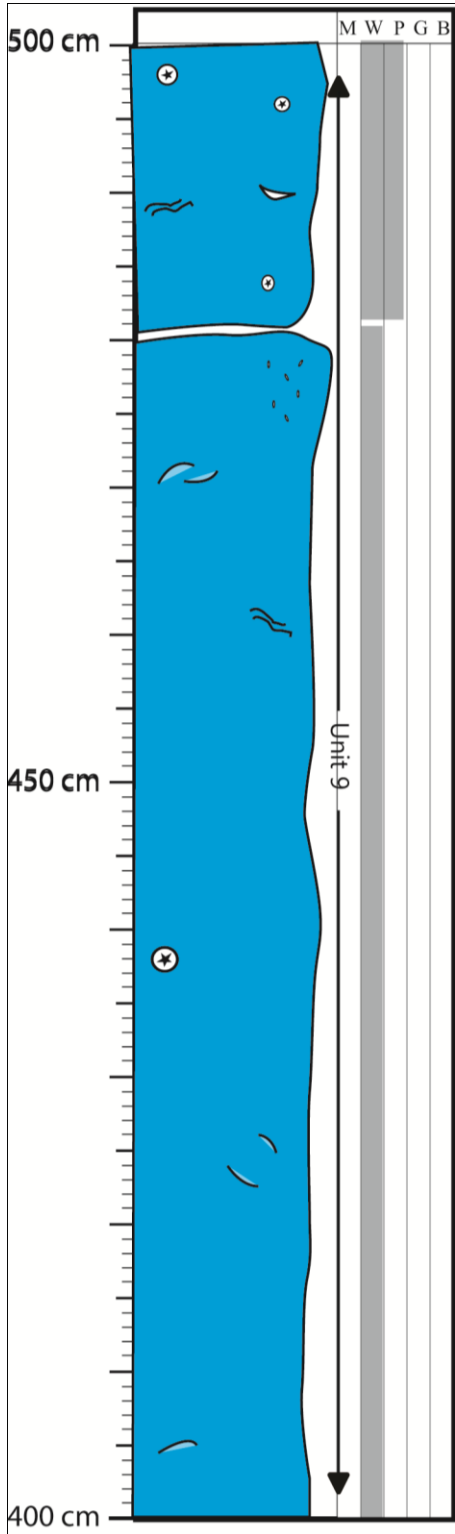




Stratigraphic Section N2 Continued  
Location: N37°11'13.44" W109°46'9.01"

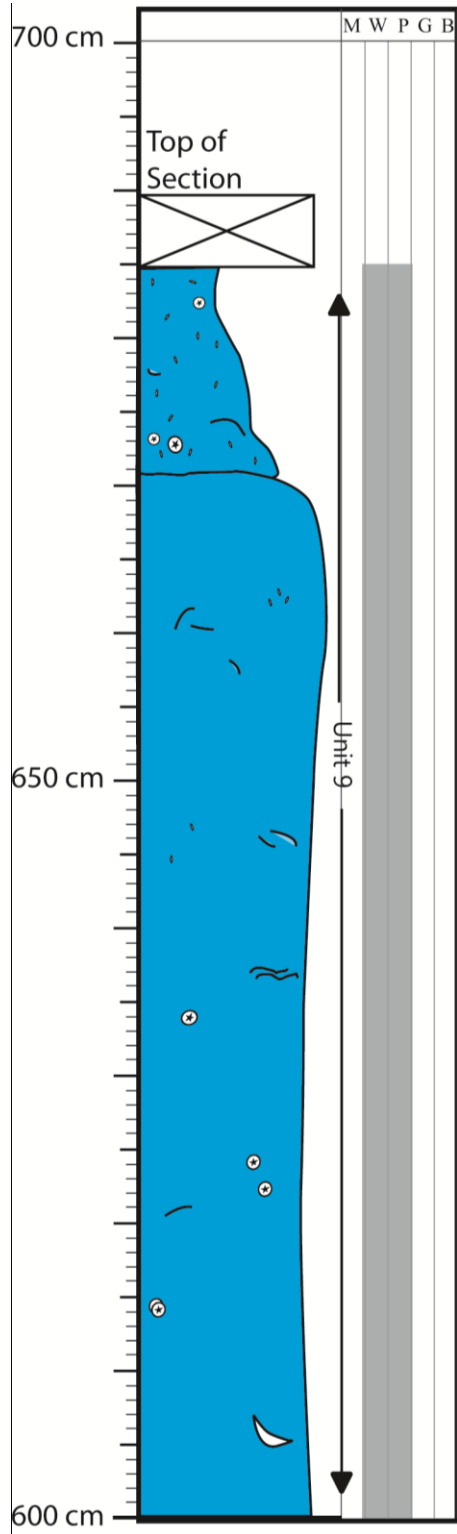


Stratigraphic Section N2 Continued  
Location: N37°11'13.44" W109°46'9.01"



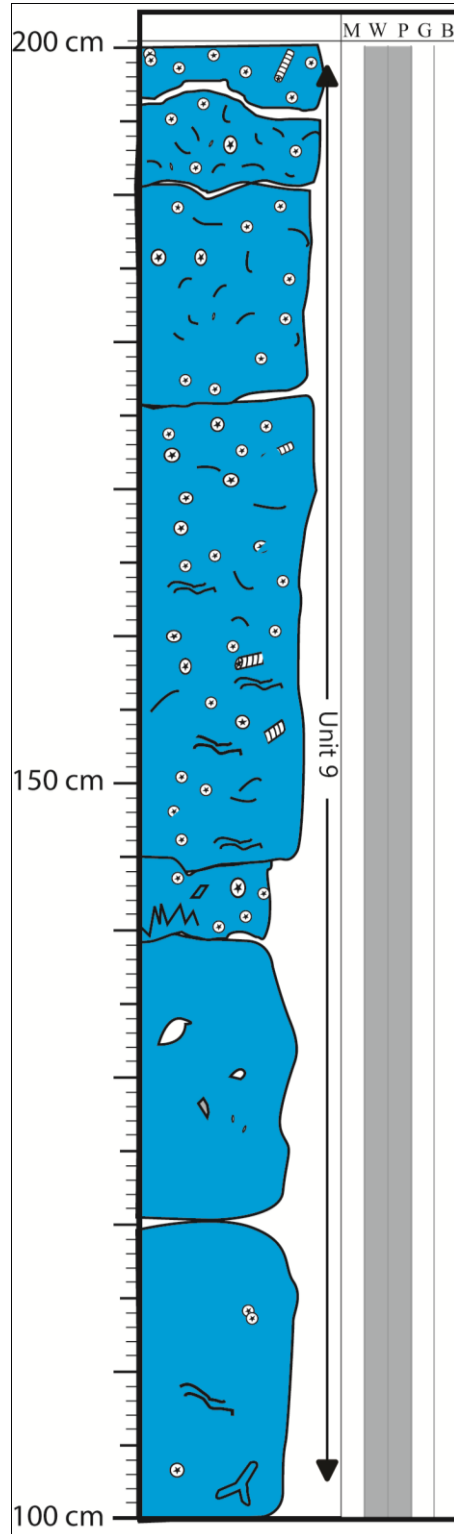
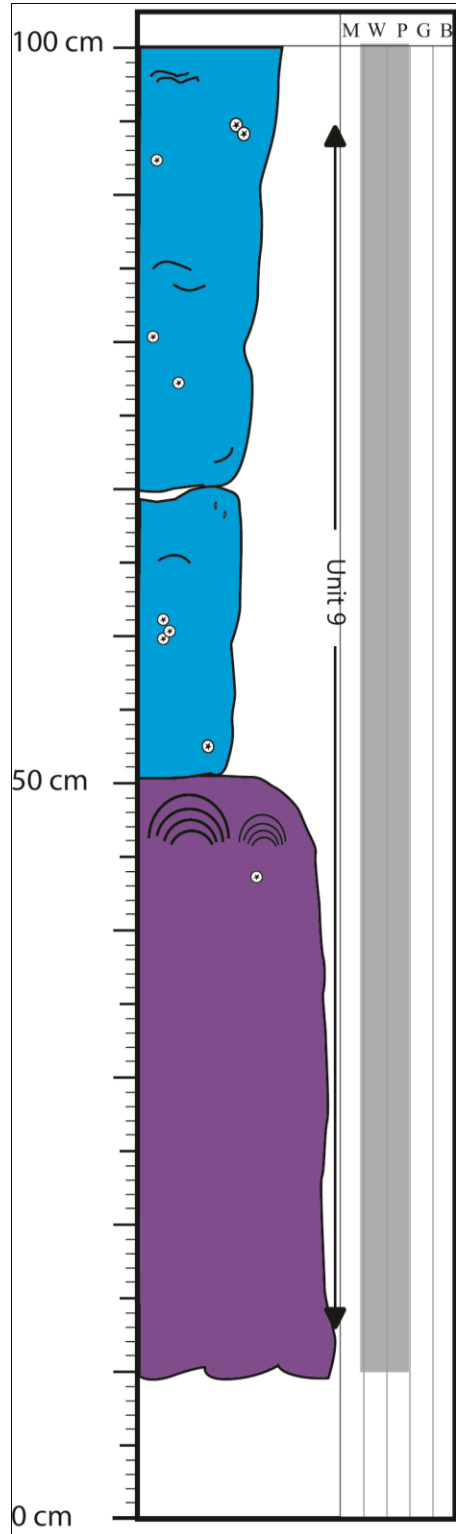
# Stratigraphic Section N2 Continued

Location: N37°11'13.44" W109°46'9.01"



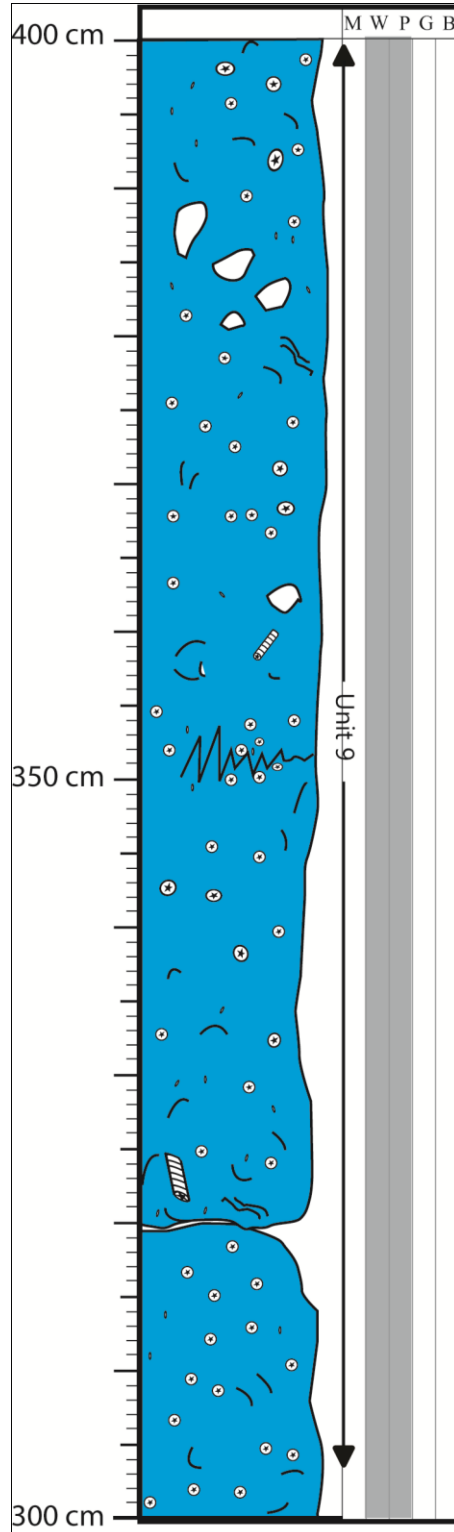
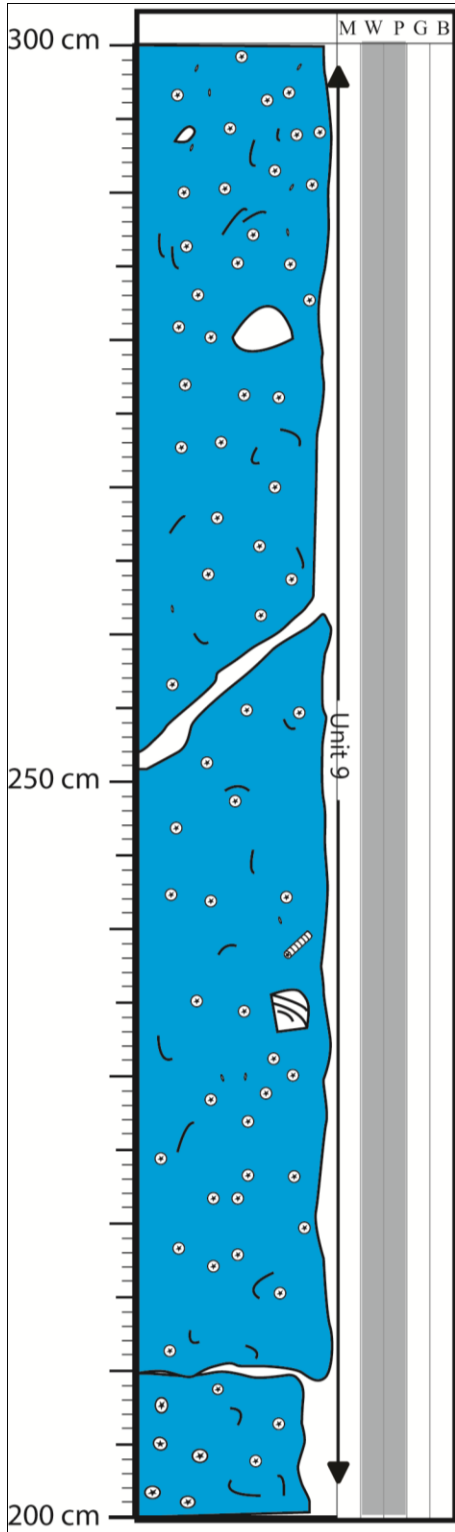
# Stratigraphic Section N3

Location: N37°11'14.12" W109°46'11.09"



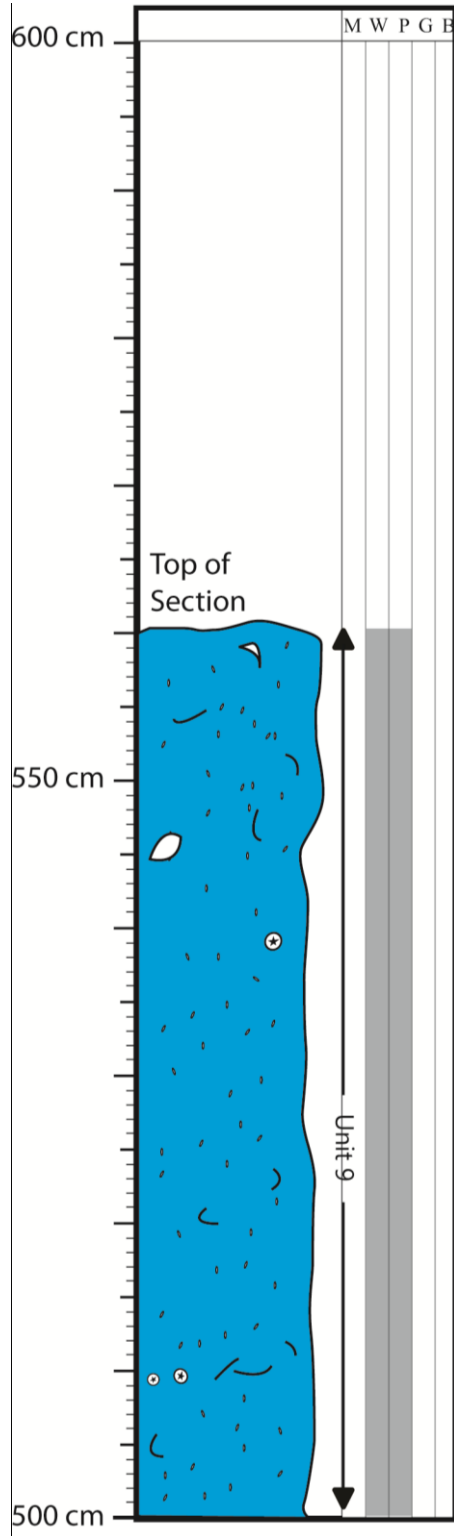
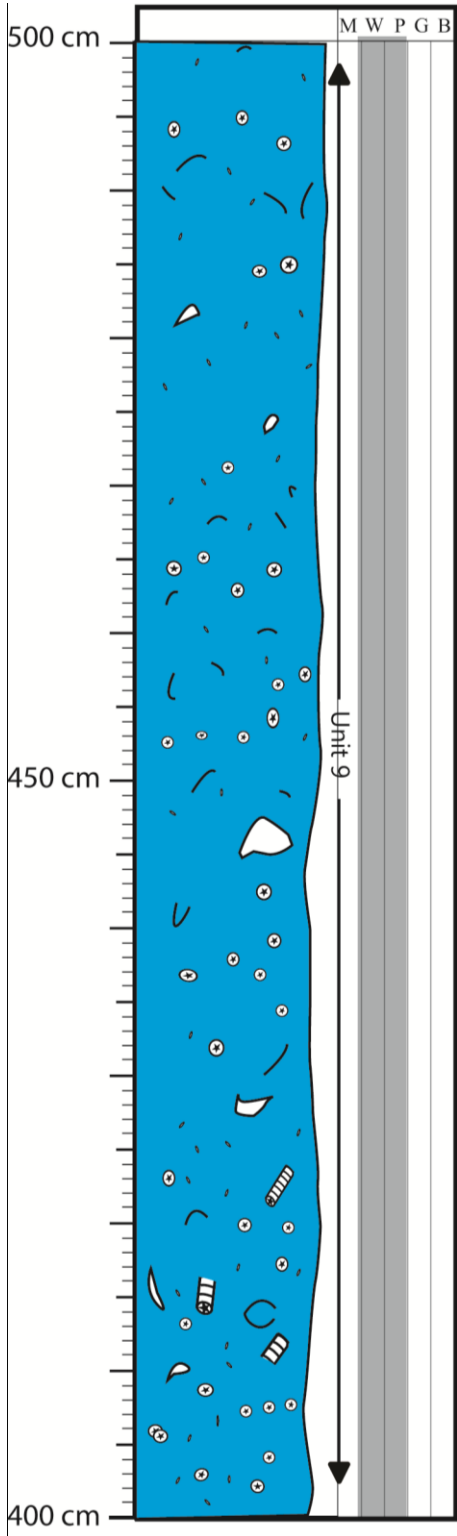
# Stratigraphic Section N3 Continued

Location: N37°11'14.12" W109°46'11.09"

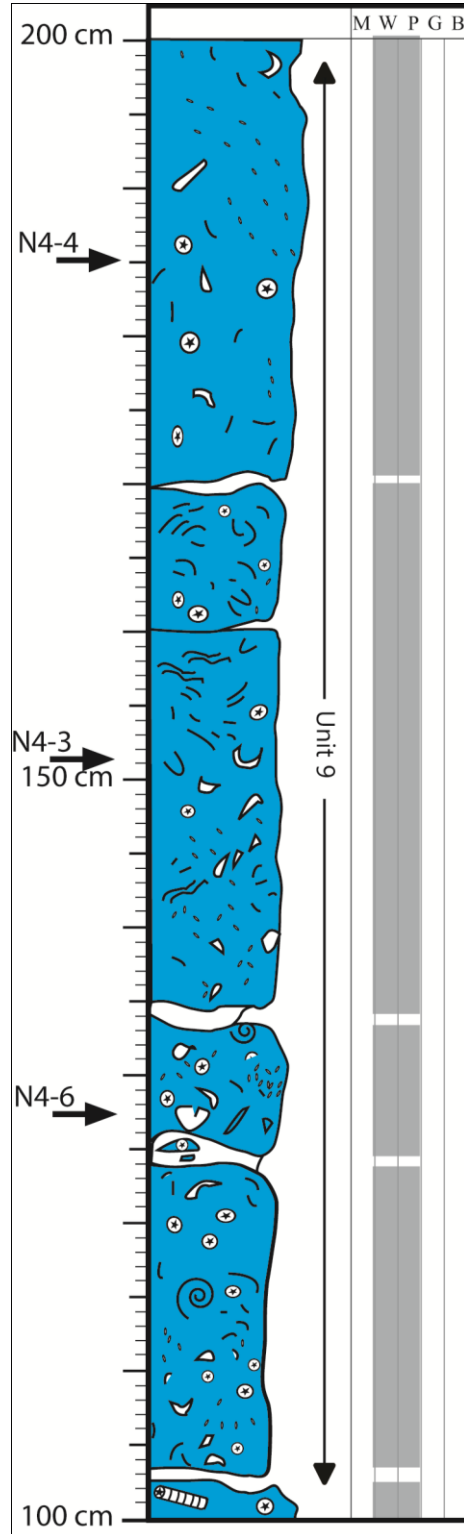
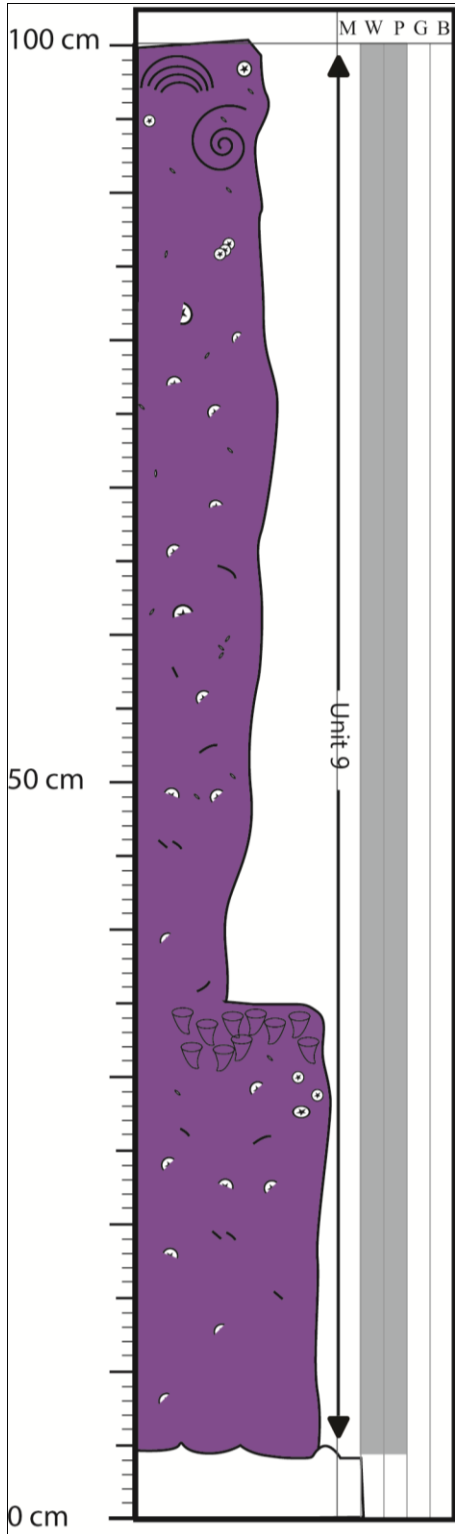


# Stratigraphic Section N3 Continued

Location: N37°11'14.12" W109°46'11.09"

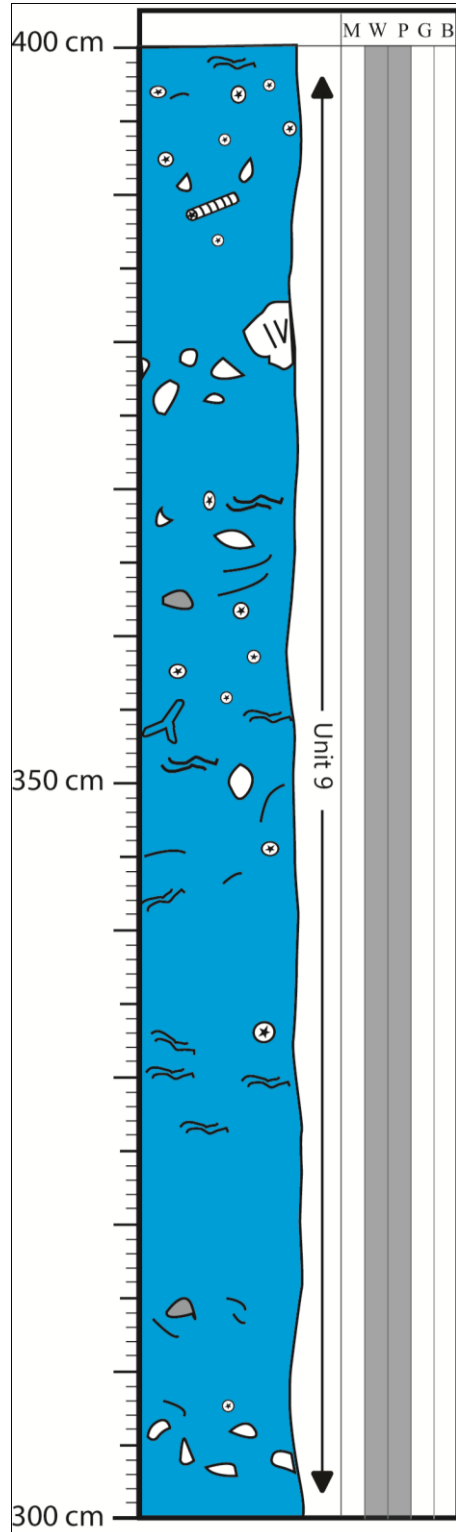
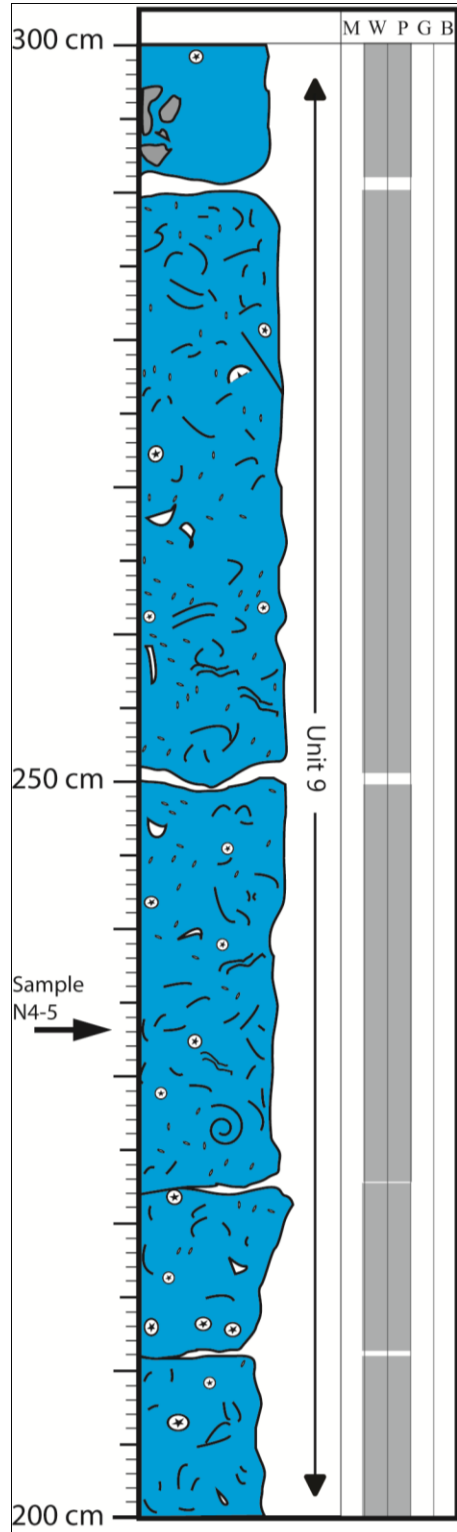


Stratigraphic Section N4  
 Location: N37°11'17.65" W109°46'15.89"



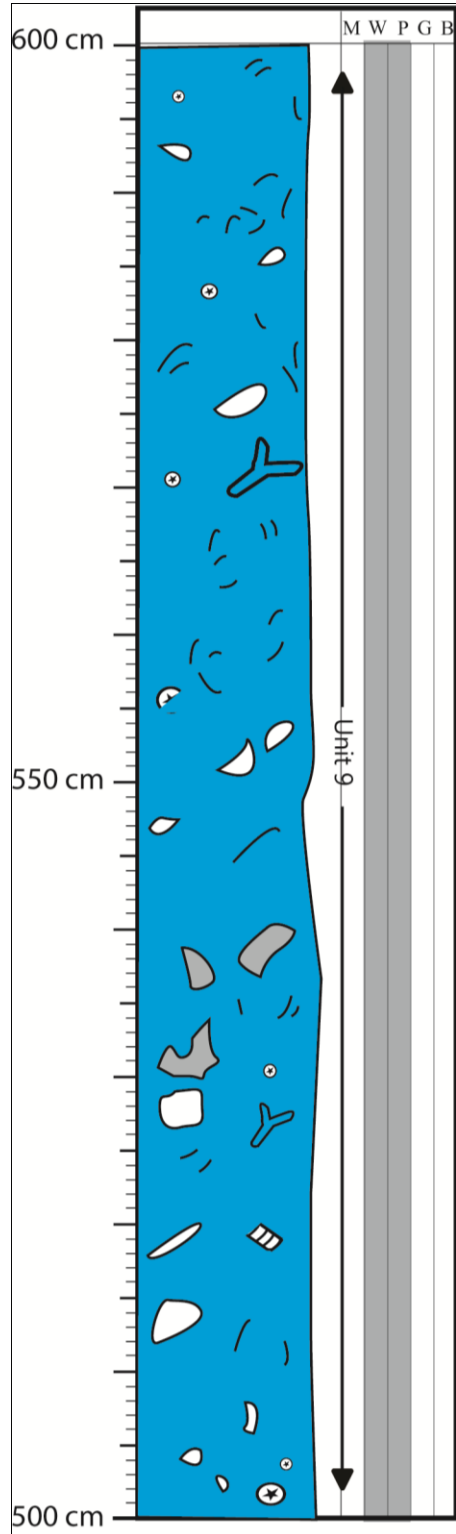
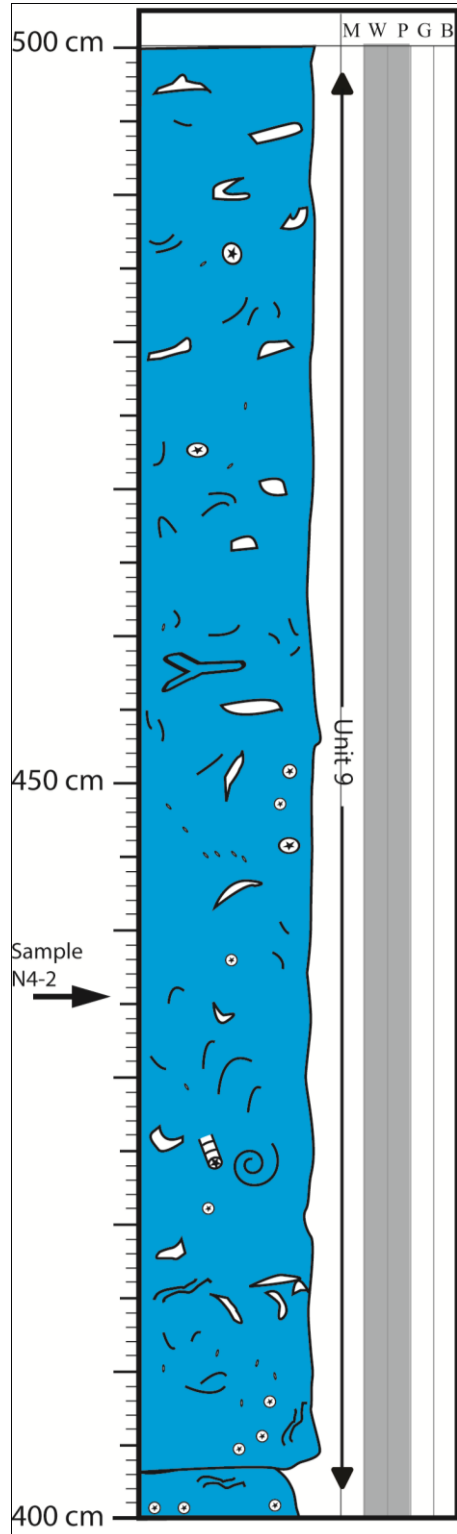
# Stratigraphic Section N4 Continued

Location: N37°11'17.65" W109°46'15.89"



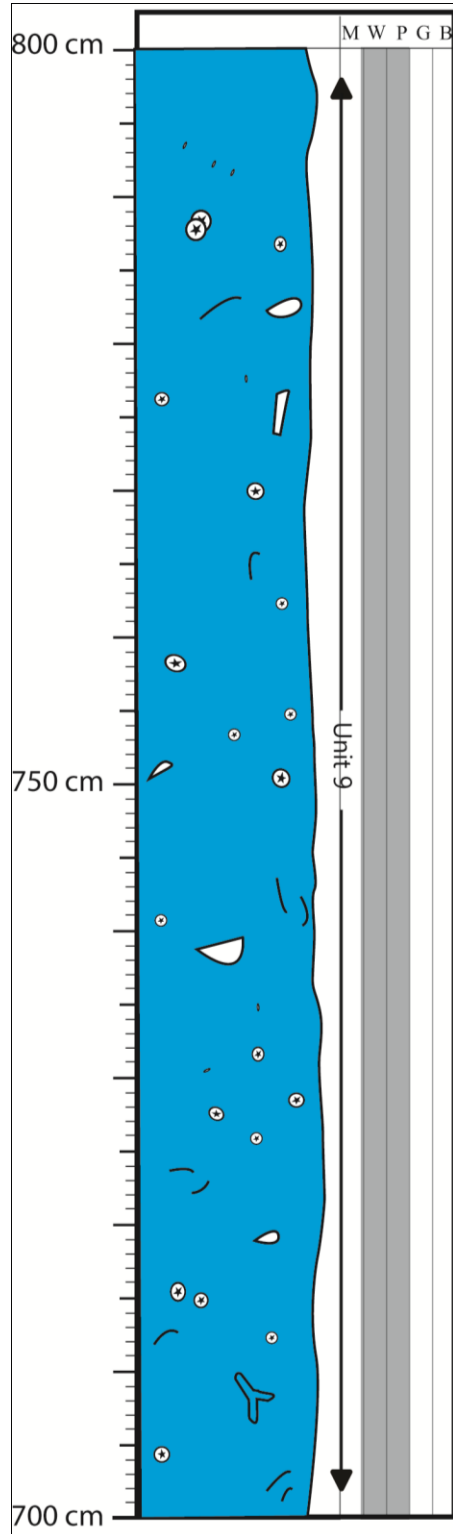
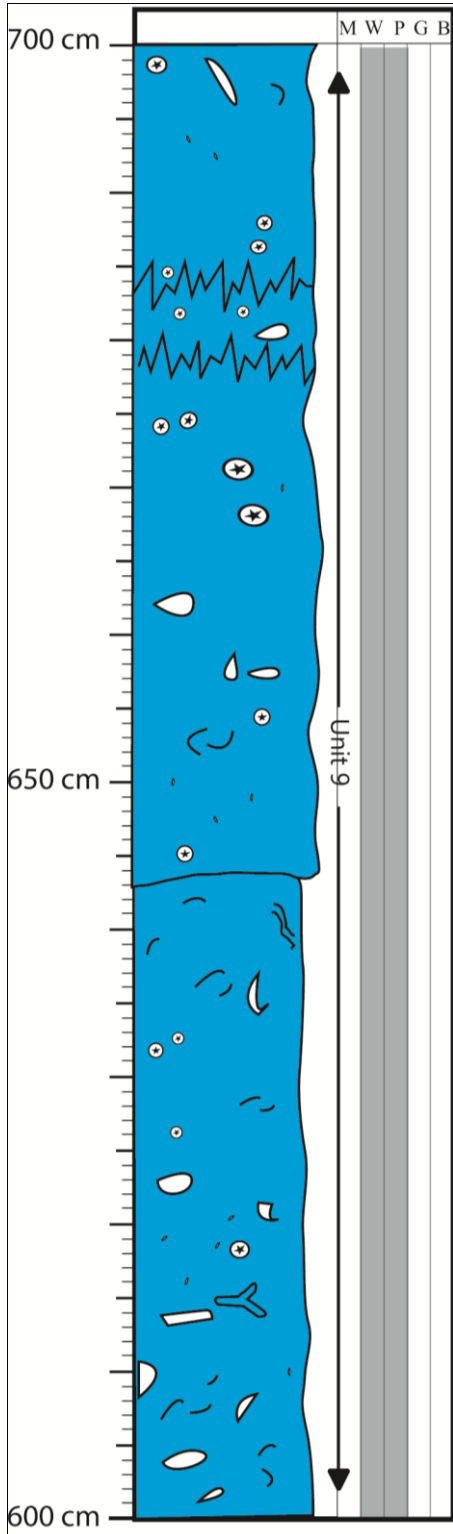


Stratigraphic Section N4  
Location: N37°11'17.65" W109°46'15.89"



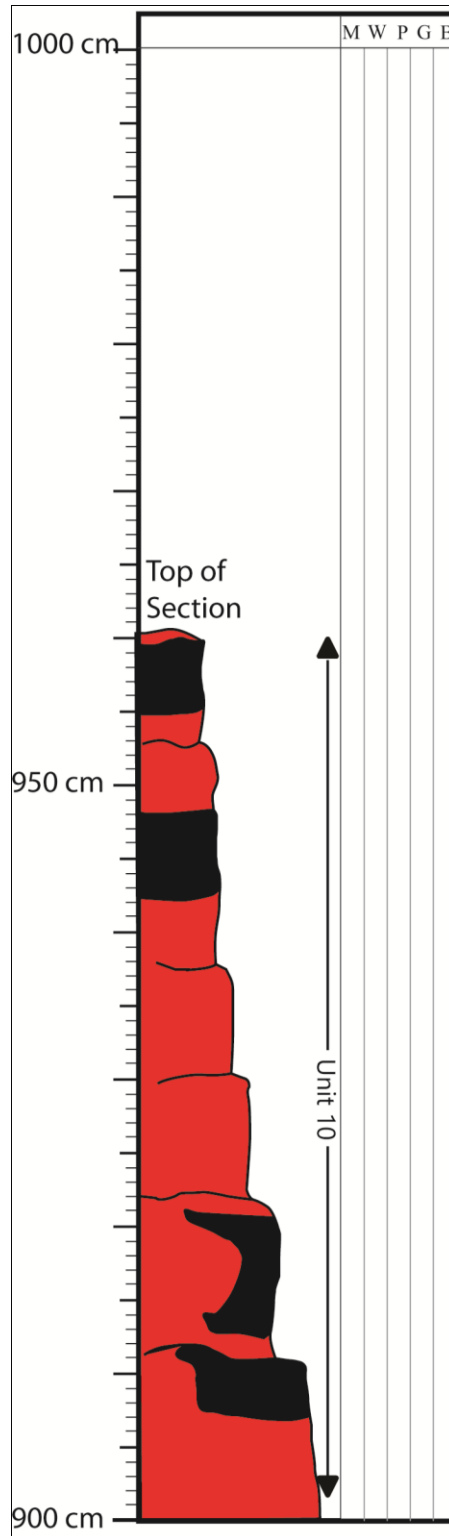
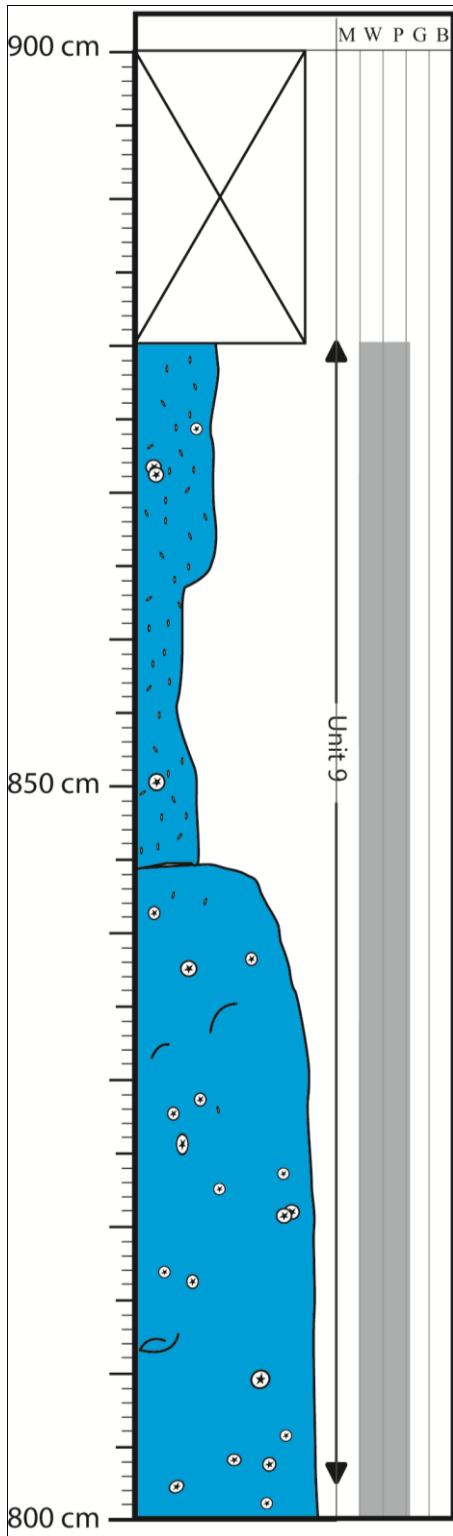
# Stratigraphic Section N4

Location: N37°11'17.65" W109°46'15.89"



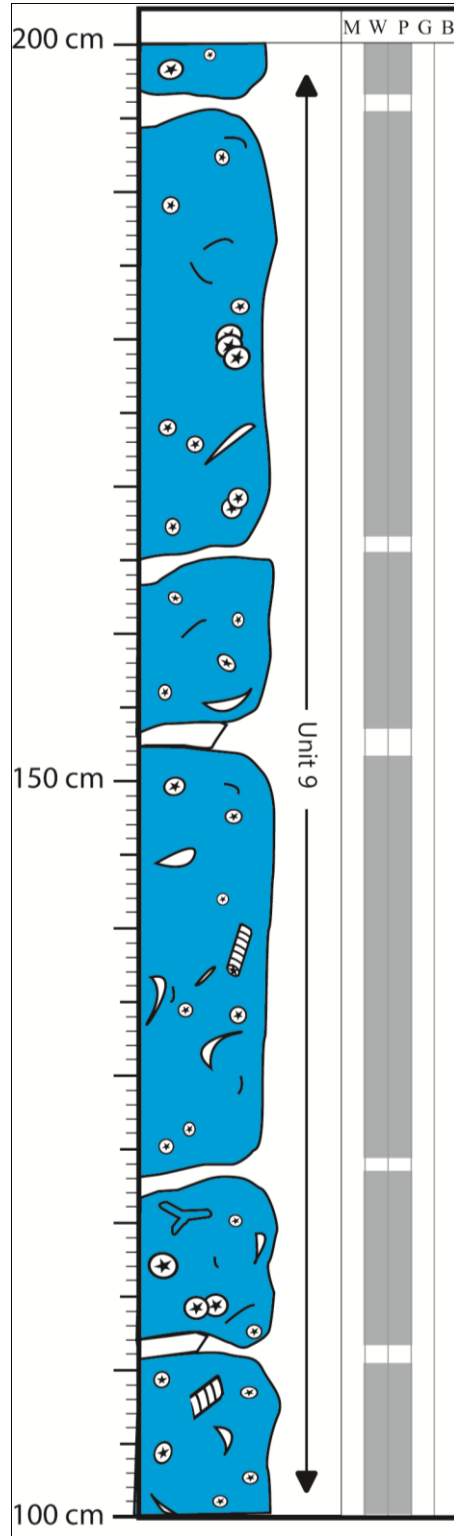
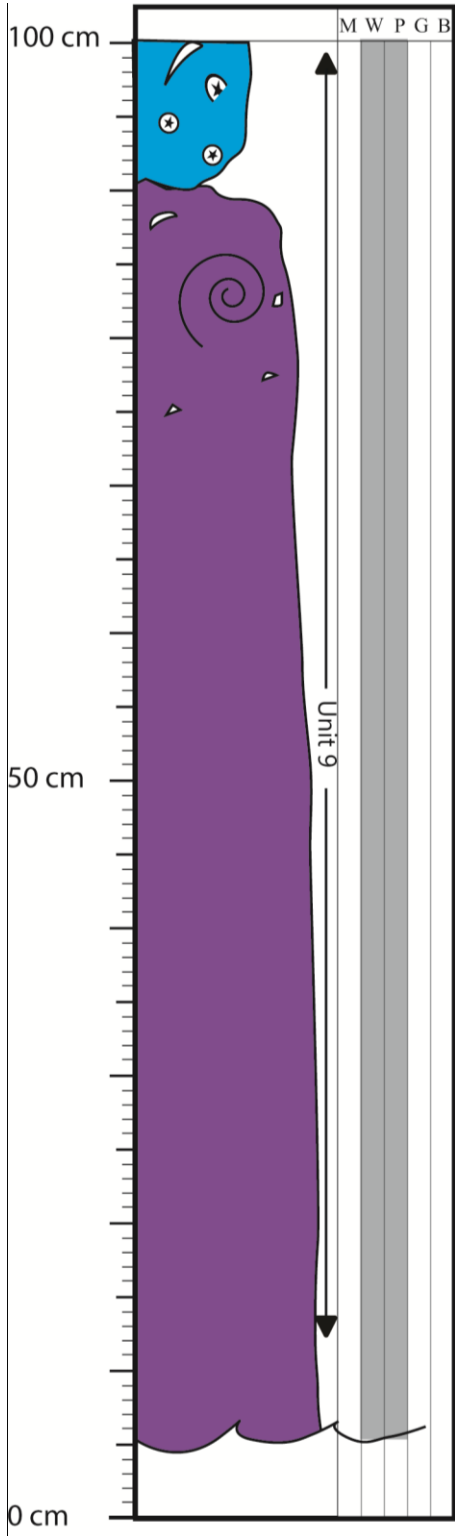
# Stratigraphic Section N4 Continued

Location: N37°11'17.65" W109°46'15.89"

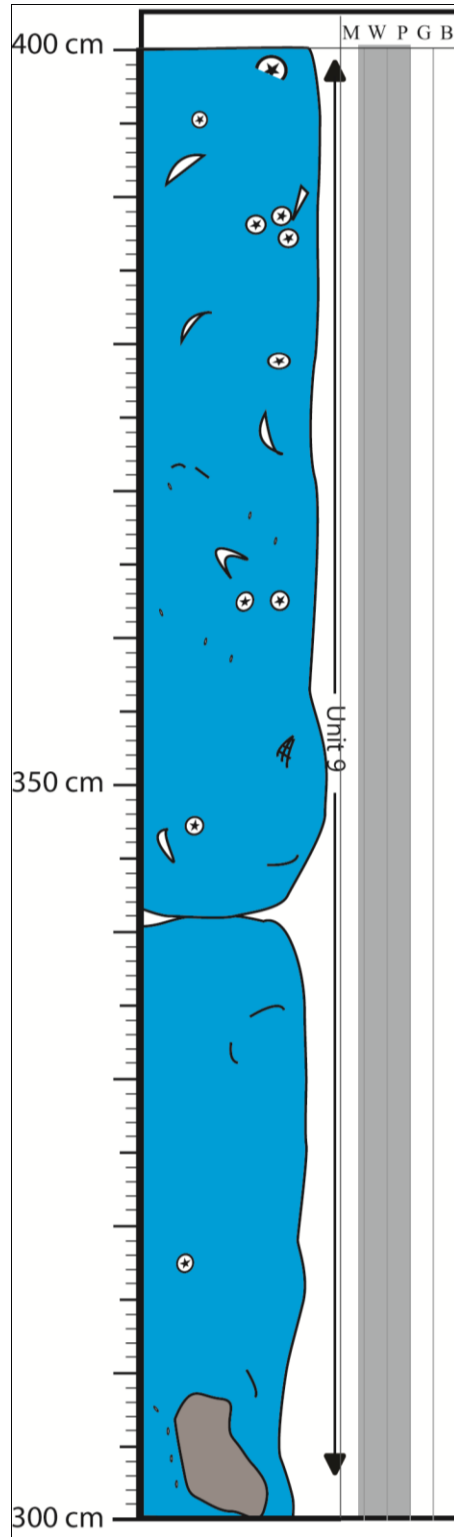
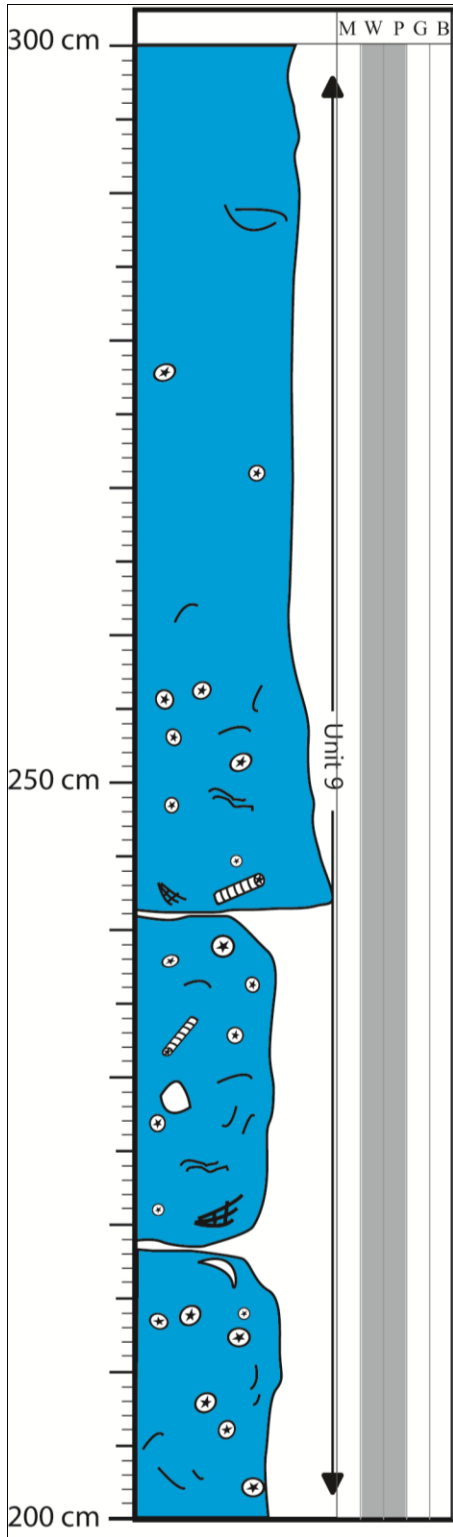


# Stratigraphic Section N6

Location: N37°11'17.19" W109°46'15.42"

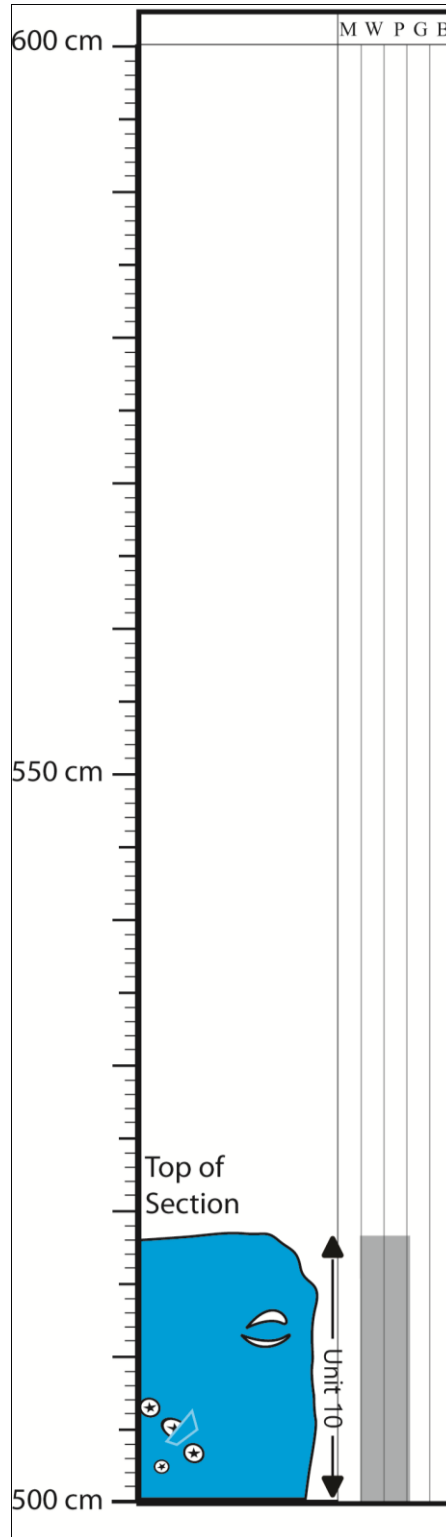
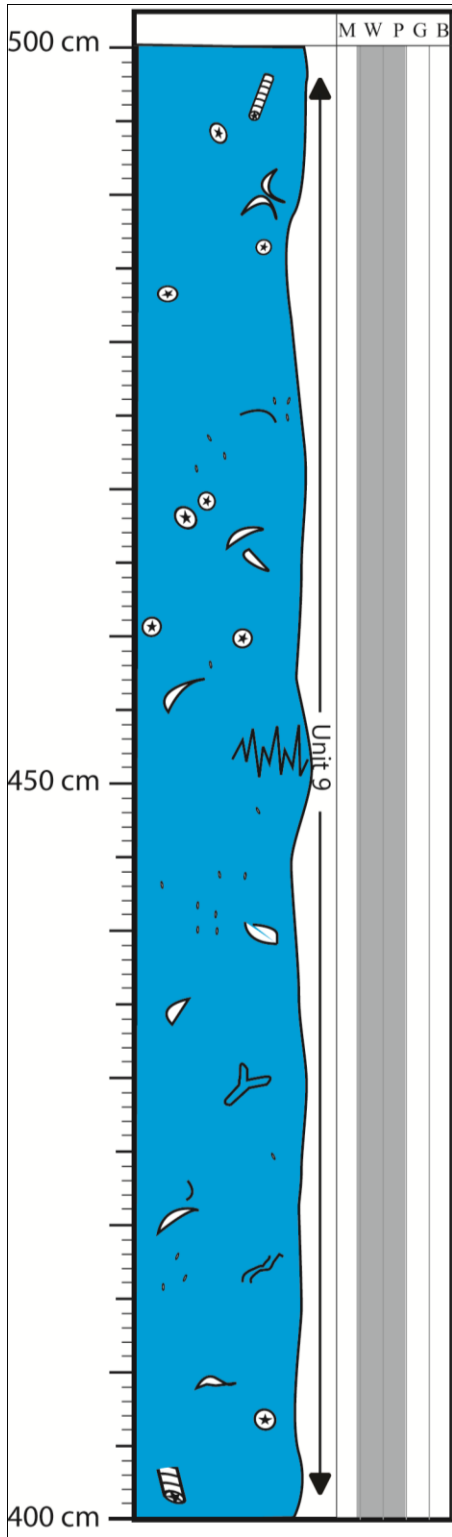


Stratigraphic Section N6 Continued  
Location: N37°11'17.19" W109°46'15.42"



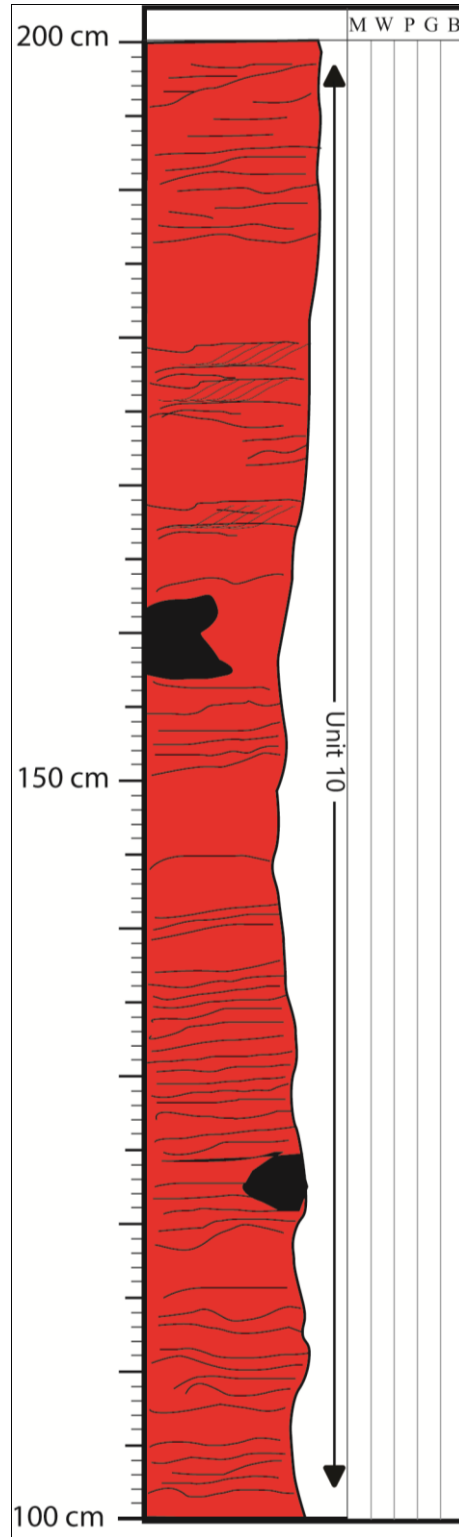
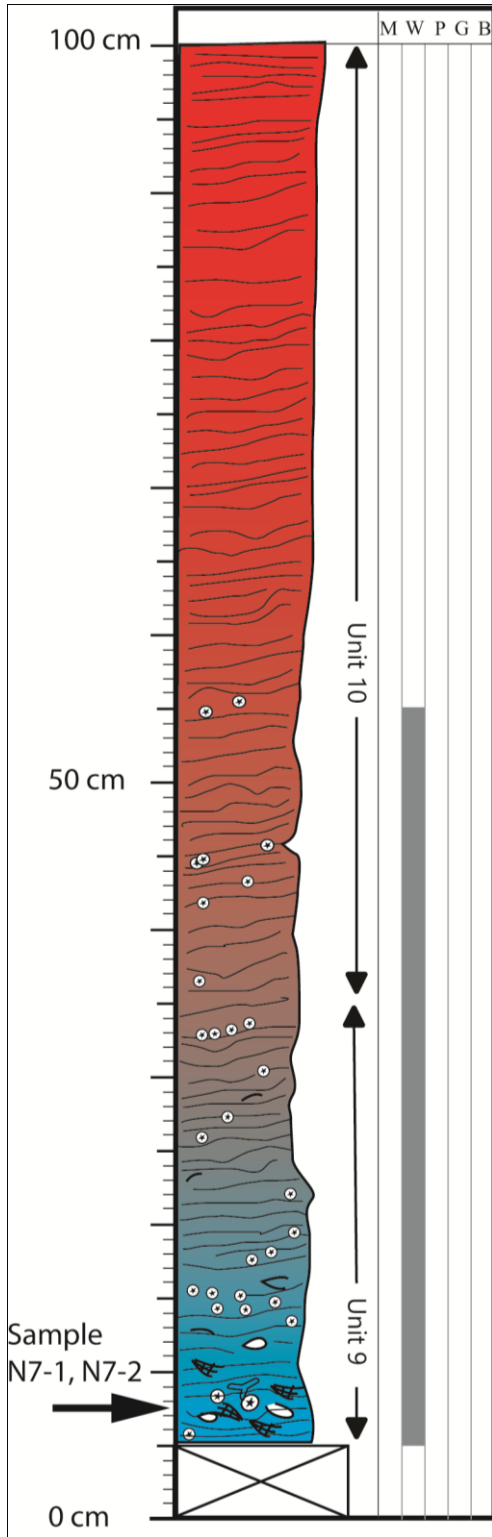
# Stratigraphic Section N6 Continued

Location: N37°11'17.19" W109°46'15.42"

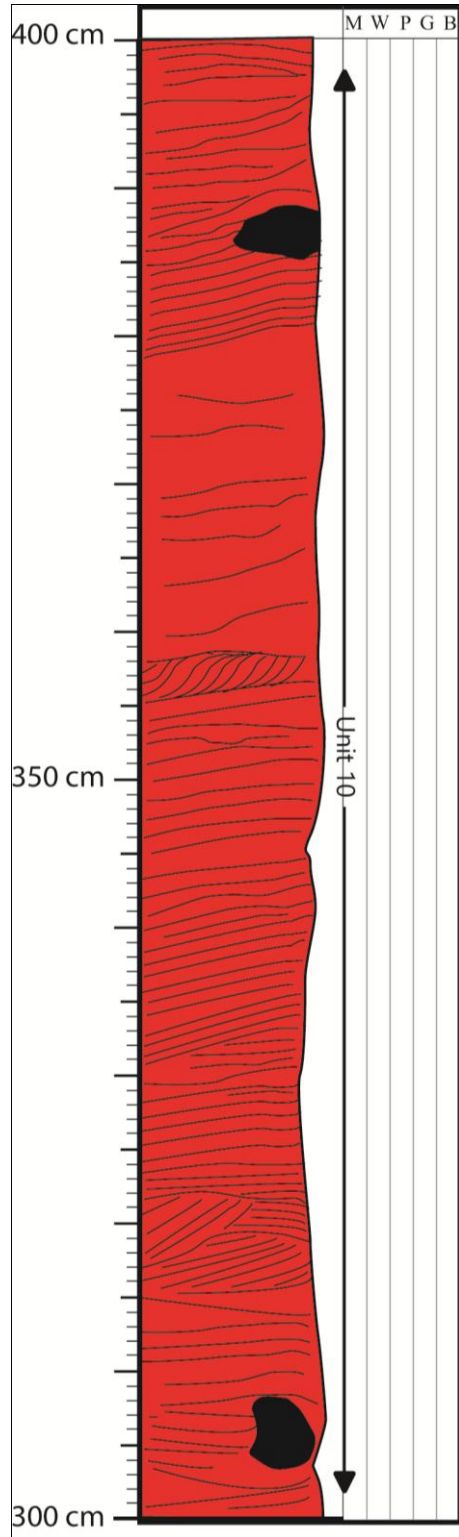
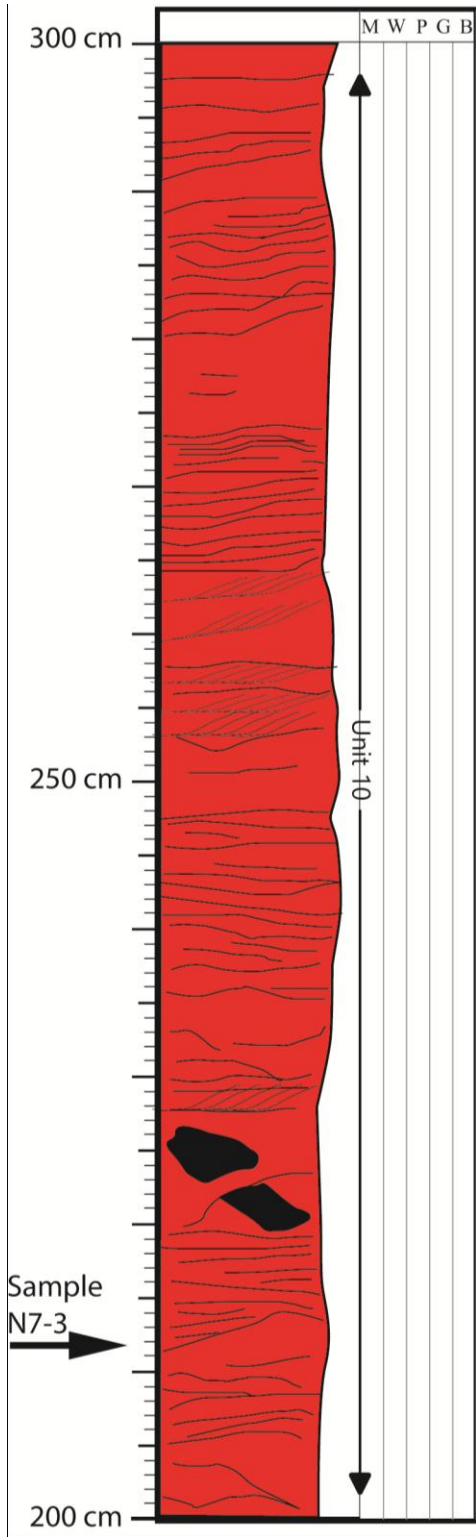


# Stratigraphic Section N7

Location: N37°11'23.35" W109°46'17.80"

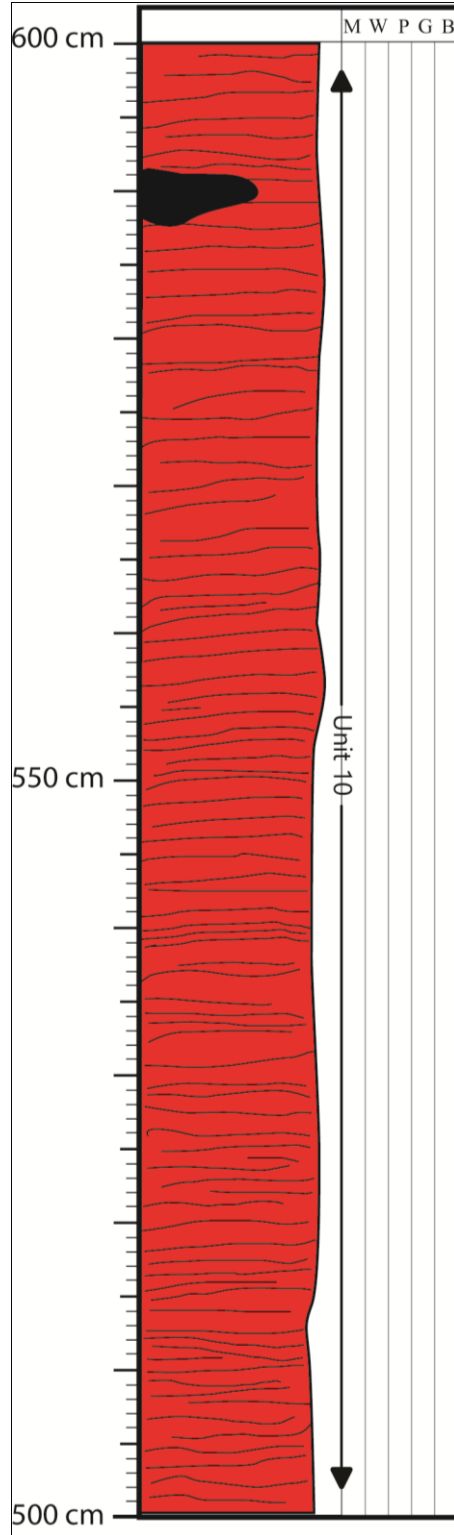
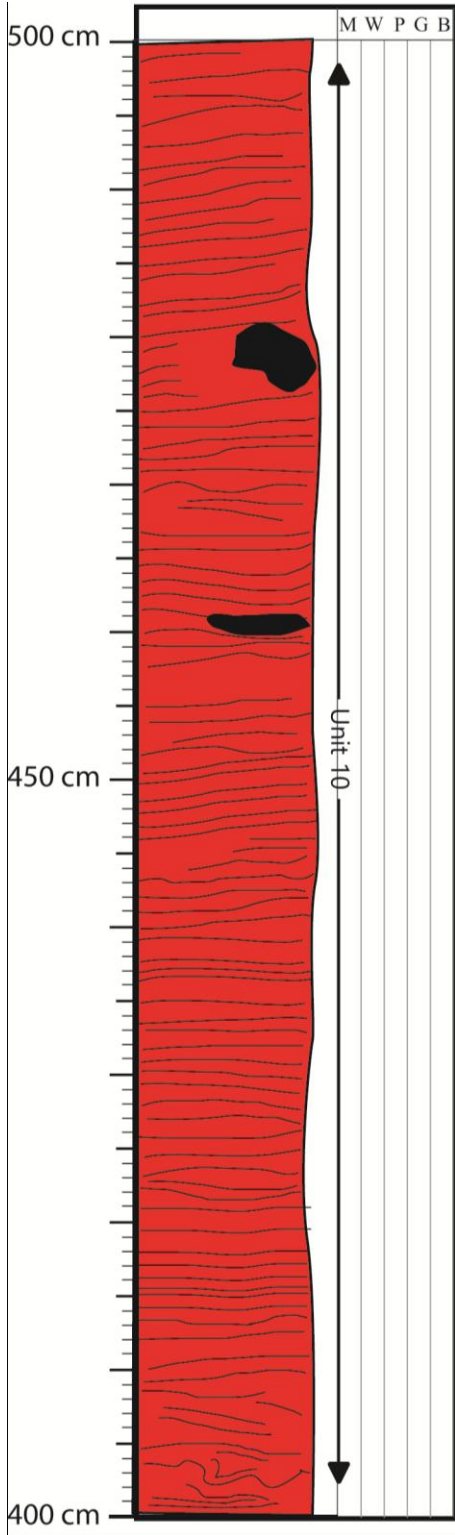


Stratigraphic Section N7 Continued  
Location: N37°11'23.35" W109°46'17.80"

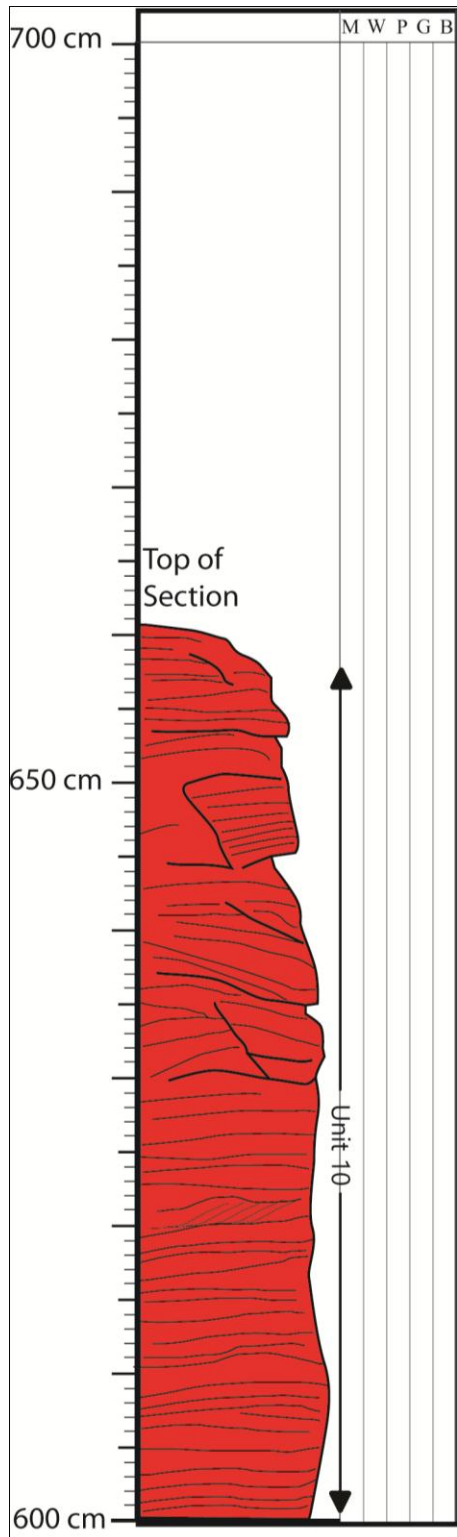




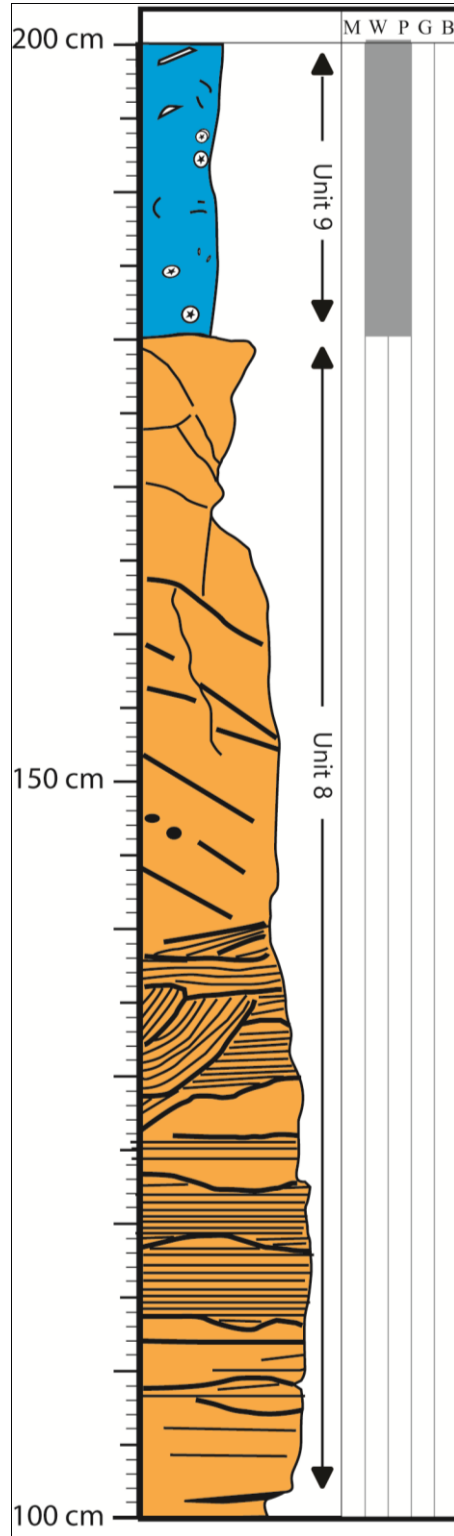
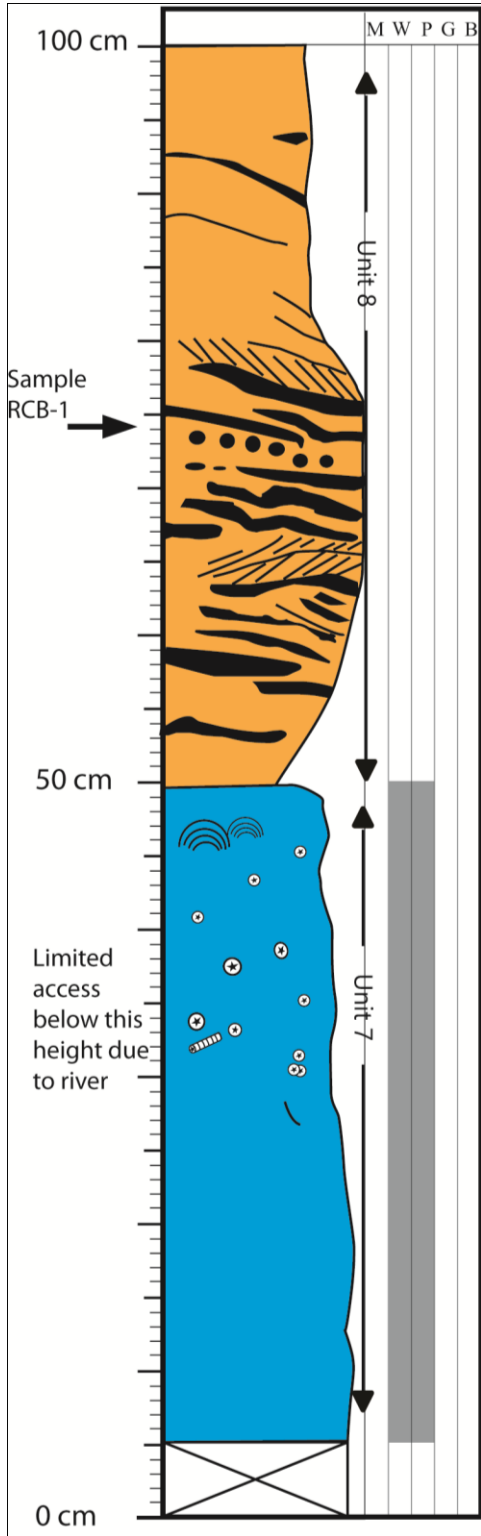
Stratigraphic Section N7 Continued  
Location: N37°11'23.35" W109°46'17.80"



Stratigraphic Section N7 Continued  
Location: N37°11'23.35" W109°46'17.80"

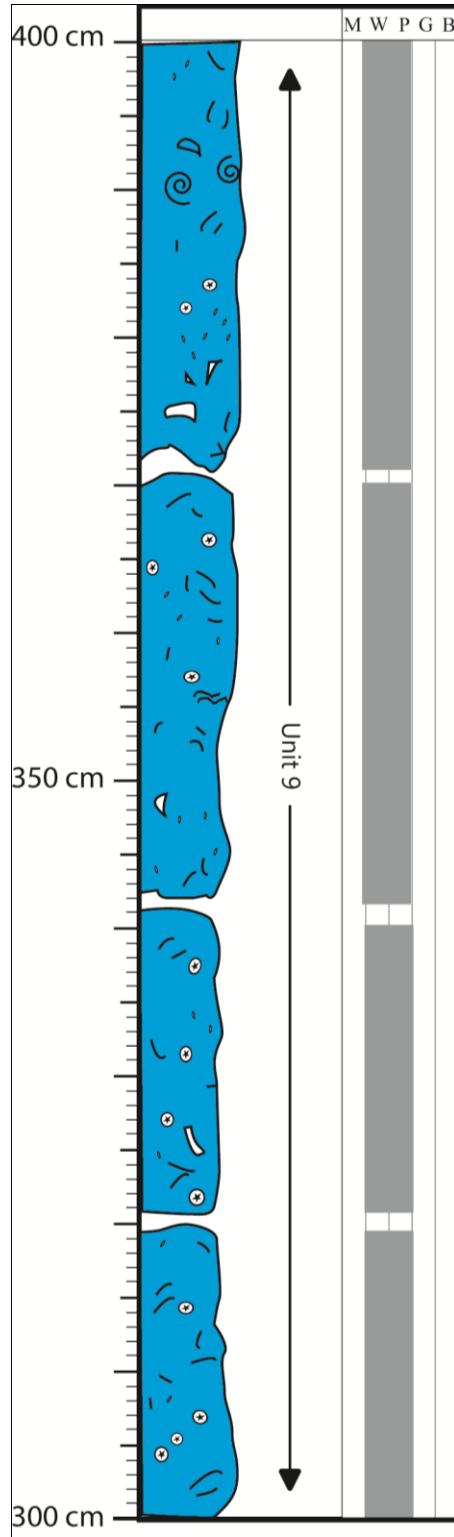
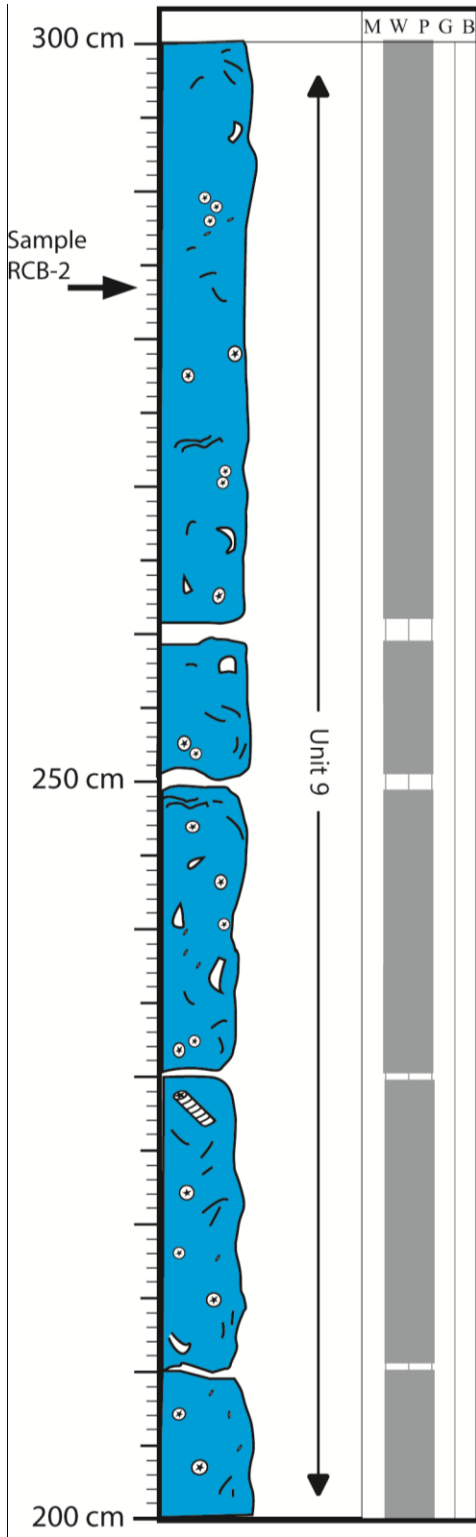


**Stratigraphic Section RCB**  
 Location: N37°11'17.65" W109°46'54.63"



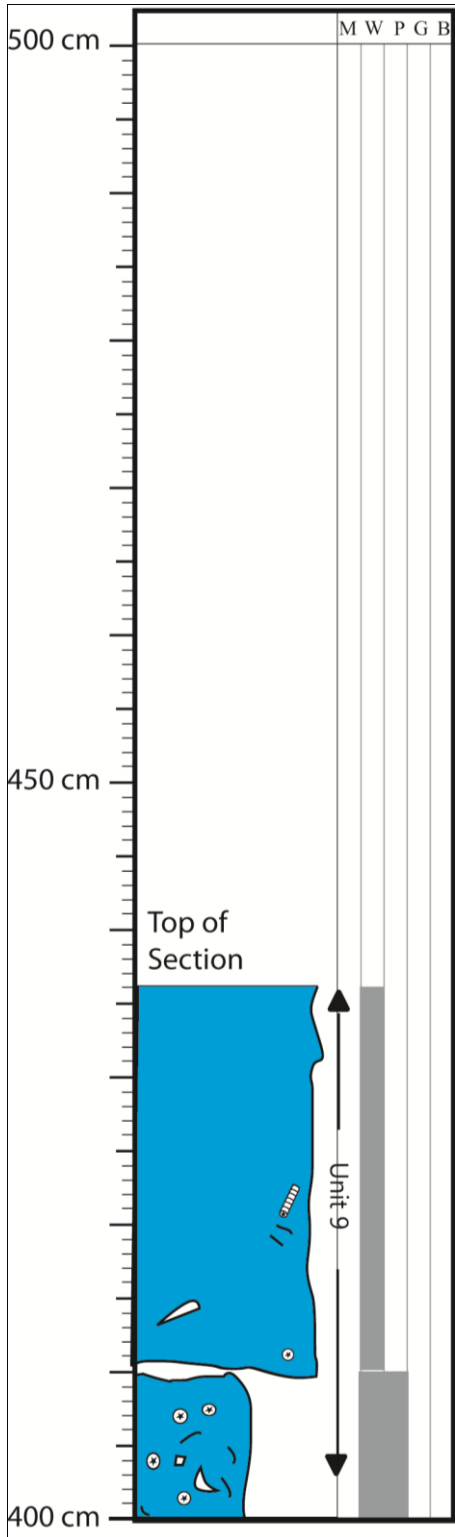
# Stratigraphic Section RCB Continued

Location: N37°11'17.65" W109°46'54.63"



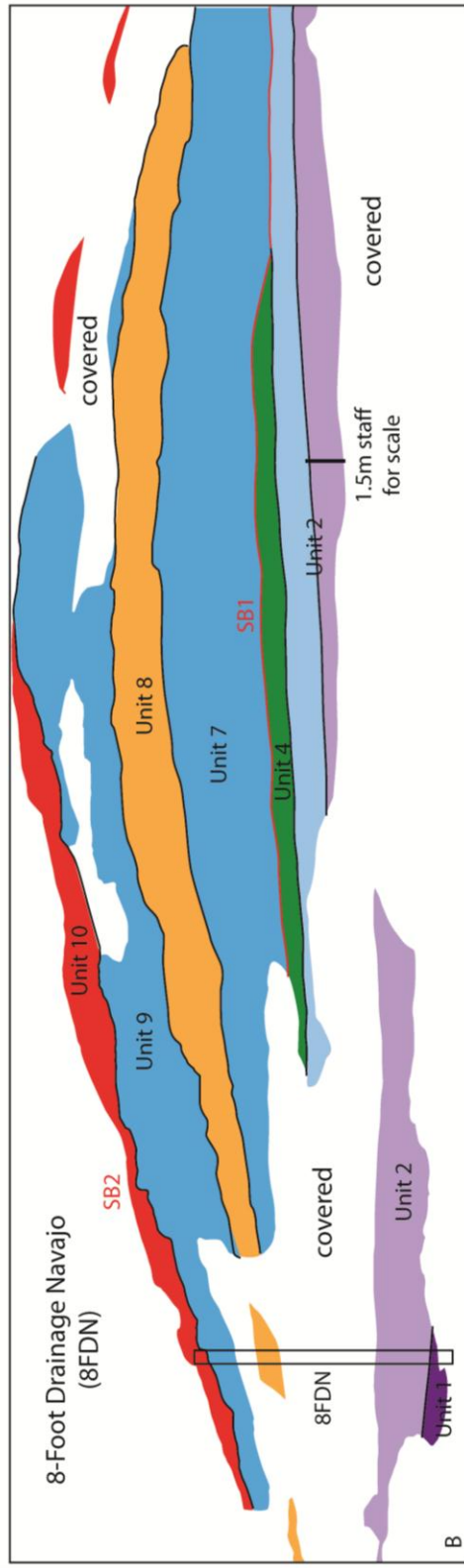
# Stratigraphic Section RCB Continued

Location: N37°11'17.65" W109°46'54.63"

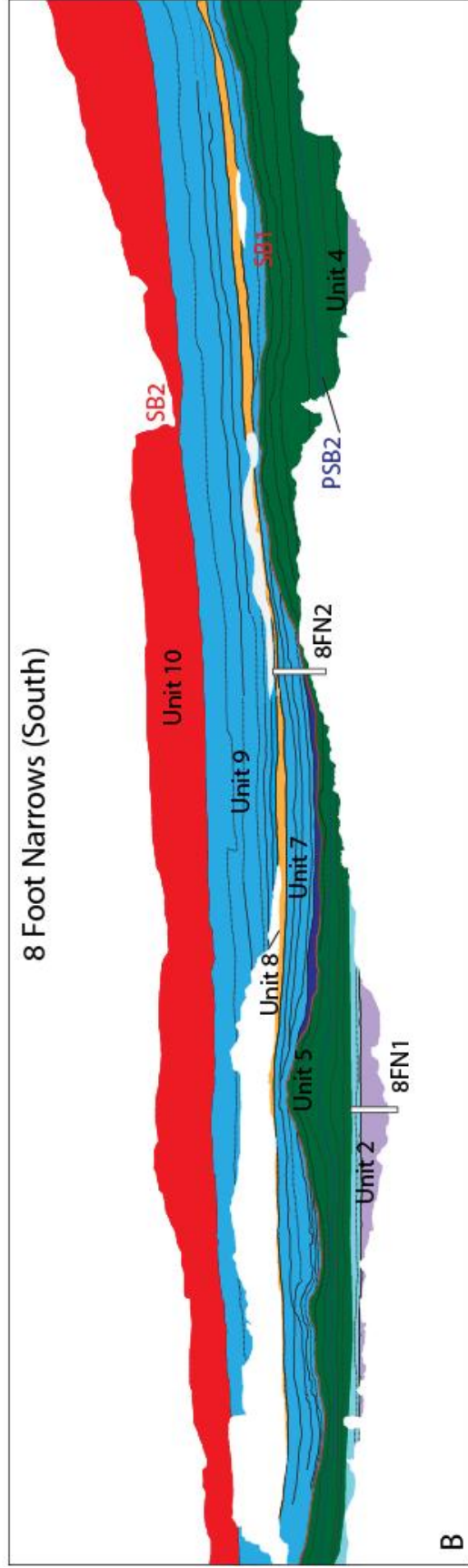


## **Appendix II**

### Photomosaics

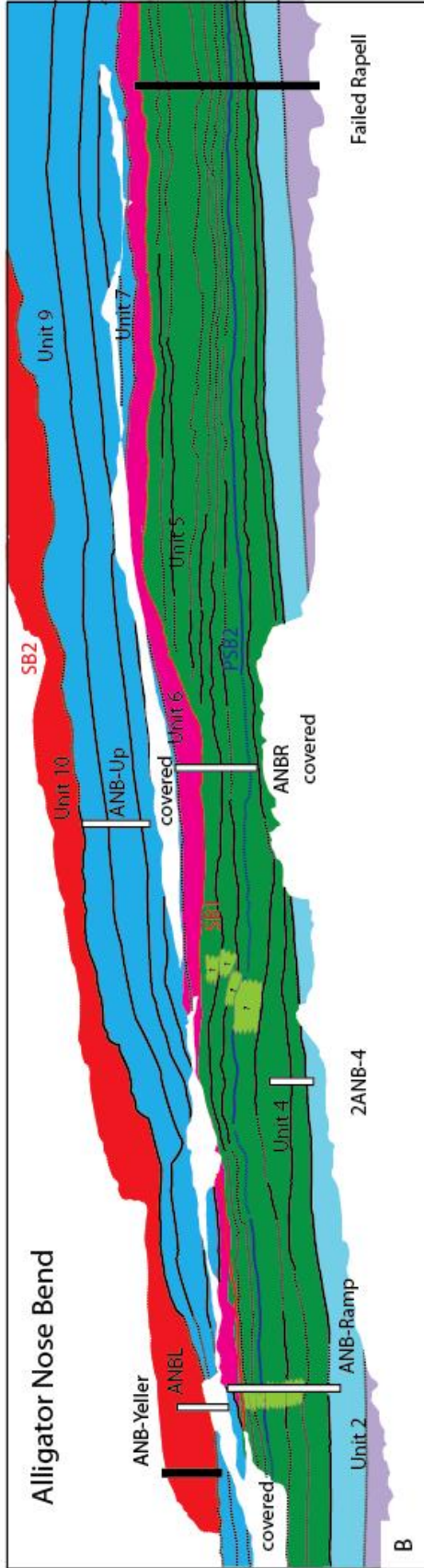
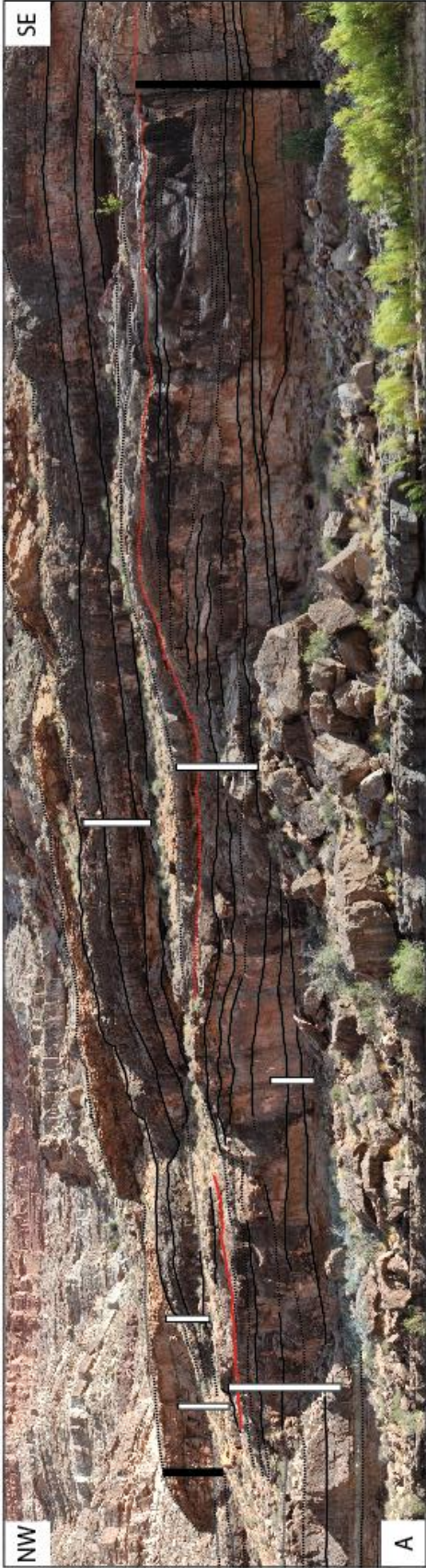


Photomosaic used in constructing cross-section C-C' (Figure 25). A) Photomosaic showing stratigraphic surfaces and location of stratigraphic section 8FDN. B) Interpretation of photomosaic in A. See Figure 10 for explanation of colors and symbols.

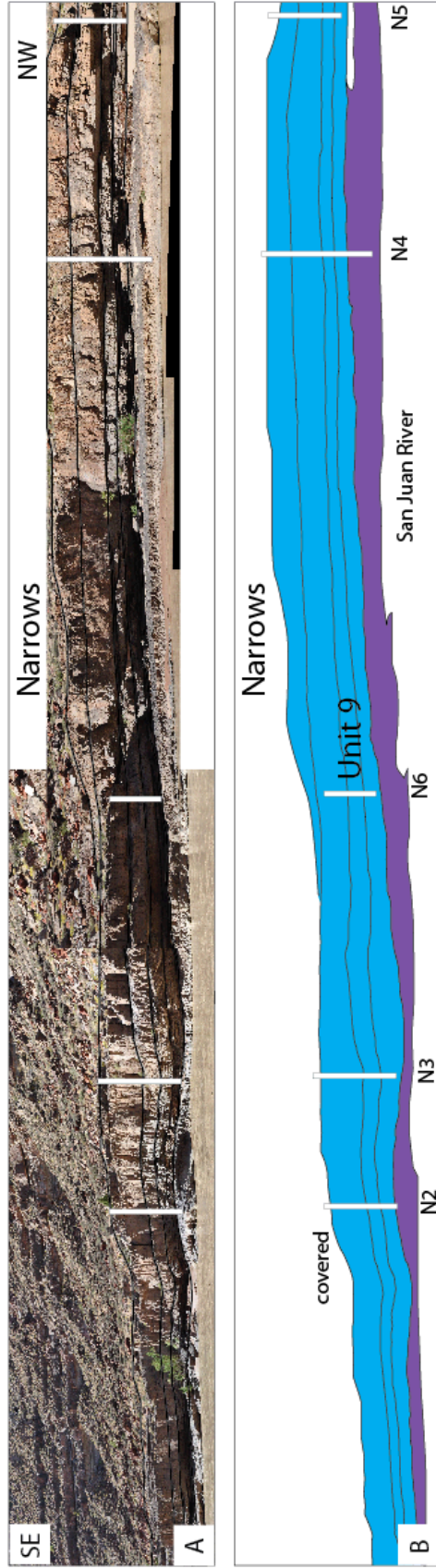


Photomosaic used in constructing cross-section C-C' (Figure 25). A) Photomosaic showing stratigraphic surfaces and location of stratigraphic section 8FN1 and 8FN2. B) Interpretation of photomosaic in A. See Figure 10 for explanation of colors and symbols.

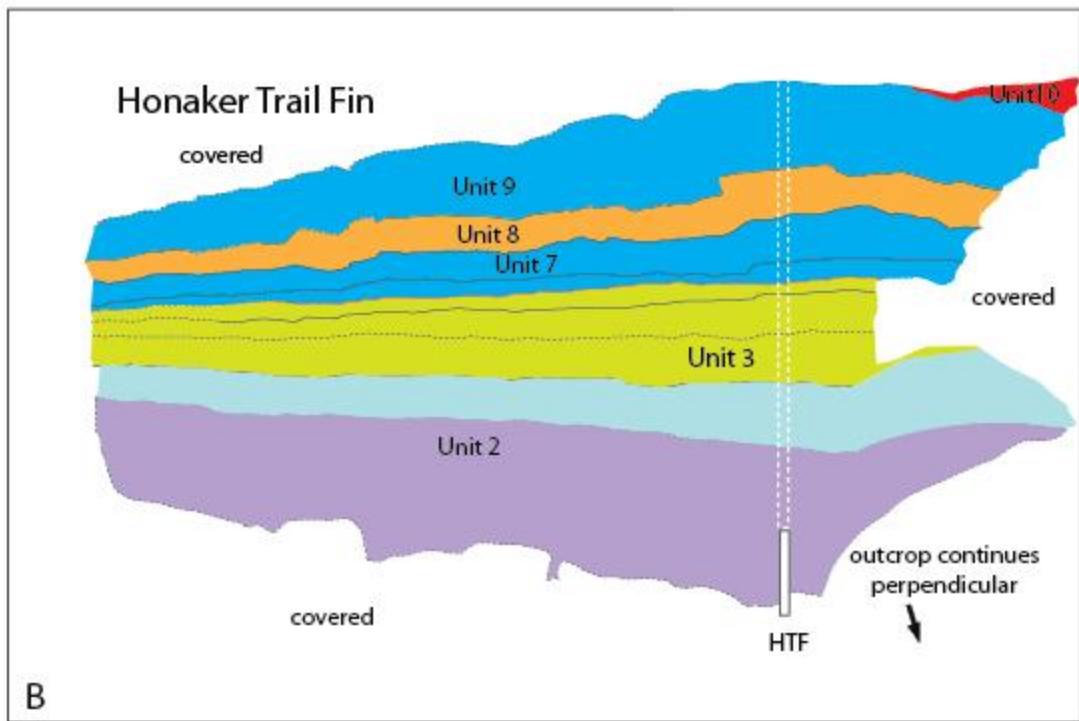




Photomosaic used in constructing cross-section B-B' (Figure 24). A) Photomosaic showing stratigraphic surfaces and location of ANB stratigraphic sections. Detailed measured sections are white and sections where only thicknesses were measured are in black. B) Interpretation of photomosaic in A. See Figure 10 for explanation of colors and symbols.



Photomosaic used in constructing cross-section A-A' (Figure 23). A) Photomosaic showing stratigraphic surfaces and location of Narrows stratigraphic sections. B) Interpretation of photomosaic in A. See Figure 10 for explanation of colors and symbols.



## **Appendix III**

### Thin Section Descriptions

Description lithofacies in thin section, sorted by lithofacies. For explanation of description criteria, see Lithofacies and Depositional Environments. See Appendix I for sample locations.

### Lithofacies 1: Black Laminated Mudstone

Sample ID: 8FN3-5					
Sample Type: Thin Section					
Texture: Black Laminated Mudstone					
Sorting: Well sorted					
Grains	Area %	Abrasion	Sizes	Orientation	Notes
quartz	20	subangular	very fine-grained; 81.3um-146.3um, average 124.7 um	random	
biotite	sparse	subangular- subrounded	194.2um - 339.2um. average 240.3 um	random	
sponge spicules	sparse	little-no abrasion	13.7 um - 184.5 um, average 15.9 um	random	most cut along short axis
pyrite	5	little-no abrasion	19.4um - 28.7um, average 20.1 um	random	cubic
clays	10				
mud	60				appears to be peloidal in origin
cement	5				pore-filling dentic and equant calcite, recrystallization
void space	0				intraparticle porosity filled with calcite

## Lithofacies 2: Spicule Mudstone

<b>Sample ID:</b> 8FN1-1 Thin <b>Sample Type:</b> Section Spicule Mudstone <b>Texture:</b> Moderately sorted					
Grains	Area %	Abrasion	Sizes	Orientation	Notes
quartz silt	30	subangular-subrounded	silt to very fine-grained; 53.2um - 67.8 um, average 60.2 um	random	
sponge spicules	20	little abrasion, fragmented	12.0um-270.9um, average 80.1um	horizontal	
brachiopod	5	moderately abraded	40.38um-1773.1um, average 1088.5um	horizontal	whole and individual shells
pyrite	sparse	little-no abrasion	80.2um-89.3um, average 83.4um	random	cubic
clays	5				
mud	35				peloidal in origin
cement	5				equant calcite, recrystallization
void space	0				

### Lithofacies 3: Crinoid Packstone

<b>Sample ID: HTF-3</b> Thin Sample Type: Section Texture: Crinoid Packstone Sorting: Moderately sorted					
Grains	Area %	Abrasion	Sizes	Orientation	Notes
crinoid	30	moderately to highly abraded, moderately fragmented	255.0um-1550.0um, average 879.9um	random	concentrated along stylolites
brachiopod	25	moderately to highly abraded, highly fragmented	218.7um-7419.6um, average 2015.4um	random	individual shells, mostly recrystallized
bryozoa	10	moderately abraded, highly fragmented	196.2um-7126.8um, average 2497.1um	random	concentrated along stylolites
sponge spicules	7	moderately abraded, fragmented	11.7um-255.9um, average 106.4um	random	
ostrocods	2	moderately abraded, moderately fragmented	33.9um-41.5um, average 3608um	random	whole and individual shells, porespace often filled with equant calcite
pellets	1	little to moderate abrasion, no fragmentation	55.5um-88.0um, average 67.8um	random	
brachipod spine	sparse	moderately abraded, moderately fragmented	341.7um	random	
mud	15				peloidal in origin
cement	8				pore-filling dentic and equant calcite, recrystallization cements
void space	1				interparticle and intercrystalline porosity

### Lithofacies 4: Algal Bafflestone

Sample ID: ANB-6a					
Thin					
Sample Type: Section					
Texture: Algal Bafflestone					
Sorting: Poorly sorted					
Grains	Area %	Abrasion	Sizes	Orientation	Notes
phylloid algae	10	little abrasion, some fragmentation of large pieces	790.9um-5977.6um, average 3869.7um	horizontal to subhorizontal	poorly preserved, highly recrystallized with large equant calcite, some cortical layers preserved, Ivanovia
brachiopod	3	little-moderately abraded, fragmented	524.9um-1132.1um, average 683.5um	random	mostly individual shells, often recrystallized
ostracod	5	moderately abraded, fragmented	159.7um-372.6um, average 246.6um	random	whole and individual shells in mud matrix
foraminifera	5	moderately abraded, fragmented	342.8um-1615.7um, average 959.7um	random	
gastropod	sparse	moderately abraded, fragmented	350.9um-803.3um, average 602.5um	random	
caliche nodule with soil pizoids	20				irregular voids with sparry rims filled with mud and pizoids
mud	35				peloidal in origin, concentrated in sediment traps created by algal plates, brecciated due to algal-plate collapse, pedoturbation
cement	15				pore-lining and pore-filling dentic and equant calcite (13%), chalcedony (2%)
void space	7				intercrystalline, moldic, and fracture porosity



<b>Sample ID: ANB-6b</b> Thin <b>Sample Type: Section</b> <b>Texture: Algal Bafflestone</b> <b>Sorting: Poorly sorted</b>					
Grains	Area %	Abrasion	Sizes	Orientation	Notes
phylloid algae	10	little abrasion, some fragmentation of large pieces	639.3um-32836.5um, average 11020.96um	horizontal to subhorizontal	poorly preserved, highly recrystallized with large equant calcite, some cortical layers preserved, Ivanovia
brachiopod	5	little-moderately abraded, fragmented	729.4um-4391.5um, average 2387.1um	random	whole and individual shells, act as shelter geopetals
ostracod	5	moderately abraded, fragmented	118.3um-227.3um, average 174.1um	random	whole and individual shells in mud matrix
bryozoa	sparse	moderately abraded, fragmented	668.8um-1093.6um, average 881.2um	random	
foraminifera	5	moderately abraded, fragmented	257.8um-1712.5um, average 691.7um	random	Fusulinids (4%), biserial forams (1%)
caliche nodule with soil pizoids	20				irregular voids with sparry rims filled with mud and pizoids
mud	30				peloidal in origin, concentrated in sediment traps created by algal plates, brecciated due to algal-plate collapse, pedoturbation
cement	15				pore-lining and pore-filling dentic and equant calcite (14%), chalcedony (1%)
void space	10				intercrystalline and fracture porosity

**Sample ID:** ANB-7  
 Thin  
**Sample Type:** Section  
**Texture:** Algal Bafflestone  
**Sorting:** Poorly sorted

Grains	Area %	Abrasion	Sizes	Orientation	Notes
phylloid algae	20	little abrasion, fragmented	1060.4um-11187.2um, average 4191.2um	horizontal to subhorizontal	poorly preserved, highly recrystallized with large equant calcite, some cortical layers preserved, Ivanovia
ostracod	8	moderately abraded, fragmented	46.0um-179.4um, average 101.5um	random	whole and individual shells in mud matrix
brachiopod	2	little-moderately abraded, fragmented	718.5um-3429.6um, average 2074.1um	random	mostly individual shells
crinoid	sparse	highly abraded, fragmented	248.6um	random	one large crinoid towards the top
foraminifera	sparse	fragmented	606.8um	random	unidentifiable
pellets	sparse	little abrasion, fragmented	770.1um	random	
mud	15				peloidal in origin, concentrated in sediment traps created by algal plates, brecciated due to algal-plate collapse
cement	25				pore-filling dentic, bladed, and equant calcite
void space	30				intercrystalline, moldic, and fracture porosity

Notes: bladed calcite indicates marine cementation

**Sample ID:** 2ANB-4  
 Thin  
**Sample Type:** Section  
**Texture:** Algal Bafflestone  
**Sorting:** Poorly sorted

Grains	Area %	Abrasion	Sizes	Orientation	Notes
phylloid algae	15	little abrasion, fragmented	668.3um-11363.1um, average 2740.9um	horizontal-subhorizontal	poorly preserved, highly recrystallized with large equant calcite, collapsed, or dissolved, some cortical layers preserved, Ivanovia
brachiopod	5	little abrasion, fragmented	1458.4um-4497.1um, average 2676.9um	random	
ostracod	5	moderately abraded, whole or fragmented	223.1um-1036.5um, average 439.7um	random	
pellets	5	little abrasion	593.6um-681.6um, average 637.6um	random	center is often dissolved and/or recrystallized
bryozoa	3	moderately abraded, fragmented	356.6um-3261.8um, average 2009.6um	random	
foraminifera	sparse	moderately abraded, fragmented	522.8um-4831.0um, average 2676.9um	random	Fusulinid
crinoid	sparse	fragment	711.4um	random	
gastropod	sparse	moderate abrasion	3085.6um	random	filled with mud and small shell fragments
mud	20				peloidal in origin, concentrated in sediment traps created by algal plates, brecciated due to algal-plate collapse
cement	40				pore- and fracture-filling dentic and equant calcite, recrystallization
void space	7				moldic, shelter, and intercrystalline porosity

Notes: large sediment traps with an increase of fragmented algal and cement content. Dissolution of cement adds to porosity.

<b>Sample ID: 2ANB-12</b> Thin <b>Sample Type: Section</b> <b>Texture: Algal Bafflestone</b> <b>Sorting: Poorly sorted</b>					
Grains	Area %	Abrasion	Sizes	Orientation	Notes
phylloid algae	30	little abrasion, some fragmenting but mostly whole	1133.9um-16001.2um, average 4260.3um	horizontal to subhorizontal	poorly preserved, highly recrystallized with large equant calcite or dissolved, some cortical layers preserved, Ivanovia
ostracod	5	moderately abraded, fragmented	173.7um-354.9um, average 243.1um	random	whole or individual shells
pellet	1	little abrasion, fragmented	595.9um-754.7um, average 675.3um	random	
bryozoa	sparse	moderately abraded, fragmented	615.1um-8308.0um, average 3405.7um	random	
brachiopod	sparse	moderately abrasion, fragmented	802.2um-1670.0um, average 1164.9um	random	individual shells, often recrystallized
mud	25				peloidal in origin, concentrated in sediment traps created by algal plates, brecciated due to algal-plate collapse
cement	29				pore- and fracture-filling dentic and equant calcite, recrystallization
void space	10				fracture and intercrystalline porosity

**Sample ID:** 2ANB-13  
 Thin  
**Sample Type:** Section  
**Texture:** Algal Bafflestone  
**Sorting:** Poorly sorted

Grains	Area %	Abrasion	Sizes	Orientation	Notes
phylloid algae	10	little abrasion, fragmented	805.5um-9416.5um, average 3588.8um	horizontal-subhorizontal	poorly preserved, highly recrystallized with large equant calcite or dissolved, some cortical layers preserved, Ivanovia
foraminifera	10	moderately-highly abraded, fragmented	42.3um-3408.6um, average 1118.0um	random	
ostracod	7	moderately abraded, fragmented	73.4um-471.8um, average 220.5um	random	whole or individual shells
bryozoa	5	moderately abraded, fragmented	268.7um-1861.6um, average 767.9um	random	
brachiopod	3	moderately abrasion, fragmented	494.7um-1586.7um, average 1035.6um	random	individual shells, often recrystallized
crinoid	sparse	highly abraded	464.8um-1422.8um, average 988.4 um	random	
gastropod	sparse	moderately abraded, fragmented	571.2um-3960.9um, average 2266.1um		
mud	30				peloidal in origin, concentrated in sediment traps created by algal plates, brecciated due to algal-plate collapse
cement	25				pore- and fracture-filling dentic and equant calcite, recrystallization
void space	10				fracture and intercrystalline porosity

**Sample ID:** 2ANB-14

Thin

**Sample Type:** Section

**Texture:** Algal Bafflestone

**Sorting:** Poorly sorted

Grains	Area %	Abrasion	Sizes	Orientation	Notes
phylloid algae	15	little abrasion, fragmented	779.1um-10453.1um, average 3743.3um	horizontal-subhorizontal	poorly preserved, highly recrystallized with large equant calcite or dissolved, some cortical layers preserved, Ivanovia
bryozoa	5	moderately abraded, fragmented	525.9um-4146.7um, average 1379.9um	random	
brachiopod	3	little abrasion, whole or fragmented	867.3um-8830.3um, average 3564.9um	random	mostly whole
ostracod	3	moderately abraded, whole or fragmented	164.1um-466.7um, average 299.4um	random	
pellet	5	little abrasion	534.3um-870.6um, average 694.2um	random	center is often dissolved and/or recrystallized
brachiopod spine	sparse	little abrasion	293.2um-627.7um, average 460.5um	random	
foraminifera	sparse	little abrasion	351.3um-387.5um, average 369.4um	random	
gastropod	sparse	little abrasion	2381.0um	random	
mud	20				peloidal in origin, concentrated in sediment traps created by algal plates, brecciated due to algal-plate collapse
cement	39				pore- and fracture-filling dentic and equant calcite, recrystallization
void space	10				moldic, shelter, and intercrystalline porosity

Notes: Same level as 2ANB-4, large sediment traps with an increase of fragmented algal and cement content. Dissolution of cement adds to porosity.

**Sample ID:** 2ANB-14  
 Thin  
**Sample Type:** Section  
**Texture:** Algal Bafflestone  
**Sorting:** Poorly sorted

Grains	Area %	Abrasion	Sizes	Orientation	Notes
phylloid algae	10	little abrasion, little fragmentation	474.5um-6902.5um, average 3376.6um	horizontal-subhorizontal	poorly preserved, highly recrystallized with large equant calcite or dissolved, some cortical layers preserved, Ivanovia
bryozoa	7	moderately abraded, fragmented	531.3um-3327.4um, average 1414.6um	random	
brachiopod	7	little abrasion, whole or fragmented	338.5um-8785.8um, average 3625.6um	random	mostly whole
pellet	5	little abrasion	634.1um-800.7um, average 725.7um	random	center is often dissolved and/or recrystallized
ostracod	1	moderately abraded, fragmented	314.0um-625.6um, average 469.8um	random	
crinoid	sparse	little abrasion	682.7um-772.1um, average 727.4um	random	
foraminifera	sparse	little abrasion	215.3um-541.1um- average 318.1um	random	
evaporite crystal	sparse		1224.3um-1308.5um, average 1266.4um		found near the top of thin section in a group
mud	28				peloidal in origin, concentrated in sediment traps created by algal plates, brecciated due to algal-plate collapse
cement	35				pore- and fracture-filling dentic and equant calcite, recrystallization
void space	7				moldic, shelter, and intercrystalline porosity

Notes: Below 2ANB-17, sediment traps from thin Ivanovia, small forams, sparse crinoid, appearance of pellets, bryozoan less fragmented, whole brachiopods and large brachiopods

**Sample ID:** 2ANB-16  
 Thin  
**Sample Type:** Section  
**Texture:** Algal Bafflestone -highly weathered  
**Sorting:** Poorly sorted

Grains	Area %	Abrasion	Sizes	Orientation	Notes
phylloid algae	50	little abrasion, some fragmentation	858.6um-11628.6um, average 3248.2um	horizontal to subhorizontal	poorly preserved, highly recrystallized with large equant calcite, some cortical layers preserved, Ivanovia
bryozoa	sparse	moderately abraded, fragmented	337.8um-597.8um, average 496.0um	random	
crinoid	5	little-no abrasion	7783.3um	random	one large crinoid towards the top
ostracod	sparse	moderately abraded, fragmented	213.2um-415.5um, average 296.9um	random	whole and individual shells
foraminifera	3	no abrasion	120.2um-1300.3um, average 310.5um	encrusting	encrusts phylloid algae
mud	7				peloidal in origin, concentrated in sediment traps created by algal plates, brecciated due to algal-plate collapse
cement	30				pore-filling dentic and equant calcite
void space	5				intercrystalline porosity

Notes: Mostly made up of Ivanovia plates with little mud and encrusters.



**Sample ID:** 2ANB-20  
 Thin  
**Sample Type:** Section  
**Texture:** Algal Bafflestone  
**Sorting:** Poorly sorted

Grains	Area %	Abrasion	Sizes	Orientation	Notes
phylloid algae	10	little abrasion, fragmented	541.1um-4405.4um, average 2805.0um	horizontal-subhorizontal	poorly preserved, highly recrystallized with large equant calcite, some cortical layers preserved, Ivanovia
bryozoa	5	moderately abraded, fragmented	401.7um-7189.9um, average 2788.2um	random	large pieces of stick bryozoans preserved
brachiopod	5	moderately abraded, whole or fragmented	151.4um-1656.7um, average 845.5um	random	
ostracod	3	moderately abraded, fragmented	173.0um-348.3um, average 281.9um	random	whole and individual shells
crinoid	1	moderately abraded, fragmented	470.5um-1615.1um, average 1042.8um	random	
brachiopod spine	sparse	little abrasion	242.1um	random	
foraminifera	sparse	little abrasion	161.4um-332.9um, average 218.1um	random and encrusting	Fusulinids, encrusting byozoa and crinoid
mud	35				peloidal in origin, concentrated in sediment traps created by algal plates, brecciated due to algal-plate collapse
cement	40				pore-filling dentic and equant calcite
void space	1				intercrystalline porosity

Notes: Sediment fills contain geopetals that are depositionally up

**Sample ID:** 2ANB-23  
 Thin  
**Sample Type:** Section  
**Texture:** Algal Bafflestone  
**Sorting:** Moderately sorted

Grains	Area %	Abrasion	Sizes	Orientation	Notes
phylloid algae	30	little abrasion, little fragmentation	331.6um-6585.2um, average 3356.2um	horizontal to subhorizontal	poorly preserved, recrystallized with medium-large equant calcite, some cortical layers preserved, bladed-calcite rinds around algae fragments, Ivanovia
brachiopod	5	moderately abraded, fragmented	726.1um	random	whole or individual shells
ostracod	7	little abrasion, fragmented	180.5um-341.4um, average 236.0um	random	whole or individual shells found in mud
pellet	5	little abrasion, fragmented	252.2um-861.2um, average 556.7um	random	
mud	15				peloidal in origin, concentrated in sediment traps created by algal plates, brecciated due to algal-plate collapse
cement	28				pore-filling dentic and equant calcite (15%), bladed-calcite rinds around algal grains (8%), recrystallization (5%)
void space	10				fracture, brecciation and intercrystalline porosity

Notes: appearance of bladed calcite rinds around algal plates

### Lithofacies 5: Algal Packstone

Sample ID: 2ANB-5					
Thin					
Sample Type: Section					
Texture: Algal Packstone					
Sorting: Poorly sorted					
Grains	Area %	Abrasion	Sizes	Orientation	Notes
phylloid algae	35	moderately abraded, highly fragmented	661.4um-28279.6um, average 4867.2um	random	moderately preserved, recrystallized with large equant calcite, many cortical layers preserved, Ivanovia
pellet	5	little abrasion, fragmented	352.4um-750.9um, average 540.1um	random	
ostracod	3	little abrasion, fragmented	131.3um-241.6um, average 193.5um	random	whole or individual shells found in mud
bryozoa	sparse	moderately abraded, fragmented	448.4um-1439.8um, average 944.1um	random	
mud	20				peloidal in origin, concentrated in sediment traps created by algal plates, brecciated due to algal-plate collapse
cement	32				pore-filling dentic and equant calcite, recrystallization
void space	5				fracture, moldic, and intercrystalline porosity

Notes: Some phylloids are lined with brown equant calcite, but show no fibrous chalcedony

**Sample ID:** 2ANB-11  
 Thin  
**Sample Type:** Section  
**Texture:** Algal packstone  
**Sorting:** poorly sorted

Grains	Area %	Abrasion	Sizes	Orientation	Notes
phylloid algae	27	little abrasion, highly fragmented	907.5um-9432.1um, average 4182.7um	random	poorly preserved, highly recrystallized with large equant calcite, some cortical layers preserved, Ivanovia
brachiopod	5	little-moderately abraded, fragmented	606.7um-1893.0um, average 1053.2um	random	mostly individual shells, some recrystallized
ostracod	5	moderately abraded, fragmented	141.0um-407.5um, average 214.2um	random	whole and individual shells in mud matrix
bryozoa	3	moderately abraded, fragmented	327.5um-1310.7um, average 888.2um	random	
gastropod	sparse	highly abraded	836.6um	random	
mud	20				peloidal in origin, concentrated in sediment traps created by algal plates, brecciated due to algal-plate collapse
cement	30				pore-filling dentic and equant calcite
void space	10				intercrystalline, moldic, and fracture porosity

<b>Sample ID: 2ANB-17</b> Thin <b>Sample Type: Section</b> <b>Texture: Algal Packstone</b> <b>Sorting: Poorly sorted</b>					
Grains	Area %	Abrasion	Sizes	Orientation	Notes
phylloid algae	10	little abrasion, little fragmentation	1266.6um-9142.4um, average 4254.0um	horizontal-subhorizontal	poorly preserved, highly recrystallized with large equant calcite, some cortical layers preserved, Ivanovia
brachiopod	7	moderately abraded, whole or fragmented	413.1um-3427.1um, average 1520.7um	random	mostly whole
brachiopod spine	5	little abrasion	600.4um-658.2um, average 638.6um	random	
bryozoa	3	moderately abraded, fragmented	219.8um-4198.4um, average 1303.3um	random	
crinoid	3	moderately abraded	460.5um-1984.6um, average 907.2um	horizontal-subhorizontal	mostly whole
ostracod	1	moderately abraded, fragmented	229.1um-327.3um, average 278.2um	random	
foraminifera	sparse	little abrasion	292.3um-379.8um, average 333.9um	encrusting	encrusting byrozoa and crinoid
mud	40				peloidal in origin, concentrated in sediment traps created by algal plates, brecciated due to algal-plate collapse
cement	30				pore-filling dentic and equant calcite
void space	1				fracture and intercrystalline porosity

Notes: Sediment fills contain geopetals that are depositionally up

<b>Sample ID: 2ANB-21</b> Thin <b>Sample Type: Section</b> <b>Texture: Algal Packstone</b> <b>Sorting: Poorly sorted</b>					
Grains	Area %	Abrasion	Sizes	Orientation	Notes
phylloid algae	25	moderately abraded, highly fragmented	1627.0um-17126.9um, average 4148.3um	random	moderately preserved, highly recrystallized with large equant calcite, collapsed, or dissolved, some cortical layers preserved, Ivanovia
pellets	2	little abrasion	489.7um-775.1um, average 632.4um	random	center sometimes dissolved and/or recrystallized
bryozoa	sparse	fragment	1566.9um	random	
crinoid	sparse	fragment	367.0um	random	
mud	13				peloidal in origin, concentrated in sediment traps created by algal plates, brecciated due to algal-plate collapse
cement	20				pore- and fracture-filling dentic and equant calcite, recrystallization
void space	40				moldic, shelter, and intercrystalline porosity

Notes: Above 2ANB-4 and 14. High porosity. Great preservation of ivanovia, highly fragmented.

**Sample ID:** 2ANB-22  
 Thin  
**Sample Type:** Section  
**Texture:** Algal Packstone  
**Sorting:** Moderately sorted

Grains	Area %	Abrasion	Sizes	Orientation	Notes
phylloid algae	30	little abrasion, highly fragmented	1829.4um-10302.5um, average 4261.7um	random	poorly preserved, recrystallized with medium-large equant calcite, some cortical layers preserved, bladed-calcite rinds around algae fragments, Ivanovia
brachiopod	2	moderately abraded, fragmented	400.0um-482.9um, average 441.5um	random	whole or individual shells
ostracod	sparse	little abrasion, fragmented	83.8um-127.5um, average 105.7um	random	individual shells found in mud
pellet	sparse	little abrasion, fragmented	606.0um-773.2um, average 703.3um	random	
foraminifera	3	little abrasion	107.9um-255.3um, average 188.1um	encrusting	encrusting phylloid algae
bryozoa	5	moderately abraded, fragmented	951.2um-1860um, average 1207.7um	random	
mud	5				peloidal in origin, concentrated in sediment traps created by algal plates, brecciated due to algal-plate collapse
cement	30				pore-filling dentic and equant calcite (10%), bladed-calcite rinds around algal grains (10%), botryoidal aragonite fans (5%), recrystallization (5%)
void space	25				shelter, fracture, brecciation and intercrystalline porosity

Notes: appearance of bladed calcite rinds around algal plates, possible botryoidal aragonite

<b>Sample ID: 2ANB-24</b> Thin <b>Sample Type: Section</b> <b>Texture: Algal Packstone</b> <b>Sorting: Poorly sorted</b>					
Grains	Area %	Abrasion	Sizes	Orientation	Notes
phylloid algae	15	little abrasion, some fragmentation	437.8um-8939.5um, average 4228.9um	subhorizontal to random	poorly preserved, recrystallized with medium-large equant calcite, some cortical layers preserved, bladed-calcite rinds around algae fragments, Ivanovia
brachiopod	5	moderately abraded, fragmented	385.7um-975.8um, average 557.1um	random	whole or individual shells
ostracod	3	little abrasion, fragmented	150.3um-245.9um, average 194.6um	random	whole or individual shells found in mud
foraminifera	2	moderately abraded, fragmented	82.8um-378.0um, average 162.2um	random and encrusting	Fusulinids (2%), encrusting (sparse)
mud	10				peloidal in origin, concentrated in sediment traps created by algal plates, brecciated due to algal-plate collapse
cement	60				pore-filling dentic and equant calcite (20%), bladed-calcite rinds around some grains (10%), botryoidal aragonite (20%), recrystallization of grains (10%)
void space	5				fracture, brecciation and intercrystalline porosity

Notes: Below 2ANB-17, sediment traps from thin Ivanovia, small forams, sparse crinoid, appearance of pellets, bryozoan less fragmented, whole brachs and large brachs



<b>Sample ID: 2ANB-25</b> Thin <b>Sample Type: Section</b> <b>Texture: Algal Packstone</b> <b>Sorting: well sorted</b>					
Grains	Area %	Abrasion	Sizes	Orientation	Notes
phylloid algae	40	moderately abraded, highly fragmented	3784.6um-8796.3um, average 5372.8um	random	poorly preserved, highly recrystallized with large equant calcite, some cortical layers preserved, Ivanovia
brachiopod	sparse	moderately abraded, whole or fragmented	1021.8um-3558.5um, average 2290.2um	random	recrystallized
ostracod	sparse	moderately abraded, fragmented	610.5um	random	whole and individual shells
mud	10				peloidal in origin, concentrated in sediment traps created by algal plates, brecciated due to algal-plate collapse
cement	45				large botryoidal aragonite fans (20%), chalcedony lining around recrystallized algal grains (12%), pore-filling dentic and equant calcite (10%), replacement quartz near chalcedony (3%)
void space	5				intercrystalline and fracture porosity

Notes: First appearance of abundant chalcedony in mound

### Lithofacies 6: Fusulinid Packstone

<b>Sample ID: 2ANB-6</b> Thin Sample Type: Section Texture: Fusulinid Packstone Sorting: Poorly sorted					
Grains	Area %	Abrasion	Sizes	Orientation	Notes
Foraminifera	50	zero-little abrasion	232.5um-2972.2um, average 1278.0um	random	Fusulinids (59%), biserial foram (possibly Deekerella, 1%)
Crinoid	12	moderately abraded, fragmented	242.5um-2198.6um, average 1042.2um	random	
Bryozoa	5	little abrasion, fragmented	375.0um-1041.7um, average 632.9um	random	fragments
Brachiopod Shell	5	little abrasion, fragmented	226.7um-5024.0um, average 1078.7um	random	individual shells
Ostracod	5	fragmented	137.9um-274.9um, average 204.8um	random	mostly individual shells
Brachiopod Spine	3	fragmented	314.4um-550.4um, average 432.4um	random	
mud	15				appears to be peloidal in origin
cement	5				pore-filling dentic and equant calcite, recrystallization
void space	0				intraparticle porosity filled with calcite

<b>Sample ID: 2ANB-9</b>					
Thin					
Sample Type: Section					
Texture: Skeletal wackestone					
Sorting: Poorly sorted					
Grains	Area %	Abrasion	Sizes	Orientation	Notes
foraminifera	60	zero-little abrasion, fragmented	222.5um-2415.8um, average 827.8um	random	Fusulinids (59%), uniserial foram (1%)
brachiopod	10	little abrasion-moderately fragmented	465.4um-4913.1um, average 1717.0um	random	
ostracod	3	little abrasion-fragmented	251.4um-305.3um, average 278.4um	random	
crinoid	10	moderately abraded, little fragmentation	147.5um-2783.1um, average 964.2um	random	
bryozoa	5	moderately abraded, fragmented	339.2um-1366.8um, average 930.7um	random	
gastropods	sparse	no abrasion, fragmented	1017.4um	random	
mud	7				appears to be peloidal in origin
cement	5				dentic and equant calcite replacement cement
void space	0				

Note: Very grainy matrix

## Lithofacies 7: Skeletal Wacke-Packstone

<b>Sample ID: 2ANB-7</b> Thin Sample Type: Section Texture: Skeletal Packstone Sorting: Moderately sorted					
Grains	Area %	Abrasion	Sizes	Orientation	Notes
foraminifera	25	zero-little abrasion	308.5um-4661.4um, average 2107.1um	horizontal-subhorizontal	Fusulinids (24%), uniserial (1%)
crinoid	25	moderately abraded, fragmented	310.8um-7262.0um, average 3402.1um	horizontal-subhorizontal	
bryozoa	10	little abrasion, fragmented	537.4um-3862.1um, average 1530.4um	horizontal-subhorizontal	
brachiopod	8	little abrasion, fragmented	314.0um-1128.7um, average 697.0um	horizontal-subhorizontal	mostly individual shells
ostracod	5	no abrasion, fragmented	226.5um-614.3um, average 420.4um	horizontal-subhorizontal	whole or individual shells
brachiopod spine	sparse	little abrasion, fragmented	301.2um-473.1um, average 390.7um	horizontal-subhorizontal	grouped together
gastropod	sparse	moderately abraded, fragmented	859.7um	horizontal-subhorizontal	
mud	15				peloidal in origin
cement	10				pore-filling dentic and equant calcite, recrystallization
void space	2				fractures

<b>Sample ID: 2ANB-10</b> Thin Sample Type: Section Texture: Skeletal Wacke-Packstone Sorting: Moderately sorted					
Grains	Area %	Abrasion	Sizes	Orientat ion	Notes
pellets	sparse	little abrasion, fragmented	373.3um-722.3um, average 574.8um	random	
phylloid algae	17	little abrasion, fragmented	2181.0um- 11919.0um, average 4631.7um	random	poorly preserved, highly recrystallized with large equant calcite or dissolved, some cortical layers preserved, Ivanovia
foraminifera	12	moderatelyabrad ed, fragmented	409.7um-3880.2um, average 1989.3um	random	Fusulinids
brachiopod	12	moderately abrasion, fragmented	618.9um-5596.2um, average 2918.2um	random	large whole and individual shells, act as geopetals
bryozoa	5	moderately abraded, fragmented	827.2um-4929.5um, average 1958.6um	random	
brachiopod spine	5	little abrasion	362.8um-2578.4um, average 994.9um	random	
crinoid	2	highly abraded, fragmented	231.9um-2071.5um, average 1469.5um	random	
ostracod	2	moderately abraded, fragmented	260.4um-325.1um, average 292.8um	random	whole or individual shells
mud	30				peloidal in origin, some mud concentrated in sediment traps created by algal plates, brecciated due to algal-plate collapse
cement	15				pore- and fracture-filling dentic and equant calcite, recrystallization
void space	0				

**Sample ID:** 8FDN-7  
 Thin  
**Sample Type:** Section  
**Texture:** Skeletal Packstone  
**Sorting:** Poorly sorted

Grains	Area %	Abrasion	Sizes	Orientation	Notes
rugose coral	35	little abrasion, fragmented around edges	3967.5um-18552.9um, average 13485.2um	grouped with other rugose corals	large and colonial
bryozoa	sparse	highly abraded, fragmented	875.6um	horizontal	
foraminifera	sparse	highly abraded, fragmented	829.2um	horizontal	unidentifiable
brachiopod	10	highly abraded, fragmented	597.9um-1657.1um, average 949.0um	horizontal	individual shells
crinoid	10	highly abraded, fragmented	264.5um-1008.0um, average 491.7um	horizontal	
phylloid algae	sparse	fragmented	3321.3um	horizontal	
ostracod	3	highly abraded, fragmented	302.2um-646.0um, average 499.8um	horizontal	individual shells
mud	35				micritized
cement	5				micrite-psuedo spar, recrystallized grains
void space	2				intercrystalline porosity

**Sample ID:** 8FN1-2  
 Thin  
**Sample Type:** Section  
**Texture:** Skeletal wackestone  
**Sorting:** Poorly sorted

Grains	Area %	Abrasion	Sizes	Orientation	Notes
phyllloid algae	15	fragmented	50.2um-2570.3um, average 819.9um	horizontal - subhorizontal	either completely dissolved or recrystallized with equant calcite, found in groups; Ivanovia
brachiopod	7	moderately abraded-fragmented	417.8um-667.0um, average 513.5um	random	some act as geopetals with orientation up
sponge spicules	2	moderately abraded-fragmented	14.3um-47.1um, average 28.9um	random	
foraminifera	1		105.3um-437.5um, average 193.4um	random	Fusulinids (0.75%), milliod morphology (0.25%)
bryozoa	1	moderately abraded-fragmented	191.6um-2540.5um, average 737.0um	random	
ostracod	1	fragmented	153.6um-1741.7um, average 831.2	random	act as geopetals with orientation up
crinoid	sparse	fragmented	317.9um-823.7um, average 554.1um	random	
mud	65				
cement	8				dentic and equant calcite, mostly pore and fracture filling cement
void space	1				modal porosity, fracture porosity

Notes: large stylolite

**Sample ID:** 8FN2-3  
 Thin  
**Sample Type:** Section  
**Texture:** Skeletal wacke-packstone  
**Sorting:** Poorly sorted

Grains	Area %	Abrasion	Sizes	Orientation	Notes
foraminifera	7	moderately abraded-fragmented	198.4um-2971.7um, average 836.6um	random	Fusulinids (6%), biserial foram (possibly Deekerella, 1%), endothyrid foram (sparse)
bryozoa	1	moderately abraded-fragmented	244.8um-1603.7um, average 934.8um	random	highly fragmented
crinoid	7	highly abraded-fragmented	483.7um-5010.2um, average 1416.9um	random	
brachiopod	1	moderately abraded-fragmented	334.2um-3555.5um, average 1663.4um	random	
brachiopod spine	sparse	moderately abraded	874.8um-1775.5um, average 1325.2	random	
phylloid algae	5	fragmented	75306um-2760um, average 1570.4um	random	poorly preserved, highly recrystallized with large equant calcite, some cortical layers preserved
trilobite	sparse	fragmented	2364.6um	random	
mud	55				
cement	30				dentic and equant calcite, calcite recrystallization of grains, pore and fracture filling cement
void space	1				intraparticle, moldic, and fracture porosity



**Sample ID:** 8FN2-5  
 Thin  
**Sample Type:** Section  
**Texture:** Skeletal Wackestone  
**Sorting:** poorly sorted

Grains	Area %	Abrasion	Sizes	Orientation	Notes
foraminifera	5	moderately abraded-fragmented	270.4um-2091.8um, average 1106.9um	random	Fusulinids (4%), biserial foram (possibly Deekerella, 1%)
brachiopod	3	moderately abraded-fragmented	537.4um-2119.8um, average 1167.4um	random	
brachiopod spine	3	moderately abraded	247.6um-1820.9um, average 724.2um	random	
bryozoa	1	moderately-highly abraded-fragmented	798.0um-3965.0um, average 2113.2um	random	highly fragmented
crinoid	sparse	highly abraded-fragmented	1768.8um	random	
phylloid algae	sparse	fragmented	119.9um-3404.6um, average 1780.5um	random	poorly preserved, highly recrystallized with large equant calcite, some cortical layers preserved
mud	80				appears to be peloidal in origin, bioturbated
cement	8				dentic and equant calcite, calcite recrystallization of grains, pore and fracture filling cement
void space	0				intraparticle and fracture porosity filled with calcite

**Sample ID:** 8FN2-7  
 Thin  
**Sample Type:** Section  
**Texture:** Skeletal Packstone  
**Sorting:** poorly sorted

Grains	Area %	Abrasion	Sizes	Orientation	Notes
brachiopod	25	highly abraded-fragmented	262.4um-9330.2um, average 1251.0um	random	
crinoid	15	highly abraded-fragmented	219.6um-3184.0um, average 740.4um	random	often in groups
foraminifera	7	moderately abraded-fragmented	168.7um-657.3um, average 334.0um	random	Fusulinids (3%), endothyrid foram (3%), biserial foram (possibly Deekerella, 1%)
ostracod	7	highly abraded - fragmented	205.7um-927.1um, average 481.7um	random	
brachiopod spine	1	moderately abraded-fragmented	111.5um-1159.9um, average 391.5um	random	
bryozoa	1	highly abraded-fragmented	872.8um-1011.5um, average 937.0um	random	
mud	35				appears to be peloidal in origin
cement	7				dentic and equant calcite replacement cement (4%), botryoidal chalcedony pore-lining cement often filling entire pore (3%)
void space	2				intraparticle and fracture porosity

**Sample ID:** 8FN2-8  
 Thin  
**Sample Type:** Section  
**Texture:** Skeletal Packstone  
**Sorting:** poorly sorted

Grains	Area %	Abrasion	Sizes	Orientation	Notes
foraminifera	10	moderately abraded-fragmented	298.3um-7468.0um, average 1525.9um	random	Fusulinids (7%), biserial foram (possibly Deekerella, 3%)
brachiopod	10	moderately-highly abraded-fragmented	520.3um-5294.6um, average 2202.7	random	
brachiopod spine	1	moderately abraded-fragmented	462.6um-651.6um, average 539.8	random	
ostracod	5	little-moderate abraded	281.5um-2261.5um, average 809.8um	random	
sponge spicules	3	fragmented	90.0um-153.2um, average 121.6um	random	
crinoid	sparse	highly abraded-fragmented	528.6um-4467.3um, average 539.8um	random	
mud	64				appears to be peloidal in origin
cement	7				dentic and equant calcite, pore-filling cement
void space	0				intraparticle and fracture porosity filled with calcite

<b>Sample ID: 8FN2-9</b> Thin <b>Sample Type: Section</b> <b>Texture: Skeletal Wacke-packstone</b> <b>Sorting: poorly sorted</b>					
Grains	Area %	Abrasion	Sizes	Orientation	Notes
brachiopod	15	highly abraded-fragmented	323.6um-9680.4um, average 1613.0um	random	
crinoid	15	highly abraded-fragmented	221.8um-3198.8um, average 1084.6um	random	
ostracod	5	moderately - highly abraded - fragmented	250.2um-1311.3um, average 758.3um	random	
foraminifera	3	moderately abraded-fragmented	333.3um-1147.5um, average 730.8um	random	Fusulinids (2%), endothyrid foram (1%)
bryozoa	sparse	moderately-highly abraded - fragmented	421.5um-605.6um, average 730.8um	random	
brachiopod spine	sparse	moderately abraded-fragmented	344.4um-971.8um, average 658.1um	random	
trilobite	sparse	fragmented	1730.3um	random	
mud	57				appears to be peloidal in origin
cement	3				dentic and equant calcite replacement cement (1%), botryoidal chalcedony pore-lining cement often filling entire pore (2%)
void space	2				intraparticle and fracture porosity

<b>Sample ID: ANB-2</b> <b>Thin</b> <b>Sample Type: Section</b> <b>Texture: Skeletal Wackestone</b> <b>Sorting: Poorly sorted</b>					
Grains	Area %	Abrasion	Sizes	Orientation	Notes
brachiopod	20	little abrasion, whole or fragmented	921.7um-9309.4um, average 3294.9um	random	often whole or partially fragmented
phylloid algae	10	moderately abraded, fragmented	303.6um-5671.1um, average 1694.8um	subhorizontal, disturbed by fragmenting	poorly preserved, highly recrystallized with large equant calcite, some cortical layers preserved, Ivanovia
crinoid	2	moderately-highly abraded	857.2um-2291.3um, average 1450.4um	random	
bryozoa	1	moderately abraded, fragmented	957.9um-3883.7um, average 2410.8um	random	
foraminifera	1	moderately abraded, fragmented	198.5um-1750.9um, average 726.3um	random	Endothyrid foram (0.5%), Fusulinids (0.25%), biserial foram (possibly Deekerella, 0.25%)
brachiopod spine	1	little abrasion	328.5um-1088.3um, average 821.2um	random	
ostracod	1	moderately abraded, fragmented	119.0um-248.3um, average 175.6um	random	
gastropod	sparse	moderately abraded	1780.0um	random	
mud	53				peloidal in origin, muddy matrix concentrated in sediment fills created by phylloid sediment traps
cement	10				intraparticle and interparticle equant calcite
void space	1				fracture porosity

**Sample ID:** 2ANB-1  
 Thin  
**Sample Type:** Section  
**Texture:** Skeletal Wackestone  
**Sorting:** Poorly sorted

Grains	Area %	Abrasion	Sizes	Orientation	Notes
crinoid	7	little abrasion	794.9um-2137.6um, average 1219.0um	horizontal-subhorizontal	mostly whole
bryozoa	5	moderately abraded, fragmented	561.8um-1532.8um, average 820.6um	random	
brachiopod	5	little abrasion, whole or fragmented	952.3um-1408.0um, average 1225.8um	random	mostly whole
ostracod	3	little abrasion	47.8um-367.6um, average 248.9um	random	
sponge spicule	1	fragmented	89.1um-174.9um, average 142.2um	random	
phylloid algae	sparse	little abrasion, fragmented	5070.7um-7169.8um, average 6120.3um	horizontal-subhorizontal	poorly preserved, highly recrystallized with large equant calcite, some cortical layers preserved, Ivanovia
gastropod	sparse	fragmented	679.5um-1052.4um, average 865.6um	random	
foraminifera	sparse	little abrasion	135.6um-183.4um, average 159.5um	encrusting	encrusting byrozoa and crinoid
evaporite crystal	10		478.7um-3584.6um, average 1454.8um	fans	found near the bottom of thin section in a group, found as small crystals throughout sample
mud	64				peloidal in origin
cement	5				intraparticle and fracture-filling equant calcite
void space	<1				dissolution of evaporites

Notes: Transition between underlying wackestone to mound facies

**Sample ID:** 2ANB-3  
 Thin  
**Sample Type:** Section  
**Texture:** Skeletal Wackestone  
**Sorting:** Poorly sorted

Grains	Area %	Abrasion	Sizes	Orientation	Notes
brachiopod	7	moderately abraded, fragmented	842.2um-1683.8um, average 1246.5um	random	
ostracod	7	moderately abraded, fragmented	447.9um-705.8um, average 557.7um	random	
crinoid	5	moderately abraded, fragmented	762.1um-2265.4um, average 1443.6um	random	
phylloid algae	3	moderately abraded, fragmented	446.0um-3439.8um, average 1904.5um	random	poorly preserved, highly recrystallized with large equant calcite, some cortical layers preserved, Ivanovia
bryozoa	3	moderately abraded, fragmented	203.9um-885.9um, average 571.5um	random	
foraminifera	sparse	moderately abraded	530.3um-2011.1um, average 1270.7um	random	Fusulinid and encrusting
brachiopod spine	sparse	no apparent abrasion	557.6um	random	
mud	60				peloidal in origin, brecciated
cement	15				pore-filling, replacement equant calcite
void space	0				

Notes: Intraclasts? Brecciated matrix

**Sample ID:** 2ANB-8  
 Thin  
**Sample Type:** Section  
**Texture:** Skeletal Wackestone  
**Sorting:** Poorly sorted

Grains	Area %	Abrasion	Sizes	Orientation	Notes
phyllloid algae	15	little abrasion, fragmented	1328.5um-5346.0um, average 2754.9um	random	poorly preserved, highly recrystallized with large equant calcite, some cortical layers preserved, Ivanovia
crinoid	7	moderately-highly abraded	283.5um-1951.2um, average 983.7um	random	
ostracod	5	moderately abraded, fragmented	95.6um-338.2um, average 227.3um	random	whole and individual shells
foraminifera	5	moderately abraded, fragmented	406.5um-1854.0um, average 1343.2um	random	Fusulinids
brachiopod	5	moderately abraded, fragmented	875.4um-1538.7um, average 1201.1um	random	
pellets	3	little abrasion, fragmented	363.0um-722.0, average 590.8um	random	
brachiopod spine	sparse	fragmented	951.0um	random	
mud	30				peloidal in origin, concentrated in sediment traps created by algal plates, brecciated due to algal-plate collapse
cement	25				pore-filling dentic and equant calcite
void space	5				intercrystalline porosity



**Sample ID:** 2ANB-18  
 Thin  
**Sample Type:** Section  
**Texture:** Skeletal Wackestone  
**Sorting:** Poorly sorted

Grains	Area %	Abrasion	Sizes	Orientation	Notes
foraminifera	sparse	moderately abraded	265.6um	random	Fusulinid and encrusting
brachiopod spine	sparse	no abrasion	443.4um	random	found next to brachiopod shell fragments
gastropod	sparse	moderately abraded, fragmented	828.3um	random	
brachiopod	20	moderately abraded, fragmented	253.0um-4650.1um, average 1499.8um	random	often whole or partially fragmented
bryozoa	7	moderately abraded, fragmented	392.8um-8720.1um, average 1718.3um	random	
crinoid	7	little to moderately abraded	259.7um-2090.8um, average 1101.7um	random	
ostracod	5	moderately abraded, fragmented	107.2um-598.9um, average 256.3um	random	
phylloid algae	sparse	moderately abraded, fragmented	2470.0um-5728.8um, average 4099.4um	random	poorly preserved, highly recrystallized with large equant calcite, some cortical layers preserved, Ivanovia
mud	51				peloidal in origin
cement	10				pore-filling, replacement equant calcite
void space	<1				intercrystalline in pore-filling calcite

**Sample ID:** FUS-1a  
 Thin  
**Sample Type:** Section  
**Texture:** Skeletal wacke-packstone  
**Sorting:** Poorly sorted

Grains	Area %	Abrasion	Sizes	Orientation	Notes
foraminifera	10	moderately abraded-fragmented	443.4um-2840.5um, average 1860.0um	random	intraparticle porosity filled with cement Fusulinids
crinoid	6	moderately - highly abraded	615.9um-1042.7um, average 856.0um	random	
brachiopod	5	moderately abraded-fragmented	602.4um-1283.0um, average 746.0um	random	
phylloid algae	sparse	moderately abraded-fragmented	3188.3um	random	Ivanovia
rugose coral	sparse	fragmented	91806.0um	random	
mud	35				peloidal in origin
cement	44				3 generations of pore-filling cement (replacement quartz (38%), chalcedony (5%), dentic and equant calcite (1%))
void space	1				fracture porosity

**Sample ID:** FUS-1b  
 Thin  
**Sample Type:** Section  
**Texture:** Skeletal wacke-packstone  
**Sorting:** Poorly sorted

Grains	Area %	Abrasion	Sizes	Orientation	Notes
foraminifera	15	moderately abraded-fragmented	486.4um-2004.4um, average 1140.5um	random	intraparticle porosity filled with cement; Fusulinids
crinoid	3	moderately - highly abraded	353.3um-3062.0um, average 1488.4um	random	
brachiopod	7	moderately abraded-fragmented	729.2um-1606.3um, average 956.2um	random	
mud	37				peloidal in origin
cement	37				three generations of pore-filling cement (replacement quartz (30%), chalcedony (6%), dentic and equant calcite (1%))
void space	1				intraparticle, moldic, and fracture porosity

**Sample ID:** N3-2  
**Sample Type:** Thin Section  
**Texture:** Skeletal Packstone  
**Sorting:** Poorly sorted

Grains	Area %	Abrasion	Sizes	Orientation	Notes
brachiopod	25	little-moderate abrasion, fragmented	533.5um-4560.4um, average 1586.7um	random	large whole and individual shells
phylloid algae	20	little abrasion, little fragmentation	888.8um-5083.3um, average 5893.8um	random	poorly preserved, highly recrystallized with large equant calcite or dissolved, some cortical layers preserved, Ivanovia
crinoid	10	highly abraded, fragmented	645.3um-2221.3um, average 1285.2um	random	
foraminifera	5	moderately abraded	175.0um-428.7um, average 339.9um	random	Fusulinids (4%), uniserial foram (0.5%), endothyrid foram (0.5%)
gastropod	5	moderately abraded	1533.3um-5083.3um, average 2893.8um	random	
ostracod	5	little abrasion, fragmented	235.4um-812.0um, average 431.5um	random	whole or individual shells
rugose coral	3	little abrasion, fragmented	4444.1um	random	
bryozoa	sparse	moderately abraded, fragmented	691.5um	random	
brachiopod spine	sparse	little abrasion	80.6um-231.9um, 170.6um	random	
mud	20				peloidal in origin
cement	5				dentic and equant calcite, recrystallization
void space	2				intercrystalline porosity

### Lithofacies 8: Peloid Mudstone

<b>Sample ID: 8FN2-4</b> Thin <b>Sample Type: Section</b> Peloid mudstone <b>Texture:</b> well sorted <b>Sorting:</b>					
Grains	Area %	Abrasion	Sizes	Orientation	Notes
brachiopod	3	moderately abraded-fragmented	295.1um-2324.9um average 930.8um	random	
foraminifera	2	moderately abraded	40.5um-1054.9um average 334.0um	random and encrusting	Fusulinids (0.5%), endothyrid foram (0.25%), encrusting (0.25%), biserial foram (possibly Deekerella, sparse)
crinoid	sparse	highly abraded-fragmented	187.2um-1009.3um average 650.1um	random	
gastropod	sparse	moderately abraded	548.6um- 1008.8um, average 778.7um	random	
mud	89				measurable peloids range in size from 62.8um-129.3um average 89.3um; unmeasureable ones were compacted
cement	2				interparticle pore- filling equant calcite
void space	4				interparticle porosity

### Lithofacies 9: Quartz Sandstone

<b>Sample ID: 8FDN-8</b> Thin Sample Type: Section Texture: Quartz Sandstone Sorting: well sorted					
Grains	Area %	Abrasion	Sizes	Orientation	Notes
quartz	70	subangular-subrounded	42um-76.3um, average 57.8um	trough crossbedded	
peloids	10	subrounded-rounded	49.6um-86.7um, average 64.4um	random within quartz crystals, surrounds skeletal grains along crossbed plains	skeletal grains surrounded by clumps of peloids ranging from 667.6um-1844.5um
foraminifera	7	highly abraded - fragmented	231.3um-1279.0um, average 789.4um	found along crossbed planes	surrounded by peloids
brachiopod	2	highly abraded-fragmented	471.1um-1890.2um, average 1240.8um	found along crossbed planes	surrounded by peloids
feldspar	1	subangular	56.7um-109.1um, average 77.8um	random	
crinoid	1	highly abraded - fragmented	382.4um-1202.6um, average 825.2um	found along crossbed planes	surrounded by peloids
brachiopod spine	sparse	highly abraded - fragmented	208.1um-278.9um, average 232.4um	found along crossbed planes	surrounded by peloids
ostracod	sparse	highly abraded - fragmented	332.8um-1381um, average 728.3um	found along crossbed planes	surrounded by peloids
pyrite	sparse		153.9um-160um, average 156.2um	found along crossbed planes	
cement	3				intraparticle and intercrystalline equant calcite
void space	6				interparticle porosity

### Lithofacies 10: Quartz Siltstone

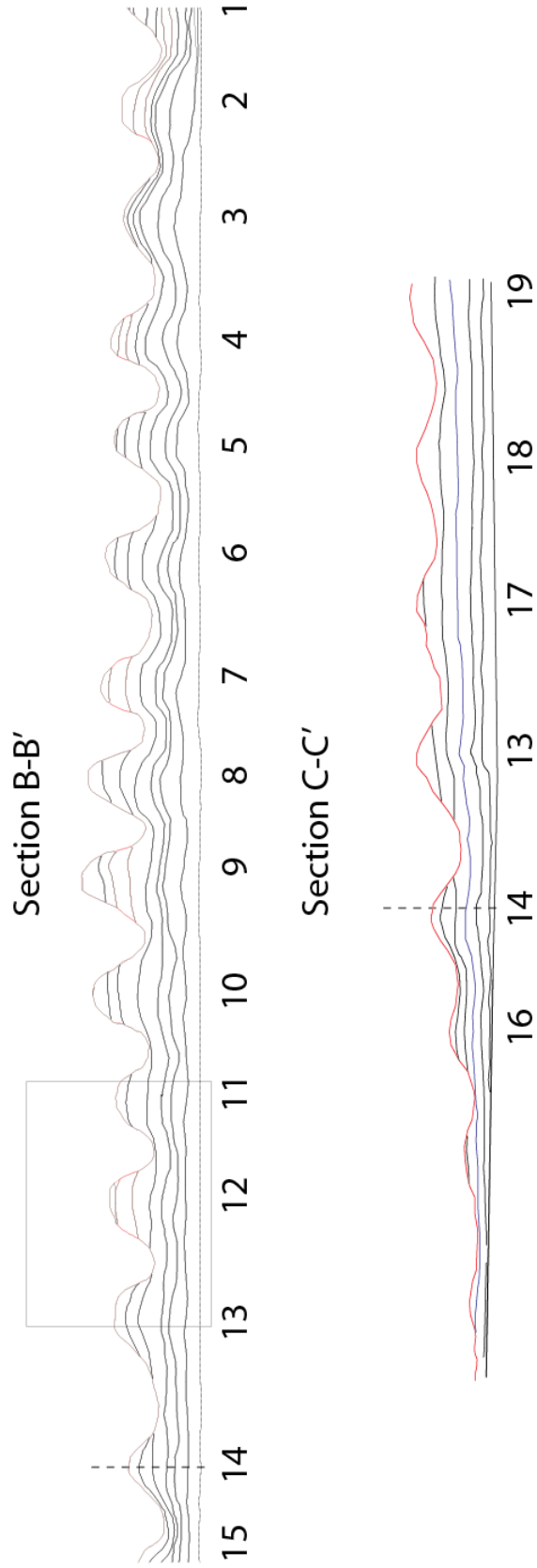
<b>Sample ID: OY-1</b> Thin Sample Type: Section Texture: Quartz Siltstone Sorting: well sorted					
Grains	Area %	Abrasion	Sizes	Orientation	Notes
quartz	93	rounded	silt	random	
brachiopod	1	highly abraded-fragmented	123.3um-8251.4um, average 1987.8um	random	
foraminifera	sparse	moderately abraded-fragmented	1204.1um-1073.6um, average 1138.9um	random	Fusulinids (2%), endothyrid foram (1%)
brachiopod spine	sparse	moderately abraded-fragmented	165.6um-265.3um, average 219.5um	random	
ostracod	sparse	moderately - highly abraded - fragmented	187.0um-299.9um, average 243.5um	random	
bryozoa	1	moderately- highly abraded - fragmented	475.8um-1952.1um, average 933.7um	random	
cement	2				calcite cement
void space	2				intraparticle and fracture porosity

## **Appendix IV**

### *Algal Facies Measurements*

Measurements of the algal facies geometries (Lithofacies 4 and Lithofacies 5). See Appendix I for stratigraphic sections and Appendix II for annotated photomosaics.





The mound number designations in the following tables refer to the specific mounds noted in the above cross-section diagrams. The dashed line on mound 14 shows the location where the cross-sections intersect. The box on Section B-B' shows the interpreted mounds that were removed by the modern-day San Juan river.

Unit	Sect.	Bed	Mound*	Strike/ Dip?	Spacing (m)	Thick (m)	Thin (m)	Relief (m)	Dip Extent (m)	Strike Extent (m)	
4	B	D	1	Strike							
			2	Strike	40.94	0.75	0.29	0.46		37.78	
			3	Strike	34.61	2.41	0.32	2.10		39.75	
			4	Dip	44.89	2.11	1.06	1.05	43.61		
			5	Dip	42.33	1.99	0.95	1.04	36.00		
			6	Dip	29.67	1.76	1.06	0.70	33.53		
			7	Dip	37.38	2.00	1.27	0.73	37.18		
			8	Dip	36.98	1.93	1.45	0.47	30.31		
			9	Dip	23.64	1.67	1.15	0.52			
			10	Dip		1.52	1.18	0.35			
			11	Dip			1.14				
			12	Dip							
			13	Dip		1.76		1.76			
			14	Dip		1.76	1.17	0.59			
			15	Dip			1.17				
		E	1	Strike							
			2	Strike	38.49	2.11	0.54	1.56		39.77	
			3	Strike	41.05	1.41	0.92	0.49		38.63	
			4	Dip	36.20	1.15	0.92	0.23	39.70		
			5	Dip	43.20	1.00	0.59	0.41	43.78		
			6	Dip	44.35	1.06	0.73	0.33	37.36		
			7	Dip	30.36	1.75	0.70	1.05	33.72		
			8	Dip	37.08	1.89	0.94	0.95	37.90		
			9	Dip	38.72	1.62	1.65		43.94		
			10	Dip	49.16	1.62	0.65	0.97			
			11	Dip			0.64				
			12	Dip							
			13	Dip	49.16	1.33		1.33			
			14	Dip		1.22		1.22			
			15	Dip			0.70				
		F	1	Strike							
			2	Strike	37.50	1.43	0.47	0.95		41.85	
			3	Strike	46.20	1.67	0.92	0.75		40.80	
			4	Dip	35.39	1.66	0.92	0.74	40.40		
			5	Dip	45.40	1.39	1.27	0.12	43.03		
			6	Dip	40.65	1.08	0.62	0.46	38.74		
			7	Dip	36.83	0.74	0.42	0.32	37.01		
			8	Dip	37.18	0.85	0.48	0.37	40.57		
			9	Dip	43.95	0.58	0.54	0.04			
			10	Dip		1.19	0.70	0.49			
			11	Dip			1.13				
			12	Dip							
			13	Dip							
			14	Dip		1.20	0.85	0.35			
			15	Dip			0.31				
			<b>Averages</b>		<b>38.64</b>	<b>1.14</b>	<b>0.78</b>	<b>0.68</b>	<b>38.55</b>	<b>39.76</b>	
			<b>Min</b>		<b>23.64</b>	<b>0.58</b>	<b>0.29</b>	<b>0.04</b>	<b>30.31</b>	<b>37.78</b>	
			<b>Max</b>		<b>49.16</b>	<b>2.41</b>	<b>1.65</b>	<b>2.10</b>	<b>43.94</b>	<b>41.85</b>	

Unit	Sec	Bed	Mound*	Strike/Dip?	Spacing (m)	Thick (m)	Actual Thin (m)	Relief (m)	Dip Extent (m)	Strike Extent (m)		
5	B	G	1	Strike								
			2	Strike	38.43	0.40	0.85			40.59		
			3	Strike	42.74	0.63	0.32	0.32			38.50	
			4	Dip	34.26	0.86	0.77	0.09	38.80			
			5	Dip	43.34	1.14	0.84	0.30	42.94			
			6	Dip	42.53	1.45	1.11	0.34	39.59			
			7	Dip	36.64	1.31	1.04	0.27	35.64			
			8	Dip	34.64	1.54	0.84	0.70	35.55			
			9	Dip	36.46	1.20	1.01	0.19				
			10	Dip		2.01	0.98	1.03				
			11	Dip			1.52					
			12	Dip								
			13	Dip	48.92	1.90		1.90				
			14	Dip		1.41	0.52	0.90				
			15	Dip			0.24					
		H	1	Strike								
			2	Strike	33.20	0.70	0.61	0.09			35.90	
			3	Strike	38.60	0.60		0.60			41.12	
			4	Dip	43.64	1.00		1.00	39.52			
			5	Dip	35.40	1.28		1.28	39.67			
			6	Dip	43.95	1.43		1.43	43.43			
			7	Dip	42.91	1.32	0.90	0.42	36.62			
			8	Dip	30.32	1.41	1.20	0.22	30.55			
			9	Dip	30.77	1.10	1.00	0.10				
			10	Dip		2.04	0.59	1.45				
			11	Dip			0.21					
			12	Dip								
			13	Dip	45.50	1.30		1.30	46.09			
			14	Dip	46.68	1.20		1.20				
			15	Dip		1.24	0.60	0.64				
		I	1	Strike								
			2	Strike	36.30	1.16	0.40	0.76			39.69	
			3	Strike	43.07	0.29		0.29			38.64	
			4	Dip	34.20	0.68		0.68	38.22			
			5	Dip	42.23	1.04		1.04	43.87			
			6	Dip	45.51	1.63		1.63	39.46			
			7	Dip	33.40	1.81		1.81	32.24			
			8	Dip	31.07	1.64		1.64	34.28			
			9	Dip	37.49	0.99		0.99				
			10	Dip		1.08		1.08				
			11	Dip								
			12	Dip								
			13	Dip	50.21				41.86			
			14	Dip	33.50	0.97		0.97				
			15	Dip				0.34				

Unit	Sec	Bed	Mound*	Strike/Dip?	Spacing (m)	Thick (m)	Actual Thin (m)	Relief (m)	Dip Extent (m)	Strike Extent (m)	
5	B	J	1	Strike		0.52		0.52			
			2	Strike			0.40				
			3	Strike							
			4	Dip							
			5	Dip							
			6	Dip							
			7	Dip							
			8	Dip							
			9	Dip			2.01		2.01		
			10	Dip							
			11	Dip							
			12	Dip							
			13	Dip							
			14	Dip							
			15	Dip							
						<b>Average</b>		<b>39.17</b>	<b>1.21</b>	<b>0.74</b>	<b>0.86</b>
			<b>Min</b>		30.32	0.29	0.21	0.09	30.55	35.90	
			<b>Max</b>		50.21	2.04	1.52	2.01	46.09	41.12	

Unit	Sec	Bed	Mound*	Strike/Dip?	Spacing (m)	Thick (m)	Thin (m)	Relief (m)
4	C	D	19	Strike				
			18	Strike				
			17	Strike				
			13	Dip	55.18	0.41		0.41
			14	Dip		0.11	0.20	
			16	Dip				
		E	19	Strike				
			18	Strike				
			17	Strike				
			13	Dip	57.75	0.50		0.50
			14	Dip		0.55	0.40	0.16
			16	Dip				
		F	19	Strike				
			18	Strike				
			17	Strike				
			13	Dip	60.42	0.59		0.59
			14	Dip		0.51	0.65	
			16	Dip		0.44		0.44
			<b>Average</b>		<b>57.79</b>	<b>0.44</b>	<b>0.42</b>	<b>0.32</b>
			<b>Min</b>		55.185	0.114	0.2	0.15
			<b>Max</b>		60.42	0.59	0.65	0.59

Unit	Sec	Bed	Mound*	Stike/ Dip?	Spacing (m)	Thick (m)	Thin (m)	Relief (m)
5	C	G	19	Strike				
			18	Strike				
			17	Strike				
			13	Dip	44.86	1.16		1.16
			14	Dip		1.48	0.74	0.74
			16	Dip		0.71		
		H	19	Strike				
			18	Strike				
			17	Strike				
			13	Dip	64.22	1.37		1.37
			14	Dip		1.26		1.26
			16	Dip				
		I	19	Strike				
			18	Strike				
			17	Strike				
			13	Dip	43.74	1.62		1.62
			14	Dip		0.80		0.80
			16	Dip				
		J	19	Strike				
			18	Strike				
			17	Strike				
			13	Dip		0.33		0.33
			14	Dip				
			16	Dip				
		K	19	Strike				
			18	Strike				
			17	Strike				
			13	Dip				
			14	Dip				
			16	Dip				
			<b>Average</b>		<b>50.94</b>	<b>1.09</b>	<b>0.74</b>	<b>1.04</b>
			<b>Min</b>		43.74	0.33	0.74	0.33
			<b>Max</b>		64.22	1.62	0.74	1.62

Unit	Sec	Mound	Strike/ Dip	Spacing of Mound	Total Mound Thick (m)	Total Mound Thin (m)	Total Relief (m)	Confidence
SE	B	1	Strike					High
		2	Strike	38.33	7.21	3.65	3.56	High
		3	Strike	43.74	7.05	3.91	3.14	High
		4	Dip	34.67	8.17	4.08	4.09	High
		5	Dip	40.68	7.76	3.64	4.12	High
		6	Dip	45	8.63	3.62	5.02	Low
		7	Dip	29.47	9.00	4.45	4.55	Low
		8	Dip	37.33	10.15	4.94	5.22	Low
		9	Dip	40.13	10.65	4.97	5.69	High
		10	Dip	39.97	9.84	4.93	4.90	High
		11	Dip			4.55		n/a
		12	Dip					n/a
		13	Dip	48.35				n/a
		14	Dip		6.63	3.77	2.87	High
		15	Dip			3.28		High
		<b>Average</b>		<b>39.77</b>	<b>6.55</b>	<b>4.15</b>	<b>3.92</b>	
		<b>Min</b>		29.47	6.6329	3.28224	2.867	
		<b>Max</b>		48.35	10.654	4.96544	5.689	

